# MOLECULAR EXCITED STATE DYNAMICS VIA HIGH RESOLUTION ELECTRONIC SPECTROSCOPY IN THE GAS PHASE

by

**Leonardo Alvarez-Valtierra**

B.S., University of Guanajuato, 1999

Submitted to the Graduate Faculty of

Arts and Sciences in partial fulfillment

of the requirements for the degree of

Doctor of Philosophy

University of Pittsburgh

2007

UNIVERSITY OF PITTSBURGH

ARTS AND SCIENCES

This dissertation was presented by

Leonardo Alvarez-Valtierra

It was defended on

September 28, 2007

and approved by

Committee Members:

Dr. Paul E. Floreancig, Associate Professor
Department of Chemistry, University of Pittsburgh

Dr. David H. Waldeck, Professor and Departmental Chair
Department of Chemistry, University of Pittsburgh

Dr. David N. Beratan, R. J. Reynolds Professor of Chemistry
Department of Chemistry, Duke University

Dissertation Director:

Dr. David W. Pratt, Professor
Department of Chemistry, University of Pittsburgh

David W. Pratt, PhD

# MOLECULAR EXCITED STATE DYNAMICS VIA HIGH RESOLUTION ELECTRONIC SPECTROSCOPY IN THE GAS PHASE

Leonardo Alvarez-Valtierra, PhD

University of Pittsburgh, 2007

Dynamical processes can be studied using the high resolution spectroscopy technique. Often, the connection between dynamics and spectroscopy is the uncertainty principle $\Delta E \Delta t \approx \hbar$; in other cases, dynamics makes its appearance via extra rovibronic peaks, tunneling splittings, anomalous line intensities, and anomalous line broadenings. Among others, these particular spectral details are related to crucial dynamical information occurring in the molecules upon excitation. Through this work, the electronic origin and some vibronic transitions have been investigated where such phenomena are manifested. Consequently, dynamical analyses are performed to explain the apparent unique characteristics present in their experimental spectra.

The molecules studied here include 2-methoxynaphthalene, *S*-(+)- and *R*-(-)- *naproxen*, acenaphthene, acenaphthene-argon complex, 9,10-dihydrophenanthrene, 2-methylanisole, 3-methylanisole, 2-methylpyrimidine, 5-methylpyrimidine, dibenzothiophene, 2,5-diphenylfuran, and 2,5-diphenyl-1,3,4-oxadiazole. The results of the present work lead to interesting insights into the vibrational inversion motion, the hindered methyl group torsional motion, and some dynamical relaxation processes of selected molecules studied. In the case of *naproxen*, the results obtained to date shed light on the origins of optical activity.

## TABLE OF CONTENTS

## LIST OF ABBREVIATIONS

| | |
|---|---|
| $0_0^0$ | electronic origin or zero point vibrational electronic transition |
| {\|k>} | bath of triplet dark states |
| \|0> | ground state |
| \|s> | prepared bright state |
| 2MA | 2-methylanisole |
| 2MP | 2-methylpyrimidine |
| 2MXN | 2-methoxynaphthalene |
| 3MA | 3-methylanisole |
| 5MP | 5-methylpyrimidine |
| Å | Angstroms |
| ACN | acenaphthene |
| ACN-Ar | acenaphthene-argon var der Waals complex |
| amu | atomic mass units |
| BBO | β-barium borate |
| BIPH | biphenyl |
| $b_N$ | *b*-inertial axis of naphthalene |
| CAR | carbazole |
| CIS | configuration interaction-singles |
| $cm^{-1}$ | wavenumbers |
| CW | continuous-wave |
| DBF | dibenzofuran |
| DBT | dibenzothiophene |
| DCM | 4-dicyanomethylene-2-methyl-6-(*p*-dimethylaminostyryl)-4H pyran |
| DF | dispersed fluorescence |
| DHPH | 9,10-dihydrophenanthrene |
| DPF | 2,5-diphenylfuran |
| DPO | 2,5-diphenyl-1,3,4-oxadiazole |
| FC | Franck-Condon |
| FLU | fluorene |
| FWHM | full width at half maximum |
| HF | Hartree-Fock |
| HT | Herzberg-Teller |
| Hz | Hertz |

| | |
|---|---|
| IC | internal conversion |
| ISC | intersystem crossing |
| IVR | intramolecular vibrational relaxation |
| JB95 | spectral fitting program |
| JBA95 | data acquisition software |
| K | Kelvin |
| KDP | potassium dihydrogen phosphate |
| LIF | laser induced fluorescence |
| MHz | megahertz |
| MO | molecular orbital |
| MP2 | second order Moller-Plesset |
| NAPH | naphthalene |
| $Nd^{3+}$ | neodymium III |
| NEA | 1-(1-naphthyl)ethylamine |
| ns | nanoseconds |
| NSAID | non-steroidal anti-inflammatory drugs |
| OMC | observed minus calculated (standard deviation) |
| PES | potential energy surface |
| PFI-ZEKE | pulsed field ionization zero kinetic energy |
| PHEN | phenanthrene |
| PMT | photomultiplier tube |
| psi | $lb/in^2$ |
| $Q_n$ | n-vibrational coordinate |
| $S_0$ | ground electronic state |
| $S_1 \leftarrow S_0$ | the lowest electronic transition |
| $S_2 \leftarrow S_0$ | the second lowest electronic transition |
| $S_1$ | first excited electronic state |
| $S_2$ | second excited electronic state |
| SOC | spin-orbit coupling |
| $T_k$ | $k^{th}$-triplet state |
| TM | transition moment |
| TOF-MS | time of flight-mass spectrometry |
| UV | ultraviolet light |
| vdW | van der Waals |
| YAG | yttrium aluminum garnet |
| ZPL | zero point vibrational level |
| $\Delta I$ | inertial defect |
| $\mu$W | micro-watts |
| $\upsilon_{sk}$ | singlet-triplet coupling terms |
| $\varphi$ | torsional ring (twisting) angle |

## LIST OF TABLES

## LIST OF FIGURES

## LIST OF SCHEMES

# PREFACE

The collection of research projects presented here is a summary of many exciting ideas that came to my mind from different sources while being enrolled in graduate school at the Department of Chemistry at the University of Pittsburgh.

One afternoon as a first-year grad student, I became incredibly attracted by the high resolution spectral landscapes when I saw a poster in front of the elevators in the sixth floor of Chevron Science Center; this work belonged to a senior member of Dr. Pratt's group. After that moment in my life, I became fascinated by the beauty of this creation of nature, but I was even more astonished when I learned that such beautiful landscapes were able to be fully analyzed by using computer programs with appropriate Hamiltonians written therein. For me, this became the best tool to prove my previous experiences in computational chemistry with real experimental results. I do believe I was very fortunate to land in this paradise of research field in science, and I thank GOD because of this invaluable gift in life.

All that I have described here was possible thanks to my advisor Professor David Pratt. His knowledge and passion about science have always been a great admiration to me. Also, his endless support and freedom in the lab have allowed me to accomplish my own inspirations in science. I am really thankful to him.

I also would like to thank the many members of the Pratt group over the years. In particular, Dr. John Yi helped me tremendously by speeding up the learning curve of the "high

resolution" technique and spending many nights in the lab trying to get the best mode hop free spectrum ever. Dr. Cheolhwa Kang was of great help in the theoretical side of spectroscopy; his explanations about symmetries, energy level diagrams and Hamiltonians simplified my efforts tremendously in understanding spectroscopy better. Dr. David Plusquellic and Dr. David Borst provided constant support on programming issues regarding JB95 and lbrot; their help on the data analysis is strongly appreciated. Dr. Jim Pfanstiel offered valuable experimental help with the ring dye laser. I also want to thank the current members of the group who have been supportive in many aspects during my stay here, especially Jessica Thomas and Justin Young.

I would like to extend my gratitude to the key people that made possible the acquisition and analysis of many projects presented here. My friends, Bob Muha and Chuck Fleishaker in the electronics shop, Tom Gasmire and Jeff Sicher in the machine shop, and Bob Greer in the glass shop; many thanks to all of them for the countless help provided, when needed, to run the experiments properly.

I thank the members of my dissertation committee, Dr. Paul Floreancig for being a committee member and my teacher of Phys. Org. Chem.; Dr. David Beratan an old friend from 1997 willing to participate in my defense traveling from Duke University, NC; and Dr. David Waldeck because he always has offered me a warm friendship and strong motivation to be successful in life. I would also thank Dr. David Nesbitt (JILA, Colorado) for recent helpful conversations and Dr. Brooks Pate (U. Virginia) for the opportunity to join his research group with a postdoctoral position in microwave spectroscopy.

My whole family deserves special thanks: My parents, brothers, relatives, and family-in-law. My aunt Catita always blessed me; unfortunately, she is no longer with us. And finally, to

my lovely wife, Lupita León Verdín, who always provided encouragement, support, love, and help, whenever I needed. I am in great debt to her.

May GOD bless all of you.

Pittsburgh, PA

September 2007

Leonardo Alvarez-Valtierra.

# 1.0 INTRODUCTION

The study of various molecular dynamical processes is nowadays a relevant topic in modern experimental spectroscopy. Issues like the evolution of the excited states, coupling between different vibrational modes, charge transfer, and fluorescence decay behavior of the electronically excited states are of predominant importance in physics, chemistry, and biology. The understanding of these dynamical phenomena and processes will reveal inter- and intra-molecular potential energy surfaces, the electronic structure of molecules, the coupling mechanisms between different quantum states, and the various channels through which chemical reactions may occur.

In this work, we exploit the *ultra*high resolution electronic spectroscopy technique to study supersonically expanded molecules in the gas phase by using a highly collimated (~1 MHz linewidth) UV light beam coming from a continuous-wave $Ar^+$ pumped ring dye laser, and a Doppler-reduced (~18 MHz) molecular beam formed in a differentially pumped vacuum system.

In Chapter 2, we study the preferred conformations of molecules in the gas phase. 2-methoxynaphthalene (2MXN) was chosen as our target molecule due to its apparent preference to exist in one conformation (*cis*-) than in the other (*trans*-). Moreover, we have further extended this study by attaching a chiral (isopropionic acid) substituent to the *cis*-2MXN frame and consequently generate *S*-(+)- and *R*-(-)-*naproxen*. Our preliminary results reveal the apparent existence of different structures just by exchanging the chiral center of the molecule.

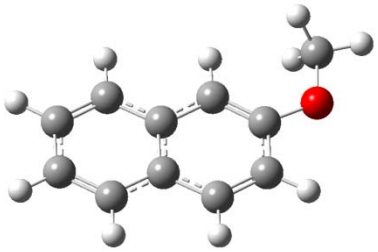

**2-methoxynaphthalene**

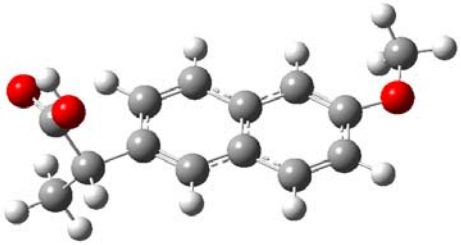

***S*-(+)-*naproxen***

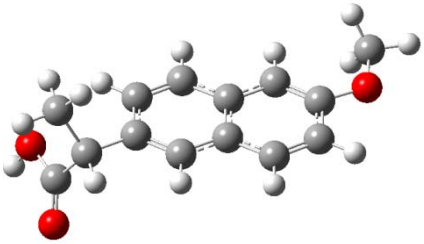

***R*-(-)-*naproxen***

In Chapter 3, we present the study of a molecule of $C_{2v}$ symmetry (acenaphthene) that exhibits intensity anomalies in some of its vibronic transitions. We have found that a pseudo-Coriolis coupling mechanism is likely to be occurring between these almost isoenergetic totally symmetric vibronic transitions. The study of a van der Waals complex of the molecule with an argon atom is also included, revealing the most likely position of the argon atom with respect to the bare molecule by Kraitchman analysis.

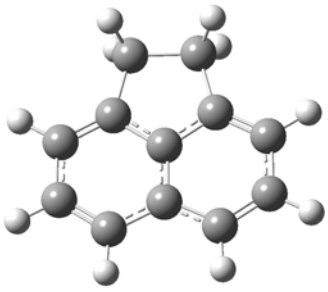

**acenaphthene**

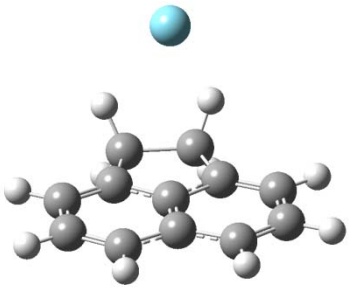

**acenaphthene-argon**

In Chapter 4, we move to a more dynamical problem dealing with a very floppy molecule in the gas phase (9,10-dihydrophenanthrene). Upon a detailed study of the inertial defects of many of the vibronic bands, we were able to unambiguously assign the vibrational modes (or combinations of them) responsible for the extensive Franck-Condon activity revealed in the low resolution spectrum of this molecule. Interestingly, in the last two vibronic transitions analyzed, we have discovered the presence of tunneling splittings assigned to the inversion motion coordinate involving cooperative motion along two totally symmetric vibrational modes.

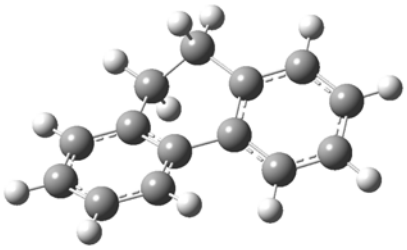

**9,10-dihydrophenanthrene**

In Chapter 5, we focus our attention on the dynamics of the methyl group torsional motion in aromatic frames. 2- and 3-methylanisole molecules were selected due to previous study in our research group about their "parent" molecules, toluene and anisole. The crucial finding in this project was the clear evidence that the potential energy barriers hindering the motion of the methyl group in both electronic states remarkably depend on the position and conformation of the methoxy group.

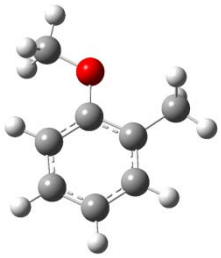

**2-methylanisole**

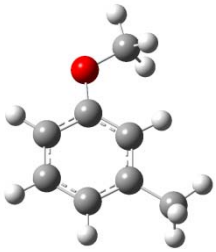

**3-methylanisole**

In Chapter 6, we continue the study of hindered methyl groups, but now in chemical systems dealing with intersystem crossing (ISC) dynamics due to the nature of the chromophore (pyrimidine) to which the methyl group is attached. It has been known that pyrimidine itself exhibits ISC in the "intermediate-case" molecule limit. Therefore, the coupling of the methyl group and the intersystem crossing dynamics are revealed in the spectra of 2- and 5-methylpyrimidine by the manifestation of extra peaks, the formation of clumps of lines, and the lifetime broadening of individual transitions.

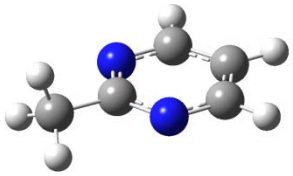

**2-methylpyrimidine**

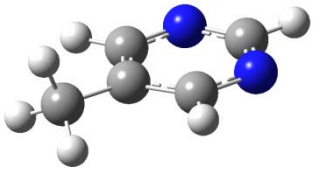

**5-methylpyrimidine**

In Chapter 7, we conclude with the study of molecules falling in the large molecule (statistical) limit of ISC. Natural lifetime broadening of peaks is remarkably manifested in sulfur-containing heterocycles, so we investigate this phenomenon in dibenzothiophene (DBT). For comparison, we include the fluorescence lifetimes previously obtained for its analogs (fluorene, carbazole, and dibenzofuran); the difference manifested in DBT is extraordinary due to a presumably large density of dark states in the vicinity of the bright state. 2,5-Diphenylfuran and 2,5-diphenyl-1,3,4-oxadiazole also exhibit small fluorescence lifetimes; the presence of 5-member ring heterocycles in the structures is known to enhance the spin-orbit coupling terms, and this is demonstrated in these two molecules.

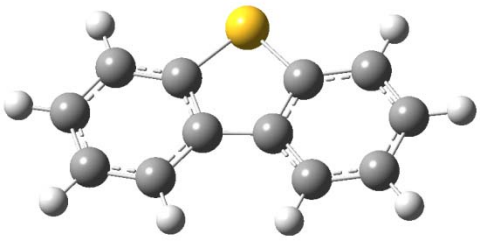

**dibenzothiophene**

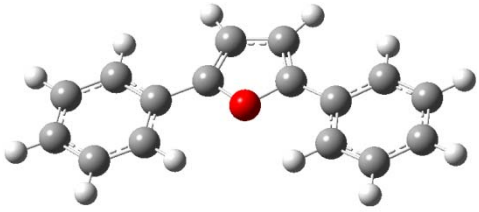

**2,5-diphenylfuran**

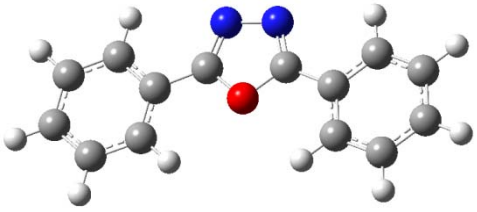

**2,5-diphenyl-1,3,4-oxadiazole**

Finally, we include three appendices at the end; two of which describe the MATHCAD codes used to solve particular problems dealing with tunneling splittings (Appendix A), and methyl group torsion-rotation first- and second-order perturbation terms (Appendix B). Appendix C describes some work in collaboration with other members of the group, and some projects that need to be further analyzed.

## 2.0 CONFORMATIONAL STUDY OF 2-METHOXYNAPHTHALENE AND *NAPROXEN* BY HIGH RESOLUTION ELECTRONIC SPECTROSCOPY IN THE GAS PHASE. ARE *S*-(+)-*NAPROXEN* AND *R*-(-)-*NAPROXEN* TRUE MIRROR IMAGES OF EACH OTHER?

## 2.1 ABSTRACT

Rotationally resolved fluorescence $S_1 \leftarrow S_0$ excitation spectra of the zero point vibrational level transitions of 2-methoxynaphthalene (2MXN), *S*-(+)-*naproxen* and *R*-(-)- *naproxen* were studied in the collision-free environment of a molecular beam. The $0_0^0$ band of the $S_1 \leftarrow S_0$ transition of *cis*-2MXN is an *a*/*b*-hybrid band with 84.2% *b*-type character. The $S_1 \leftarrow S_0$ $0_0^0$ transitions of both *S*-(+)- and *R*-(-)-*naproxen* are *a/b/c* hybrid bands with a high percentage of *b*-type character, as observed in 2MXN. The two *naproxen* molecules are derivatives of 2MXN, having a chiral isopropionic acid group attached at the 6-position. As expected, *S*-(+) and *R*-(-)-*naproxen* exhibit identical vibrationally resolved electronic spectra. However, the two optical isomers exhibit *different* rotational constants. Thus, even though the electronic transitions on each of the two isomers show up at the same frequencies, noticeable differences are found in their inertial parameters in both electronic states. This behavior seems to suggest that the two isomers of this molecule are diastereomers, rather than enantiomers, which should have identical inertial parameters.

## 2.2 INTRODUCTION

Stereoisomers are defined as isomers (*i.e.*, compounds having the same molecular formula but different structures) differing only in configuration and/or conformation. There are two types of stereoisomers, enantiomers and diastereomers. The terms enantiomer and diastereomer relate to molecules as a whole. Thus, if two molecules have the same constitution (connectivity) but different spatial arrangements of the atoms (*i.e.*, they are stereoisomeric), they must either be

related as mirror images or not. In the former case they are enantiomers, in the latter case they are diastereomers. A chiral center is a focus of chirality; in the case of carbon it corresponds to the asymmetric tetrahedral atom. The existence of enantiomers is usually, but not invariably, guaranteed by the existence of at least one chiral center or chiral torsional axis (axis of chirality). Diastereomers often contain two or more chiral centers, chiral axes, or combination of thereof; however, this is not necessarily the case. On the other hand, stereogenic centers (axes or atoms), which are the foci of diastereoisomerism, might or might not be chiral. Interchange of ligands at a stereogenic center leads to a stereoisomer (enantiomer or diastereomer).[1]

The chemical and physical properties of stereoisomers have been the focus of attention of many physical organic chemists in the past century due to nature's degree of chiral purity. Almost all natural amino acids rotate the plane of polarized light to the left (*S*), whereas natural sugars rotate it to the right (*R*). In turn, many types of ligand-receptor (lock-and-key) processes in biosynthesis and enzymatic catalysis are highly chirospecific.[2] Additionally, it has been recently reported by Mons *et al*.[3] that the presence of a chiral center in amino acids nominally influences the direction of the so-called $\gamma$-turns in the secondary structure of short peptides in the gas phase.

Enantiodifferenciation of jet-cooled chiral aromatic molecules in the gas phase has been the subject of extensive research by Lahmani, Zehnacker, and co-workers in the past few years.[4-11] These studies involve the formation of van der Waals complexes in the jet, which exhibit different spectroscopic features depending on the chirality of the complexing agent with respect to the chiral target molecule. It has been revealed that certain *S*-chiral species prefer forming complexes with *S*-chiral rather than with *R*-chiral solvents, mimicking the lock-and-key phenomena observed in chiral biomolecules.[4,5,9-11]

Naphthalene and many of its derivatives have been extensively studied in the past years by high resolution electronic spectroscopy of jet-cooled molecules in the gas phase.[12-19] In these studies, a great deal was learned about their structural and dynamical properties of the molecules in their ground and electronically excited states. Many structural isomers were detected; additionally, several of the attached groups were discovered to vibrate along low-frequency vibrational coordinates whose potentials differed greatly in the two electronic states. In general, it was also found that the electronic transition moment (TM) vectors of the $S_1 \leftarrow S_0$ transitions are parallel to the (long) *a*-inertial axis in 1-substituted naphthalenes and parallel to the (short) *b*-axis in 2-substituted naphthalenes. An important exception was found for 1-aminonaphthalene, which exhibits a short-axis polarized TM orientation in its rotationally resolved electronic spectrum. This anomalous behavior was explained in terms of the conjugative properties between the amino group and the naphthalene aromatic framework.[19]

Several spectroscopic studies have also been performed on 2MXN using laser induced fluorescence (LIF), dispersed fluorescence (DF), hole-burning, and time resolved emission spectroscopy.[20,21] From these studies and theoretical calculations,[21] it is known that 2MXN exhibits several electronic transitions mainly originating in its *cis*-conformer. The corresponding *trans*-conformer transitions are relatively weak; the relative energy difference between the conformers is about 700 $cm^{-1}$ in their ground electronic states. No further experimental evidence in the literature is available concerning the electron density distribution or transition moment orientations in 2MXN or its derivatives.

*Naproxen* is a 2MXN derivative formed upon attachment of an isopropionic acid group to the 6-position of the aromatic frame (see Scheme 2.1). The *S*-enantiomer of this molecule belongs to the arylacetic acid group of non-steroidal anti-inflammatory drugs (NSAID) due to its

analgesic and antipyretic properties. It is believed that the mechanism of action of *S*-(+)-*naproxen* in the body is related to prostaglandin synthetase inhibition.[22-24] Despite being "mirror image" identical, the *S*- and *R*-enantiomers of a chiral drug can function to affect drastic physiological differences, as evidenced by penicillamine [*R* (toxic) and *S* (antiarthritic)].[25] The possibility of deleterious side effects of the wrong enantiomer is one of the principal driving forces for the synthesis of enantiomerically pure drugs.

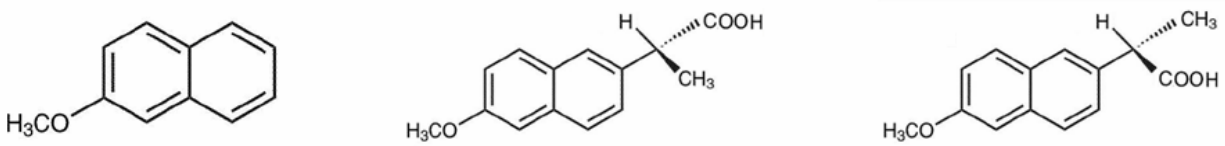


2MXN *S*-(+)-*naproxen* *R*-(-)-*naproxen*

**Scheme 2.1. Structures of *cis*-2-methoxynaphthalene and *S*-(+)- and *R*-(-)-*naproxen*.**

The present study emerges from the therapeutic relevance of *S*-(+)-*naproxen* as a chiral drug and the interest to study the electronic spectra of both enantiomers at rotational resolution in the jet. From our preliminary results of the analysis of the spectra of both isomers in the gas phase, apparently *S*-(+)-*naproxen* and *R*-(-)-*naproxen* are not exact mirror images of each other, due to a presumed torsional motion of another functional group upon excitation. In fact, instead of *S*-(+)- and *R*-(-)-*naproxen* being enantiomers, they tend to behave as diastereomers. We speculate that this diastereometric behavior is a consequence of the incipient development of a second chiral element in the isolated molecule.

## 2.3 EXPERIMENTAL

2MXN (>99% pure), *S*-(+)-*naproxen* (>98% pure) and *R*-(-)-*naproxen* (>98% pure) were purchased from Aldrich and used without further purification. In the vibrationally resolved electronic experiments, the sample was seeded into 45 psi of helium gas and expanded into a vacuum chamber ($10^{-5}$ torr) through a 1 mm diameter orifice pulsed valve (General Valve Series 9) operating at 10 Hz. Two centimeters downstream of the valve, the sample was excited with the second harmonic of a Quanta Ray $Nd^{3+}$:YAG (Model DCR-1A) pumped dye laser (Model PDL-1). The dye (DCM) laser output was frequency doubled with an external potassium dihydrogen phosphate (KDP) crystal providing a spectral resolution of ~0.6 $cm^{-1}$ in the UV. From the point of intersection between the nozzle and the laser, the molecules were excited and the fluorescence was collected with a photomultiplier tube (PMT). Finally, the collected data were processed by a boxcar integrator (Stanford Research Systems) and recorded with Quick Data Acquisition software version 1.0.5.

The rotationally resolved electronic experiments were performed using a molecular beam laser spectrometer, described in detail elsewhere.[26] Briefly, the molecular beam was formed by expansion of the vaporized sample seeded in argon carrier gas (-17 psi) through a heated (~328 K for 2MXN and ~483 K for *naproxen*) 200 $\mu$m quartz nozzle into a differentially pumped vacuum system. The expansion was skimmed 2 cm downstream and crossed 15 cm further downstream by a continuous wave (CW) $Ar^+$ pumped ring dye laser. The CW laser was operated with DCM dye and intracavity frequency doubled in a 640 nm $LiIO_3$ crystal, yielding ~350 $\mu$W of UV radiation.

The fluorescence excitation spectrum was detected using spatially selective optics, a photomultiplier tube, and a photon counting system. This signal together with the iodine

absorption spectrum and the relative frequency markers were simultaneously collected and processed by the JBA95 data acquisition system.[26] Absolute frequency calibration of the excitation spectrum was performed by comparison with the $I_2$ absorption spectrum. The relative frequency markers were obtained from a stabilized etalon with a free spectral range of 299.7520 ± 0.0005 MHz.

## 2.4 RESULTS

Figure 2.1 shows the first ~1200 $cm^{-1}$ of the vibrationally resolved fluorescence excitation spectrum of 2MXN in a supersonic jet. The LIF spectrum is similar to the one previously reported by Troxler *et al*.;[20,21] it exhibits what appear to be two origin bands; a strong transition at ~31028 $cm^{-1}$ and a much weaker origin lying 661 $cm^{-1}$ to the red. The two bands were assigned to *cis*- and *trans*-2MXN, respectively based on comparison with previous results obtained for *cis*- and *trans*-hydroxynaphthalenes.[14,20] Vibronic bands displaced by +449 and +461 $cm^{-1}$ from the origin band of *cis*-2MXN (see bottom panel of Figure 2.1) have been assigned to totally symmetric in-plane modes of the *cis*-conformer, which exhibit extensive vibrational mixing.[21]

Figure 2.2 shows the rotationally resolved $S_1 \leftarrow S_0$ fluorescence excitation spectrum of the $0_0^0$ band of *cis*-2MXN at 31028.0 $cm^{-1}$. The spectrum spans approximately 3.0 $cm^{-1}$, and exhibits *a/b*-hybrid character of 15.8/84.2%. Its signal/noise ratio is about 18/1. To fit this spectrum, approximately 3000 *b*-type rovibronic transitions were generated based on *ab initio*[18] [MP2/6-31G (d,p)] estimates of rotational constants and rigid rotor Hamiltonians for both electronic states. Then, quantum number assignments of single transitions in the simulated

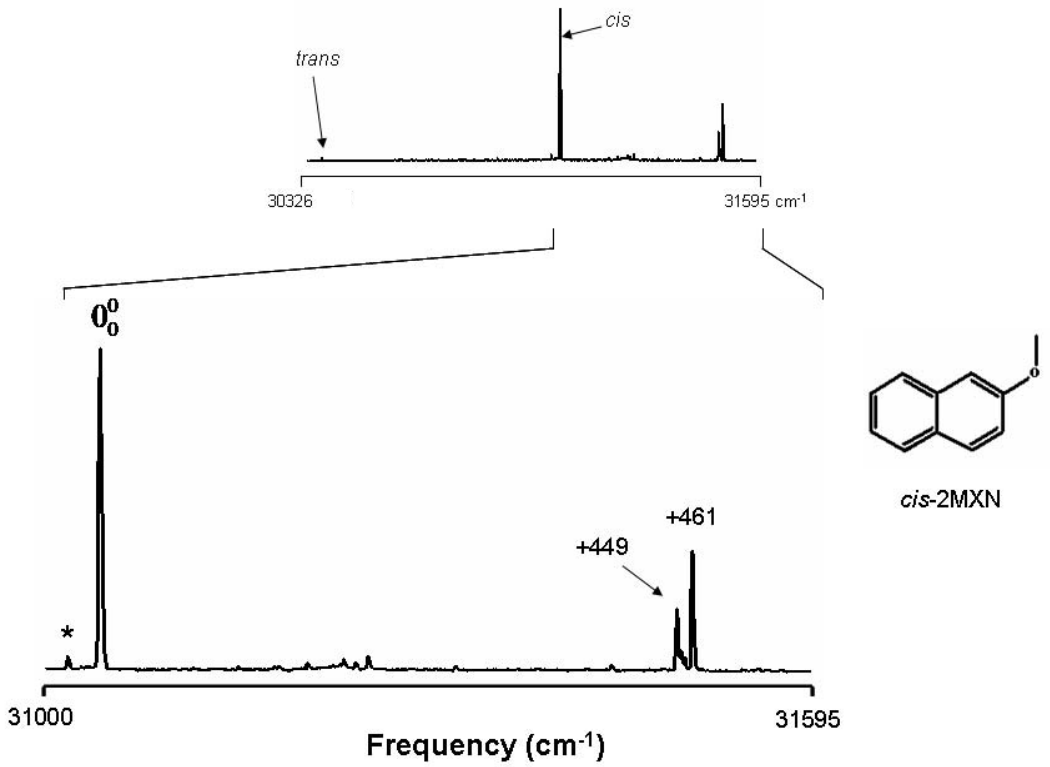


**Figure 2.1. Vibrationally resolved fluorescence excitation spectrum of 2MXN in a molecular beam. The top trace makes evident the relative difference in intensities between the *cis*- and *trans*-conformers of the molecule. The bottom trace shows the portion corresponding to *cis*-2MXN, where the small transition marked with the asterisk presumably corresponds to its hydrogen bonded water complex.**

spectrum were made to the corresponding transitions in the experimental spectrum using the Windows-based program JB95.[28] Finally, a least-squares fitting procedure was used to optimize the rotational constants, based on comparisons of the observed and calculated line positions. The final fit utilized ~150 assigned lines, including some *a*-type ones, and resulted in a standard deviation (OMC) of ~3.5 MHz. The quality of the fit is shown in the bottom panel of Figure 2.2. Here, a portion of the *P* branch at full experimental resolution is shown with its corresponding simulated spectra with and without a calculated lineshape function. The Voigt lineshape function applied utilized 18 MHz Gaussian and 22 MHz Lorentzian contributions, yielding an overall full width at half maximum (FWHM) linewidth of ~30 MHz. The rotational temperature of the fit is 4.0 K. The inertial parameters of this spectrum are summarized in Table 2.1.

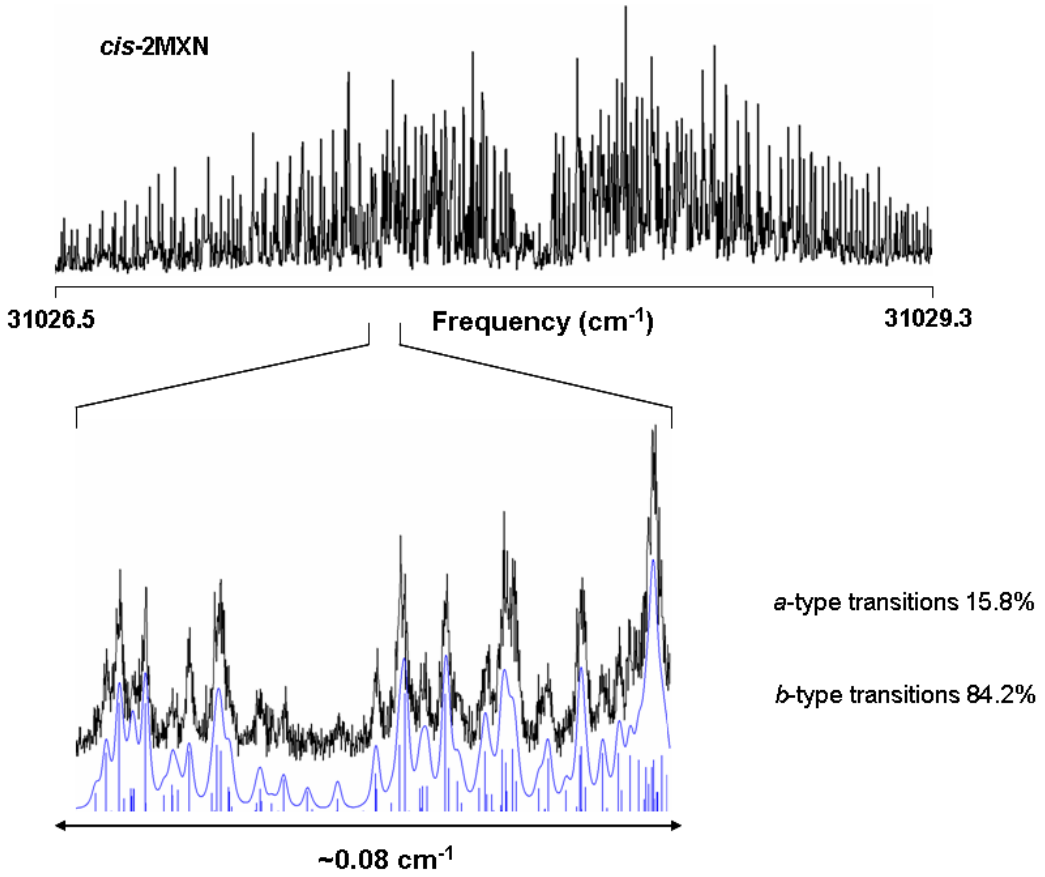


**Figure 2.2. Rotationally resolved fluorescence excitation spectrum of the $0_0^0$ band of jet-cooled *cis*-2MXN in the gas phase (top panel). Portions of the *P* branch at full experimental resolution together with a simulated spectrum, with and without a calculated lineshape function, are also shown (bottom panel).**

The vibrationally resolved LIF spectrum of *S*-(+)-*naproxen* has been recently reported by Lahmani, *et al*.[9] and shown in Figure 2.3. The presence of two conformers, "red" and "blue", were clearly identified in the spectrum. With the help of theoretical calculations, the structures and their relative energies have been assigned to each transition. These two conformers correspond to the two minimum energy conformations of the molecule by rotating the chiral substituent by ~176° along the C–C bond from the naphthalene framework; the preferred orientation of the methoxy group in these two transitions corresponds to the one observed in *cis*-2MXN and the frequency spacing between them is about 102 $cm^{-1}$. The rest of the observed vibrational activity corresponds to vibronic transitions of both identified conformers.

**Table 2.1. Inertial parameters of the origin band of *cis*-2-methoxynaphthalene.**

| Parameter[a] | Experimental | Theory [MP2/6-31G (d,p)] | |
|---|---|---|---|
| | | ***cis*-2MXN** | ***trans*-2MXN** |
| **$S_0$** | | | |
| ***A″* (MHz)** | 2336.5 (1) | 2333.6 | 2776.7 |
| ***B″* (MHz)** | 621.8 (1) | 622.0 | 575.3 |
| ***C″* (MHz)** | 492.8 (1) | 492.6 | 478.0 |
| **$\Delta I''$ (amu Å$^2$)** | -3.48 (5) | -3.19 | -3.20 |
| **$S_1$** | | | |
| ***A′* (MHz)** | 2267.3 (1) | | |
| ***B′* (MHz)** | 620.3 (1) | | |
| ***C′* (MHz)** | 488.8 (1) | | |
| **$\Delta I'$ (amu Å$^2$)** | -3.61 (5) | | |
| **TM angle with respect to $b_N$** | 23°(2) | 19.4° | 11.2° |
| **Band origin (cm$^{-1}$)** | 31028.0(<1) | | |
| **OMC (MHz)** | 3.5 | | |
| **Temp (K)** | 3.0 | | |

[a] Standard deviations shown in parentheses are relative to the last significant figure.

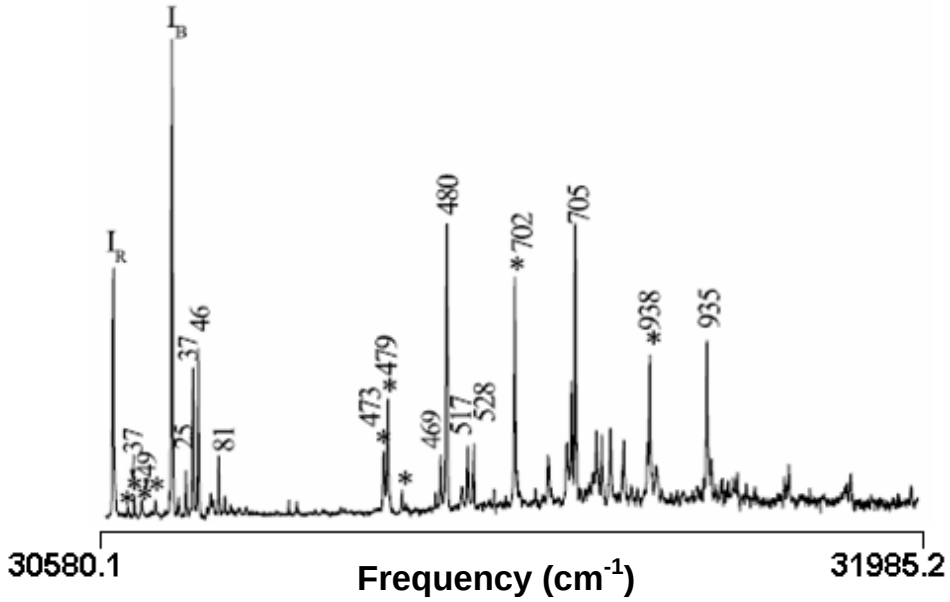


**Figure 2.3. Vibrationally resolved fluorescence excitation spectrum of jet-cooled *S*-(+)-*naproxen* in the gas phase. Two conformers [red ($I_R$) and blue ($I_B$)] have been identified. The transitions marked with asterisks belong to the blue conformer. Taken from Reference 9.**

Figure 2.4 shows the rotationally resolved fluorescence excitation spectrum of the red conformer of *S*-(+)-*naproxen* at 30585.3 $cm^{-1}$. The spectrum spans approximately 2 $cm^{-1}$ and exhibits *a/b/c* hybrid character of 22.7/70.4/8.9. Its signal/noise ratio is about 3/1. The spectrum was fit using rigid rotor Hamiltonians in both electronic states by means of a procedure similar to that used for 2MXN. The final fit used ~120 assigned lines to yield an OMC of 4.86 MHz. A fully resolved portion of the experimental spectrum and its simulated spectral traces are shown in the bottom panel of Figure 2.4. The lineshape function used 18 MHz Gaussian and 20 MHz Lorentzian contributions. The rotational temperature of the fit is 5.0 K. The inertial parameters of the fit are reported in Table 2.2.

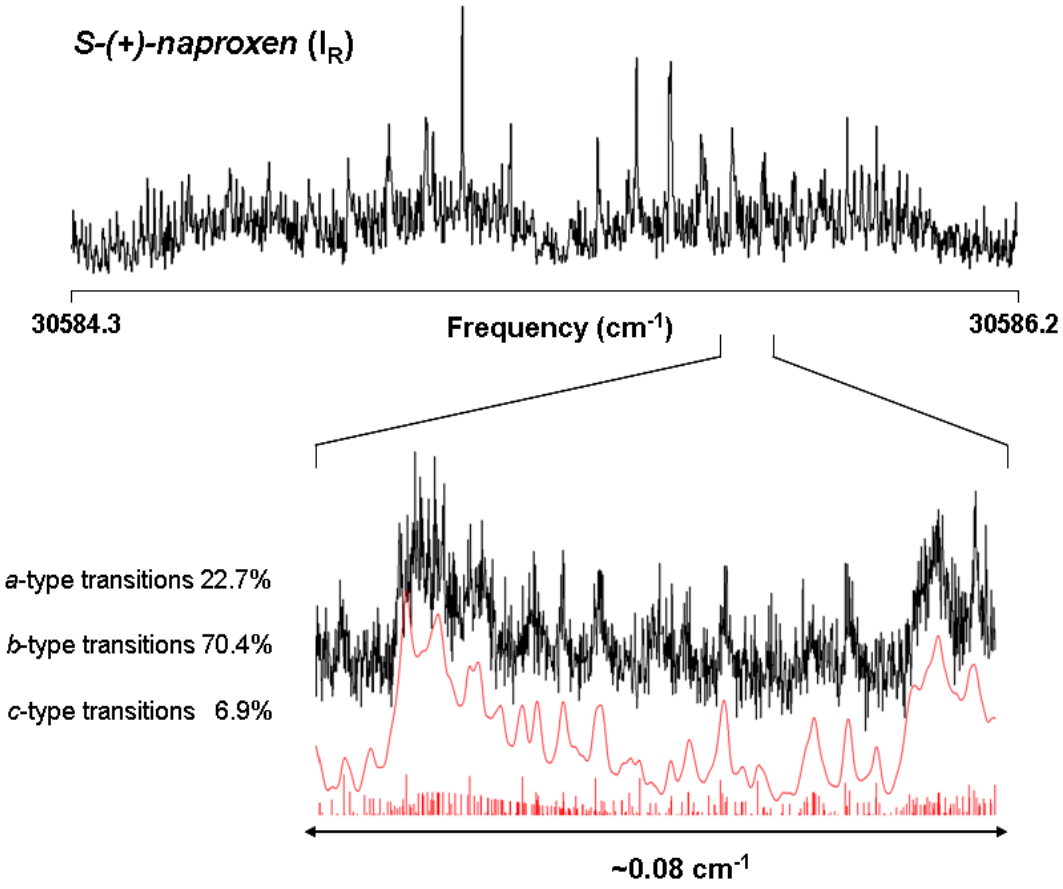


**Figure 2.4. Rotationally resolved fluorescence excitation spectrum of the $0_0^0$ band of the red conformer of *S*-(+)-*naproxen* in the gas phase (top panel). Portions of the *R* branch at full experimental resolution together with a simulated spectrum, with and without a calculated the lineshape function, are also shown (bottom panel).**

Figure 2.5 shows the rotationally resolved electronic spectrum of the blue conformer of *S*-(+)-*naproxen* at 30687.2 $cm^{-1}$. The spectrum spans ~2 $cm^{-1}$ and exhibits *a/b/c* hybrid character of 16.7/76.3/7.0. Its signal/noise ratio is about 4/1. Approximately 130 lines were assigned in the fit of the high resolution spectrum, which resulted in an OMC of 6.20 MHz. The Voigt profile lineshape function required 18 MHz Gaussian and 30 MHz Lorentzian contributions. The rotational temperature of the fit is 6.5 K. The inertial parameters of the fit are reported in Table 2.2.

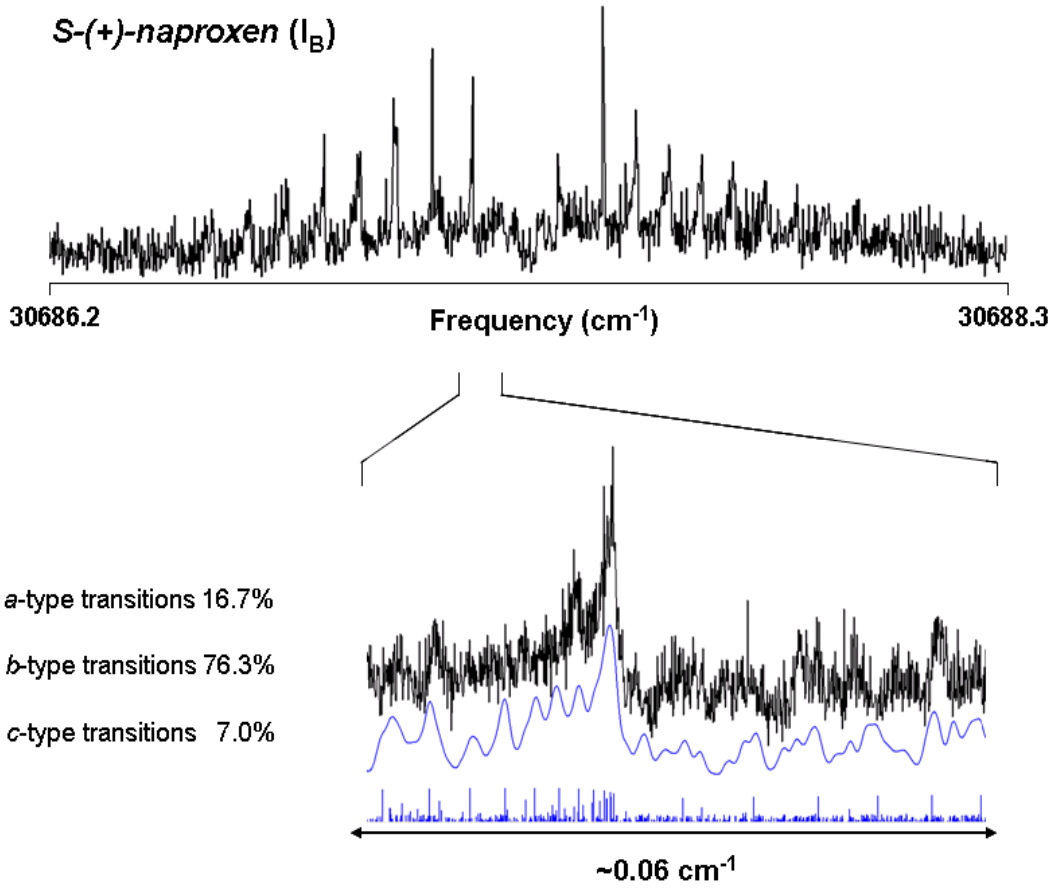


**Figure 2.5. Rotationally resolved fluorescence excitation spectrum of the $0_0^0$ band of the blue conformer of *S*-(+)-*naproxen* in the gas phase (top panel). Portions of the *P* branch at full experimental resolution together with a simulated spectrum, with and without a calculated lineshape function, are also shown (bottom panel).**

*R*-(-)-*naproxen* was also probed in our high resolution apparatus. Two conformers were also identified at the same frequencies where the "red" and "blue" conformers of *S*-(+)-*naproxen* were found. Figure 2.6 shows the rotationally resolved fluorescence excitation spectrum of the blue conformer of *R*-(-)-*naproxen* at 30687.2 $cm^{-1}$. The spectrum spans ~2 $cm^{-1}$ and exhibits *a/b/c* hybrid character of 15.8/72.8/11.4; its signal/noise ratio is about 6/1. Approximately 70 lines were assigned in the fit, yielding an OMC of 3.85 MHz. The lineshape function applied for the simulated spectrum used 18 MHz Gaussian and 30 MHz Lorentzian contributions. The rotational temperature of the fit is 6.0 K. The ground and excited state rotational constants of the fit are reported in Table 2.2.

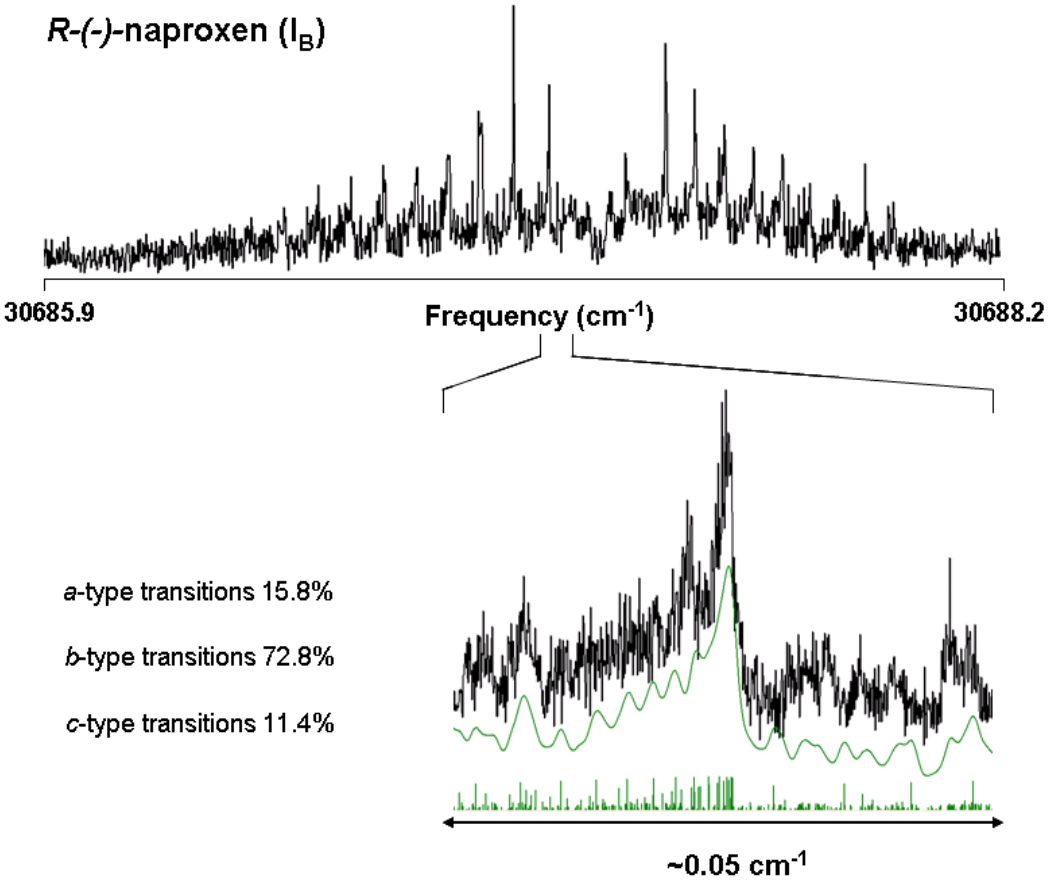


**Figure 2.6. Rotationally resolved fluorescence excitation spectrum of the $0_0^0$ band of the blue conformer of *R*-(-)-*naproxen* in the gas phase (top panel). Portions of the *P* branch at full experimental resolution together with a simulated spectrum, with and without a calculated lineshape function, are also shown (bottom panel).**

**Table 2.2. Inertial parameters of the experimental fits corresponding to the two conformers (red and blue) of the *S*-(+)- and *R*-(-)-*naproxen* in the gas phase.**

| Parameter[a] | *S*-(+)-*naproxen* ($I_R$) | *S*-(+)-*naproxen* ($I_B$) | *R*-(-)-*naproxen* ($I_B$) |
|---|---|---|---|
| **$S_0$** | | | |
| ***A″* (MHz)** | 1240.6 (5) | 1313.2 (6) | 1316.2 (5) |
| ***B″* (MHz)** | 216.3 (3) | 207.1 (3) | 204.9 (2) |
| ***C″* (MHz)** | 202.4 (3) | 193.2 (3) | 195.0 (2) |
| **$\Delta I''$ (amu Å$^2$)** | -247.4 (2) | -209.5 (2) | -258.9 (1) |
| **$S_1$** | | | |
| ***A′* (MHz)** | 1216.7 (5) | 1303.3 (6) | 1304.6 (5) |
| ***B′* (MHz)** | 217.2 (3) | 206.3 (3) | 204.4 (2) |
| ***C′* (MHz)** | 202.6 (3) | 192.1 (3) | 194.3 (2) |
| **$\Delta I'$ (amu Å$^2$)** | -248.8 (2) | -205.9 (2) | -258.6 (1) |
| ***a/b/c*-character** | 23/70/7 (3) | 17/76/7 (3) | 16/73/11 (3) |
| **Band origin (cm$^{-1}$)** | 30585.3 (<1) | 30687.2(<1) | 30687.2 (<1) |
| **OMC (MHz)** | 4.9 | 6.2 | 3.8 |
| **Temp (K)** | 5.0 | 6.5 | 6.0 |
| **Assignment** | *S*-(*II*) | *S*-(*I*) | *R*-(*II*) |

[a] Standard deviations shown in parentheses are relative to the last significant figure.

The corresponding spectrum of the red conformer of *R*-(-)-*naproxen* has not yet been fully analyzed, owing to the poor signal-to-noise ratio. But, a physical mixture of the two *naproxen* enantiomers was tried in our beam machine. Approximately equal amounts of each enantiomer were mixed and probed with our high resolution laser system. Figure 2.7 shows the rotationally resolved fluorescence excitation spectrum that was obtained for the blue transition at 30687.2 cm$^{-1}$. A small portion of the *P* branch at full experimental resolution is shown in the bottom panel of Figure 2.7, where two simulated spectra were required to better fit the experimental trace. Surprisingly, the two spectra share the same excitation frequency, but they exhibit different rotational parameters; one corresponding to the *S*-(+)- and the other to the *R*-(-)-*naproxen* enantiomer, as previously reported for each "blue" transition band in Table 2.2.

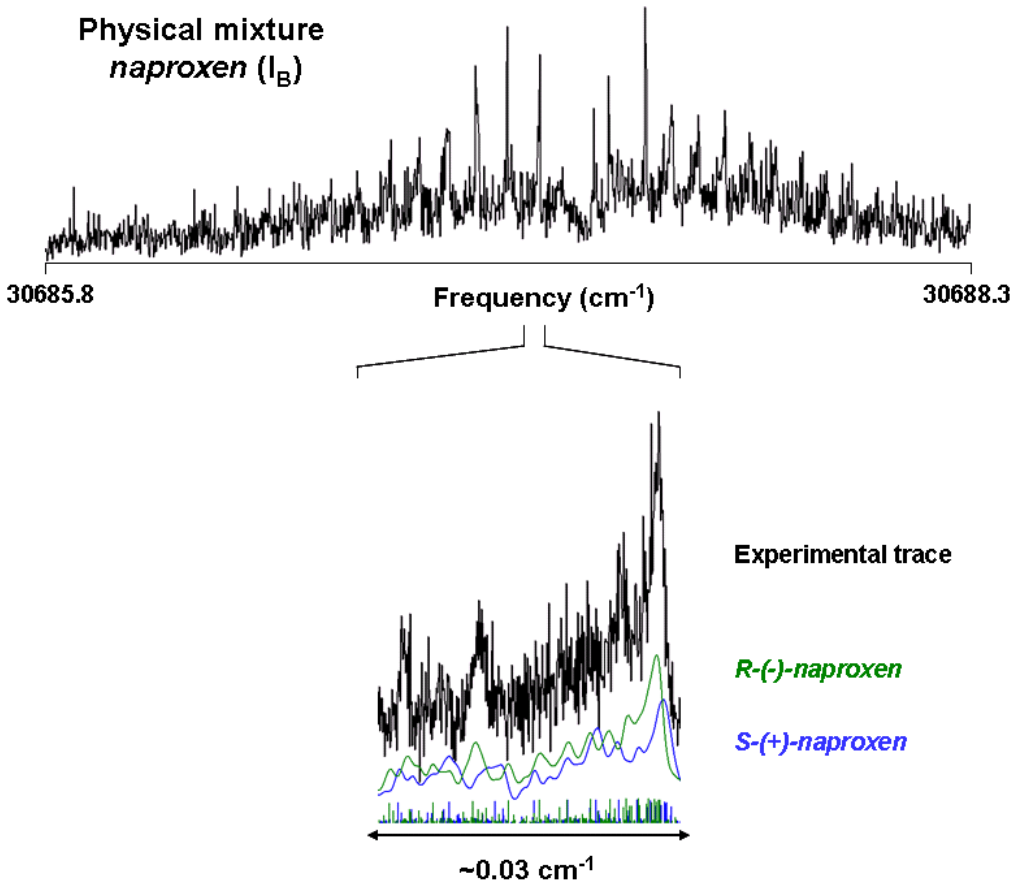


**Figure 2.7. Rotationally resolved fluorescence excitation spectrum of the $0_0^0$ band of the blue conformers of *S*-(+)- and *R*-(-)-*naproxen* in the gas phase (top panel). Portions of their *P* branches at full experimental resolution together with the simulated spectra, with and without calculated lineshape functions, are also shown (bottom panel).**

## 2.5 DISCUSSION

### 2.5.1 *cis*-2-methoxynaphthalene

The conformational preference of the *cis*- with respect to the *trans*- configuration in 2MXN has been previously reported in detail for the ground electronic state,[21] in which the energy difference between the two minima was determined to be about 700 $cm^{-1}$ (approximately the frequency spacing between the two conformers in the LIF spectrum of Figure 2.1). However,

with the help of our experimental results from the fit of the high resolution spectrum in Figure 2.2 and by comparison with the theoretical ground state rotational constants (*c.f.* Table 2.1), we unambiguously assign the strongest transition of the spectrum in Figure 2.1 to the *cis*-conformer of 2MXN. This latter result reveals that the two conformers are presumably equally stable in the $S_1$ state, but the relative Boltzmann populations in the ground $S_0$ state are the important factor that contributes to the large *cis/trans* intensity ratio in the LIF spectrum. In the present work, we have focused on the study of the *cis*-conformer in further detail. The experimental 15.8/84.2 *a/b*-hybrid character of the $0_0^0$ band of *cis*-2MXN yields an angle of the TM vector of the molecule with respect to its *b*-inertial axis of ± 23.4º (± 2). Therefore, the TM orientation follows the one observed for the parent molecule, NAPH and other 2-substituted naphthalenes,[12,14] polarized along the short in-plane inertial axis ($^1L_a$ state). *Ab initio* calculations [MP2/6-31G (d,p)] have been performed to corroborate this experimental result.[29] The optimized geometry calculation yields an angle of rotation of +19.8º for the new *b*-inertial axis with respect to the *b*-axis of naphthalene [see Figure 2.8 (a)]. Thus, we predict that the $S_1 \leftarrow S_0$ TM vector should make an angle of -19.8° with respect to the *b*-axis of 2MXN, if the transition is "pure" $^1L_a$. This last result and the calculated rotational constants in the ground electronic state of the molecule are in fairly good agreement with our experimental results (*cf.* Table 2.1).

The excited state *A′*, *B′*, and *C′* values are smaller than their ground state counterparts, owing to small ring expansions that are typical of $\pi\pi^*$ states. Apparently, 2MXN is essentially planar in both electronic states. It has an inertial defect of -3.48 amu Å$^2$ in its ground state, a value that is consistent with two out-of-plane C–H bonds; this value does not change substantially when the molecule absorbs light, since the torsional barrier for the torsional motion of the methyl group is very high in both electronic states.

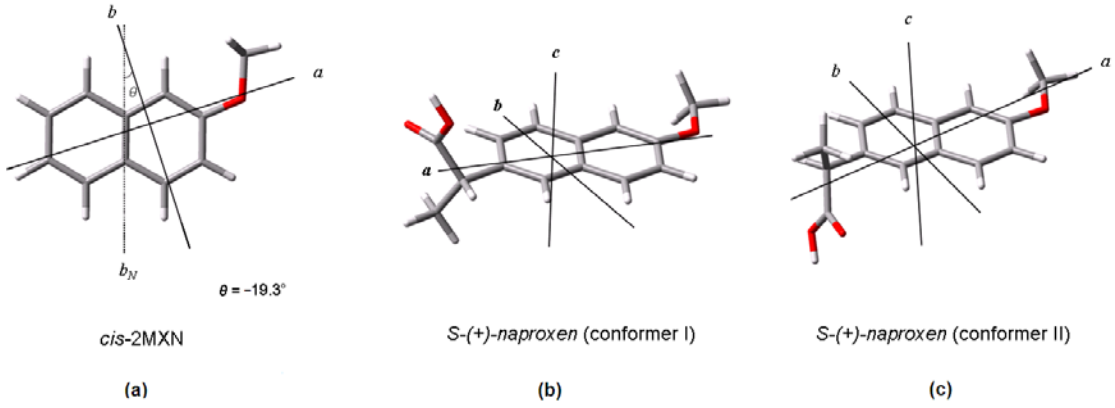


**Figure 2.8. Theoretical inertial axes in *cis*-2MXN, and the conformers I and II of *S*-(+)-*naproxen*. In *cis*-2MXN (a) the angle of rotation of the *ab*-plane with respect to the *b*-axis of naphthalene ($b_N$) is also shown.**

### 2.5.2 *S*-(+)- and *R*-(-)-*naproxen*

The most interesting finding in the present work is the discovery that the experimental high resolution electronic spectra corresponding to the same blue conformer of both *naproxen* enantiomers do not appear to be identical. They were found to exhibit slightly different inertial parameters. If this is true, then the two chemical species should not be referred as enantiomers, since they are not mirror images of each other, and should rather be referred to as diastereomers.

If the two species are diastereomers, then there must be some additional difference in their geometries, apart from the difference in their chiral centers. To probe this question, several *ab initio* calculations[29] have been performed for different *naproxen* structures, similar to the ones previously reported in the literature, where the six more stable conformers have been studied.[9] The theoretical results obtained for the ground electronic state structures that better match with the experimental ground state rotational constants are shown in Figure 2.9. Upon detailed analysis of the results, we have concluded that (1) the calculated rotational constants of *S*-Conformer II better match those of *S*-(+)-*naproxen*, $I_R$; (2) the calculated rotational constants

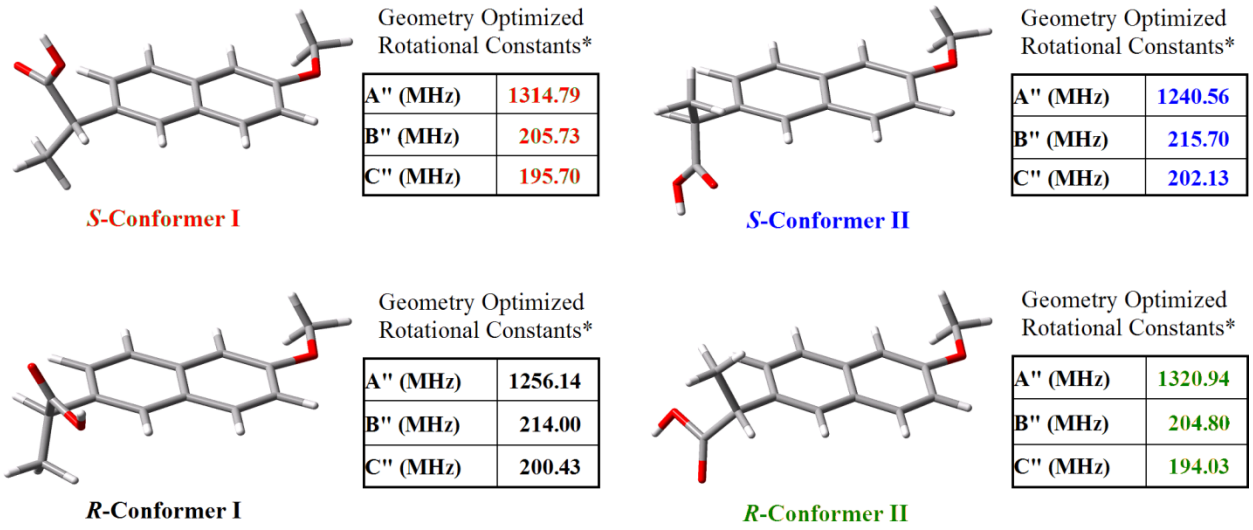


**Figure 2.9. Theoretical structures of *S*-(+)- and *R*-(-)-*naproxen* that best match the ground state rotational constants of the experimental fits. Note the relative rotation of the carboxylic group when going from *S*-I to *R*-II and from *S*-II to *R*-I.**

of *S*-Conformer I better match those of *S*-(+)-*naproxen*, $I_B$; and that (3) the calculated rotational constants of *R*-Conformer II better match those of *R*-(-)-*naproxen*, $I_B$. *S*-Conformer I and *R*-Conformer II are not enantiomers of each other, they differ in the orientation of the carboxylic acid functional group attached to the chiral center.

This is an unexpected result. But it is not unprecedented. Mons and co-workers[3] have recently shown that single peptides having single chiral centers are not mirror images of each other, and have suggested that this is caused by the presence of a second chiral element, an incipient γ turn or helix. In our system, however, there seems to be no stereogenic center other than the asymmetrical carbon in the isopropionic acid functional group of the molecule. It is possible that the asymmetric location of the methoxy functional group might work as an additional stereogenic center for the molecule; thus, generating structural differences among the two *naproxen* "enantiomers" in the jet.

Analogous conformational studies have been performed on 1-(1-naphthyl)ethylamine (NEA) by Plusquellic and co-workers.[30] In this work, it was shown that the rotationally resolved electronic spectrum of the origin band of this molecule required only one single simulated spectrum to fit the experimental trace in an experimental mixture of (±)-NEA. They required the use of circular dichroism techniques in order to enantio-differentiate both enantiomers in the sample. Therefore, in this molecule, both enantiomers are in fact mirror images and do not exhibit differences in structure that can be distinguished by means of high resolution electronic spectroscopy in the gas phase.

In our *naproxen* experiments, the signal/noise ratio in the high resolution electronic spectra is unfortunately very low, and the differences between theoretical and experimental rotational constants of the two enantiomers are relatively small. Attempts to fit the *R*-(-)-*naproxen* spectrum of the blue conformer using the inertial parameters of the *S*-(+)-enantiomer resulted in an overall shape of the simulation significantly worse than the one shown in Figure 2.6. But better spectra with higher signal/noise ratio will be required before it can be unambiguously concluded that the *S*- and *R*-molecules are, in fact, not enantiomers of each other. Our new wave train frequency doubler should help us accomplish this task. We also plan CHIRPED-pulse microwave experiments[31] on this system.

Additional experiments and calculations are also planned on other naphthalene derivatives to further test our conjecture that the orientation of the methoxy group provides an incipient chiral element in the isolated molecule.

## 2.6 SUMMARY

Rotationally resolved $S_1 \leftarrow S_0$ fluorescence excitation spectra of the $0_0^0$ bands of 2MXN and the two most stable conformers of *S*-(+)- and *R*-(-)-*naproxen* enantiomers have been recorded in the collision-free environment of a molecular beam. *cis*-2MXN exhibits an *a/b*-hybrid band character due to the rotation of the axes system upon the addition of the $–OCH_3$ group to the naphthalene frame. On the other hand, *naproxen* is a chiral molecule that preserves the *a/b/c*-hybrid band character of the spectra relative to what is observed in *cis*-2MXN. *S*-(+)- and *R*-(-)-*naproxen* enantiomers apparently exhibit different, initially distinguishable structures in the gas phase. It is suggested that a torsional motion of the attached carboxylic group in one of the chiral entities is responsible for the differences in the inertial parameters observed.

## 2.7 ACKNOWLEDGMENTS

L. Alvarez thanks M. G. León for motivating him to perform this pharmacologically relevant project in the laser laboratory. The authors also thank Brooks H. Pate (U. Virginia) and Peter Wipf (U. Pittsburgh) for helpful comments and discussions on chiral issues. This project has been supported by NSF (CHE-0615755).

## 2.8 REFERENCES

1. E. L. Eliel and S. H. Wilen, *Stereochemistry of Organic Compounds*, John Wiley & Sons, Inc. New York, 1994.

2. L. Stryer, *Biochemistry*, 3rd ed., Freeman, New York, 1988.

3. V. Brenner, F. Piuzzi, I. Dimicoli, B. Tardivel, and M. Mons*, J. Phys. Chem*. **111A**, 7347 (2007).

4. A. R. Al-Rabaa, K. Le Barbu, F. Lahmani, and A. Zehnacker-Rentien, *J. Photochem. Photobiol.* **105A**, 277 (1997).

5. K. Le Barbu, V. Brenner, Ph. Millie, F. Lahmani, and A. Zehnacker-Rentien, *J. Phys. Chem.* **102A**, 128 (1998).

6. M. Mons, F. Puzzi, I. Dimicoli, A. Zehnacker, and F. Lahmani, *Phys. Chem. Chem. Phys*. **2**, 5065 (2000).

7. K. Le Barbu, F. Lahmani, and A. Zehnacker-Rentien. *J. Phys. Chem*. **106A**, 6271 (2002).

8. K. Le Barbu-Debus, N. Seurre, F. Lahmani, and A. Zehnacker-Rentien, *Phys. Chem. Chem. Phys*. **4**, 4866 (2002).

9. F. Lahmani, K. Le Barbu-Debus, N. Seurre, and A. Zehnacker-Rentien, *Chem. Phys. Lett.* **375**, 636 (2003).

10. N. Seurre, K. Le Barbu-Debus, F. Lahmani, A. Zehnacker-Rentien, and J. Sepiol, *J. Mol. Struc*. **692**, 127 (2004).

11. N. Seurre, K. Le Barbu-Debus, F. Lahmani, A. Zehnacker, N. Borho, and M. A. Suhm, *Phys. Chem. Chem. Phys*. **8**, 1007 (2006).

12. W. A. Majewski and W. L. Meerts, *J. Mol. Spectrosc*. **104**, 271 (1984).

13. W. A. Majewski, D. F. Plusquellic, and D. W. Pratt, *J. Chem. Phys.* **90**, 1362 (1989).

14. J. R. Johnson, K. D. Jordan, D. F. Plusquellic, and D. W. Pratt, *J. Chem. Phys*. **93**, 2258 (1990).

15. G. Berden, W. L. Meerts, and W. Kreiner, *Chem. Phys*. **174**, 247 (1993).

16. S. Jagannathan and D. W. Pratt, *J. Chem. Phys.* **100**, 1874 (1994).

17. S. J. Humphrey and D. W. Pratt, *Chem. Phys. Lett.* **257**, 169 (1996).

18. L. Alvarez-Valtierra, D. F. Plusquellic, J. T. Yi, and D. W. Pratt, in preparation.

19. G. Berden, W. L. Meerts, D. F. Plusquellic, I. Fujita, and D. W. Pratt, *J. Chem. Phys*. **104**, 3935 (1996).

20. T. Troxler, B. A. Pryor, and M. R. Topp, *Chem. Phys. Lett.* **274**, 71 (1997).

21. T. Troxler, *J. Phys. Chem.* **102A**, 4775 (1998).

22. D. Bougie and R. Aster, *Blood* **97**, 3846 (2001).

23. Roche Pharmaceuticals, Medication Guide for EC-NAPROSYN® (*naproxen*), 2006, http://www.rocheusa.com/products/naprosyn/pi.pdf

24. PDR Drug Information for *Naproxen*, Drugs.com ™ (Drug information online), 2006, http://www.drugs.com/pdr/NAPROXEN.html

25. P. Schreier, A. Bernreuther, and M. Huffer, *Analysis of Chiral Organic Molecules, Methodology and Applications*, Walter de Gruyter, Berlin, 1995.

26. W. A. Majewski, J. F. Pfanstiel, D. F. Plusquellic, and D. W. Pratt, in *Laser Techniques in Chemistry*. T. R. Rizzo, and A. B. Myers, Eds., J. Wiley & Sons, New York, 1995.

27. S. M. Beck, D. E. Powers, J. B. Hopkins, and R. E. Smalley, *J. Chem. Phys.* **73**, 2019 (1980).

28. D. F. Plusquellic, *Jb95 Spectral fitting program*, NIST, http://physics.nist.gov/jb95.

29. M. J. Frisch, *et al*. *Gaussian 03*, Revision C.02, Gaussian, Inc., Pittsburgh, PA, 2003.

30. D. F. Plusquellic, R. J. Lavrich, T. Petralli-Mallow, S. Davis, T. M. Korter, and R. D. Suenram, *Chem. Phys.* **283**, 355 (2002).

31. For a description of the instrumental setup, see, G. G. Brown, B. C. Dian, K. O. Douglass, S. M. Geyer, and B. H. Pate, *J. Mol. Spectrosc.* **238**, 200 (2006).

# 3.0 ON THE ELECTRONIC EXCITED STATE DYNAMICS OF VIBRONIC TRANSITIONS. HIGH RESOLUTION ELECTRONIC SPECTRA OF ACENAPHTHENE AND ITS ARGON VAN DER WAALS COMPLEX IN THE GAS PHASE

## 3.1 ABSTRACT

Rotationally resolved fluorescence excitation spectroscopy has been used to study the dynamics, electronic distribution, and the relative orientation of the transition moment vector in several vibronic transitions of acenaphthene (ACN) and in its Ar van der Waals (vdW) complex. The $0_0^0$ band of the $S_1 \leftarrow S_0$ transition of ACN exhibits a transition moment orientation parallel to its *a*-inertial axis. However, some of the vibronic bands exhibit a transition moment orientation parallel to the *b*-inertial axis, suggesting a Herzberg-Teller coupling with the $S_2$ state. Additionally, some other vibronic bands exhibit anomalous intensity patterns in several of their rotational transitions. A pseudo-Coriolis coupling mechanism involving two near degenerate vibrations has been proposed to explain this behavior. The high resolution electronic spectrum of the ACN-Ar vdW complex has also been obtained and fully analyzed. The results indicate that the weakly attached argon atom is located on top of the plane of the bare molecule at ~3.48 Å away from its center of mass in the $S_0$ electronic state.

## 3.2 INTRODUCTION

Naphthalene (NAPH) has been extensively investigated using different spectroscopic techniques to determine the symmetry properties of its lowest excited states. Fifty years ago, it was discovered that the lowest $\pi\pi^*$ transition of NAPH is weak and polarized along its *a*-inertial axis, pumping to a $^1B_{3u}$ ($^1L_b$) excited electronic state; meanwhile, the second $\pi\pi^*$ transition is strong and *b*-axis polarized, pumping to a $^1B_{2u}$ ($^1L_a$) excited electronic state.[1,2] Later studies using high resolution spectroscopy have confirmed such findings.[3] It was also found that 1-substituted

naphthalenes exhibit properties[4-6] similar to the parent molecule but that 2-substituted naphthalenes are quite different. These molecules exhibit *b*-axis polarized lowest $S_1 \leftarrow S_0$ transitions owing to the different nodal properties of their frontier molecular orbitals (MO's).[7] Conversely, 1-aminonaphthalene is an exception to this trend; its $S_1 \leftarrow S_0$ transition also is *b*-axis polarized,[8] suggesting a reversal of the $^1L_b$ and $^1L_a$ states owing to the conjugative properties of the amino group.

In acenaphthene (ACN), the $D_{2h}$ point group symmetry of NAPH has been reduced to $C_{2v}$ (see Scheme 3.1). The extra five-membered ring in ACN causes a breakdown of the symmetry properties of NAPH, and the lowest $\pi\pi^*$ transition is no longer a nearly equal mixture of two near degenerate excitations ($\pi_4\pi_6^* - \pi_5\pi_7^*$).[9] What is not known, therefore, is the effect that this breakdown will have on the properties of its low-lying excited states.

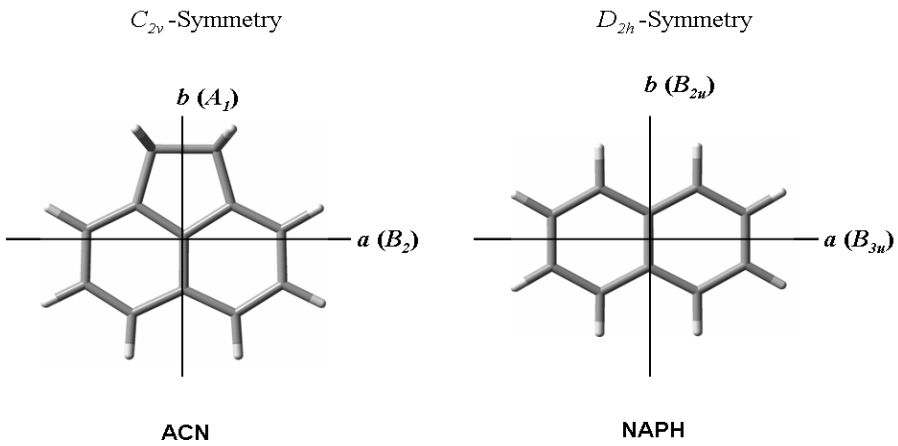


**Scheme 3.1. Sketch of the in-plane inertial axes of ACN ($C_{2v}$) and NAPH ($D_{2h}$).**

In this work, we report the rotationally resolved $S_1 \leftarrow S_0$ fluorescence excitation spectra of several vibronic bands of ACN (including the $0_0^0$ transition), as well as the corresponding van der Waals (vdW) complex of this molecule with an argon atom. Evidence for significant electronic state mixing was found in higher energy transitions of ACN. Additionally, at even

higher energy, an anomalous intensity pattern is identified for selected rotational lines, providing a new route for electronic decay *via* what appears to be a pseudo Coriolis-coupling mechanism.

## 3.3 THEORY

### 3.3.1 Herzberg-Teller (HT) mechanism

Dealing with large polyatomic molecules like ACN or NAPH, many vibronic transitions are allowed by symmetry. According to HT vibronic coupling theory,[10] the transition moment $\boldsymbol{R_{evr}}$ for an electric dipole transition between two vibronic states is given by

$$R_{evr} = \int \psi'_{evr}{}^{*} \mu \psi''_{evr} d\tau \,, \tag{3.1}$$

where $\mu$ is the electric dipole moment operator and the integral is over all the electronic and vibrational coordinates. The requirement for $\boldsymbol{R_{evr}}$ to be nonzero is that the product of the symmetry species inside the integral at least contains the totally symmetric representation in the molecular point group, so the corresponding transition is symmetry allowed. For pure electronic transitions ($0_0^0$ bands), the electronic transition moment must be independent of the nuclear motion and hence, the vibrational overlap integral. Therefore, all vibronic transitions associated with allowed electronic transitions are allowed by symmetry, but their intensities are governed by the Franck-Condon (FC) principle.[12] In addition, the intensities of the vibronic progressions are proportional to the square of $\boldsymbol{R_{evr}}$ in Equation (3.1).

A HT (*intensity stealing*) mechanism may also contribute to the intensities of vibronic transitions at higher frequencies. A specific transition which is forbidden by symmetry may show

vibronically induced bands involving non-totally symmetric vibrations. In this case, the electronic transition moment $\boldsymbol{R_e}$ is no longer independent of the vibrational motion, revealing a breakdown of the Born-Oppenheimer approximation. This effect is taken into account by expanding $\boldsymbol{R_e}$ as a Taylor series

$$R_{evr} = R_r \cdot (R_e)_{eq} \cdot \int \psi_v' \psi_v'' \, d\tau_v + \sum_s \left( \frac{\partial R_e}{\partial Q_s} \right)_{eq} \int \psi_v' Q_s \psi_v'' \, d\tau_v + \sum_a \left( \frac{\partial R_e}{\partial Q_a} \right)_{eq} \int \psi_v' Q_a \psi_v'' \, d\tau_v + \cdots \qquad \textbf{(3.2)}$$

here, the subscript '*eq'* refers to the equilibrium configuration of the molecule, and the involved vibrations have been conveniently classified into '*s*' totally symmetric and '*a*' non-totally symmetric vibrations. For an electronically forbidden transition, the first two terms in the right hand side of Equation (3.2) are zero and the third term is nonzero. The transition is then said to be electronically forbidden but *vibronically allowed* or *vibrationally induced*. In this mechanism, the upper electronic state interacts with a higher electronic state through a non-totally symmetric vibration, *stealing* intensity from the transition between two excited electronic states.

### 3.3.2 Coriolis coupling mechanism

The above discussion assumes that the transition moment operator ($\mu$) includes only pure electronic, vibrational and rotational Hamiltonians; *i.e.*, no interaction terms exist between the rotational and vibrational motions of the molecule. Therefore, when Coriolis coupling is considered, the rotational-vibrational Hamiltonian ($H_{vr}$) must incorporate a coupling term in the Hamiltonian, *i.e.*, $H_{vr} = H_v + H_r + H'$. Here, $H_v$ is a sum of non-interacting harmonic oscillators, $H_r$ is the rigid-rotor Hamiltonian, and $H' \approx \sum_\alpha (-p_\alpha J_\alpha)/I_\alpha$ is a coupling term, where $J_\alpha$ ($\alpha = a, b, c$) is a component of the total angular momentum, $I_\alpha$ is the moment of inertia, and $p_\alpha$ is the component of the vibrational angular momentum about the molecular $\alpha$ axis[13]

$$p_\alpha = \sum_m \sum_n \zeta_{mn}^\alpha \left[ Q_m P_n - Q_n P_m \right]. \tag{3.3}$$

In Equation (3.3), $Q_m$ denotes the $m$th normal coordinate, $P_m = -i\hbar(\partial/\partial Q_m)$ is the momentum conjugate to that coordinate, and $\zeta_{mn}^\alpha$ are the *Coriolis zeta constants*.[11] The sums in Equation (3.3) are taken over all pairs of normal coordinates. As a consequence of Jahn's rule,[14] the only nonvanishing $\zeta_{mn}^\alpha$ will be those for which the product of the symmetry species of $Q_m$ and $Q_n$ contains the rotation $R_\alpha$. Since the terms $Q_m$ and $Q_n$ obey the selection rule that $\upsilon' = \upsilon \pm 1$, a $p_\alpha$ matrix element may be written as

$$\left\langle \upsilon_m + 1, \upsilon_n \left| p_\alpha \right| \upsilon_m, \upsilon_n + 1 \right\rangle = -\frac{i\hbar}{2} \zeta_{mn}^\alpha \left[ (\upsilon_m + 1)(\upsilon_n + 1) \right]^{1/2} \cdot \left[ \left( \frac{\nu_n}{\nu_m} \right)^{1/2} + \left( \frac{\nu_m}{\nu_n} \right)^{1/2} \right]; \tag{3.4}$$

where the vibrational quantum numbers ($\upsilon_m$ and $\upsilon_n$) change in opposite directions, the most common case, and $\nu_m$ and $\nu_n$ are the vibrational frequencies of the modes $m$ and $n$, respectively.

## 3.4 EXPERIMENTAL

ACN (99% pure) was purchased from Aldrich and used without further purification. In the vibrationally resolved experiments, the sample was seeded into 10 psi of argon gas and expanded into a vacuum chamber ($10^{-5}$ torr) through a 1 mm diameter orifice pulsed valve (General Valve Series 9) operating at 10 Hz. Two centimeters downstream of the valve, the sample was excited with the second harmonic of a Quanta Ray $Nd^{3+}$:YAG (Model DCR-1A) pumped dye laser (Model PDL-1). The dye (DCM) laser output was frequency doubled with an external potassium dihydrogen phosphate crystal providing a spectral resolution of ~0.6 $cm^{-1}$ in the ultraviolet. From the point of intersection between the nozzle and the laser, the molecules were excited and the

fluorescence was collected with a photomultiplier tube (PMT). Finally, the collected data were processed by a boxcar integrator (Stanford Research Systems) and recorded with Quick Data Acquisition software version 1.0.5.

Rotationally resolved experiments were performed using a molecular beam laser spectrometer, described in detail elsewhere.[15] Briefly, the molecular beam was formed by expansion of the vaporized sample and seeded in argon carrier gas (-18 psi) through a heated (~313 K) 240 $\mu$m quartz nozzle into a differentially pumped vacuum system. The expansion was skimmed twice and crossed 110 cm downstream by a continuous wave (CW) $Ar^+$ pumped ring dye laser. [For the ACN-Ar complex, the expansion was skimmed only once and crossed 15 cm downstream by the laser beam.] The CW laser was operated with DCM special dye and was intracavity frequency doubled in either a 630 nm $LiIO_3$ or a 620 nm BBO crystal, yielding approximately 350 $\mu$W of UV radiation with a resolution of ~1 MHz. The fluorescence excitation spectrum was detected, using spatially selective optics, by a PMT and photon counting system. This signal, together with the iodine absorption spectrum and the relative frequency markers, was simultaneously collected and processed by the JBA95 data acquisition system.[15] Absolute frequency calibration of the spectra was performed by comparison with the $I_2$ absorption spectrum. Relative frequency markers were obtained from a stabilized etalon having a free spectral range of 299.7520 ± 0.0005 MHz.

## 3.5 RESULTS

Figure 3.1 shows the vibrationally resolved fluorescence excitation spectrum of jet-cooled ACN in the gas phase. In agreement with previous results,[16,17] we observe that the electronic origin

( $0_0^0$ band) of ACN is red shifted by ~542 $cm^{-1}$ from that of NAPH.[2,3] In addition, frequency labels are used to identify the stronger vibronic bands in the spectrum. The +431 $cm^{-1}$ band is close in frequency to the $\bar{8}_0^1$ vibration, the strongest band in the spectrum of NAPH. Interestingly, the remaining vibronic bands in the spectrum of Figure 3.1 were not detected in the low resolution spectrum of the parent molecule, NAPH.[2]

Extensive studies have been performed on every single band in Figure 3.1 at high resolution, to investigate the origin of such transitions and provide further information about other phenomena that might occur upon excitation with light. Figure 3.2 shows the rotationally resolved $S_1 \leftarrow S_0$ fluorescence excitation spectrum of the $0_0^0$ band of ACN at 31477.1 $cm^{-1}$. The spectrum spans approximately 3.5 $cm^{-1}$ and exhibits pure *a*-type character ($^1L_b$ excited state), *i.e.*, the transition moment vector lies parallel to the *a*-inertial axis of the molecule. To fit this spectrum, we first generated ~3000 *a*-type rovibronic transitions based on *ab initio*[18] estimates of rotational constants and rigid rotor Hamiltonians for both electronic states. Then, we made

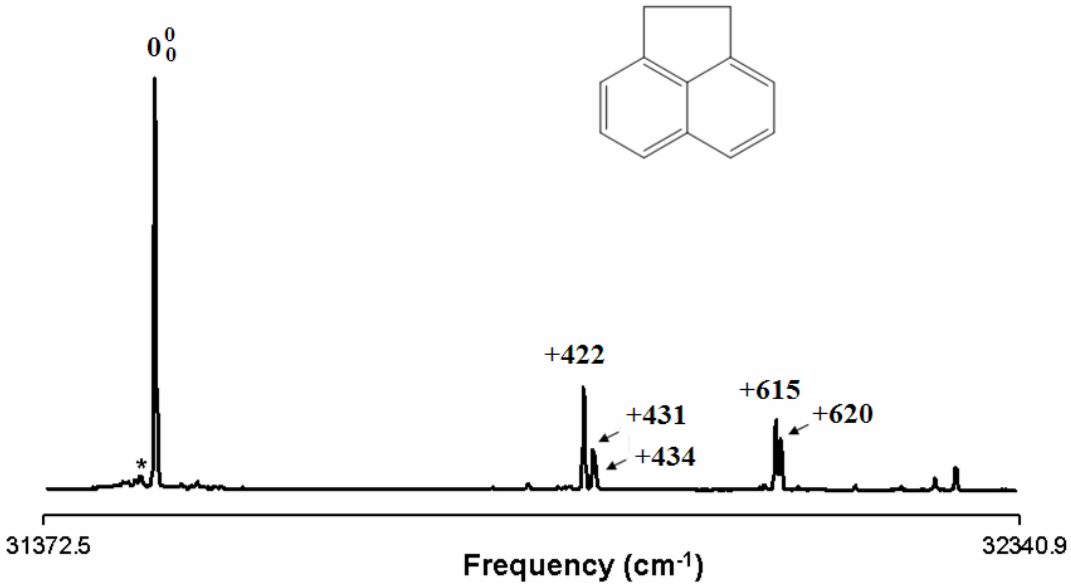


**Figure 3.1. Vibrationally resolved fluorescence excitation spectrum of acenaphthene in a supersonic jet. The small transition marked with the asterisk corresponds to the argon complex.**

quantum number assignments of single transitions in the simulated spectrum to the corresponding transitions in the experimental spectrum, using the Windows-based program JB95.[19] Finally, we used a least-squares fitting procedure to optimize the rotational constants, based on comparisons of the observed and calculated line positions. The final fit utilized ~300 assigned lines and resulted in a standard deviation (OMC) of ~1.9 MHz. The quality of the fit is shown in the bottom panel of Figure 3.2. Here, trace 1 shows a portion of the *Q* branch of the

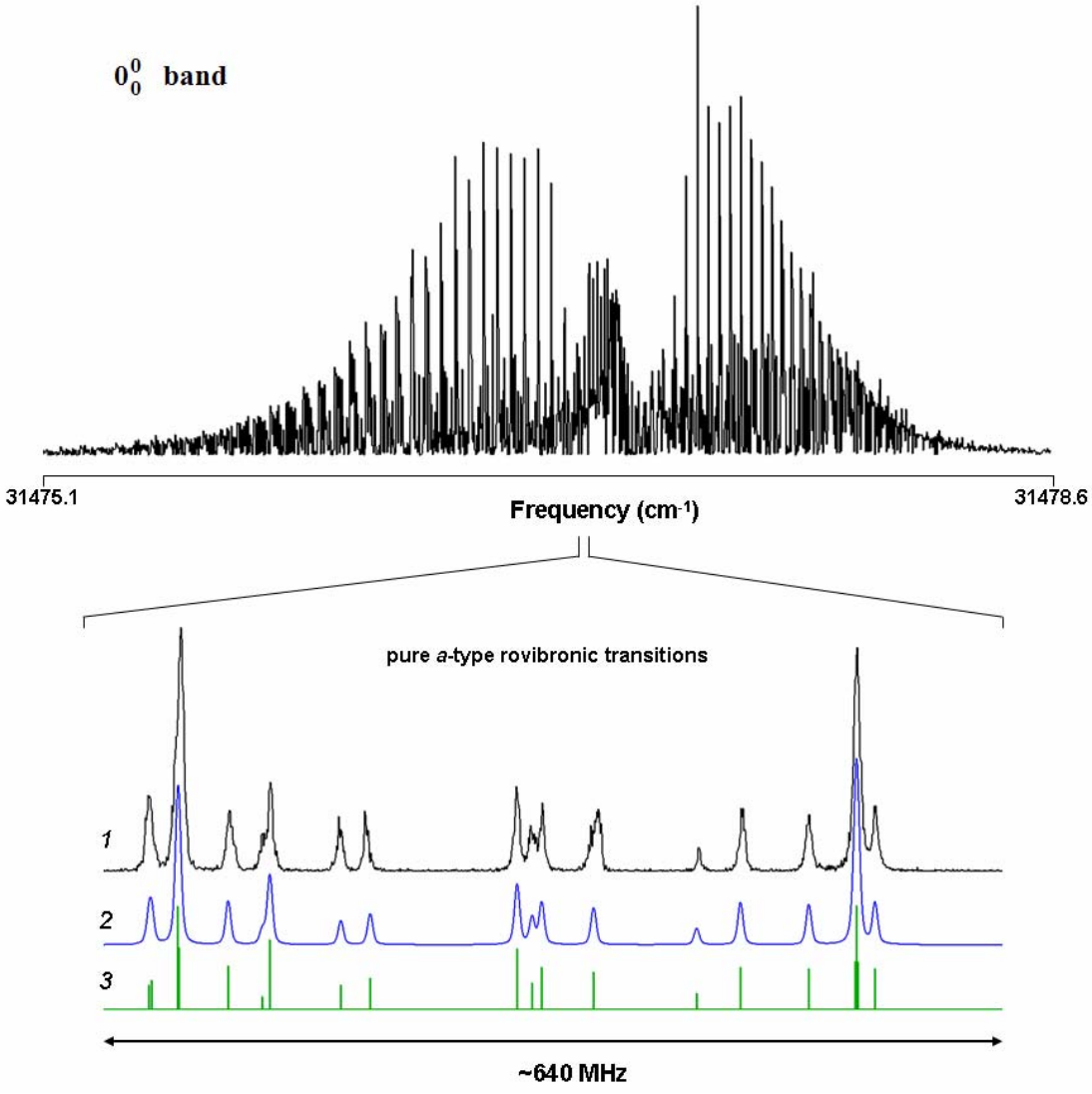


**Figure 3.2. Rotationally resolved fluorescence excitation spectrum of the $S_1 \leftarrow S_0$ electronic origin band of ACN. Portions of the fully resolved experimental spectrum (1) and the corresponding simulated spectrum, with (2) and without (3) a convoluted lineshape function, are also shown in the bottom panel.**

fully resolved experimental spectrum, and traces 2 and 3 show the simulated spectra. Trace 3 is in a "stick-type" spectrum and trace 2 is the simulation with a Voigt lineshape function applied (~3 MHz Gaussian and ~2 MHz Lorentzian contributions) with a linewidth of 2.7 MHz at FWHM. The rotational temperature of the fit is 3.5 K. The inertial parameters of this band are summarized in Table 3.1.

Figures 3.3 and 3.4 show the high resolution spectra of three vibronic bands of ACN at 422, 431, and 434 $cm^{-1}$ above the origin band. Surprisingly, all three of these bands exhibit *b*-type polarized spectra. Therefore, their polarization is perpendicular to that of the $0_0^0$ band

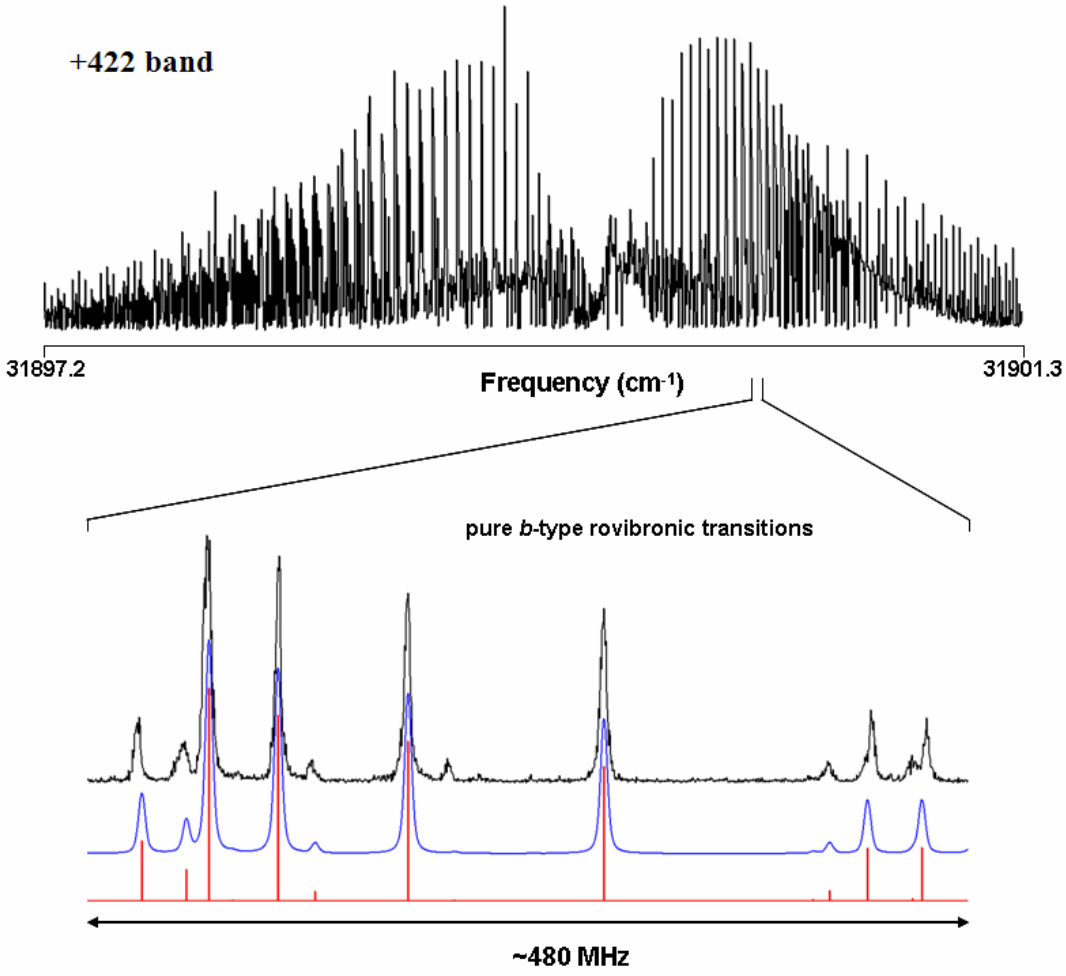


**Figure 3.3. Rotationally resolved fluorescence excitation spectrum of the +422 band of ACN. Portions of the fully resolved experimental spectrum and the corresponding simulated spectrum are also shown in the bottom panel.**

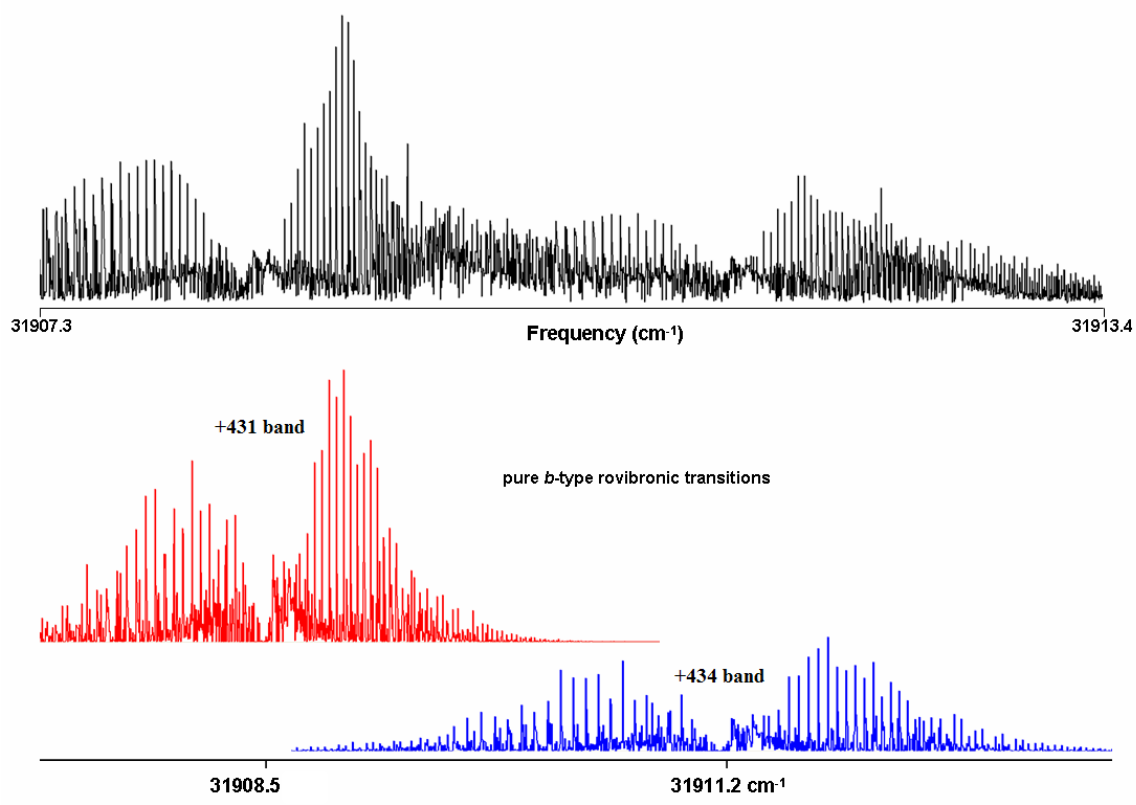


**Figure 3.4. Rotationally resolved fluorescence excitation spectra of the +431 and +434 bands of ACN. The two simulated spectra are shown in the bottom panel.**

(*i.e.*, parallel to the $C_2$ symmetry axis of the molecule). Analyses of these spectra proceeded in a manner similar to the previously described origin band. In the case of the +422 band (see Figure 3.3), ~5300 *b*-type rovibronic transitions were simulated. Of these, ~200 lines were assigned and fit using rigid rotor Hamiltonians for both electronic states. In the bottom panel of Figure 3.3, the experimental trace and the corresponding simulations, with and without a lineshape function are also shown. The OMC of the fit is ~1.49 MHz, the lineshape Voigt profile has ~3 MHz Gaussian and ~2 MHz Lorentzian contributions. The rotational temperature of the fit is ~8 K. For the +431 and +434 bands (see Figure 3.4), ~220 lines out of ~7500 were assigned, resulting in standard deviations of ~1.5 MHz; the rotational temperatures of the fits are ~9.5 and ~17 K, respectively. Voigt profile components similar to those used in the +422 band were used in these fits. The

bottom panel of Figure 3.4 shows two simulated spectra for each experimental transition along with their corresponding frequency origin labeled in the horizontal axis. The inertial parameters of these three bands are reported in Table 3.1.

Two higher vibronic transitions (+615 and +620 bands in Figure 3.1) of ACN were also fully analyzed at rotational resolution. Both of these transitions exhibit parallel polarizations. Therefore, their band contour is analogous to the spectrum shown in Figure 3.2 for the $0_0^0$ band. Interestingly, both bands reveal evident perturbations in their rotational structure. Their experimental spectra exhibit rotational line intensities which cannot be simulated using rigid rotor Hamiltonians at any rotational temperature (*cf*. Figure 3.5). Moreover, attempts to fit some transitions exhibiting anomalous frequency shifts (especially lines where $K_c' = 10$), with a Watson distortion Hamiltonian[20] for the $S_1$ state were also unsuccessful. Nonetheless, ignoring a very few shifted transitions, fits have been performed for these bands by assigning ~1000 lines of the ~15000 simulated rovibronic transitions. The standard deviations of the fits are 1.40 and 1.25

**Table 3.1. Inertial parameters of the origin band and some higher $S_1$ vibronic bands of acenaphthene.**

| **Parameter**[ab] | $\mathbf{0_0^0}$ | **+422.4** | **+431.4** | **+434.2** | **+615.4** | **+620.3** |
|---|---|---|---|---|---|---|
| **$S_0$** | | | | | | |
| ***A″* (MHz)** | 1410.3 (1) | 1410.3 (1) | 1410.3 (1) | 1410.7 (1) | 1410.2 (1) | 1410.2 (1) |
| ***B″* (MHz)** | 1193.9 (1) | 1193.9 (1) | 1193.9 (1) | 1194.2 (1) | 1193.8 (1) | 1193.8 (1) |
| ***C″* (MHz)** | 652.0 (1) | 652.0 (1) | 652.0 (1) | 652.3 (1) | 652.1 (1) | 652.0 (1) |
| **$S_1$** | | | | | | |
| ***A′* (MHz)** | 1394.1 (1) | 1394.6 (1) | 1394.3 (1) | 1394.8 (1) | 1393.4 (1) | 1393.3 (1) |
| ***B′* (MHz)** | 1175.8 (1) | 1376.0 (1) | 1176.0 (1) | 1176.4 (1) | 1176.2 (1) | 1176.2 (1) |
| ***C′* (MHz)** | 643.2 (1) | 643.1 (1) | 643.7(1) | 644.0 (1) | 643.4 (1) | 643.3 (1) |
| **Band type** | *a* | *b* | *b* | *b* | *a* | *a* |
| **Band origin ($cm^{-1}$)** | 31477.11 | 31899.53 | 31908.52 | 31911.26 | 32092.56 | 32097.38 |
| **OMC (MHz)** | 1.94 | 1.49 | 1.52 | 1.40 | 1.40 | 1.25 |
| **Temp (K)** | 3.5 | 8.0 | 9.5 | 17.0 | 11.0 | 11.0 |

[a] Standard deviations shown in parentheses are relative to the last significant figure.
[b] MP2/6-31G** values: $A'' = 1410.1$, $B'' = 1194.4$, and $C'' = 651.8$ MHz.

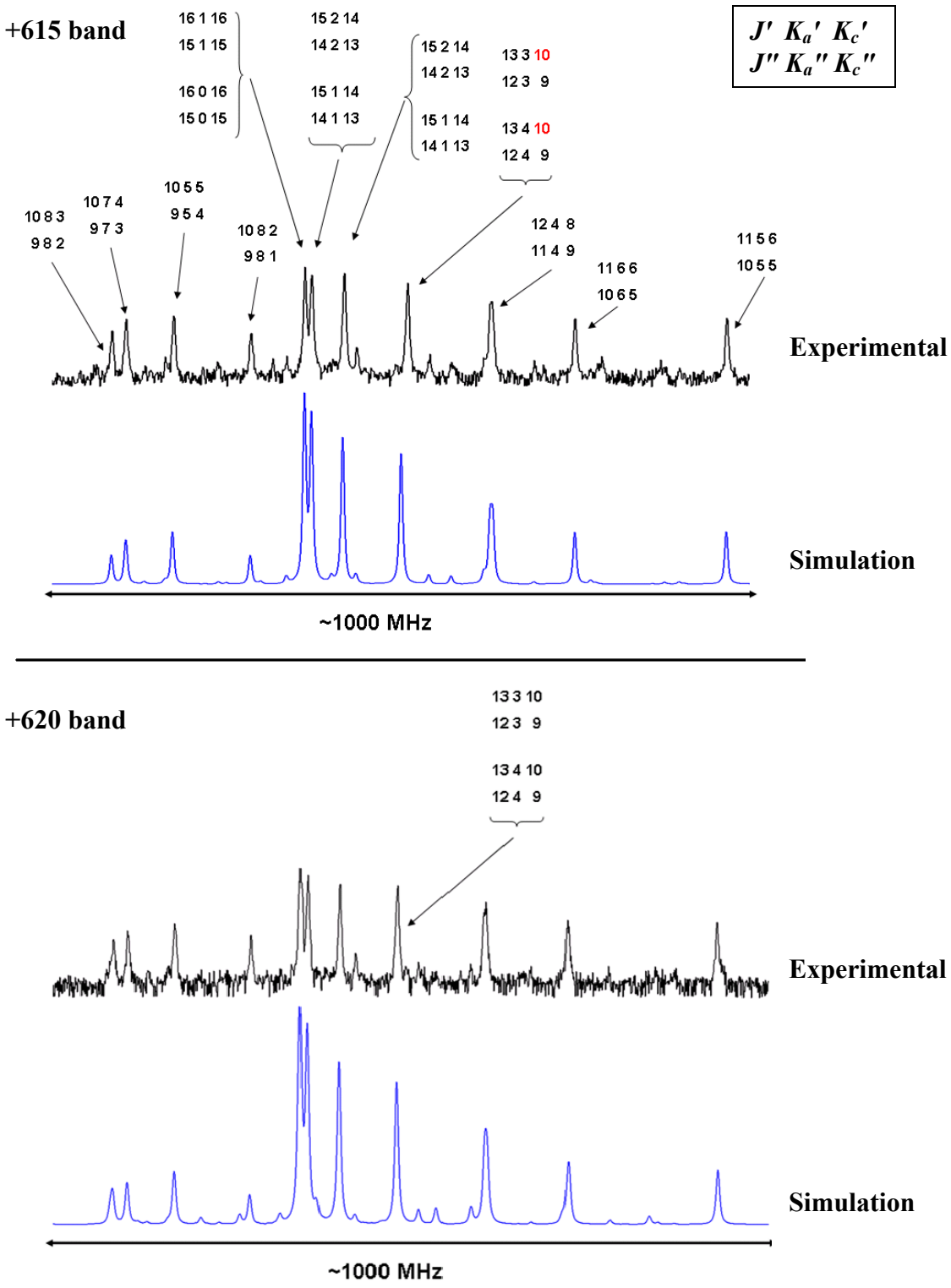


**Figure 3.5. Similar portions of the *R* branch in the high resolution electronic spectra of the +615 and +620 bands of ACN. The simulated spectra show that the experimental traces exhibit anomalous intensity patterns on several rotational transitions. Some of the lines have been identified using their angular momentum quantum numbers, as indicated in the box.**

MHz for the +615 and +620 bands, respectively. The Voigt lineshape profiles required 5 MHz Gaussian and 3 MHz Lorentzian contributions. The rotational temperature that best fit the observed line intensities in both spectra was 8 ± 2 K. The inertial parameters of these bands are included in Table 3.1.

Finally, the $S_1 \leftarrow S_0$ origin band of the ACN-Ar vdW complex (the small transition marked with an asterisk in Figure 3.1) was studied and found to be red shifted by 13.6 $cm^{-1}$ from the $0_0^0$ band of the bare molecule. Figure 3.6 shows its rotationally resolved fluorescence excitation spectrum. It spans ~2.1 $cm^{-1}$ and exhibits *a*/*c*-type hybrid character; consequently, the center of mass of the complex is no longer on the *ab*-plane of the ACN bare molecule. The

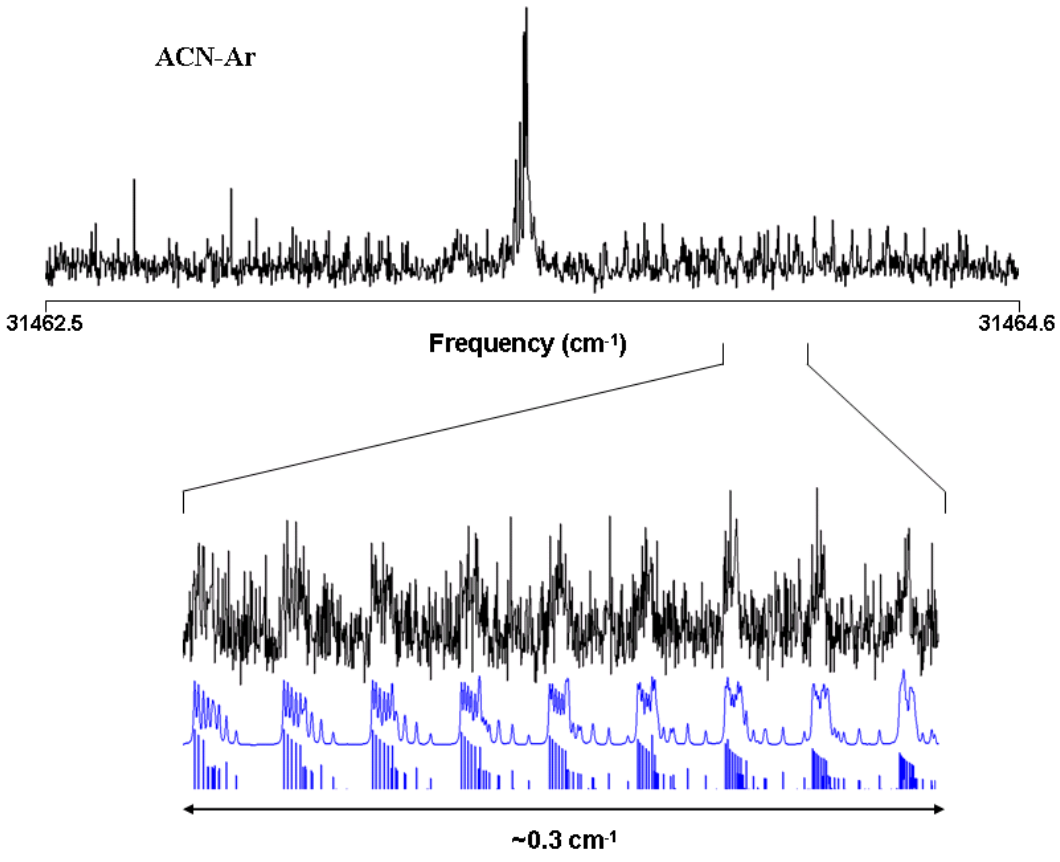


**Figure 3.6. Rotationally resolved fluorescence excitation spectrum of the ACN-Ar vdW complex in the gas phase. Portions of the fully resolved experimental spectrum and the corresponding simulation are also shown in bottom panel.**

spectrum was fit using Watson Hamiltonians for both electronic states, incorporating some centrifugal distortion terms.[20] The standard deviation of the fit is ~4.0 MHz and the Voigt profile for the lineshape function required 22 MHz Gaussian and 3 MHz Lorentzian components. The rotational temperature of the fit is 5 K. The inertial parameters of this band are summarized in Table 3.2.

**Table 3.2. Inertial parameters of the acenaphthene-argon vdW complex.**

| Parameter[a] | ACN-Ar[b] |
|---|---|
| **$S_0$** | |
| ***A″* (MHz)** | 681.6 (1) |
| ***B″* (MHz)** | 666.2 (1) |
| ***C″* (MHz)** | 616.1 (1) |
| **$S_1$** | |
| ***A′* (MHz)** | 682.1 (1) |
| ***B′* (MHz)** | 658.1 (1) |
| ***C′* (MHz)** | 614.9 (1) |
| **Band type *a/b/c*** | *90/10/0* |
| **Band origin ($cm^{-1}$)** | 31463.52 |
| **OMC (MHz)** | 3.98 |
| **Temp (K)** | 5.0 |

[a] Standard deviations shown in parenthesis are relative to the last significant figure.
[b] The following Watson distortion terms were required in the fit: $\Delta J''$ = 0.00236, $\Delta JK''$ = -0.00671, $\Delta K''$ = 0.00193, $\delta J''$ = -0.00065, $\delta K''$ = -0.00351 MHz; $\Delta J'$ = 0.00235, $\Delta JK'$ = -0.00256, $\Delta K'$ = -0.01039, $\delta J'$ = -0.00094, and $\delta K'$ = -0.00087 MHz.

## 3.6 DISCUSSION

### 3.6.1 Origin band

The $0_0^0$ band of ACN was experimentally found to be polarized parallel to the *a*-inertial axis of the molecule; *i.e.*, no *b*- or *c*-type rovibronic transitions were observed in the high resolution spectrum of Figure 3.2. This finding indicates that the $S_1$ electronic state of ACN is an $^1L_b$ state,

analogous to the *a*-type polarized weak electronic origin found in NAPH.[1,2] The intensity enhancement of this transition in ACN is believed to be a consequence of the lower symmetry of the molecule. Thus, as shown in Figure 3.7, the two one-electron excitations $\Psi_4\Psi_6^*$ and $\Psi_5\Psi_7^*$ make unequal contributions to the $S_1$ state, and thus do not cancel, as they do in NAPH. Analyses of the inertial parameters of the $0_0^0$ band (*cf.* Table 3.1) reveal that ACN is a near-oblate asymmetric top with $\kappa'' = 0.429$.

The calculated rotational constants[18] of the molecule in its ground state are in excellent agreement with the experimental values (*cf.* Table 3.1). Generally, the excited state *A′*, *B′*, and *C′* values are smaller than their ground state counterparts, owing to small ring expansions that are typical of $\pi\pi^*$ states. Apparently, ACN is nonplanar in both electronic states. It has an inertial defect of -6.58 amu Å$^2$ in its ground state, a value that is consistent with four out-of-plane C–H bonds; this value does not change substantially when the molecule absorbs light.

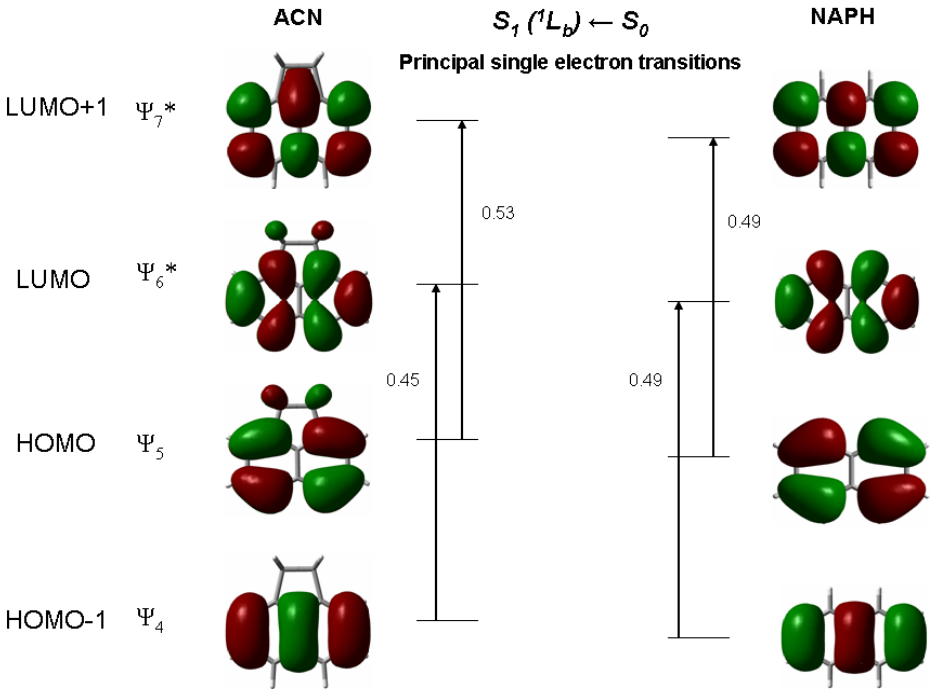


**Figure 3.7. CIS/6-31G* frontier molecular orbitals of acenaphthene (ACN) and naphthalene (NAPH). The energy level diagrams indicate the principal single electronic transitions and their corresponding contributions to the $S_1 \leftarrow S_0$ electronic excitation.**

Figure 3.7 shows a sketch of the relevant MO's of the geometry optimized structures of ACN that were derived from these calculations; a comparison with NAPH is performed for clarity purposes. According to CIS, the principal one-electron excitation that contributes to the $S_1$ state is the LUMO+1 ← HOMO transition (~53%); the other main contribution comes from the LUMO ← HOMO-1 transition (~45%). The oscillating charge distribution that is associated with the $S_1 \leftarrow S_0$ transition is oriented along the *a*-inertial axis. Thus, CIS calculations predict the electronic excited state $S_1$ as an $^1L_b$ state ($B_2$ symmetry in $C_{2v}$ point group), in agreement with our experimental results for the origin band of ACN, see Figure 3.8 for details.

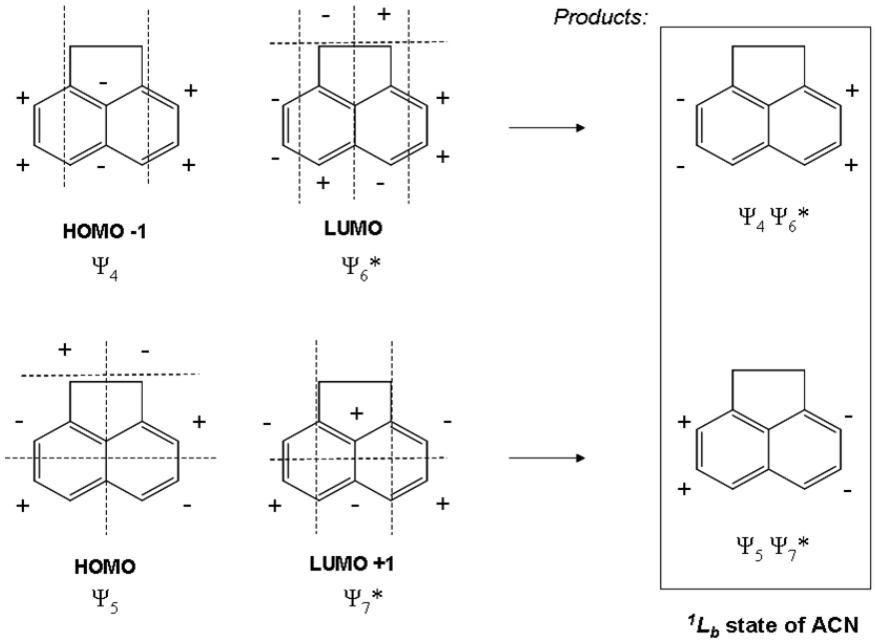


**Figure 3.8. Product wavefunctions of acenaphthene in its $S_1 \leftarrow S_0$ electronic transition.**

### 3.6.2 Perpendicular transitions

The study of vibronic transitions in electronic excited states has been a topic of intense interest in our research group in the last few years.[6,8] Recently, we have studied how the replacement of the central group of atoms in fluorene causes drastic changes in the observed electronic transition

moment orientations in the origin bands of carbazole and dibenzofuran.[21] In those cases, the $S_1$ state of fluorene was assigned as $^1L_b$ state whereas the $S_1$ states for carbazole and dibenzofuran were assigned as $^1L_a$ states in Platt's notation.[22] Upon investigating the molecules' vibronic bands, one band for each molecule was discovered with a different transition moment orientation relative to their $0_0^0$ bands. This finding has been explained by the interaction between the vibronic transition and a second nearby electronic excited state ($S_2$) *via* Herzberg-Teller coupling.[10]

The +422, +431 and +434 vibronic bands in ACN were found to be polarized parallel to the *b*-inertial axis of the molecule (see Figures 3.3 and 3.4). Hence, a HT mechanism must also be responsible for the observation of these symmetry-forbidden vibronic bands. Apparently, the oscillator strength is being borrowed form the $S_2 \leftarrow S_0$ electronic transition in ACN, which is polarized parallel to its short inertial axis. The $S_2$ state has been assigned as an $^1L_a$ state ($A_1$ symmetry in the $C_{2v}$ point group) and the appearance of these bands is through the last term of Equation 3.2. *Ab initio* frequency calculations (MP2 for the $S_0$ state and CIS for the $S_1$ state with 6-31G** basis sets)[18] have been performed to identify the vibrational modes involved in these transitions. By frequency comparisons, the +422 band is assigned to the asymmetric in-plane bending mode of the 5-membered ring; whereas the +431 band is assigned to the asymmetric in-plane distortion mode ($\bar{8}_0^1$) that also appears in the corresponding spectrum of NAPH (and is also *b*-polarized).[2] Lastly, the +434 band is likely to be a hot vibronic band, presumably originating from the +431 band, due to the relative frequency separation and the evident difference of its ground state rotational constants with respect to the rest of the bands analyzed (*cf.* Table 3.1). Sketches of the vibrational modes involved in these vibronic transitions are shown in the top panel of Figure 3.9.

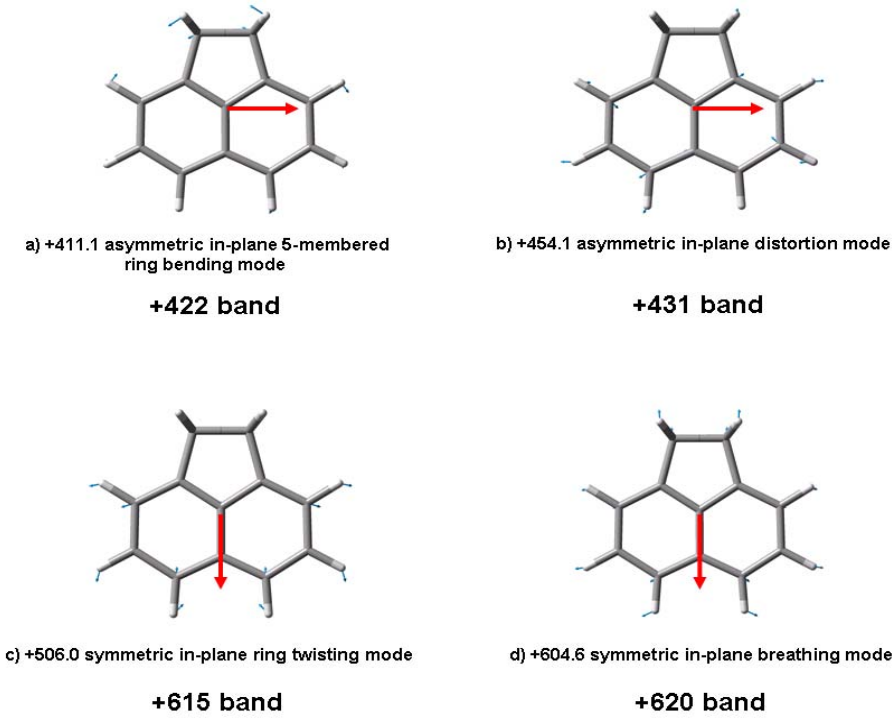


**Figure 3.9. CIS 6-31+G* vibrational modes and vibronic band assignments of acenaphthene in its $S_1$ state.**

### 3.6.3 Parallel transitions

Based on their frequencies, the +615 band in ACN presumably corresponds to the totally symmetric in-plane ring twisting mode, whereas the +620 band is assigned to the symmetric breathing mode of the isolated molecule. Neither band appears in the corresponding low resolution spectrum of NAPH.[2,16] Portions of the *R* branches in the high resolution spectra of the +615 and +620 bands of ACN are shown in Figure 3.5. Some intensity anomalies have been observed in both experimental spectra, where some particular rovibronic transitions are either too weak or too strong compared to the calculated spectra. Clearly, in the +615 band, the doubly degenerate transitions with $K_a'$ or $K_c'$ values less than two, are expected to exhibit more intensity than what it is experimentally observed [*cf.* the transitions terminating in 16 0 16 (16 1 16) and 15 2 14 (15 1 14) in the $S_1$ state]; the remaining single rotational lines do exhibit the intensity

pattern expected in the experimental trace. The transitions with $K_c' = 10$ are special in terms of frequency; these lines were found to be particularly shifted; an example is the double line terminating in 13 3 10 (13 4 10) in the top panel of Figure 3.5. Similar anomalies in intensity (not in frequency) were observed in the +620 band; *i.e.*, all the lines fit in frequency including the $K_c' = 10$ rotational transitions.

One possible source of these frequency and intensity anomalies, together with the overall intensity enhancement, is a pseudo-Coriolis coupling mechanism taking place within the two nearly degenerate vibrational modes in the excited electronic state at frequencies 615 and 620 $cm^{-1}$. Due to the relatively close proximity (~5 $cm^{-1}$) of these bands and their analogous polarizations, the coupling outlined in Equation 3.3 might occur through rotation about the *c*-inertial axis of the molecule.[11,13] ACN is a near-oblate asymmetric top. *True* oblate symmetric tops exhibit such behaviors. An example is found in the electronic spectrum of $Na_3$. As has been discussed in detail by Ernst *et al.*[23], a fractional quantization of the vibronic states of the $Na_3$ cluster appears when the two potential energy surfaces interact *via* a conical intersection, and the corresponding vibrational and electronic wave functions are affected. The observed features in the rotational structure of the spectrum were through a pseudo Jahn-Teller coupling of a degenerate state with a nearby non-degenerate state. The rovibronic energy corrections were accomplished by fitting the spectra using the following expression,

$$E = BJ(J + 1) - (B - C) K_c^2 \pm 2C\zeta K_c. \quad \textbf{(3.5)}$$

Here, the last term describes the Coriolis interaction, $J$ and $K_c$ are the angular momentum quantum numbers, $B$ and $C$ are the oblate rotational constants, and $\zeta$ is the effective Coriolis constant. For strong pseudo Jahn-Teller coupling, $\zeta = |j|$ holds,[24] and the last term in Equation 3.5

has the form ± $2CjK_c$ ($j$ is the vibronic angular momentum described by a cyclic motion of the nuclei on the potential surface).

For the particular value of $K_c$ = 10 and a rotational constant $C'$ = 643.4 MHz (~0.021 $cm^{-1}$) in ACN, the dynamics contained in $j$ plays an important role on the energy of the rotational eigenstates. This may be the source of the frequency perturbations observed in the +615 totally symmetric vibronic band. Moreover, the intensity mismatches in the +615 and +620 bands occur for quantum numbers $10 \leq J' \leq 25$ and $K_c'$ ($K_a'$) $\leq 2$. These energy eigenstates happen to be doubly degenerate (*cf*. Figure 3.5). Therefore, they may exhibit further Coriolis perturbations *via* a conical intersection occurring between the two vibrational energy surfaces in the vicinity.

By frequency and symmetry comparison between the experimental results and the theoretical calculations performed on this molecule in the ground and excited electronic states, we assign the band appearing at +615 $cm^{-1}$ above the origin to the totally symmetric in-plane ring twisting mode and the band at +620 $cm^{-1}$ above the origin to the totally symmetric breathing mode. The bottom panel of Figure 3.9 shows sketches of these two vibrational modes.

### 3.6.4 Acenaphthene-argon vdW complex

Extensive investigations of vdW complexes have focused on rare gas complexes of aromatic molecules.[25-27] These complexes are of particular interest since the rare gas acts as a structureless probe of the shape of the intermolecular energy surface. Structural and dynamical studies of vdW molecules also provide information needed to elucidate the nature of weak chemical forces that dominate their behavior. In the present study, experimental information about the ACN-Ar vdW complex was obtained from the analysis of the inertial parameters obtained from the fit of its rotationally resolved electronic spectrum in Figure 3.6 (see Table 3.2). Thereafter, a Kraitchman

analysis was performed to determine the position of the argon atom with respect to the bare acenaphthene frame by structural analysis in the vdW complex in both electronic states.[28] As a result of this study, involving transformation of coordinate systems, it was determined that the argon atom is located 3.48 Å away from the center of mass of the ACN frame in its $S_0$ state (see Figure 3.10) and 3.44 Å away in its $S_1$ electronic state. This last result is consistent with the observation that the complex transition is 13.6 $cm^{-1}$ redshifted from the $0_0^0$ band band of the bare molecule. The van der Waals interaction is stronger in the $S_1$ state of the argon complex. Finally, an angle of 18° (2) has been measured between the *c*-inertial axis and the plane of the ACN frame in the vdW complex.

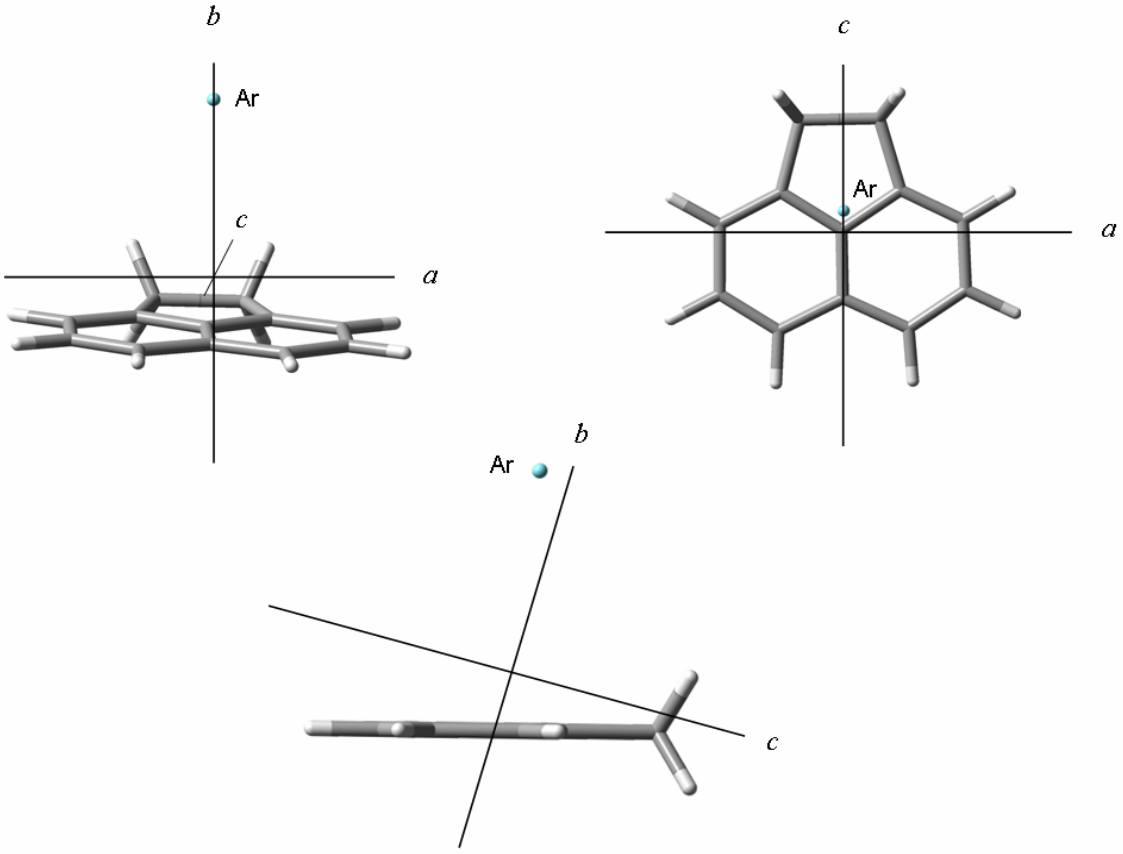


**Figure 3.10. Relative position of the Ar atom in the ACN-Ar complex in its $S_0$ electronic state. The inertial axes are shown as a reference framework.**

## 3.7 SUMMARY

Two different coupling mechanisms have been observed in acenaphthene by the careful analysis of its rotationally resolved electronic spectra in the gas phase. The $0_0^0$ band exhibits a polarization parallel to the *a*-inertial axis of the molecule; the +422, +431, and +434 $cm^{-1}$ vibronic bands exhibit perpendiculars polarizations with respect to the origin band, this result signals a HT coupling mechanism taking place within the $S_2$ state. In contrast, the +615 and +620 $cm^{-1}$ vibronic bands exhibit a parallel polarization with respect to the $0_0^0$ band, but reveal some intensity and frequency inconsistencies in their fits. A pseudo-Coriolis coupling mechanism, involving near-degenerate vibrational modes, has been suggested to be responsible for this finding. Lastly, it was observed that acenaphthene forms a vdW complex with an argon atom from the carrier gas. From the fit of the observed rotational structure analysis, it was determined that the argon atom lies 3.4 Å above the plane of the bare molecule.

## 3.8 ACKNOWLEDGMENTS

This work has been supported by NSF (CHE-0615755) to whom we are grateful.

## 3.9 REFERENCES

1. a) M. J. S. Dewar and H. C. Longuet-Higgins, *Proc. Phys. Soc.* (London) **67**, 795 (1954).
b) D. S. McClure, *J. Chem. Phys*. **22(10)**, 1668 (1954).

2. S. M. Beck, D. E. Powers, J. B. Hopkins, and R. E. Smalley, *J. Chem. Phys.* **73**, 2019 (1980).

3. W. A. Majewski and W. L. Meerts, *J. Mol. Spec*. **104**, 271 (1984).

4. G. Berden, W. L. Meerts, and W. Kreiner, *Chem. Phys*. **174**, 247 (1993).

5. S. Jagannathan and D. W. Pratt, *J. Chem. Phys.* **100**, 1874 (1994).

6. S. J. Humphrey and D. W. Pratt, *Chem. Phys. Lett.* **257**, 169 (1996).

7. J. R. Johnson, K. D. Jordan, D. F. Plusquellic, and D. W. Pratt, *J. Chem. Phys*. **93**, 2258 (1990).

8. G. Berden, W. L. Meerts, D. F. Plusquellic, I. Fujita, and D. W. Pratt, *J. Chem. Phys*. **104**, 3935 (1996).

9. L. Salem. *The Molecular Orbital Theory of Conjugated Systems*, 397 (Benjamin, New York, 1966).

10. G. Herzberg and E. Teller, Z. *Phys. Chem*. **21**, 410 (1933).

11. W. Gordy and R. L. Cook, *Microwave Molecular Spectra*, 2nd Ed., 289 (Wiley, New York, 1984).

12. J. M. Hollas, *High Resolution Spectroscopy*, 326 (Butterworth, London, 1982).

13. R. Nanes and E. K. C. Lee, *J. Chem. Phys*. **84**, 5290 (1986).

14. H. A. Jahn, *Phys. Rev.* **56**, 680 (1939).

15. W. A. Majewski, J. F. Pfanstiel, D. F. Plusquellic, and D. W. Pratt, *Laser Techniques in Chemistry*. T. R. Rizzo, A. B. Myers, 101 (Wiley, New York, 1995).

16. T. Chakraborty and M. Chowdhury, *Chem. Phys*. **159**, 439 (1992).

17. N. A. Borisevich, L. B. Vodovatov, G. G. D'jachenko, V. A. Petukhov, and M. A. Semenov, *Optika i Spektroskopiya* **81**, 757 (1996).

18. M. J. Frisch, *et al*. *Gaussian 03*, Revision B.05, Gaussian, Inc.: Pittsburgh PA, 2003.

19. D. F. Plusquellic, *Jb95 Spectral fitting program*, NIST, Gaithersburg, MD, http://physics.nist.gov/jb95.

20. J. K. G. Watson, *J. Chem. Phys*. **48**, 4517 (1968).

21. J. T. Yi, L. Alvarez-Valtierra, and D. W. Pratt, *J. Chem. Phys*. **124**, 244302 (2006).

22. J. R. Platt, *J. Chem. Phys*. **17(5)**, 484 (1949).

23. W. E. Ernst and S. Rakowsky, *Phys. Rev. Lett.*, **74**, 58 (1995).

24. G. Herzberg, *Molecular Spectra and Molecular Structure*, *Vol. III*, 63 (Van Nostrand, New York, 1966).

25. W. E. Sinclair and D. W. Pratt, *J. Chem. Phys*. **105**, 7942 (1996).

26. C. Kang and D. W. Pratt, *J. Chem. Phys*. **123**, 094306 (2005).

27. C. Kang and D. W. Pratt, *Intl. Rev. Phys. Chem*. **24**, 1 (2005).

28. J. Kraitchman, *Am. J. Phys*., **21**, 17 (1953).

# 4.0 ROTATIONALLY RESOLVED ELECTRONIC SPECTRA OF 9,10-DIHYDROPHENANTHRENE. A "FLOPPY" MOLECULE IN THE GAS PHASE

This work is published in *J. Chem. Phys.* **126**, 224308 (2007).

## 4.1 ABSTRACT

Rotationally resolved fluorescence excitation spectra of several bands in the $S_1 \leftarrow S_0$ electronic spectrum of 9,10-dihydrophenanthrene (DHPH) have been observed and assigned. Each band was fit using rigid rotor Hamiltonians in both electronic states. Analyses of these data reveal that DHPH has a non-planar configuration in its $S_0$ state with a dihedral angle between the aromatic rings ($\varphi$) of ~21.5°. The data also show that excitation of DHPH with UV light results in a more planar structure of the molecule in the electronically excited state, with $\varphi$ ~8.5°. Three prominent Franck-Condon (FC) progressions appear in the low resolution spectrum, all with fundamental frequencies lying below 300 $cm^{-1}$. Estimates of the potential energy surfaces along each of these coordinates have been obtained from analyses of the high resolution spectra. The remaining barrier to planarity in the $S_1$ state is estimated to be ~2650 $cm^{-1}$ along the bridge deformation coordinate and it is substantially reduced by excitation of the molecule along the (orthogonal) ring twisting coordinate.

## 4.2 INTRODUCTION

Low frequency vibrational modes in large molecules have been extensively studied in past years owing to their relevance in a wide variety of processes in chemical physics. These processes include intramolecular vibrational redistribution, the Duschinsky effect, Herzberg-Teller couplings, internal conversion, intersystem crossing, and many others.[1-7] Low frequency modes are relevant in these processes because they create a high density of states at the available

energy, making possible rapid energy redistribution among these modes even when there are only small couplings among them.[8]

Typical low frequency modes in large molecules possessing different functional groups include inversions, torsions, ring twists, butterfly motions, and other large amplitude out-of-plane vibrations.[9-15] An interesting example is provided by 9,10-dihydrophenanthrene (DHPH), see Scheme 4.1 below. DHPH is a homolog of stilbene and has figured prominently in

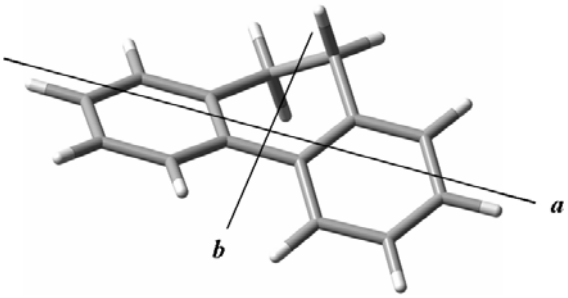


**Scheme 4.1. Optimized structure of DHPH in its $S_0$ state.**

discussions of *cis-trans* photoisomerization dynamics.[16] Previously, Chakraborty and Chowdhury (CC),[17] Zgierski *et al.* (ZZSL),[18] and Smith and Knee (SK)[19] have performed a number of low resolution fluorescence excitation, emission and depletion experiments on DHPH cooled in a supersonic jet. All authors observed essentially identical excitation spectra. The molecule exhibits an extensive, strong and apparently harmonic progression with a fundamental frequency of ~100 $cm^{-1}$, and apparently similar progressions of somewhat lower intensity at higher energies. However, the aforementioned authors differ in their interpretations of these modes. CC assigned the main progression to an out-of-plane torsional mode, ZZSL assigned it to an out-of-plane non-totally symmetric $–CH_2–CH_2–$ bridge deformation mode, and SK assigned it to a totally symmetric phenyl torsional mode that is governed by a single-minimum potential rather than a double-minimum one.

Described herein is an extensive study of the rotationally resolved $S_1 \leftarrow S_0$ fluorescence excitation spectra of several of the bands exhibited in the low resolution spectrum of DHPH. The data show that the molecule is non-planar in its $S_0$ state with a dihedral angle between the rings of $\varphi$ ~21.5°; that the molecule is also non-planar in its $S_1$ state, but with a smaller dihedral angle ($\varphi$ ~8.5°); and that three vibrational modes are active in flattening the molecule when it is excited to the $S_1$ state. Each of these modes have been identified; mode *a* is a ring twisting mode, mode *b* is a combined in-plane-bending and stretching mode, and mode *c* is a bridge deformation mode. Potential energy surfaces along each of these coordinates have been determined from analyses of these spectra. Additionally, the data show that there is a strong coupling of all these modes in the $S_1$ state, and that excitation of the ring twisting mode substantially reduces the barrier to planarity along the bridge deformation mode.

## 4.3 EXPERIMENTAL

DHPH (>94% pure) was purchased from Aldrich and used without further purification. Dry argon (Ar) was used in all experiments as an inert carrier gas.

In the vibrationally resolved fluorescence excitation experiments, samples were seeded into 20 psi of Ar gas and expanded into a vacuum chamber ($10^{-5}$ torr) through a 1 mm diameter orifice pulsed valve (General Valve Series 9) operating at 10 Hz. Two centimeters downstream of the valve, the free jet was excited with the second harmonic of a Quanta Ray $Nd^{3+}$:YAG (Model DCR-1A) pumped dye laser (Model PDL-1). The dye (Kiton Red 620) laser output was frequency doubled with an external KDP crystal providing a spectral resolution of ~0.6 $cm^{-1}$ in the ultraviolet (UV). The molecules were excited at the point of intersection between the jet and

the laser beam and the resulting fluorescence was collected with a photomultiplier tube (PMT). Finally, the collected data were processed by a boxcar integrator (Stanford Research Systems) and recorded with Quick Data Acquisition software (Version 1.0.5).

Rotationally resolved experiments were performed using a molecular beam laser spectrometer, described in detail elsewhere.[20] Briefly, the molecular beam was formed by expansion of vaporized DHPH seeded in Ar (-15 psi) through a heated (~425 K) 200 $\mu$m quartz nozzle into a differentially pumped vacuum system. The expansion was skimmed 2 cm downstream with a 1 mm diameter skimmer and crossed 13 cm further downstream by a continuous wave (CW) $Ar^+$-pumped ring dye laser. The CW laser was operated with Rhodamine 6G dye and intracavity frequency doubled in a BBO crystal, yielding ~200 $\mu$W of UV radiation with a resolution of ~1 MHz. The fluorescence excitation spectrum was detected, using spatially selective optics, by a PMT and photon counting system. The PMT signal together with the iodine absorption spectrum and the relative frequency markers were simultaneously collected and processed by the JBA95 data acquisition system.[20] Absolute frequency calibration of the spectra was performed by comparison with the $I_2$ absorption spectrum. Relative frequency markers were obtained from a stabilized etalon having a free spectral range of 299.7520 ± 0.0005 MHz.

## 4.4 RESULTS

Figure 4.1 shows the vibrationally resolved fluorescence excitation (low resolution) spectrum of DHPH. In agreement with previous results,[18,19] we observe three well-defined Franck-Condon (FC) progressions of vibrational bands, labeled **a**, **b**, and **c** in Figure 4.1. Clearly, these long FC progressions signal large differences in the potential energy surfaces along different low

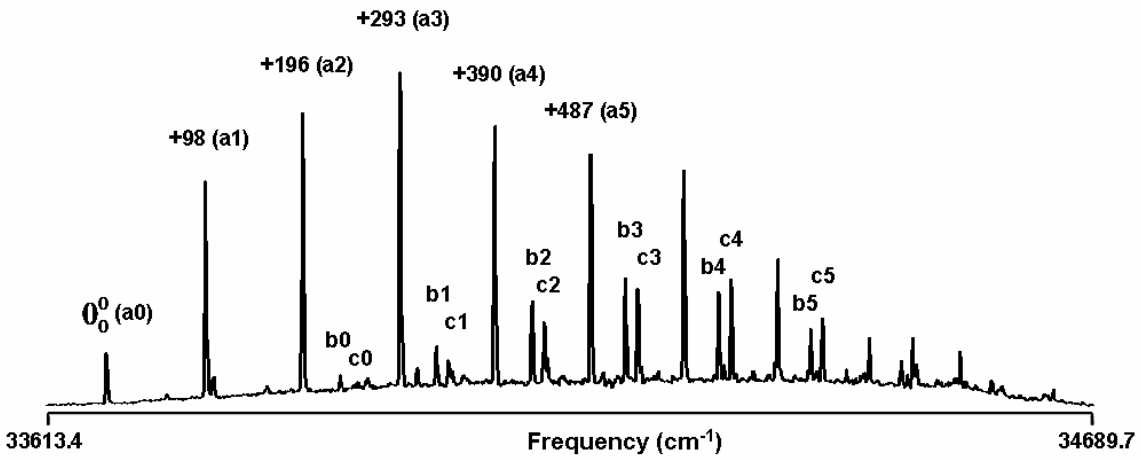


**Figure 4.1. Vibrationally resolved fluorescence excitation spectrum of DHPH in the gas phase.**

frequency coordinates of the molecule in both electronic states. The first (**a**) progression is the most intense one, while the second and the third progressions are weaker, blue shifted in frequency, and have similar intensities. The labeling scheme used in Figure 4.1 is analogous to the one used by ZZSL.[18] The $0_0^0$ transition is located at 33669.9 $cm^{-1}$ (~297 nm), blue shifted from that of phenanthrene by more than 43 nm,[21] and redshifted from that of biphenyl by ~13.5 nm.[22] The frequency spacing among the members of the **a** progression has a nearly constant value of ~97.5 $cm^{-1}$. The **b** and **c** FC progressions exhibit similar spacings but their "false" origins are shifted to the blue of the 'true" origin by ~234 $cm^{-1}$ and ~246 $cm^{-1}$, respectively.

Extensive studies of several of these bands have been performed at high resolution. Our first examples are from the **a** progression. Figure 4.2 shows the rotationally resolved $S_1 \leftarrow S_0$ fluorescence excitation spectra of the bands at +293 $cm^{-1}$ (**a3**) and +487 $cm^{-1}$ (**a5**). Each spectrum spans ~2 $cm^{-1}$ and exhibits pure *a*-type character. To fit these spectra, we first generated about 4500 *a*-type rovibronic transitions based on *ab initio*[23] estimates of rotational constants and rigid rotor Hamiltonians for both electronic states. Then, we made quantum number assignments of single transitions in each of the simulated spectra to the corresponding

transitions in each of the experimental spectra, using the Windows-based program JB95.[24] Finally, we used a least-squares fitting procedure to optimize the rotational constants, based on a comparison of observed and calculated line positions. The final fits utilized ~200 assigned rovibronic transitions and resulted in standard deviations of 2.56 and 2.97 MHz, respectively. More detailed illustrations of the quality of the fits are shown in the bottom panel of Figure 4.2. Lineshapes of individual rovibronic transitions were fit to Voigt profiles having Gaussian and Lorentzian components of 18 and 25 MHz, respectively. Rotational temperatures used for the fits were 5.5 and 4.5 K, respectively. Similar experiments were performed on four other members of the main progression; $0_0^0$, **a1**, **a2**, and **a4**.

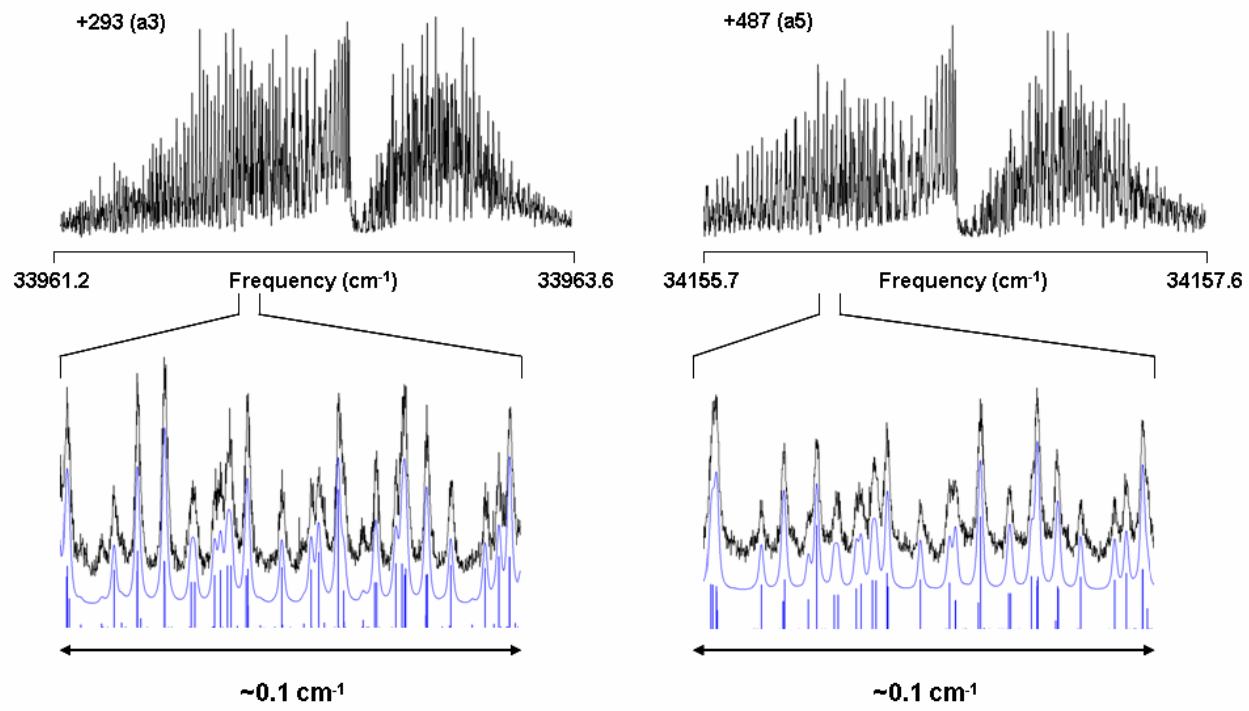


**Figure 4.2. Rotationally resolved fluorescence excitation spectra of the bands at +293 cm$^{-1}$ (a3) and +487 cm$^{-1}$ (a5) in the first Franck-Condon progression of DHPH in the gas phase (top panels). Equivalent portions of the *P* branches at full experimental resolution and the corresponding simulated spectra with and without an assumed line shape function are also shown (bottom panels).**

Several transitions in the minor **b** and **c** FC progressions were recorded and fully analyzed as well. For example, Figure 4.3 shows the rotationally resolved $S_1 \leftarrow S_0$ fluorescence excitation spectra of the bands at +523 $cm^{-1}$ (**b3**) and +714 $cm^{-1}$ (**b5**). Each spectrum spans ~2 $cm^{-1}$ and again exhibits 100% *a*-type character. Similar strategies were used to fit these bands; comparisons of experimental and simulated portions of these bands are also shown in Figure 4.3. The standard deviations of the fits are 3.24 and 3.53 MHz, respectively. Each spectrum exhibits a Voigt profile having 18 MHz Gaussian and 30 MHz Lorentzian contributions. The rotational temperatures of the fits are 6.0 and 5.5 K, respectively. Two other **b** bands were also examined in detail, **b2** and **b4**.

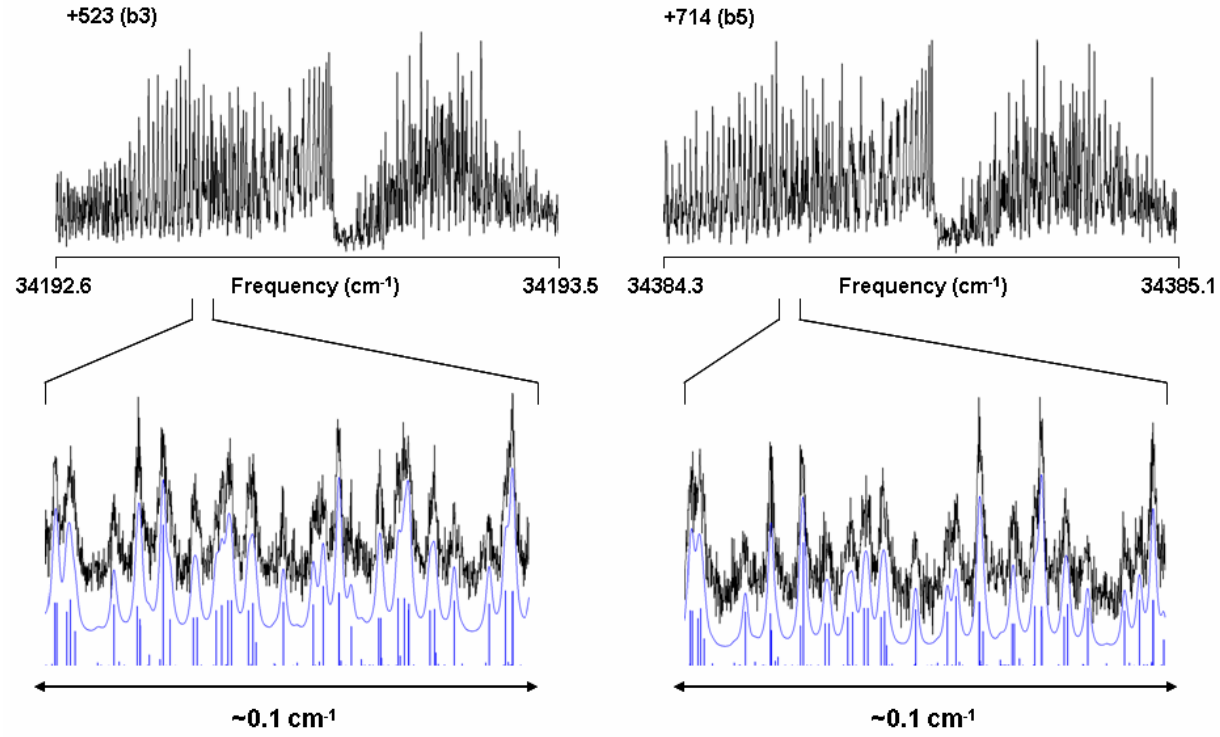


**Figure 4.3. Rotationally resolved fluorescence excitation spectra of the bands at +523 $cm^{-1}$ (b3) and +714 $cm^{-1}$ (b5) in the second Franck-Condon progression of DHPH in the gas phase (top panels). Equivalent portions of the *P* branches at full experimental resolution and the corresponding simulated spectra with and without an assumed line shape function are also shown (bottom panels).**

We also recorded the high resolution spectra of three members of the third FC progression, the bands located at +535 $cm^{-1}$ (**c3**), +631 $cm^{-1}$ (**c4**) and +727 $cm^{-1}$ (**c5**). Anticipating results similar to these for **a** and **b** bands, similar methods were used to fit the **c** progression bands. Band **c3** could be fit in this way, but bands **c4** and **c5** could not. Both of these latter bands were found to be split into two sub-bands with different sub-band splittings, ~27 MHz for the **c4** band and ~145 MHz for the **c5** band (see Figure 4.4). The expanded scale sections shown in the bottom panels of Figure 4.4 clearly show the remarkable differences in structure of these two bands. Rigid rotor Hamiltonians were again used to fit the observed sub-bands, all of which were again found to be 100% *a*-type. The standard deviations of the fits

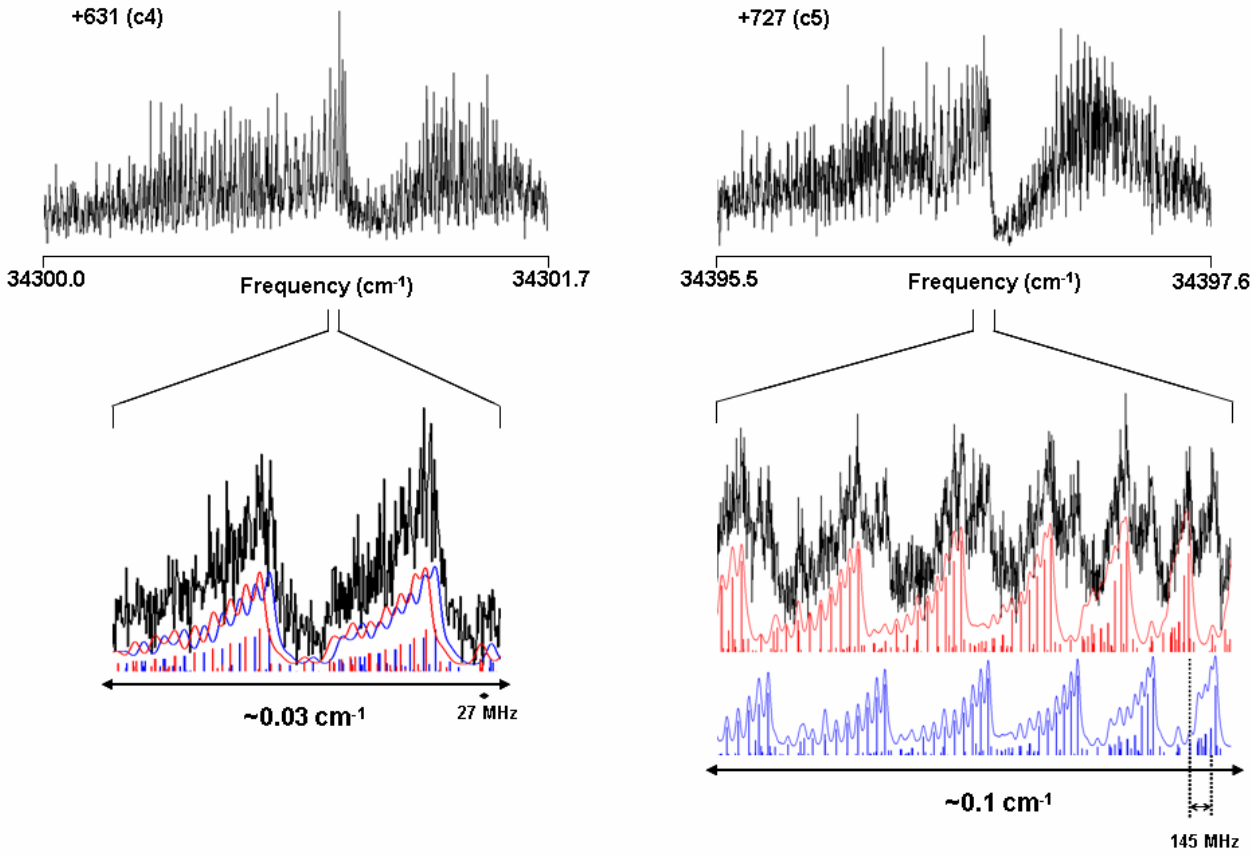


**Figure 4.4. Rotationally resolved fluorescence excitation spectra of the bands at +631 $cm^{-1}$ (c4) and +727 $cm^{-1}$ (c5) bands in the third Franck-Condon progression of DHPH in the gas phase (top panels). Similar portions of their *Q* branches at full experimental resolution and the corresponding simulated spectra are also shown. Note that these bands require two simulated spectra to fit their corresponding experimental traces; the sub-band splittings are ~27 and ~145 MHz, respectively.**

are 3.54, 3.11, and 2.56 MHz for the **c3** band and the redshifted sub-bands of **c4** and **c5**, respectively, and 2.08 and 3.74 MHz for the blueshifted sub-bands of **c4** and **c5**, respectively. Voigt line shape profiles were again observed; all five sub-bands have 18 MHz Gaussian and 25 MHz Lorentzian components, with rotational temperatures lying between 4-7 K. Inertial parameters of all studied members of the **a**, **b**, and **c** progressions in DHPH are reported in Table 4.1.

## 4.5 DISCUSSION

Every single member of each of the three vibrational progressions, that are observed in the electronic spectrum of DHPH and were examined here, exhibits a transition moment vector that is oriented parallel to the *a*-inertial axis of the molecule. Further, the ground state rotational constants of all examined bands are the same within experimental error (*cf*. Table 4.1). Therefore, it is likely that all bands originate in the zero-point vibrational level (ZPL) of the $S_0$ state and terminate in *different* vibrational levels of the *same* excited electronic state, presumably the $S_1$ state. In previous reports, ZZSL[18] and SK[19] have argued that the second and third progressions of vibronic bands originate in an $S_2$ state at ~240 $cm^{-1}$ above the $S_1$ state, but the present results suggest that this is not the case. If a second excited state participated in the spectrum shown in Figure 4.1, it would likely have differently polarized bands.

We have performed *ab initio* calculations[23] (MP2/6-31G** and CIS/6-31G) to complement our experimental observations. Theory suggests that DHPH has a dihedral angle $\varphi$ ~21.7° in its ground $S_0$ electronic state and $\varphi$ ~8.5° in the excited $S_1$ state (see Scheme 4.2), thereby explaining the extensive FC progression observed in its low resolution spectrum. Indeed,

**Table 4.1. Inertial parameters derived from the fits of the high resolution spectra of all observed bands of 9,10-dihydrophenanthrene.**

| Parameter[a] | $0_0^0$ | +98 (a1) | +196 (a2) | +293 (a3) | +390 (a4) | +427 (b2) | +487 (a5) |
|---|---|---|---|---|---|---|---|
| $S_0$ | | | | | | | |
| *A″* (MHz)[b] | 1526.8 (1) | 1527.9 (1) | 1526.8 (1) | 1526.3 (1) | 1526.8 (3) | 1527.1 (1) | 1528.1 (1) |
| *B″* (MHz)[b] | 545.5 (1) | 545.4 (1) | 545.6 (1) | 545.5 (1) | 545.5 (1) | 545.4 (1) | 545.5 (1) |
| *C″* (MHz)[b] | 412.5 (1) | 412.5 (1) | 412.5 (1) | 412.6 (1) | 412.6 (1) | 412.5 (1) | 412.6 (1) |
| $S_1$ | | | | | | | |
| *A′* (MHz) | 1491.6 (1) | 1492.6 (1) | 1491.4 (1) | 1490.7 (1) | 1491.1 (3) | 1492.2 (1) | 1492.2 (1) |
| *B′* (MHz) | 546.2 (1) | 546.0 (1) | 546.1 (1) | 545.9 (1) | 545.8 (1) | 545.9 (1) | 545.6 (1) |
| *C′* (MHz) | 405.8 (1) | 405.9 (1) | 406.0 (1) | 406.1 (1) | 406.2 (1) | 406.0 (1) | 406.3 (1) |
| Band origin ($cm^{-1}$) | 33669.9 | 33767.8 | 33865.4 | 33962.6 | 34059.8 | 34096.5 | 34156.7 |
| OMC (MHz) | 2.33 | 2.84 | 2.53 | 2.56 | 1.33 | 3.03 | 2.97 |
| Temp (K) | 4.8 | 4.5 | 5.0 | 5.5 | 5.5 | 6.5 | 4.5 |

**Table 4.1 (cont.). Inertial parameters derived from the fits of the high resolution spectra of all observed bands of 9,10-dihydrophenanthrene.**

| Parameter[a] | +523 (b3) | +535 (c3) | +619 (b4) | +631 (c4) | | +714 (b5) | +727 (c5) | |
|---|---|---|---|---|---|---|---|---|
| | | | | red | blue | | red | blue |
| $S_0$ | | | | | | | | |
| *A″* (MHz)[b] | 1526.2 (1) | 1529.1 (1) | 1527.0 (1) | 1529.7 (4) | 1526.6 (4) | 1529.0 (1) | 1530.1 (1) | 1528.3 (1) |
| *B″* (MHz)[b] | 545.6 (1) | 545.6 (1) | 545.7 (1) | 545.6 (1) | 545.4 (1) | 545.6 (1) | 545.7 (1) | 545.5 (1) |
| *C″* (MHz)[b] | 412.5 (1) | 412.5 (1) | 412.5 (1) | 412.5 (1) | 412.6 (1) | 412.5 (1) | 412.4 (1) | 412.5 (1) |
| $S_1$ | | | | | | | | |
| *A′* (MHz) | 1491.2 (1) | 1492.1 (1) | 1491.9 (1) | 1492.6 (4) | 1489.5 (4) | 1493.8 (1) | 1492.8 (1) | 1491.1 (1) |
| *B′* (MHz) | 546.0 (1) | 546.2 (1) | 546.0 (1) | 546.1 (1) | 545.9 (1) | 545.8 (1) | 546.0 (1) | 545.9 (1) |
| *C′* (MHz) | 406.1 (1) | 406.3(1) | 406.2 (1) | 406.3 (1) | 406.4 (1) | 406.3 (1) | 406.4 (1) | 406.4 (1) |
| Band origin ($cm^{-1}$) | 34192.6 | 34205.2 | 34288.8 | 34301.1 | 34301.1 | 34384.4 | 34396.7 | 34396.7 |
| OMC (MHz) | 3.24 | 3.54 | 3.58 | 3.11 | 2.08 | 3.53 | 2.56 | 3.74 |
| Temp (K) | 6.0 | 6.5 | 5.5 | 4.5 | 4.5 | 5.5 | 6.5 | 6.5 |

[a] Standard deviations shown in parentheses are uncertainties in the last significant figure.

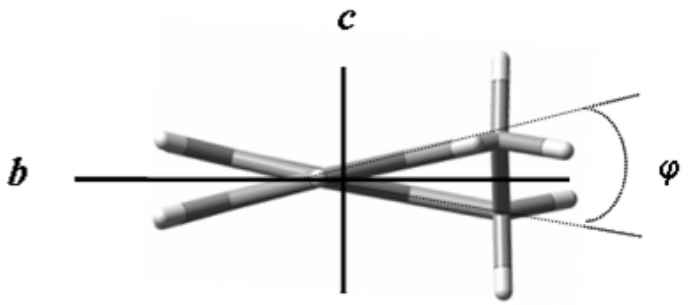


**Scheme 4.2. Torsional (twisting) angle $\varphi$ between the two aromatic rings of DHPH.**

**Table 4.2. Calculated low frequency vibrational modes of 9,10-dihydrophenanthrene in its $S_0$ and $S_1$ electronic states.**

| Model | Symmetry ($C_2$ point group) | $S_0$ Frequency[a] ($cm^{-1}$) | Sketch | $S_1$ Frequency[a] ($cm^{-1}$) |
|---|---|---|---|---|
| **1. Butterfly** | *B* | 122.8 | 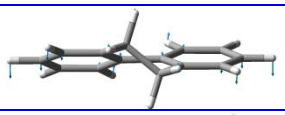 | 67.7 |
| **2. Ring twisting** | *A* | 140.1 | 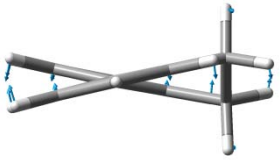 | 87.3 |
| **3. In-plane bending** | *A* | 192.9 | 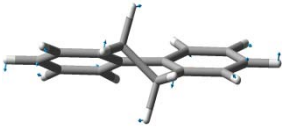 | 146.0 |
| **4. $CH_2$–$CH_2$ out-of-plane bending** | *B* | 223.4 | 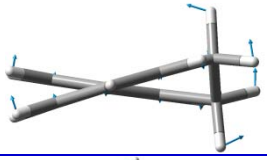 | 192.8 |
| **5. In-plane stretching** | *A* | 275.6 | 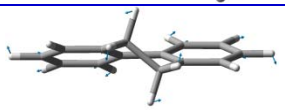 | 237.4 |
| **6. $CH_2$–$CH_2$ bridge deformation** | *A* | 333.9 | 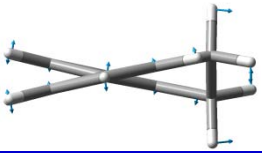 | 305.5 |

[a] Theoretical frequencies have been reduced by a factor of 0.893.[25]

the molecule is predicted to have several fundamental vibrational modes lying below 300 $cm^{-1}$ in its $S_0$ and $S_1$ states. These are listed in Table 4.2. In what follows, we compare the results of theory and experiment in order to determine which vibrational motions are responsible for the observed FC progressions, and thereby characterize the dynamical behavior of the isolated DHPH molecule when it absorbs light.

### 4.5.1 The "a" progression. Symmetric out-of-plane ring twist

Of the vibrational modes shown in Table 4.2, the most likely candidate for the first FC progression is mode 2, the symmetric ring twisting mode. Both, the symmetry of this mode (*A*) and its calculated frequency in the $S_1$ state (87.3 $cm^{-1}$) are consistent with what is observed experimentally (*a*-type bands, frequency of ~98 $cm^{-1}$). Other calculated modes either have the wrong symmetry (a *B* mode at 67.7 $cm^{-1}$) or lie at much higher frequency (the next *A* mode is predicted at 146.0 $cm^{-1}$).

This assignment was confirmed using the rotationally resolved spectra. Table 4.3 lists the values of the inertial defects ($\Delta I = I_c - I_a - I_b$) of each studied vibrational level in DHPH, derived from the measured rotational constants of both the ground and the excited electronic states. First, we note that all ground state values derived from fits of bands in the **a** progression are the same, within experimental error ($\Delta I$ = -32.4 ± 0.2 amu $Å^2$). This shows that all bands originate in the same vibrational level, presumably the ZPL of the $S_0$ state. Next, we note that the values of $\Delta I$ in the $S_1$ state are substantially less (in magnitude) than those of the $S_0$ state. This is a direct consequence of the "flattening" of the molecule, a planar molecule having a $\Delta I$ value of essentially zero.[26] Finally, we note a revealing trend; the magnitude of $\Delta I$ increases

monotonically from -18.7 to -21.2 amu Å$^2$ with increasing vibrational energy, evidencing increasingly larger average displacements along some *out-of-plane* coordinate.

**Table 4.3. Inertial defects of the observed vibrational bands in the $S_1 \leftarrow S_0$ electronic spectrum of 9,10-dihydrophenanthrene. Standard deviations are ~0.05 amu Å$^2$.**

| Band | $S_0$ $\Delta I''$ (amu Å$^2$) | $S_1$ $\Delta I'$ (amu Å$^2$) |
|---|---|---|
| First Franck-Condon progression (**a** bands) | | |
| **$0_0^0$ (a0)** | -32.35 | -18.66 |
| **+98 (a1)** | -32.21 | -19.02 |
| **+196 (a2)** | -32.18 | -19.55 |
| **+293 (a3)** | -32.58 | -20.50 |
| **+390 (a4)** | -32.39 | -20.87 |
| **+487 (a5)** | -32.15 | -21.15 |
| Second Franck-Condon progression (**b** bands) | | |
| **+427 (b2)** | -32.46 | -19.70 |
| **+523 (b3)** | -32.44 | -20.09 |
| **+619 (b4)** | -31.97 | -20.17 |
| **+714 (b5)** | -31.70 | -20.41 |
| Third Franck-Condon progression (**c** bands) | | |
| **+535 (c3)** | -31.54 | -20.05 |
| **+631 (c4)** | -31.66 | -20.29 |
| | -32.86 | -21.63 |
| **+727 (c5)** | -31.15 | -20.51 |
| | -31.91 | -21.29 |

We have modeled this behavior in the manner shown in Figure 4.5. Beginning with a geometry-optimized *ab initio* structure, DHPH was distorted from its equilibrium geometry along the symmetric ring twisting mode ($\varphi$) by 5º increments in the ground state and 1º increments in the excited state. The geometry of the molecule at each point was again energy optimized along all other coordinates at each step and then $\Delta I$ values were calculated. Figure 4.5 shows a plot of the theoretically predicted $\Delta I$ values against $\varphi$. The plot accurately reproduces the

values of $\Delta I$ for a $\varphi$ value in the $S_0$ state of ~22º and a range of $\varphi$ values in the $S_1$ state lying between 9 and 13º; the lower value being the one corresponding to the ZPL of the $S_1$ state. We thus conclude that the symmetric ring twisting mode is responsible for the major FC progression in the spectrum of DHPH. This conclusion is consistent with the earlier work of ZZSL[18] and SK[19] based on their careful studies of vibrationally resolved fluorescence spectra.

A crucial question that needs to be resolved is whether the potential energy surfaces (PES) along this vibrational coordinate are single or double wells in the $S_0$ and $S_1$ states. ZZSL[18] assumed double minimum potentials in both states, but SK[19] argued that the potentials are single welled ones. Their calculations suggested that the suspected ring twisting mode was accompanied by a simultaneous distortion of the $–CH_2–CH_2–$ group, so that motion along this

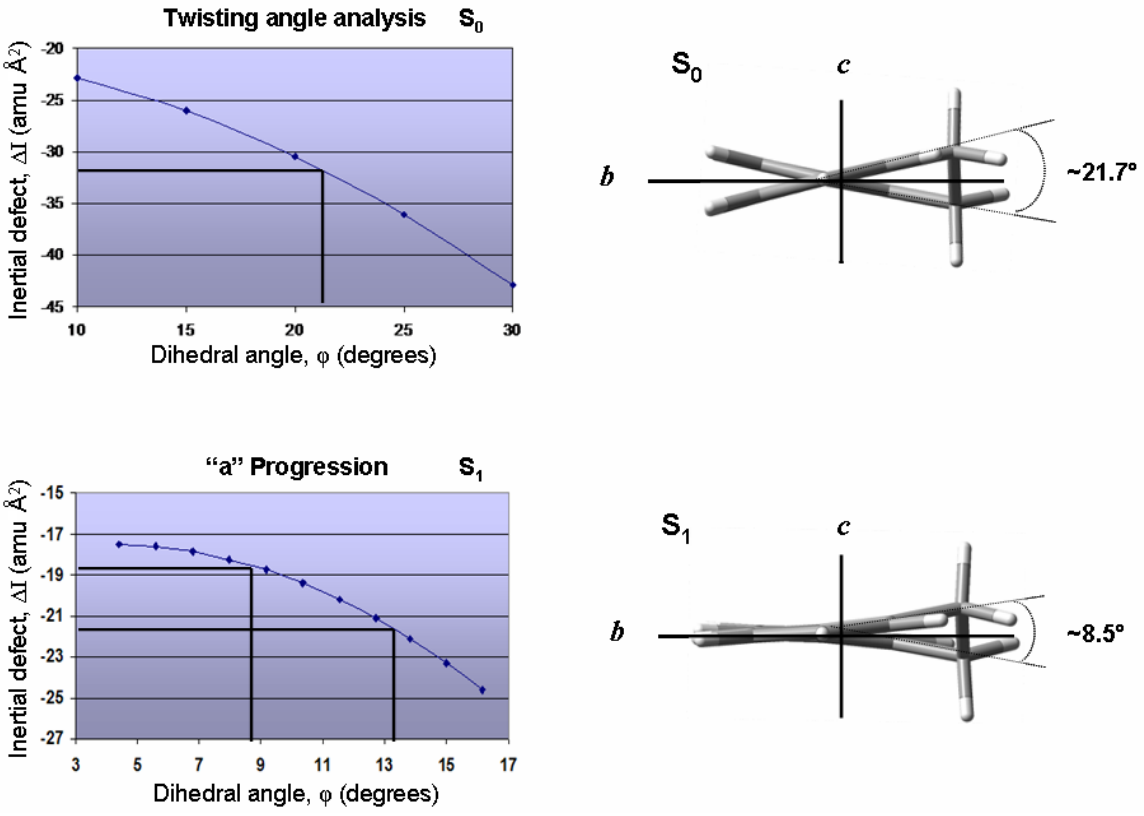


**Figure 4.5. Relationship between theoretical values of the inertial defect ($\Delta I$) and the torsional coordinate ($\varphi$) for the "a" (symmetric ring twisting) mode of DHPH in its $S_0$ and $S_1$ electronic states. The range of experimental results is marked with thick lines.**

coordinate does not "carry the molecule through planarity with respect to both the rings and the aliphatic chain".[19] Since the motion is not symmetric with respect to the planar structure, the PES is single welled along this coordinate. Their arguments (for the $S_1$ state) were supported by the observed harmonicity of the main FC progression, and (for the $S_0$ state) by a fluorescence depletion experiment.

Our results confirm both of these conclusions. There is a monotonic dependence of the inertial defect $\Delta I$ on displacement along this coordinate in the $S_1$ state. If the potential were a double well, some "zigzag" behavior in $\Delta I$ would be expected with increasing vibrational quantum number. And no "tunneling" splittings were observed in the rotationally resolved spectra, in either state. Thus, our experimental results agree with the interpretations of SK.[19] PES's along the twisting coordinate that best represent these results are shown in Figure 4.6. The frequencies of the two potentials are 105 and 97.5 $cm^{-1}$, respectively. Taking harmonic oscillator

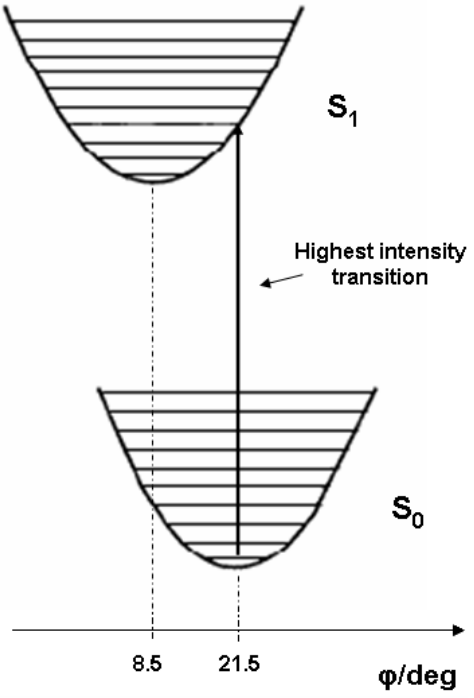


**Figure 4.6. Potential energy surfaces along the $\varphi$ twisting coordinate that best represent the "a" progression of bands of DHPH in agreement with the experimental results.**

$S_0$ minimum is located at $\varphi$ = 21.5º, and the $S_1$ minimum is located at $\varphi$ = 8.5º; the fundamental wave functions for the two states, we then calculated the FC factors to estimate the frequency profile of the main vibrational progression. The best fit of the observed intensities (see Figure 4.7) was accomplished by using a $\Delta\varphi$ value of -13° for the dihedral angle between the two rings. This value is the same as estimated from our inertial defect analysis, confirming the "one-dimensional" model of this motion in both electronic states.

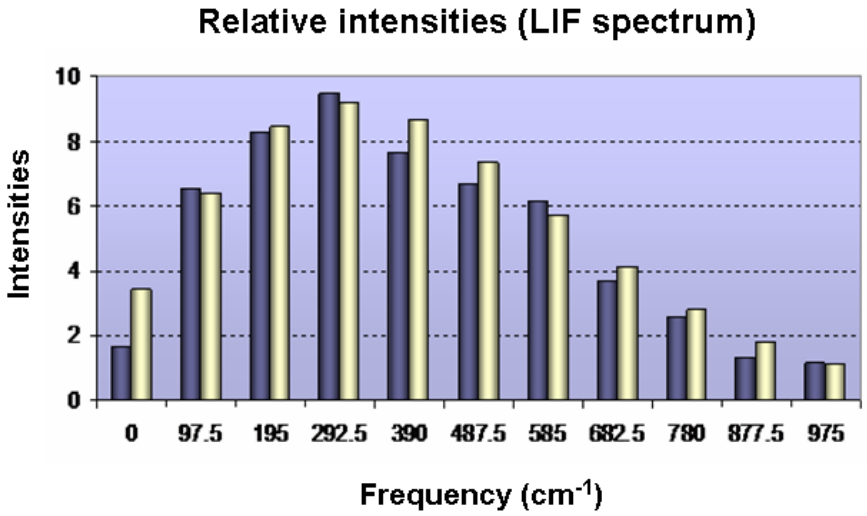


**Figure 4.7. Comparison of relative intensities for the "a" progression of transitions of DHPH. Dark bars correspond to the experimental results; light bars correspond to Franck-Condon analysis.**

### 4.5.2 The "b" progression

The key observation concerning the origin of the **b** progression in the low resolution spectrum of DHPH was made by ZZSL.[18] These authors showed that a combination of three different modes appear in the dispersed fluorescence spectrum of band **b1**; at ~98, ~173, and ~265 $cm^{-1}$. The first mode corresponds to the ring twisting mode; the second is the in-plane bending mode; and the third is the in-plane stretching mode (*cf.* Table 4.2). Thus, we assign band **b0** as a false origin

(combination of the in-plane bending and in-plane stretching modes) of the $S_1 \leftarrow S_0$ transition; the calculated frequency of this "combination" band is 146.0 + 237.4 = 383.4 $cm^{-1}$ compared to an observed displacement from the origin of ~234 $cm^{-1}$. Notably, the two contributing fundamentals are *A*-symmetry modes, explaining the *a*-type character of the band. Then, built upon this origin is a progression in the same ring twisting mode as is involved in the main progression at ~98 $cm^{-1}$.

Further support for this assignment is shown in the top panel of Figure 4.8. Illustrated there is a comparison of measured and calculated values of the inertial defect of the $S_1$ DHPH vibrational levels accessed in the **b** progression. As before, $|\Delta I'|$ increases with increasing displacement along $\varphi$ (*cf.* Table 4.3). However, the magnitudes of these increases are less than these observed in the **a** progression. Presumably, this is because excitation of **b** bands involves displacement along an in-plane mode as well as an out-of-plane mode.

### 4.5.3 The "c" progression

The third FC (**c**) progression of vibrational bands exhibited in the low resolution spectrum of DHPH is even more intriguing. Again, the magnitudes of the inertial defects increase with increasing displacement along the relevant coordinate(s), as shown in Table 4.3 and the lower panel of Figure 4.8. But the changes in $|\Delta I'|$ in the **c** progression are significantly larger than those on the **b** progression. Additionally, there is a nearly constant displacement of ~12.5 $cm^{-1}$ between each pair of **b** and **c** bands. Therefore, we believe that the two progressions are "independent" in sense that the **c** progression is built upon another false origin of different character. The most likely candidate for this origin is the "$–CH_2–CH_2–$ bridge deformation" mode, mode 6 in Table 4.2. The calculated frequency of this mode is 305.5 $cm^{-1}$ in the $S_1$ state,

compared to the displacement of the **c0** band from the true origin of ~247 $cm^{-1}$. Additionally, all measured bands in the **c** progression are *a*-type bands; the bridge deformation mode is a totally symmetric out-of-plane mode. Then, as before, a progression of vibrations along the ring twisting mode is built upon this false origin, explaining most of the remaining vibrational activity in the spectrum.

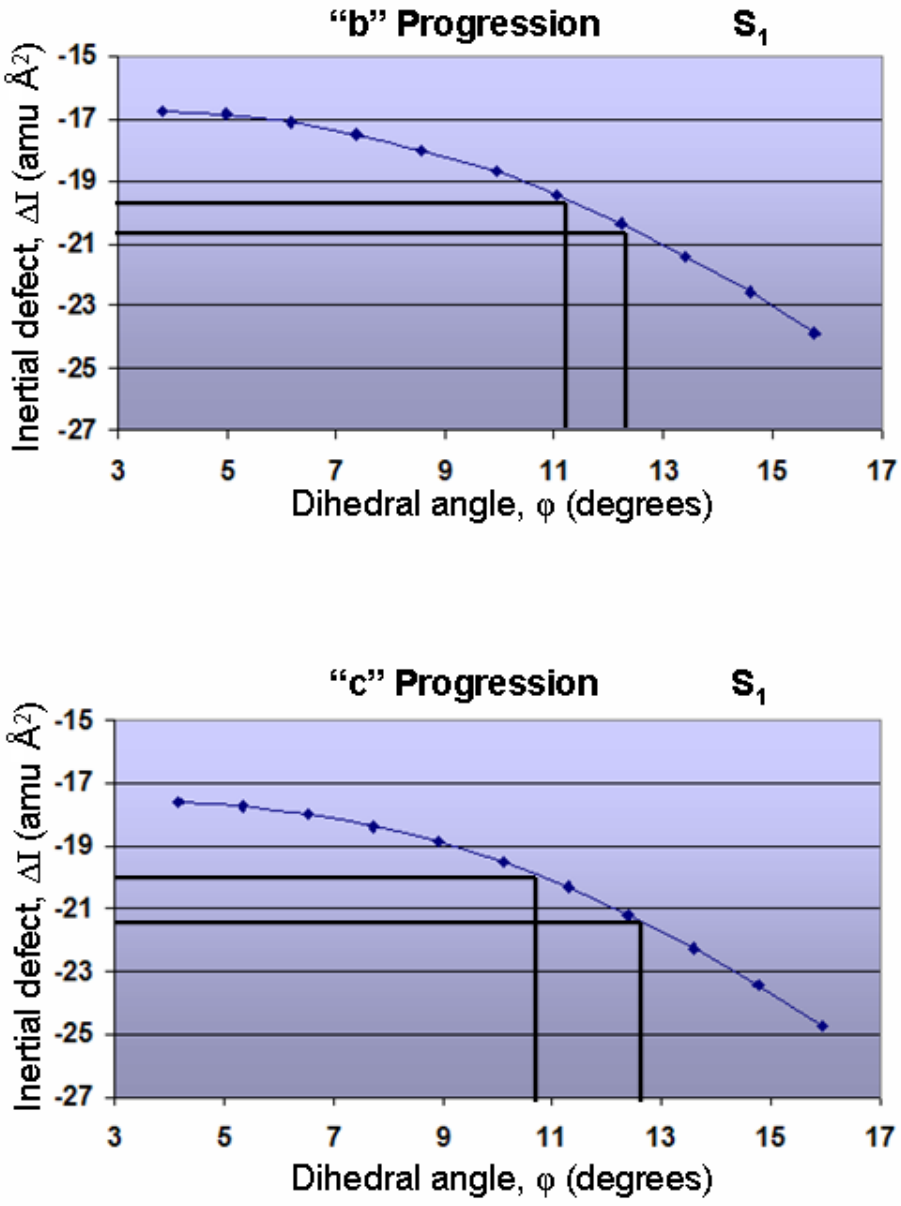


**Figure 4.8. Plots of the inertial defect vs. the dihedral angle for several vibrational levels in the $S_1$ excited state of DHPH. The top (bottom) panel shows the data for levels accessed in the "b" ("c") progression. Points are calculated values; the solid lines indicate the range of values observed experimentally.**

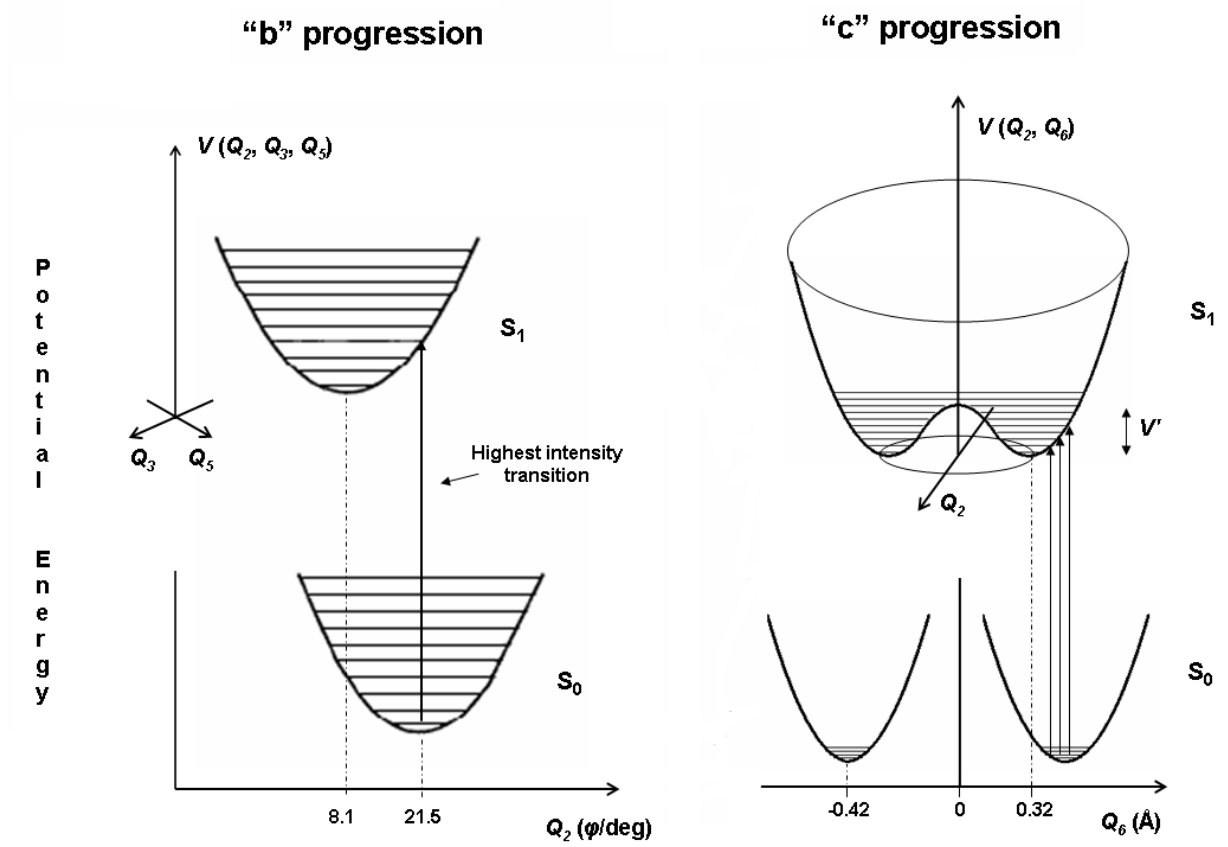


**Figure 4.9. Potential energy surfaces along the $Q_2$ (ring twisting dihedral angle $\varphi$) for the combination of modes "b" and "c" of DHPH. The "b" progression contains two extra vibrational coordinates, $Q_3$ and $Q_5$, (inactive). The "c" progression exhibits tunneling due to the combination of the $Q_2$ and $Q_6$ (–$CH_2$–$CH_2$– bridge deformation) torsional coordinates, which overcome the torsional barrier at higher energy.**

That this interpretation of the origin of the **c** progression is correct is revealed by the remarkable finding that, whereas band **c3** (and presumably bands **c0**, **c1** and **c2** as well) are single bands, bands **c4** and **c5** are each found to be split into two components at high resolution. The splittings of the two (equally intense) "sub-bands" are ~27 MHz for the **c4** band and ~145 MHz for the **c5** band. Further, as shown in Table 4.3, the blueshifted sub-bands have $|\Delta I'|$ values that are larger than those of the redshifted sub-bands. These observations provide the key to understanding the nature of the tunneling motion that is responsible for the appearance of two sub-bands in each of these spectra, as described below.

Our model is as follows. We imagine that there is a double-well potential along $Q_6$, the $–CH_2–CH_2–$ bridge deformation mode, as shown in Figure 4.9. Now, in the ground state, and in the zero point level of the $S_1$ excited state, the barrier to this motion is high. As first noted by SK,[19] "DHPH is a non-planar molecule with a high barrier to planarity. Excitation of the ring twisting mode (mode 2) does not carry the molecule through planarity with respect to both the rings and the aliphatic chain, but does bring the phenyl rings to planarity", with respect to each other. Our results show, however, that excitation of the combined vibrational motion (one quantum in mode 6 plus one or more quanta in mode 2) does allow the molecule to pass through an "all-planar" transition state, giving rise to observable tunneling splittings with four or more quanta in the ring twisting mode. Thus, we write

$$\Psi_s = c_1\psi_1 + c_2\psi_2 \qquad \textbf{(4.1a)}$$

$$\Psi_a = c_1\psi_1 - c_2\psi_2 \qquad \textbf{(4.1b)}$$

where $\psi_1$ and $\psi_2$ are vibrational wavefunctions centered in wells 1 and 2, along the bridge deformation coordinate, and $\Psi_s$ and $\Psi_a$ are symmetric and antisymmetric combinations of these, separated by a tunneling splitting, $\Delta E$,[27]

$$\Delta E = E_a - E_s = 2\hbar\nu \cdot \exp\left[ -\frac{2\sqrt{2\mu}}{\hbar} \int_{x_1}^{0} \left(V(x) - E_0\right)^{\frac{1}{2}} dx \right]. \qquad \textbf{(4.2)}$$

Here, $\nu$ is the vibrational frequency of mode 6, $\mu$ is the reduced mass of the molecule, $V(Q_6)$ is the (assumed one-dimensional) potential energy function and $E_0$ is the reference energy. The potential function is centered at $x = 0$, the hypothetical planar molecule. Hence, the antisymmetric state has a larger inertial defect than the symmetric one. Since the blueshifted sub-bands in bands **c4** and **c5** have larger $|\Delta I'|$ values, this means that the tunneling splitting (barrier height) in the $S_1$ excited state is larger (smaller) than in the ground $S_0$ state, as expected on the basis of chemical intuition.

We can calculate the barrier heights ($V$-$E_0$) in the following way. Based on the calculated minimum energy geometry of the $S_1$ state, the two minima in the potential are estimated to lie at ± 0.42 Å along the bridge deformation coordinate, this being the vertical distance of the $–CH_2–$ group above (or below) the all-planar transition state. Now, the distance to the barrier is reduced by excitation of DHPH with one quantum of the bridge deformation mode at ~254 $cm^{-1}$. An estimate of this distance is obtained by comparing the inertial defects of the upper state vibrational levels **a3** and **c3**, which yields $x_1$ = 0.32 Å. Inserting this value into Equation (4.2), we find the barrier height to be ~2650 $cm^{-1}$ if $\Delta E$ = 27 MHz (see Appendix A for details), and ~2150 $cm^{-1}$ if $\Delta E$ = 145 MHz. These values are believed to be accurate to ±100 $cm^{-1}$. Thus, the barrier to planarity along the bridge deformation coordinate is significantly (~20%) reduced by simultaneously exciting the ring twisting coordinate, evidencing a kind of cooperative motion involving the two coordinates. A similar behavior has been observed in tropolone,[28-31] where it has been shown that the barrier to intramolecular hydrogen atom transfer from the –OH to the C=O group is substantially reduced by excitation of –C=C– stretching modes in the seven-membered ring.

Because no torsional splitting is observed in the ground state, DHPH can be regarded as belonging to the $C_2$ point group, having only a $C_2$ axis of symmetry. Then the electronic transition observed is $B \leftarrow A$. But in the excited state, when torsional splitting is observed, the $C_{2v}$ point group is appropriate; each of the split components is a $B_1$, $B_2$ pair. Then it is useful to regard the zero point level of the $S_0$ state as being composed of an $A_2$, $A_1$ degenerate pair, leading to a description of the pairs of transitions in the **c** progression of DHPH as $B_2 \leftarrow A_1$ and $B_1 \leftarrow A_2$ pairs, using $C_{2v}$ symbols for each state. It will be interesting to see if, in the future, it proves

possible to resolve tunneling splittings along this coordinate in the ground state using even higher resolution methods.[32]

### 4.5.4 Electronic structure analysis

Though vibrational in nature, the fundamental driving force for structural change on excitation of DHPH (and tropolone) by light is electronic in nature. Figure 4.10 provides a comparison of the principal CIS/6-31G frontier molecular orbitals (MO's) involved in the $S_1 \leftarrow S_0$ transition of DHPH and two related molecules, biphenyl (BIPH) and phenanthrene (PHEN). The calculated MO's of DHPH and BIPH are more similar to each other, whereas those of PHEN are different. Note the reversal of the nodal patterns in PHEN, compared to DHPH and BIPH. In DHPH, the LUMO ← HOMO excitation is the principal contributor to the structure of the $S_1$ state, bringing electron density from the periphery of the rings into the $C_{12}$–$C_{13}$ bond (see Scheme 4.3), decreasing its bond length.

The increased conjugation between the two rings causes the molecule to become more planar in the $S_1$ state, as in the case of BIPH. [The relatively large change in the *A* rotational constant, ($\Delta A = A' - A''$ = -35.2 MHz) is a direct measure of the conjugative interaction of the two rings.] But ethane prefers to be staggered, rather than eclipsed, so DHPH is twisted in its $S_1$ state, rather than completely flat. Nonetheless, the competition between these two effects leads to substantial Franck-Condon activity along three different vibrational coordinates in its $S_1 \leftarrow S_0$ spectrum, as delineated here.

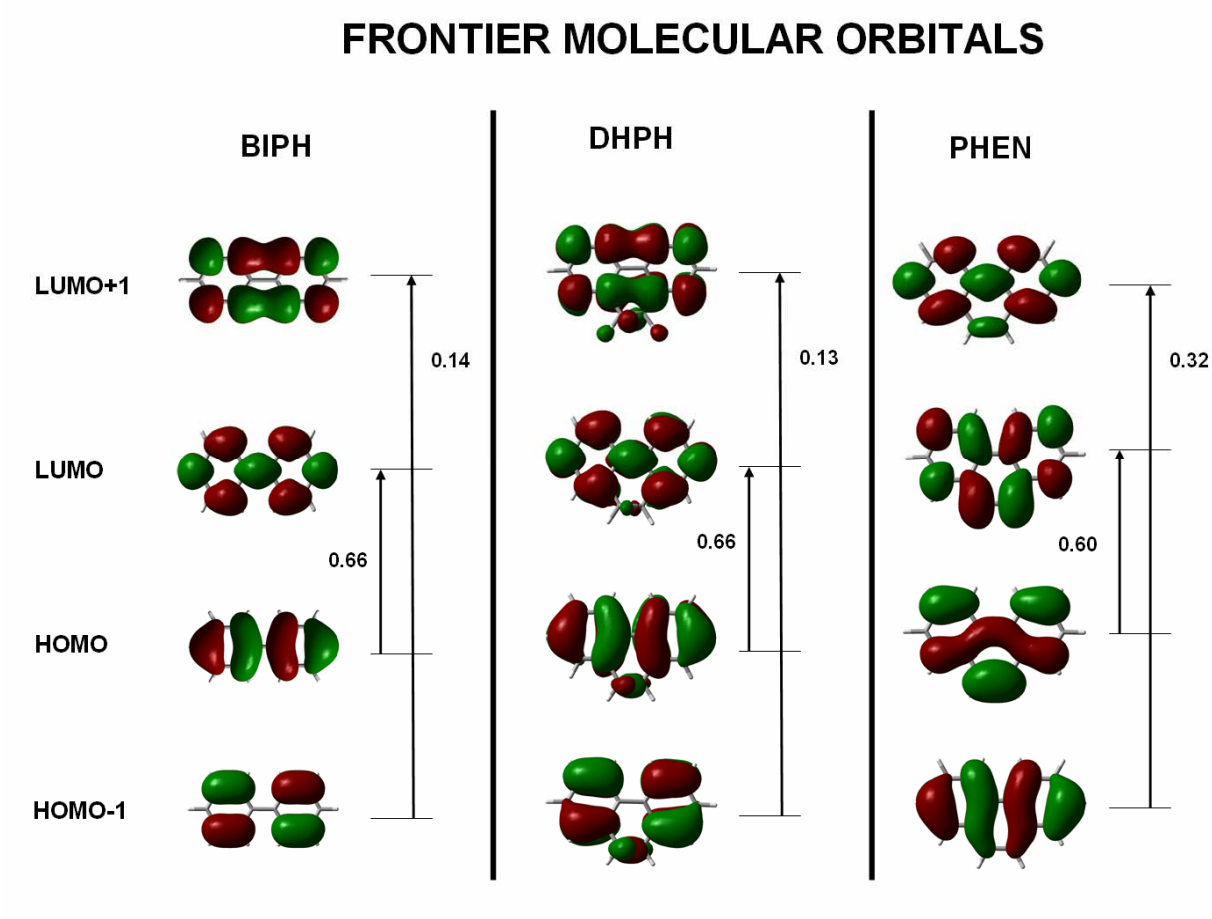


**Figure 4.10. CIS/6-31G frontier molecular orbitals with their corresponding transition probabilities of biphenyl (BIPH), 9,10-dihydrophenanthrene (DHPH), and phenanthrene (PHEN).**

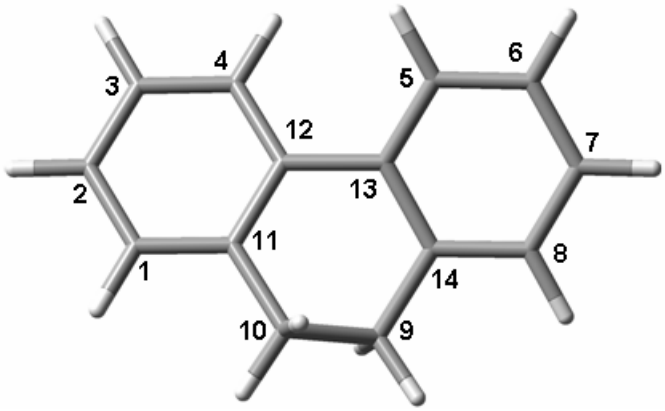


**Scheme 4.3. Atom numbering in DHPH molecule.**

## 4.6 SUMMARY

Rotationally resolved $S_1 \leftarrow S_0$ fluorescence excitation spectra of three different Franck-Condon progressions of vibrational bands in the DHPH molecule reveal that the mode responsible for their appearance is the totally symmetric ring twisting mode, whose torsional coordinate of motion is the dihedral angle between the two aromatic rings ($\varphi$). The two higher frequency progressions of bands are built upon false origins involving in-plane bending and stretching modes and a bridge deformation mode. A detailed analysis of the spectra of these bands reveals characteristics of the potential energy surface along each of these coordinates, including a coupling of two of the modes at higher energies. This coupling is a direct consequence of the second covalent link between the two aromatic rings.

## 4.7 ACKNOWLEDGMENTS

We thank Dr. John T. Yi and Dr. David R. Borst for their helpful assistance in the data analysis, and Jessica Thomas for overall comments about the manuscript. We are also grateful to an anonymous referee for suggestions regarding symmetry considerations. This work has been supported by NSF (CHE-0615755).

## 4.8 REFERENCES AND NOTES

1. T. Suzuki, N. Mikami, and M. Ito, *J. Phys. Chem.* **90**, 6431 (1986).

2. H. Kono, S. H. Lin, and E. W. Schlag, *Chem. Phys. Lett.* **145**, 280 (1988).

3. T. G. Wright, E. Cordes, O. Dopfer, and K. Mueller-Dethlefs, *J. Chem. Soc., Faraday Trans.* **89**, 1609 (1993).

4. W. E. Sinclair, H. Yu, D. Phillips, and J. M. Hollas, *J. Chem. Phys.* **106**, 5797 (1997).

5. J. M. Hollas, *J. Chem. Soc., Faraday Trans.*, **94**, 1527 (1998).

6. W. Werncke, S. Hogiu, M. Pfeiffer, A. Lau, and A. Kummrow, *J. Phys. Chem. A* **104**, 4211 (2000).

7. S. J. Baek, D. Lee, K. Choi, Y. S. Choi, and S. K. Kim, *J. Mol. Struct.* **611**, 203 (2002).

8. Y. Mikami, *J. Chem. Phys.* **73**, 3314 (1980).

9. K. W. Holtzclaw and D. W. Pratt, *J. Chem. Phys.* **84**, 4713 (1986).

10. J. H. Frederick, E. J. Heller, J. L. Ozment, and D. W. Pratt, *J. Chem. Phys.* **88**, 2169 (1988).

11. T. Chakraborty and E. C. Lim, *J. Chem. Phys.* **98**, 836 (1993).

12. M. Z. Zgierski, T. Chakraborty, and E. C. Lim, *J. Chem. Phys.* **98**, 9340 (1993).

13. K. Okuyama, Y. Numata, S. Odawara, and I. Suzuka, *J. Chem. Phys.* **109**, 7185 (1998).

14. J. Laane, *J. Phys. Chem.* **104A**, 7715 (2000).

15. M. Baba, A. Doi, Y. Tatamitani, S. Kasahara, and H. Kato, *J. Phys. Chem. A* **108**, 1388 (2004).

16. See for example, H. Petek, K. Yoshihara, Y. Fujiwara, Z. Lin, J. H. Penn, and J. H. Frederick, *J. Phys. Chem.* **94**, 7539 (1990).

17. T. Chakraborty and M. Chowdhury, *Chem. Phys. Lett.* **177**, 223 (1990).

18. M. Z. Zgierski, F. Zerbetto, Y. Shin, and E. C. Lim, *J. Chem. Phys.* **96**, 7229 (1992).

19. J. M. Smith, J. L. Knee, *J. Chem. Phys.* **99**, 38 (1993).

20. W. A. Majewski, J. F. Pfanstiel, D. F. Plusquellic, and D. W. Pratt, *Laser Techniques in Chemistry*. T. R. Rizzo, A. B. Myers, Eds. J. Wiley & Sons: New York, p 101 (1995).

21. N. Ohta and H. Baba, *Mol. Phys.* **59**, 921 (1986).

22. Y. Takei, T. Yamaguchi, Y. Osamura, K. Fuke, and K. Kaya. *J. Phys. Chem.* **92**, 577 (1988).

23. M. J. Frisch, G. W. Trucks, H. B. Schlegel, *et al*., GAUSSIAN 98, Revision A.9, Gaussian, Inc., Pittsburgh PA 1998.

24. D. F. Plusquellic, JB95 Spectral fitting program, NIST. http://physics.nist.gov/jb95.

25. J. B. Foresman and Æ. Frisch, *Exploring Chemistry with Electronic Structure Methods*, 2nd Ed. Gaussian Inc., Pittsburgh PA, p 64 (1996).

26. T. Oka and Y. Morino, *J. Mol. Spec.*, **6**, 472 (1961).

27. R. P. Bell, *The Tunnel Effect in Chemistry*. Ed. Chapman and Hall, New York, p 43 (1980). For numerical methods of analysis, see J. R. Letelier and A. Toro-Labbé, *J. Math. Chem.* **39**, 485 (2006).

28. A. C. P. Alves and J. M. Hollas, *Mol. Phys.* **23**, 927 (1972).

29. A. C. P. Alves and J. M. Hollas, *Mol. Phys.* **25**, 1305 (1973).

30. R. K. Frost, F. Hagemeister, D. Scheleppenbach, G. Laurence, and T. S. Zwier, *J. Phys. Chem.* **100**, 16835 (1996).

31. J. J. Paz, M. Moreno, and J. M. Lluch, *J. Chem. Phys.* **108**, 8114 (1998).

32. Referee comments.

# 5.0 ROTATIONALLY RESOLVED ELECTRONIC SPECTRA OF 2- AND 3-METHYLANISOLE IN THE GAS PHASE: A STUDY OF METHYL GROUP INTERNAL ROTATION

This work is published in *J. Phys. Chem. B* **110**, 19914-22 (2006).

## 5.1 ABSTRACT

Rotationally resolved fluorescence excitation spectra of several torsional bands in the $S_1 \leftarrow S_0$ electronic spectra of 2-methylanisole (2MA) and 3-methylanisole (3MA) have been recorded in the collision-free environment of a molecular beam. Some of the bands can be fit with rigid rotor Hamiltonians; others exhibit perturbations produced by the coupling between the internal rotation of the methyl group and the overall rotation of the entire molecule. Analyses of these data show that 2MA and 3MA both have planar heavy-atom structures; 2MA has *trans*-disposed methyl and methoxy groups, whereas 3MA has both *cis*- and *trans*-disposed substituents. The preferred orientations (staggered or eclipsed) in two of the conformers and the internal rotation barriers of the methyl groups in all three conformers change when they are excited by light. Additionally, the values of the barriers opposing their motion depend on the relative positions of the substituent groups, in both electronic states. In contrast, no torsional motions of the attached methoxy groups were detected. Possible reasons for these behaviors are discussed.

## 5.2 INTRODUCTION

The phenomenon of internal rotation has been a subject of considerable interest to both chemists and physicists for many years. In 1936, on the basis of thermodynamic evidence, it was concluded that the relative rotation of the two methyl groups in ethane was not entirely free but was shown to be restricted by a potential barrier.[1] Subsequently, following pioneering studies of the origins of such barriers,[2] much research has been performed on many molecules containing methyl groups.[3] Two molecules of special interest to us are toluene (methylbenzene) and anisole

(methoxybenzene). Recent studies of these two species have revealed that the methyl group internal rotation in toluene is relatively free,[4] whereas that in anisole is relatively rigid.[5] In the present study, we focus on molecules containing both of these functional groups, 2-methylanisole (2MA) and 3-methylanisole (3MA), see below. Our interest is in learning about how the torsional degrees of freedom in these two molecules might be influenced by each other.

Previous investigations of 2MA and 3MA have included studies of their TOF-MS,[6] LIF,[7,8] PFI-ZEKE,[9] hole-burning,[7,8] and dispersed fluorescence[6,7] spectra. These studies have revealed that both molecules exhibit significant low frequency Franck-Condon activity in their $S_1 \leftarrow S_0$ electronic spectra, evidencing some kind of conformational change produced by the absorption of light, presumably involving one or more torsional modes. Additionally, others[10,11] have described *ab initio* calculations of the ground state methyl group internal rotation potentials for several toluene derivatives. Computed barriers at the Hartree-Fock (HF) level using medium sized basis sets agree reasonably with experimental results, for several *ortho*-substituted toluenes. But the agreement is poor for *meta*- and *para*-substituted compounds, even in their ground states. Capturing the dependence of these barriers on the electronic state of the molecule is an even more challenging task.

More data are needed to rectify this situation. In what follows, we describe both the low and high resolution $S_1 \leftarrow S_0$ fluorescence excitation spectra of 2MA and 3MA, as isolated species in the gas phase. We derive from these data information about the structures of the molecules, the preferred orientations of their substituent groups, and the barriers to methyl group internal rotation in both electronic states. The results show that the magnitude and signs of these barriers are a sensitive function of the relative position of the substituent groups, and the electronic state of the molecules to which they are attached.

## 5.3 EXPERIMENTAL

2MA and 3MA were purchased from Aldrich and used without further purification. Dry argon and helium were used in all experiments as inert carrier gases.

In the vibrationally resolved experiments, samples were seeded into 60 psi of helium gas and expanded into a vacuum chamber ($10^{-5}$ torr) through a 1 mm diameter orifice pulsed valve (General Valve Series 9) operating at 10 Hz. Two centimeters downstream of the valve, the free jet was excited with the second harmonic of a Quanta Ray $Nd^{3+}$:YAG (Model DCR-1A) pumped dye laser (Model PDL-1). The dye (Rhodamine 575) laser output was frequency doubled with an external $\beta$-barium borate (BBO) crystal providing a spectral resolution of ~0.6 $cm^{-1}$ in the UV. From the point of intersection between the jet and the laser beam, the molecules were excited and the fluorescence was collected with a photomultiplier tube (PMT). Finally, the collected data were processed by a boxcar integrator (Stanford Research Systems) and recorded with Quick Data Acquisition software (Version 1.0.5).

Rotationally resolved electronic experiments were performed using a molecular beam laser spectrometer, described in detail elsewhere.[12] Briefly, the molecular beam was formed by expansion of the vaporized sample (either 2MA or 3MA) seeded in argon carrier gas (-18 psi) through a heated (~313 K) 240 $\mu$m quartz nozzle into a differentially pumped vacuum system. The expansion was skimmed 2 cm downstream with a 1 mm diameter skimmer and crossed 13 cm further downstream by a continuous wave (CW) $Ar^+$ pumped ring dye laser. The CW laser was operated with Rhodamine 110 dye and intracavity frequency doubled in BBO, yielding ~200 $\mu$W of UV radiation with a linewidth of ~1 MHz.

The fluorescence excitation spectrum was detected, using spatially selective optics, by a PMT and photon counting system. The PMT signal together with the iodine absorption spectrum

and the relative frequency markers were simultaneously collected and processed by the JBA95 data acquisition system.[12] Absolute frequency calibration of the spectra was performed by comparison with the $I_2$ absorption spectrum. The relative frequency markers were obtained from a stabilized etalon with a free spectral range of 299.7520 ± 0.0005 MHz.

## 5.4 RESULTS

Figure 5.1 shows the vibrationally resolved fluorescence excitation (low resolution) spectra of 2MA and 3MA. Like Breen *et al*.[6] and Ichimura and Suzuki (IS),[7] we observe extensive low frequency progressions in each spectrum. [Additional activity appears at high energies in both spectra, in combination with ring modes (*e.g*., $6b^1$, $6a^1$, and $1^1$).] The labeling scheme in Figure 5.1 is taken directly from IS[7] in which the numbers designate the vibrational quantum numbers of the methyl group torsional levels in the $S_1$ state and the letters designate their symmetries. The origin band ($0a_1$) in 2MA is at 36361.8 $cm^{-1}$ (~275 nm), red shifted from that of toluene[4] by more than 1000 $cm^{-1}$. IS[7] claim that 3MA exhibits two origin bands, one at 36049.3 $cm^{-1}$ that has been assigned as the *cis*-conformer (the lowest frequency band in Figure 5.1b, marked "$1e,0a_1$" inside the box) and a slightly higher energy band at 36115.5 $cm^{-1}$ that has been assigned as the *trans*-conformer (marked "$0a_1$" in Figure 5.1b); see Scheme 5.1 below. Clearly, the extensive Franck-Condon progressions in these two spectra signal large differences in both the orientations of the methyl groups and the barriers opposing their motions in the two electronic states, if these interpretations are correct.

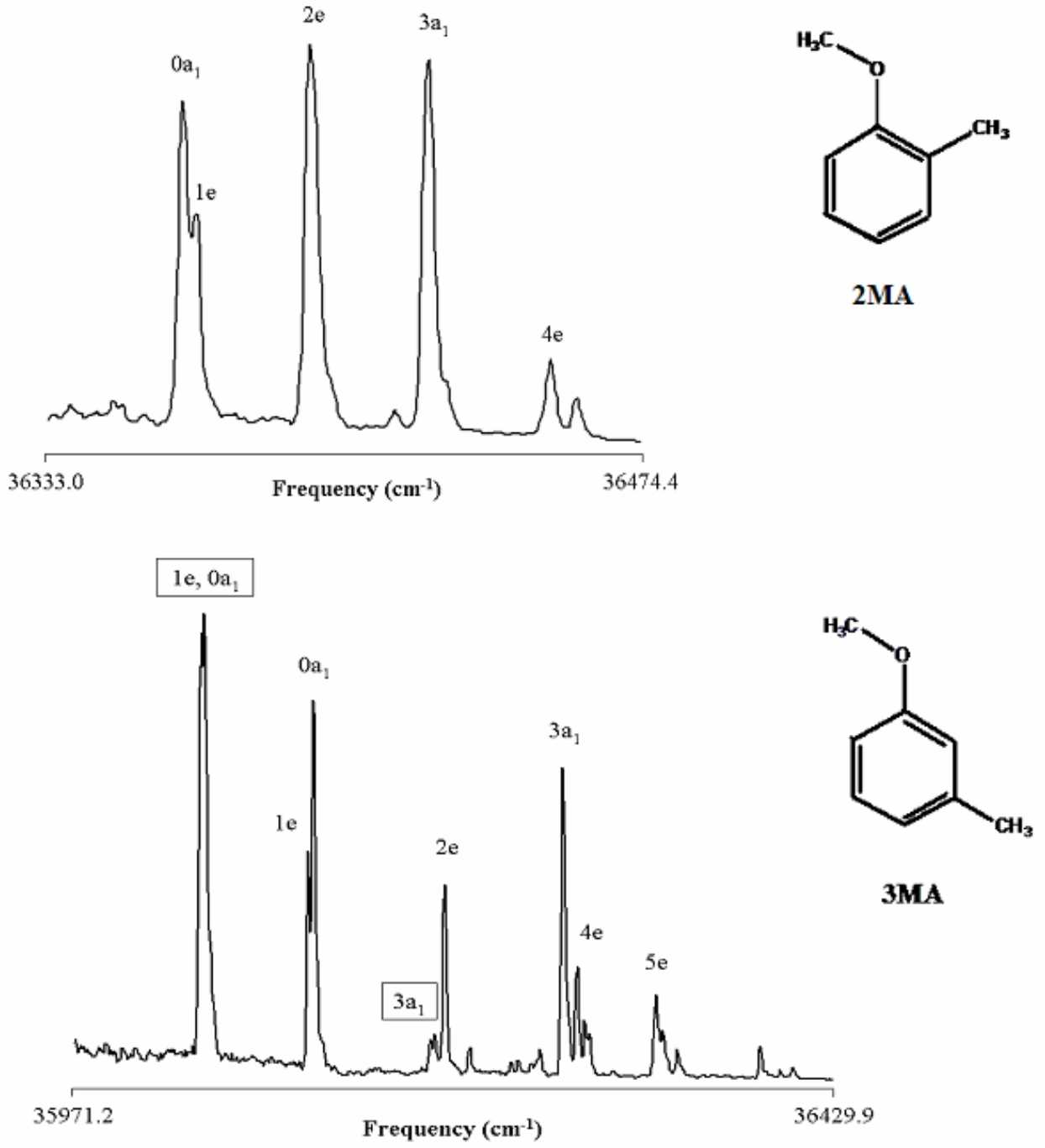


**Figure 5.1. Vibrationally resolved fluorescence excitation spectra of 2MA (top) and 3MA (bottom) in the gas phase. The "boxed" labels refer to bands of the *cis*-conformer.**


**Scheme 5.1. Geometry-optimized structures of *cis*- and *trans*-3MA (MP2/6-31G**).**

We have performed extensive studies of these spectra at high resolution, to test these hypotheses and to provide further information about the ensuing dynamics. Figure 5.2a shows the rotationally resolved $S_1 \leftarrow S_0$ fluorescence excitation spectrum of band $0a_1$ in 2MA. It spans approximately 3.3 $cm^{-1}$ and exhibits *b*-type character, evidencing a near-perpendicular orientation of the $S_1 \leftarrow S_0$ transition moment in the inertial frame. To fit this spectrum, we first generated about 2600 *b*-type rovibronic transitions based on *ab initio*[13] estimates of rotational constants and rigid rotor Hamiltonians for both electronic states. Then, we made quantum number assignments of single transitions in the simulated spectrum to corresponding transitions in the experimental spectrum, using the Windows-based program JB95.[14] Finally, we used a least-squares fitting procedure to optimize the rotational constants, based on a comparison of observed and calculated line positions. The final fit utilized 114 rovibronic transitions, including some weaker *a*-type lines and resulted in a standard deviation of 2.8 MHz. A portion of this fit is shown in Figure 5.2b. Individual lines in the fit exhibit Voigt profiles, with Gaussian widths of 18 MHz and Lorentzian widths of 28 MHz. The rotational temperature of the fit is 4 ± 1 K. The inertial parameters from the fit are reported in Table 5.1.

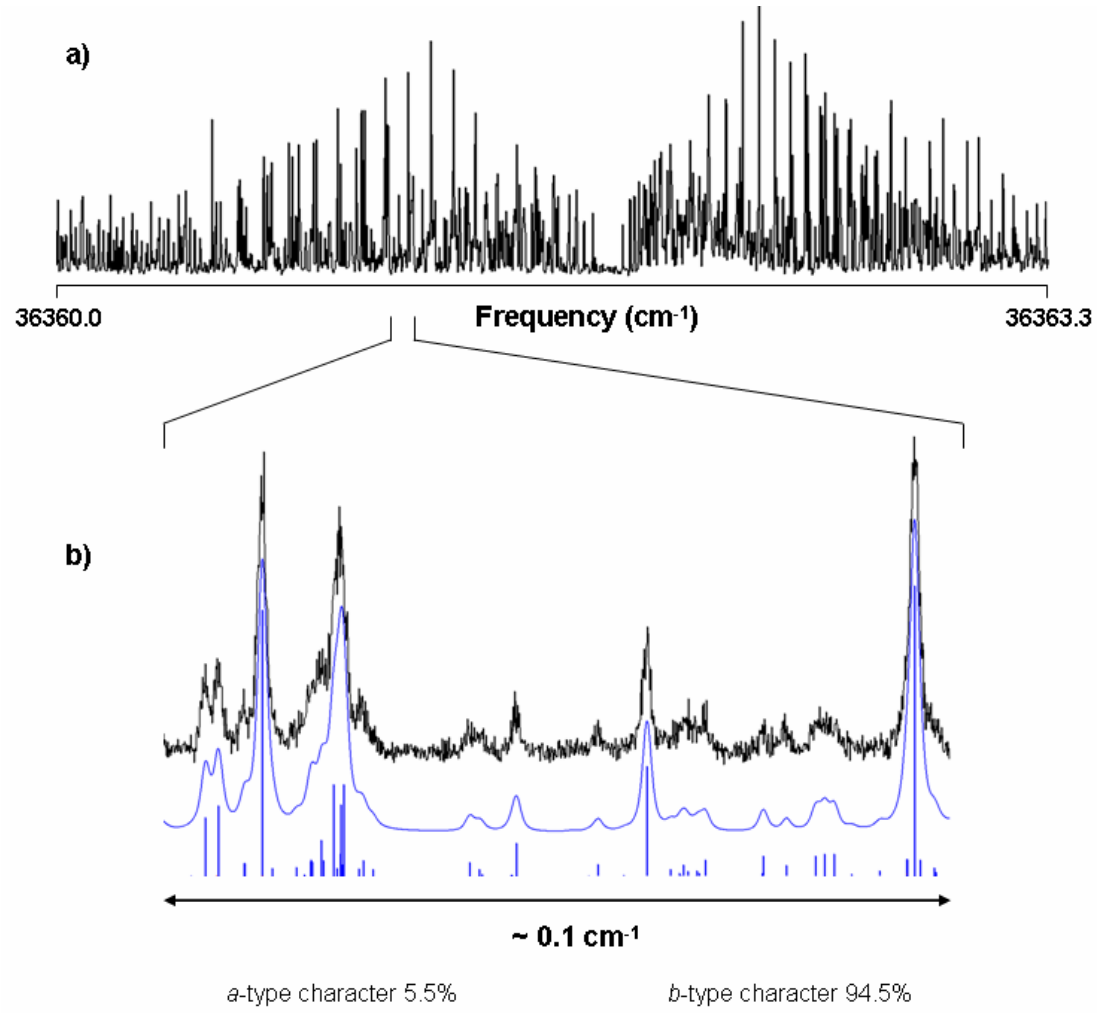


**Figure 5.2. Rotationally resolved fluorescence excitation spectrum band $0a_1$ in 2MA; the origin frequency is at 36361.8 $cm^{-1}$. A portion of the high resolution spectrum at full experimental resolution and its simulated spectrum are also shown in the bottom panel.**

Band 1e was recorded but could not be analyzed. Other higher torsional bands, shown in Figure 5.1a, were analyzed, such as bands 2e and $3a_1$ in 2MA. Figure 5.3a shows the high resolution spectrum of 2MA-2e. Comparison of this spectrum with that in Figure 5.2a shows that band 2MA-2e has a very different structure. It appears to consist of two overlapping sub-bands, as would be expected if band 2MA-2e were in fact an "e-type" transition, and the two sub-bands contained therein ($e_1$ and $e_2$) were split by the torsion-rotation interaction.[15] We therefore attempted to fit the spectrum in Figure 5.3a using the following Hamiltonian for both electronic

**Table 5.1. Rotational constants of *trans*-2-methylanisole in its ground and excited electronic states.[a]**

| Parameter | 2MA-0a$_1$ | 2MA-2e[b] | 2MA-3a$_1$[c] |
|---|---|---|---|
| **$S_0$** | | | |
| ***A″* (MHz)** | 2490.0 (1) | 2490.6 (1) | 2490.1 (1) |
| ***B″* (MHz)** | 1558.9 (1) | 1558.8 (1) | 1558.9 (1) |
| ***C″* (MHz)** | 970.7 (1) | 970.7 (1) | 970.7 (1) |
| **$\Delta I''$ (amu Å$^2$)** | -6.51 (2) | -6.52 (2) | -6.50 (2) |
| **$S_1$** | | | |
| ***A′* (MHz)** | 2407.9 (1) | 2419.2 (1) | 2543.5 (1) |
| ***B′* (MHz)** | 1550.0 (1) | 1569.7 (1) | 1830.9 (1) |
| ***C′* (MHz)** | 951.2 (1) | 952.3 (1) | 954.1 (1) |
| **$\Delta I'$ (amu Å$^2$)** | -4.64 (2) | -0.14 (2) | 54.98 (3) |
| **TM angle to the *b*-inertial axis** | 14 (2)° | 14 (2)° | 25 (2)° |

[a] Numbers in parentheses are the standard deviations of the last significant figure.
[b] See Table 5.5 for additional information about the first order torsion-rotation perturbation coefficients that were used in the fit.
[c] The following *A*-reduced Watson centrifugal distortion terms were applied to the $S_1$ state; $\Delta_J' = -0.10$, $\Delta_{JK}' = 0.15$, $\Delta_K' = -0.14$, $\delta_J' = 0.05$, $\delta_K' = 0.33$ MHz.

states

$$H_{eff}^{E} = A_E P_a^2 + B_E P_b^2 + C P_c^2 + F W_E^{(1)} \left( \rho_a P_a + \rho_b P_b \right) \tag{5.1}$$

here, $A_E$, and so forth, are the effective rotational constants given by

$$A_E = A + F W_E^{(2)} \rho_a^2, \quad B_E = B + F W_E^{(2)} \rho_b^2 \tag{5.2}$$

$F$ is the internal rotor constant, $W_E^{(1)}$ and $W_E^{(2)}$ are the first- and second-order perturbation terms, first written down by Herschbach,[16] and $\rho_a$ and $\rho_b$ are weighted direction cosines of the angle between the axis of internal rotation and the *a*- and *b*-inertial axes of the molecule, $\rho_a = \lambda_a \left( I_\alpha / I_a \right)$, and so forth. $I_\alpha$ is the moment of inertia of the methyl group, and $r$ is a reduction factor

$$r = 1 - \sum \frac{\lambda_g^2 I_\alpha}{I_g}, \quad g = a,b,c\,. \tag{5.3}$$

This fit showed excellent agreement with experiment, the OMC obtained was 3.8 MHz; see Figure 5.3b. The Gaussian linewidth in 2MA-2e is 18 MHz, the Lorentzian linewidth is 28 MHz,

and the rotational temperature is 6 K. The inertial parameters obtained from this fit are listed in Table 5.1.

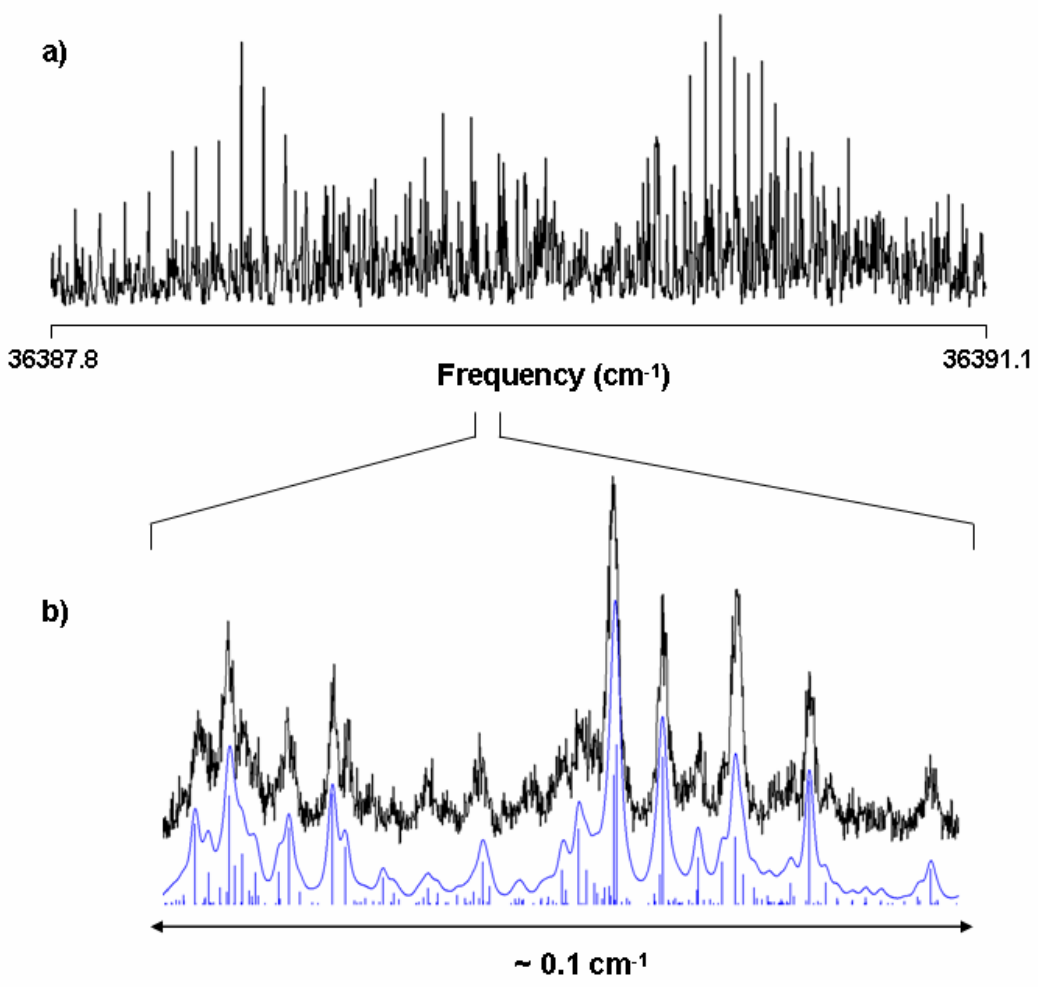


**Figure 5.3. Rotationally resolved fluorescence excitation spectrum band 2e in 2MA; the origin of frequency is at 36389.7 $cm^{-1}$. A portion of the *P* branch is also shown in the bottom panel.**

Figure 5.4a shows the high resolution spectrum of 2MA-$3a_1$. The fitting procedure for its analysis was analogous to that used for the 2MA-$0a_1$ band. Using rigid rotor Hamiltonians for both electronic states, a simulated spectrum was generated and more than 200 rovibronic simulated lines were assigned to experimental transitions, yielding an OMC of ~20 MHz. This was reduced substantially to 3.9 MHz by including Watson distortion terms[17] for the $S_1$ state.

The $3a_1$ level lies above the torsional barrier in the $S_1$ state, but no torsion-rotation perturbations were observed which is consistent with the assignment of band 2MA-$3a_1$ as an $a_1$ band. This band has a Gaussian linewidth of 18 MHz, a Lorentzian linewidth of 30 MHz, and a rotational temperature of 4.5 K. Table 5.1 lists the inertial parameters obtained from the experimental fit of this band.

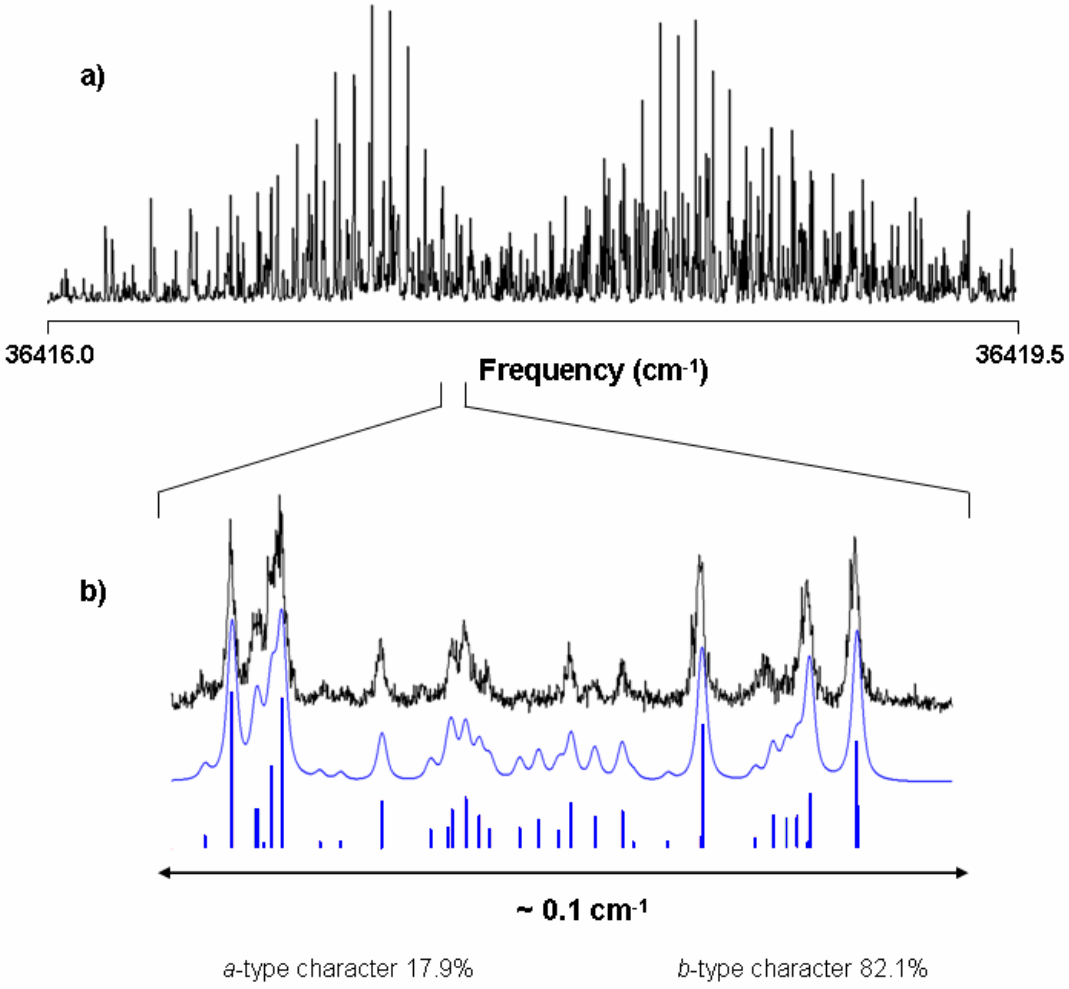


**Figure 5.4. Rotationally resolved fluorescence excitation spectrum band $3a_1$ in 2MA; the origin frequency is at 36417.7 $cm^{-1}$. Portions of the high resolution spectrum at full experimental resolution and its simulated spectrum are also shown in the bottom panel.**

Figure 5.5a shows the high resolution spectrum of the lowest energy observed bands in 3MA, the "boxed" 3MA-$1e,0a_1$ band in Figure 5.1b. It spans approximately 6.6 $cm^{-1}$ and

displays two spectra on top of each other, as illustrated in Figure 5.5b. The blue-shifted spectrum was fit using effective rigid rotor Hamiltonians for both states, which argues in favor of its assignment as the $0a_1$ transition. However, the red-shifted band required first-order perturbation

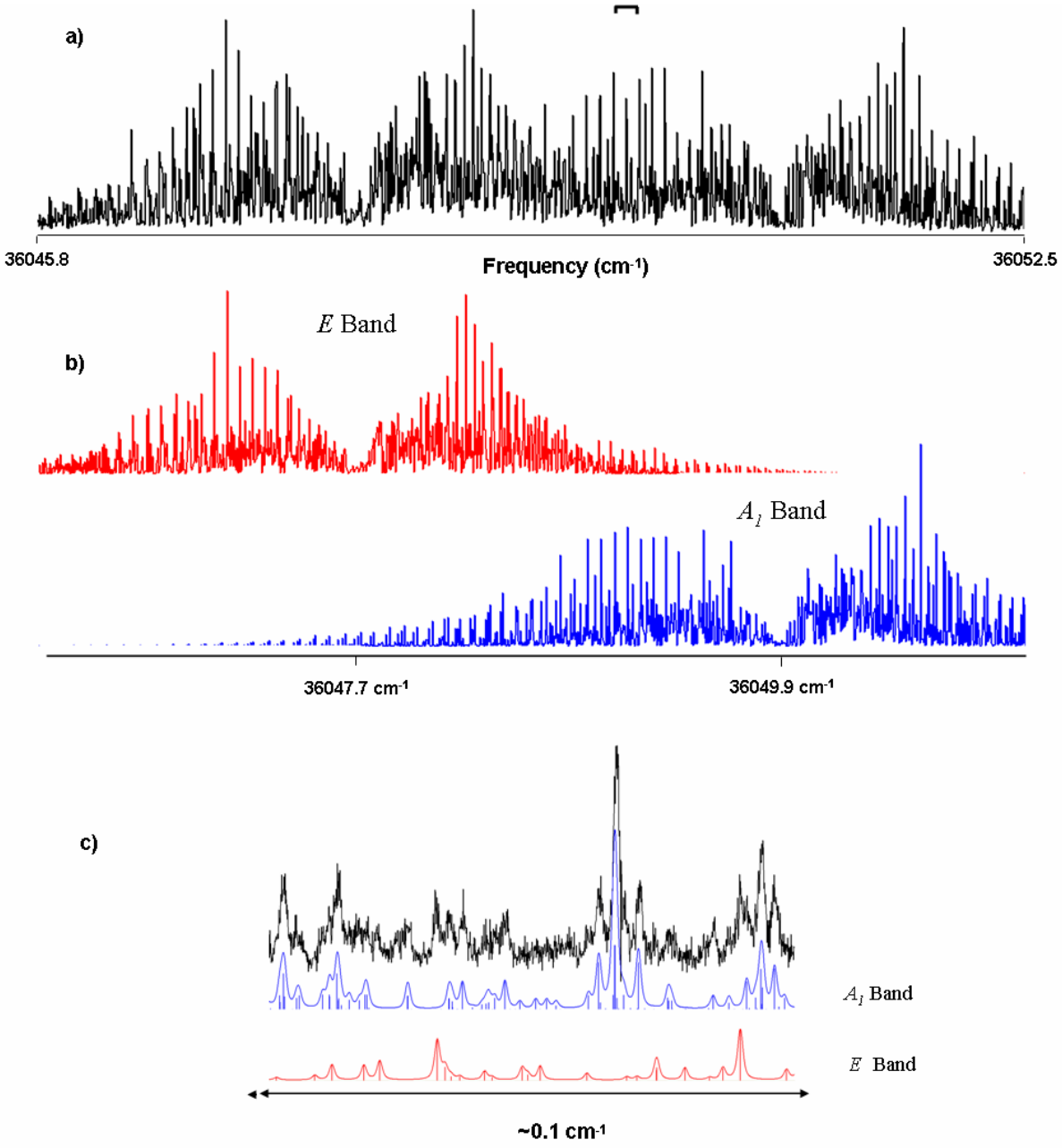


**Figure 5.5. (a) Rotationally resolved fluorescence excitation spectrum of the *cis*-3MA-1e,$0a_1$ band. (b) Two simulated spectra ($A_1$ and $E$ bands) are required to fit the experimental spectrum; the origin frequencies of each simulated spectrum are labeled in the horizontal axis. (c) A portion (see part a) of the fully resolved experimental spectrum and the detailed contribution of $A_1$- and $E$-type simulated rovibronic lines.**

terms for its analysis, which argues in favor of its assignment as the 1e transition. Figure 5.5c shows a portion of the high resolution spectrum at full experimental resolution at the overlap region to illustrate the quality of the fit. The OMC of the fits are 2.4 MHz for the $0a_1$ band and 3.1 MHz for the 1e band. The Gaussian linewidth is 18 MHz and the Lorentzian linewidth is 22 MHz for both bands. The inertial parameters for both spectra are reported in Table 5.2.

**Table 5.2. Rotational constants of *cis*-3-methylanisole in its ground and excited electronic states.[a]**

| Parameter | 3MA-1e[b] | 3MA-$0a_1$ |
|---|---|---|
| $S_0$ | | |
| $A''$ (MHz) | 2752.0 (1) | 2766.7 (1) |
| $B''$ (MHz) | 1292.5(1) | 1297.5 (1) |
| $C''$ (MHz) | 890.7(1) | 890.7 (1) |
| $\Delta I''$ (amu Å$^2$) | -7.22 (2) | -4.76 (4) |
| $S_1$ | | |
| $A'$ (MHz) | 2676.4 (2) | 2677.4 (1) |
| $B'$ (MHz) | 1279.2 (2) | 1279.6 (1) |
| $C'$ (MHz) | 875.7 (1) | 875.8 (1) |
| $\Delta I'$ (amu Å$^2$) | -6.79 (2) | -6.64 (4) |
| TM angle to the *b*- inertial axis | 28 (2)° | 25 (2)° |

[a] Numbers in parentheses are the standard deviations of the last significant figure.
[b] See Table 5.5 for additional information about the first order torsion-rotation perturbation coefficients that were used in the fit.

Figure 5.6a shows the high resolution spectrum of the band labeled 3MA-$0a_1$ in Figure 5.1b. This spectrum spans ~3.7 cm$^{-1}$ and its origin is located at 36115.5 cm$^{-1}$. Rigid rotor Hamiltonians were found to be adequate to fully analyze this band; neither distortion terms nor perturbation coefficients were required. This confirms its assignment as an $a_1$ band. In the final fit, approximately 176 rovibronic lines were assigned and resulted in a standard deviation of 3.1 MHz. The Gaussian linewidth is 18 MHz, the Lorentzian linewidth is 20 MHz, and the rotational temperature is 5 K. The inertial parameters from the fit are listed in Table 5.3.

The 3MA bands labeled "1e" and "2e" in Figure 5.1b were both observed in our high resolution experiments, located at 36111.6 and 36193.6 $cm^{-1}$, respectively. Both bands were confirmed to be "e-type" bands as each is split by torsion-rotation coupling. Unfortunately, we have not yet succeeded in completely analyzing either of these bands; they are significantly perturbed, and exhibit low signal-to-noise. Nonetheless, we can confirm that the origin of the 1e band is red shifted by 3.9 $cm^{-1}$ from $0a_1$ and that 2e is blue shifted by 82.0 $cm^{-1}$ from $3a_1$, as observed by IS.[7]

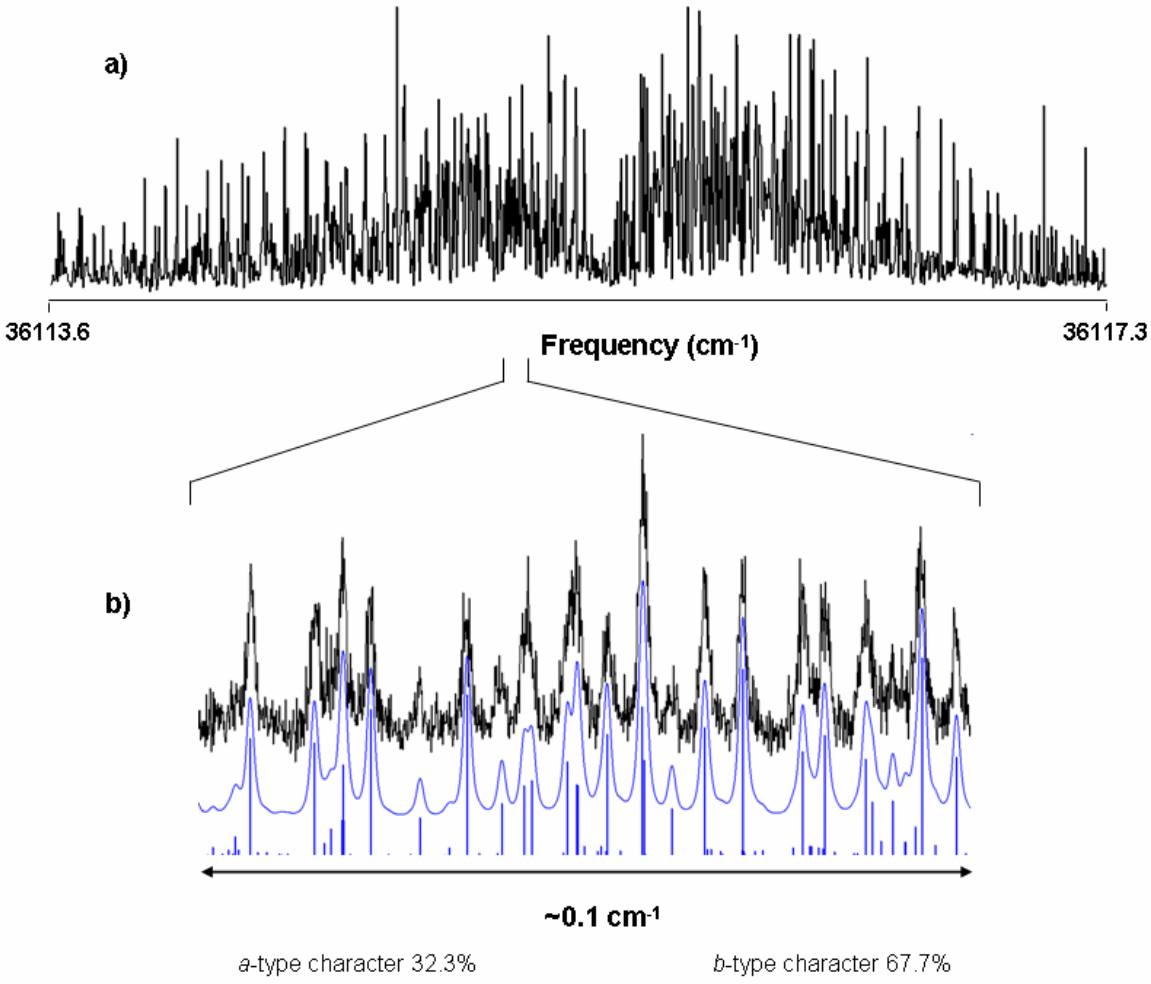


**Figure 5.6. Rotationally resolved fluorescence excitation spectrum of the *trans*-3MA-$0a_1$ band; the origin frequency is at 36115.5 $cm^{-1}$. Portions of the high resolution spectrum at full experimental resolution and its simulated spectrum are also shown at the bottom panel.**

Finally, Figure 5.7a shows the high resolution spectrum of 3MA-3$a_1$, located at 36264.3 $cm^{-1}$. It spans ~4.7 $cm^{-1}$ and has a congested *Q* branch. Effective rigid rotor Hamiltonians were used to fit this band; no Watson distortion terms or first-order perturbation terms were required in the Hamiltonians to fit the spectrum. In the final fit, the convoluted spectrum showed mainly *b*-type rovibronic transitions but included some weaker *a*-type lines. Approximately 250 transitions were assigned and resulted in a standard deviation of 4.0 MHz. Figure 5.7b shows a portion of the *R* branch at full experimental resolution to illustrate the quality of the fit. The Gaussian linewidth is 18 MHz, the Lorentzian linewidth is 20 MHz and the rotational temp. is 8 K. Table 5.3 lists the inertial parameters obtained from the fit of this higher torsional band.

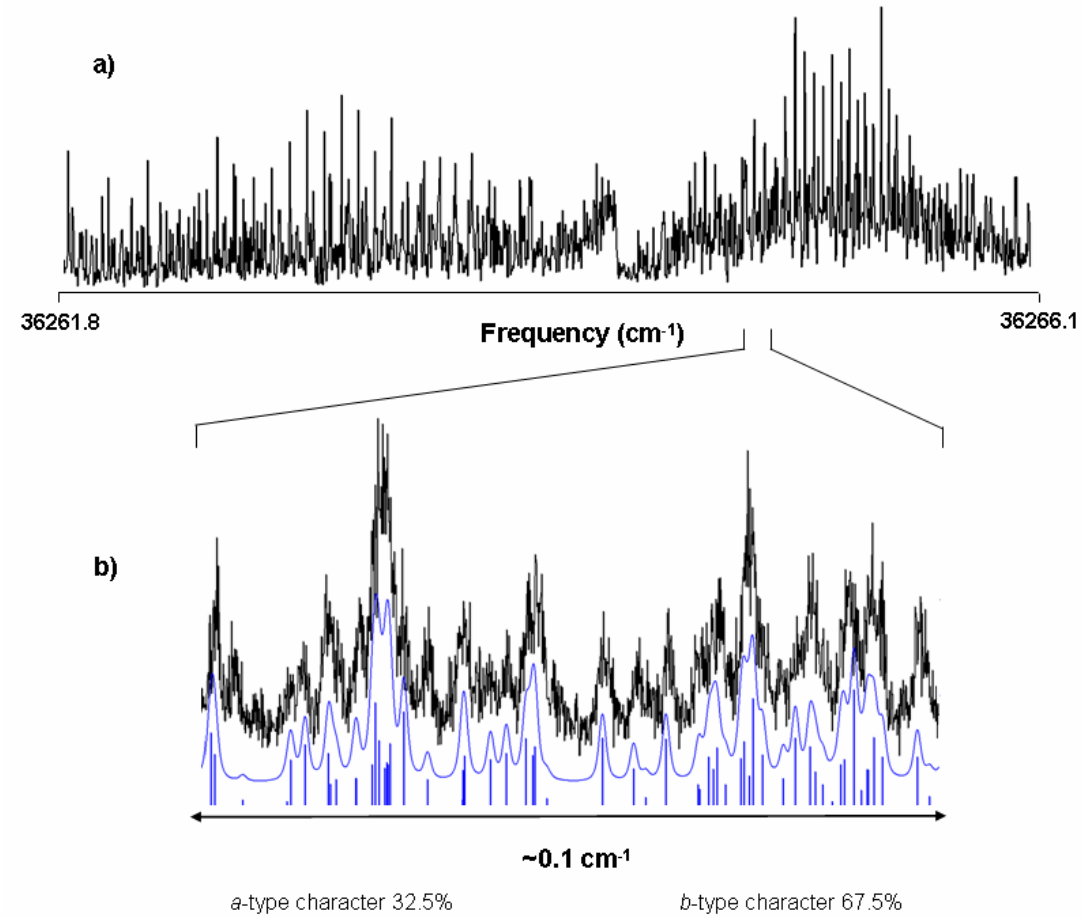


**Figure 5.7. Rotationally resolved fluorescence excitation spectrum of the *trans*-3MA-3$a_1$ band; the origin frequency is at 36264.3 $cm^{-1}$. Portions of the high resolution spectrum at full experimental resolution and its simulated spectrum are also shown in the bottom panel.**

**Table 5.3. Rotational constants of *trans*-3-methylanisole in its ground and excited electronic states.[a]**

| Parameter | 3MA-0$a_1$ | 3MA-3$a_1$ |
|---|---|---|
| **$S_0$** | | |
| ***A″* (MHz)** | 3573.1 (1) | 3572.4 (1) |
| ***B″* (MHz)** | 1124.2 (1) | 1124.1 (1) |
| ***C″* (MHz)** | 861.1 (1) | 861.1 (1) |
| **$\Delta I''$ (amu Å$^2$)** | -4.06 (2) | -4.13 (1) |
| **$S_1$** | | |
| ***A′* (MHz)** | 3406.5 (1) | 3554.4 (2) |
| ***B′* (MHz)** | 1111.3 (1) | 1114.2 (2) |
| ***C′* (MHz)** | 847.2 (1) | 846.5 (1) |
| **$\Delta I'$ (amu Å$^2$)** | -6.62 (2) | 1.26 (1) |
| **TM angle to the *b*-inertial axis** | 34 (2)° | 35 (2)° |

[a] Numbers in parentheses are the standard deviations of the last significant figure.

## 5.5 DISCUSSION

### 5.5.1 Ground state conformers

Table 5.4 compares the ground state rotational constants of the origin ($0a_1 \leftarrow 0a_1$) bands obtained from our fits with the corresponding theoretical values for the *cis*- and *trans*-conformers of 2MA, and 3MA. The data clearly show that the *cis*-2MA conformer was not present in our experiments. Therefore, we assign all the spectral features in Figure 5.1a to the *trans*-2MA conformer. On the other hand, both *cis*- and *trans*-conformers were present in our experiments on 3MA; we assign the "boxed" 3MA-1e,$0a_1$ band in Figure 5.1b to the *cis*-3MA conformer, whereas the bands 3MA-$0a_1$ and 3MA-$3a_1$ are assigned to the *trans*-3MA conformer.

**Table 5.4. Experimental and theoretical ground state rotational constants from the fits of the origin bands ($0a_1 \leftarrow 0a_1$) of *trans*-2MA, *cis*-3MA and *trans*-3MA.**

| Rotational Constant | *trans*-2MA | | *cis-2MA* | *cis*-3MA | | *trans*-3MA | |
|---|---|---|---|---|---|---|---|
| | fit | theory[a] | theory[b] | fit | theory[a] | fit | theory[a] |
| ***A″* (MHz)** | 2490.0 | 2494.1 | 3333.3 | 2766.7 | 2752.1 | 3573.1 | 3532.3 |
| ***B″* (MHz)** | 1558.9 | 1556.8 | 1461.7 | 1297.5 | 1295.2 | 1124.2 | 1121.8 |
| ***C″* (MHz)** | 970.7 | 970.2 | 1029.2 | 890.7 | 890.5 | 861.1 | 860.6 |

[a] Geometry optimization calculation (MP2/6-31G**)
[b] Single point calculation (MP2/6-31G*)

Differences among the ground state rotational constants may be easily understood. Figure 5.8 shows projections of the three geometry optimized[13] conformer structures in the *ab* plane, in their ground states. In *trans*-2MA, the *A″* rotational constant is the smallest of the three because the methyl group is maximally displaced from the *a*-inertial axis, whereas the *A″* rotational constant of the *trans*-3MA conformer is the largest among the three species because most of its heavy atoms lie close to the *a*-axis. *cis*-3MA is intermediate in this regard. The *B″* and *C″* rotational constants are similarly unique; *trans*-2MA has the largest *B″* and *C″*, whereas *trans*-3MA has the smallest *B″* and *C″*. The inertial defect values ($\Delta I = I_c - I_a - I_b$) of each conformer are expected to be near -6.6 amu Å$^2$; 2MA and 3MA should be planar structures in their $S_0$ state, with four out-of-plane hydrogen atoms, two from the methyl group and two from the methoxy group. However, the experimental values (see Tables 5.1, 5.2, and 5.3) are different; *trans*-2MA has $\Delta I''$ = -6.51 amu Å$^2$, but *cis*-3MA has $\Delta I''$ = -4.76 and *trans*-3MA has $\Delta I''$ = -4.06 amu Å$^2$. As will be seen, these deviations from experiment signal large motion along the methyl group torsional coordinate.

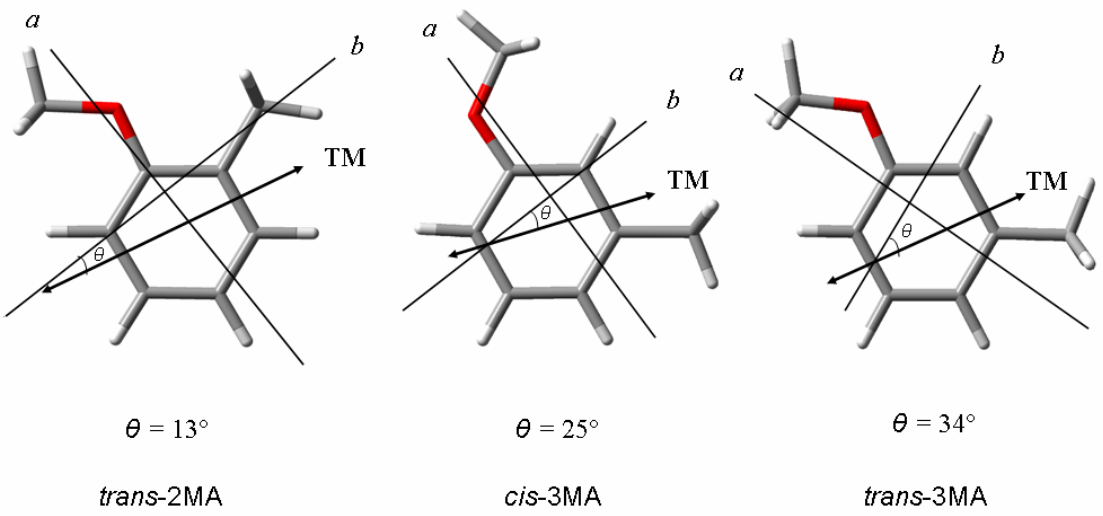


**Figure 5.8. Inertial axes and $S_1 \leftarrow S_0$ TM orientation vectors in the experimentally observed *cis*- and *trans*- conformers of 2MA and 3MA.**

### 5.5.2 Excited state conformers

Also shown in Figure 5.8 are the experimentally determined orientations of the $S_1 \leftarrow S_0$ transition moment (TM) vectors in the inertial frames of the three observed conformers of 2MA and 3MA. Immediately apparent is the fact that the observed TM vectors are approximately perpendicular to the C–O bond of the attached methoxy group, in all three cases. (Small differences in these orientation angles presumably have their origins in small rotations of the in-plane inertial axes by the attached methyl groups.) We conclude from this observation that the $S_1 \leftarrow S_0$ transition in both 2MA and 3MA is "anisole-like"; that is, the $S_1 \leftarrow S_0$ transitions in all three conformers are principally HOMO-LUMO in nature, and the nodal planes of these MOs are either parallel or perpendicular to the C–O bond. This has been confirmed by CIS calculations.[13]

The $S_1$ state of anisole is quinoidal in shape, expanded relative to the ground state, but with shorter "parallel" C–C bonds than perpendicular ones.[5,18,19] Thus, the three rotational constants $A'$, $B'$, and $C'$ are all less than those of the ground state, but $\Delta A = (A' - A'') = -233$ MHz is by far the largest in magnitude. The same is true for all three observed conformers of 2MA and 3MA; *trans*-3MA has by far the largest value, $\Delta A = -167$ MHz. So, just as in anisole itself, there is significant charge transfer from the oxygen lone pairs of the methoxy group to the aromatic ring when both 2MA and 3MA absorb light.

### 5.5.3 Methyl torsional barriers

Despite the transfer of electrons from the oxygen atom to the ring, there is little or no torsional activity in the $S_1 \leftarrow S_0$ spectrum of anisole, presumably because of hyperconjugative interactions of the (methoxy) methyl group and the "in-plane" oxygen lone pair electrons. Charge transfer is expected to involve the "out-of-plane" oxygen lone pair. Thus, assuming the same to be true in 2MA and 3MA, the low frequency activity in their $S_1 \leftarrow S_0$ spectra must have its origin in the motion of the attached methyl groups. We focus on this issue here.

Table 5.5 lists the torsional parameters $D_g$ ($= FW_E^{(1)}\rho_g P_g$, $g = a,b,c$), obtained from the fits of the 2e band in *trans*-2MA and the 1e band in *cis*-3MA. By the use of Herschbach's tables,[16] the reduced barriers ($s$) and the corresponding 3-fold barriers $V_3$ ($= \frac{9}{4} F \cdot s$) were determined. Small torsion-rotation terms were found for *trans*-2MA ($D_a'' = 4.6$ and $D_b'' = 16.3$ MHz) in its $S_0$ state, which results in a relatively small first-order perturbation coefficient ($W_E^{(1)} = 0.008$), and by interpolation, a relatively large reduced barrier height of 27.879 ($V_3'' = 345.00$ cm$^{-1}$). A similar procedure was followed for the $S_1$ state, obtaining the much

**Table 5.5. First-order torsion-rotation perturbation coefficients in the Hamiltonian and reduced barrier heights for selected *e*-symmetry torsional bands in 2MA and 3MA.[a]**

| Parameter | *trans*-2MA-2e band | *cis*-3MA-1e band |
|---|---|---|
| | Ground State ($S_0$) | |
| $D_a''$ (MHz) | 4.6 (16) | 1119.5 (3) |
| $D_b''$ (MHz) | 16.3 (24) | 667.4 (1) |
| $W^{(1)}''$ | 0.008 | 0.647 |
| $s''$ | 27.879 | 4.685 |
| $V_3''$ ($cm^{-1}$) | 345.00 | 57.07 |
| $V_6''$ ($cm^{-1}$) | -5.00 | 2.00 |
| $F''$($cm^{-1}$) | 5.50 | 5.46 |
| | Excited State ($S_1$) | |
| $D_a'$ (MHz) | -2120.0 (1) | 61.9 (3) |
| $D_b'$ (MHz) | -3970.2 (1) | 44.8 (30) |
| $W^{(1)}'$ | 2.531 | 0.038 |
| $s'$ | 3.020 | 17.195 |
| $V_3'$ ($cm^{-1}$) | -36.90 | 209.47 |
| $V_6'$ ($cm^{-1}$) | -2.76 | -26.00 |
| $F'$ ($cm^{-1}$) | 5.43 | 5.51 |

[a] Numbers in parentheses are the standard deviations of the last significant figure.

smaller barrier height of $V_3' = -36.90$ $cm^{-1}$, a value 10 times smaller than that computed for $V_3''$ [Appendix B contains the code used to determine the barrier heights in both electronic states]. Interestingly, *cis*-3MA exhibits the opposite behavior; its torsion-rotation terms are large in the ground state but small in the excited state, resulting in barriers of $V_3'' = 57.07$ $cm^{-1}$ and $V_3' = 209.47$ $cm^{-1}$. The latter result perfectly agrees with the observation that the 1e transition in *cis*-3MA is red shifted from the $0a_1$ one. For the *trans*-3MA conformer, a different approach was used to determine the methyl torsional barriers. In this case, we performed an absolute frequency (energy) study to match the energy level spacings observed in our high resolution spectra. From those differences, the $V_3$, $V_6$, and $F$ parameters were fit, $V_3'' = 30.35$ $cm^{-1}$ and $V_3' = -225.70$ $cm^{-1}$. The corresponding potential energy surfaces for the three conformers studied are shown in Figures 5.9 – 5.11. The results for the *trans*-2MA and *trans*-3MA conformers are in close

agreement with the ones obtained by IS.[7]

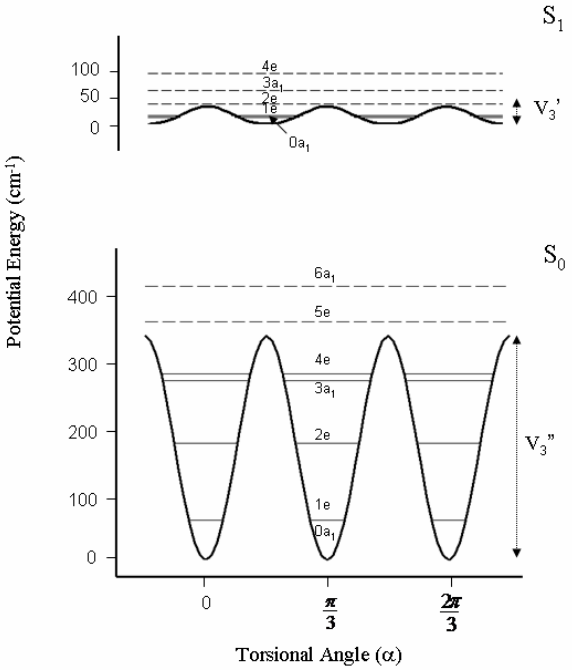


| *Parameter* | *Value ($cm^{-1}$)* |
|---|---|
| $V_3$ | - 36.90 |
| $V_6$ | -2.76 |
| F | 5.43 |

| *Parameter* | *Value ($cm^{-1}$)* |
|---|---|
| $V_3$ | 345.00 |
| $V_6$ | -5.00 |
| F | 5.50 |

**Figure 5.9. Torsional energy surfaces of *trans*-2MA. The torsional parameters from the fit are included in tables for both electronic states.**

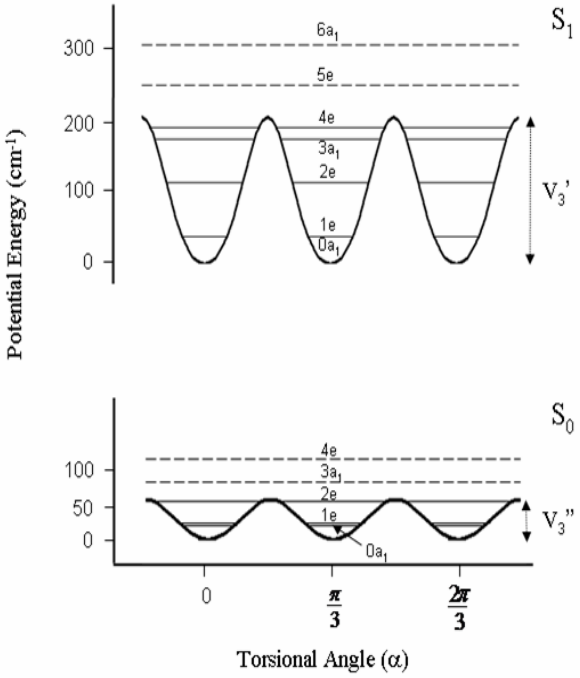


| *Parameter* | *Value ($cm^{-1}$)* |
|---|---|
| $V_3$ | 209.47 |
| $V_6$ | -26.00 |
| F | 5.51 |

| *Parameter* | *Value ($cm^{-1}$)* |
|---|---|
| $V_3$ | 57.07 |
| $V_6$ | 2.00 |
| F | 5.46 |

**Figure 5.10. Torsional energy surfaces for *cis*-3MA. The torsional parameters from the fit are included in tables for both electronic states.**

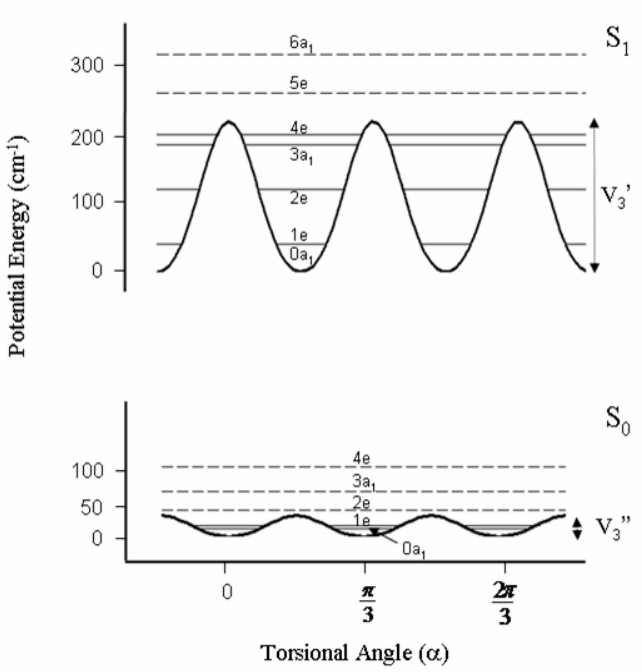


| Parameter | Value ($cm^{-1}$) |
|---|---|
| $V_3$ | -225.70 |
| $V_6$ | -24.45 |
| F | 5.51 |

| Parameter | Value ($cm^{-1}$) |
|---|---|
| $V_3$ | 30.35 |
| $V_6$ | 2.00 |
| F | 5.47 |

**Figure 5.11.Torsional energy surfaces of *trans*-3MA. The torsional parameters from the fit are included in tables for both electronic states.**

The significant differences in the ground state barriers, the excited state barriers, and the preferred orientation of the methyl groups among the three conformers have their origin in the relative positions of the substituents (S) attached to the aromatic ring, see Scheme 5.2 below.

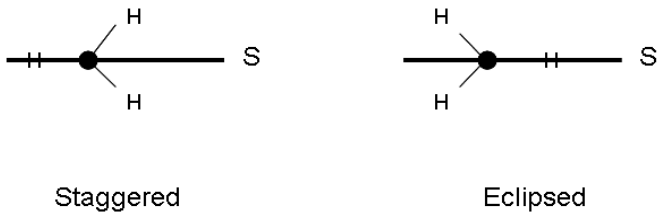


**Scheme 5.2. Relative configurations of the methyl group with respect to the other substituent (S).**

According to theory,[13] the eclipsed configuration of the methyl group is more stable in $S_0$ *trans*-2MA, presumably due to the mesomeric effect. The $C_1$–$C_2$ bond is expected to have higher double bond character than $C_2$–$C_3$. However, excitation of 2MA to its $S_1$ state increases the $\pi$-character of the $C_2$–$C_3$ bond, owing to the quinoidal distribution of the ring. This explains both

the dramatic reduction of $V_3$ on absorption of light and the conformational change of the methyl group, from the eclipsed to the staggered configuration. Apparently, the $C_2$–$C_3$ bond in *trans*-2MA has slightly more double bond character than the $C_1$–$C_2$ bond, in the $S_1$ state.[21, 22]

The most stable configurations in ground state *cis*-3MA and *trans*-3MA are eclipsed and staggered, respectively; here, the relative orientation of the methoxy group determines which of the adjacent C–C ring bonds is strengthened by the mesomeric effect. Since *cis*-3MA has an eclipsed methyl group in its $S_0$ state, excitation of this state will only increase the magnitude of $V_3$, and not change its sign. No conformational change is observed. In contrast, *trans*-3MA has a staggered methyl group in its $S_0$ state, so that excitation by light changes both the barriers and its sign, resulting in a change of the preferred orientation of the methyl group.

The most remarkable consequences of these changes are the differences in relative intensities among the torsional bands and the Franck-Condon (FC) activity in the low frequency region of the vibrationally resolved spectra. *trans*-2MA shows FC activity and its $A/E$ intensity ratio[23] is about 2; the origin is not the most intense transition in the $S_1 \leftarrow S_0$ spectrum. On the other hand, *cis*-3MA exhibits a strong origin band, no FC activity, and an $A/E$ intensity ratio of about 1; whereas *trans*-3MA shows FC activity and an $A/E$ intensity ratio near 2. These results are summarized in Figure 5.12.

A final unanticipated result of these experiments is the discovery that the inertial defects of the three observed conformers of 2MA and 3MA are markedly influenced by the torsional motion of the methyl group. Recall from Table 5.1 that $\Delta I'' = -6.51$ amu Å$^2$ for *trans*-2MA in its ground state and $\Delta I' = -4.64$ amu Å$^2$ in the zero-point vibrational level of its excited electronic state. The larger (in magnitude) value is that expected for four out-of-plane hydrogen atoms, two from the methoxy group and two from the methyl group, whereas the smaller value is

unexpected. In *cis*- and *trans*-3MA, this behavior is reversed; both molecules exhibit larger $\Delta I$ values in the excited state, and smaller $\Delta I$ values in the ground state. The smaller values must signal transition to less "localized" methyl group C–H bonds, owing to the onset of essentially free internal rotation. Toluene, a molecule having a methyl group with similar properties, has $\Delta I$ values of -0.187 and 0.029 amu Å$^2$ in its $S_0$ and $S_1$ electronic states, respectively.[4] Still more surprising are the excited state $\Delta I$ values for the two higher energy vibronic bands in *trans*-2MA, -0.14 amu Å$^2$ for the 2e band and 54.98 amu Å$^2$ for the $3a_1$ band. The latter value may signal a large in-plane distortion of the isolated molecule.

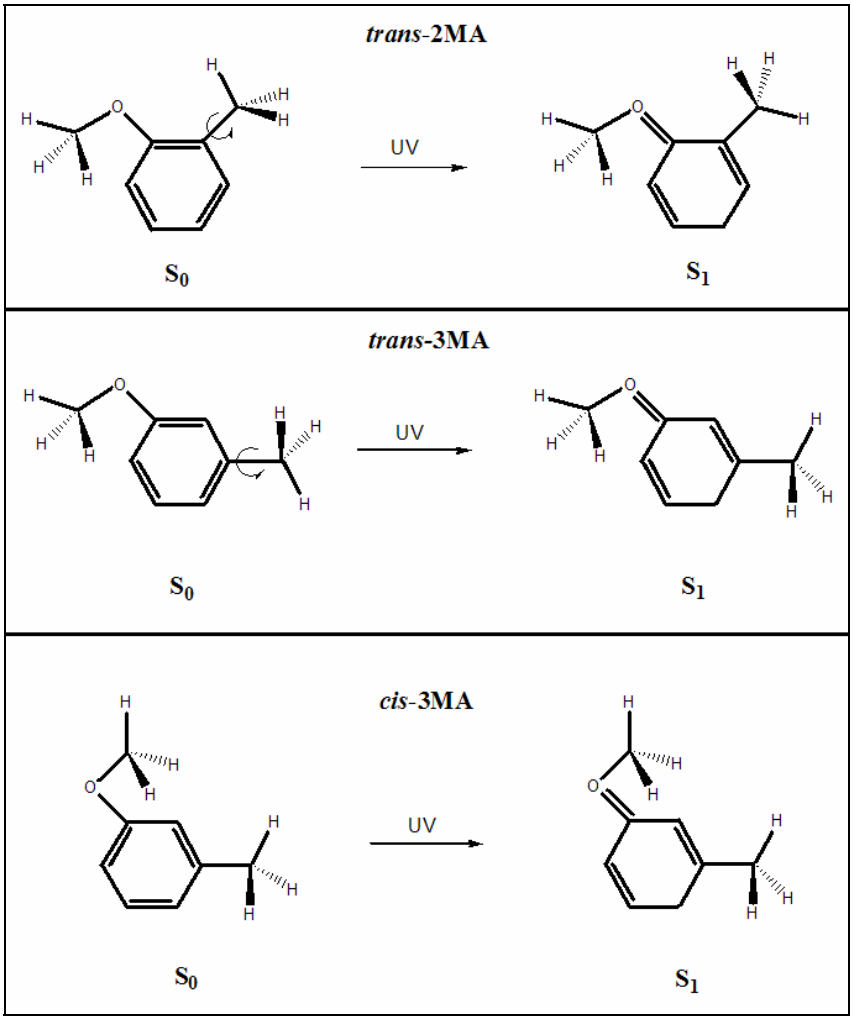


**Figure 5.12. Most stable conformers of 2MA and 3MA in the gas phase.**

## 5.6 SUMMARY

Rotationally resolved $S_1 \leftarrow S_0$ fluorescence excitation spectra of three conformers of 2- and 3-methylanisole reveal that the position of substitution of the methoxy group on the aromatic ring determines the preferred orientation and torsional barrier height of the attached methyl group. The relative position of the two groups also has a major influence on the torsional dynamics. Comparisons of the results for the different electronic states show that these effects have their origin in substituent-induced differences in the $\pi$-electron distributions in the aromatic ring.

## 5.7 ACKNOWLEDGMENTS

We thank Dr. David R. Borst, Dr. Cheolhwa Kang, and Dr. W. Leo Meerts for helpful assistance and suggestions. This work has been supported by NSF (CHE-0315584).

## 5.8 REFERENCES AND NOTES

1. (a) Kemp, J. D.; Pitzer, K. S. *J. Chem. Phys*. **1936**, 4, 749. (b) Kemp, J. D.; Pitzer, K. S. *J. Am. Chem. Soc.* **1937**, 59, 276.

2. Pophristic, V.; Goodman, L. *Nature* **2001**, 411, 565 and references therein.

3. For a review, see Spangler, L. H.; Pratt, D. W. in *Jet Spectroscopy and Molecular Dynamics*; edited by Hollas, J. M.; Phillips, D., Ed.; Chapman & Hall: London, **1995**; pp 366-398 and references therein.

4. Borst, D. R.; Pratt D. W. *J. Chem. Phys.* **2000**, 113, 3658.

5. Ribblett, J. W.; Sinclair, W. E.; Borst, D. R.; Yi, J. T.; Pratt, D. W. *J. Phys. Chem. A*. **2006,** 110, 1478.

6. Breen, P. J.; Bernstein, E. R.; Secor, H. V.; Seeman, J. I. *J. Am. Chem. Soc.* **1989,** 111, 1958.

7. Ichimura, T.; Suzuki, T. *J. Photochem. Photobiol. C* **2000,** 1, 79.

8. Kojima, H.; Miyake, K.; Sakeda, K.; Suzuki, T.; Ichimura, T.; Tanaka, N.; Negishi, D.; Takayanagi, M.; Hanazaki, I. *J. Mol. Struct.* **2003**, 665, 185.

9. Kinoshita, S.; Kojima, H.; Suzuki, T.; Ichimura, T.; Yoshida, K.; Sakai, M.; Fujii, M. *Phys. Chem. Chem. Phys*. **2001**, 3, 4889.

10. Nakai, H.; Kawai, M. *J. Chem. Phys*. **2000**, 113, 2168.

11. Del Rio, A.; Boucekkine, A.; Meinnel, J. *J. Comput. Chem*. **2003**, 24, 2093.

12. Majewski, W. A.; Pfanstiel, J. F.; Plusquellic, D. F.; Pratt D. W. *Laser Techniques in Chemistry*. Rizzo T. R., Myers A. B., Eds. J. Wiley & Sons: New York, **1995**, pp 101.

13. Frisch, M. J.; Trucks, G. W.; Schlegel, H. B.; Scuseria, G. E.; Robb, M. A.; Cheeseman, J. R.; Montgomery, J. A., Jr.; Vreven, T.; Kudin, K. N.; Burant, J. C.; Millam, J. M.; Iyengar, S. S.; Tomasi, J.; Barone, V.; Mennucci, B.; Cossi, M.; Scalmani, G.; Rega, N.; Petersson, G. A.; Nakatsuji, H.; Hada, M.; Ehara, M.; Toyota, K.; Fukuda, R.; Hasegawa, J.; Ishida, M.; Nakajima, T.; Honda, Y.; Kitao, O.; Nakai, H.; Klene, M.; Li, X.; Knox, J. E.; Hratchian, H. P.; Cross, J. B.; Adamo, C.; Jaramillo, J.; Gomperts, R.; Stratmann, R. E.; Yazyev, O.; Austin, A. J.; Cammi, R.; Pomelli, C.; Ochterski, J. W.; Ayala, P. Y.; Morokuma, K.; Voth, G. A.; Salvador, P.; Dannenberg, J. J.; Zakrzewski, V. G.; Dapprich, S.; Daniels, A. D.; Strain, M. C.; Farkas, O.; Malick, D. K.; Rabuck, A. D.; Raghavachari, K.; Foresman, J. B.; Ortiz, J. V.; Cui, Q; Baboul, A. G.; Clifford, S.; Cioslowski, J.; Stefanov, B. B.; Liu, G.; Liashenko, A.; Piskorz, P.; Komaromi, I.; Martin, R. L.; Fox, D. J.; Keith, T.; Al-Laham, M. A.; Peng, C. Y.; Nanayakkara, A.; Challacombe, M.; Gill, P. M. W.; Johnson, B.; Chen, W.; Wong, M. W.; Gonzalez, C.; Pople, J. A. *Gaussian 03*, Revision A.1; Gaussian, Inc.: Pittsburgh, PA, **2003**.

14. Plusquellic, D. F. *JB95* Spectral fitting program, NIST, Gaithersburg, MD. http://physics.nist.gov/jb95.

15. (a) Tan, X. -Q.; Majewski, W. A.; Plusquellic, D. F.; Pratt, D. W.; Meerts, W. L. *J. Chem. Phys.* **1989**, 90, 2521. (b) Tan, X. -Q.; Majewski, W. A.; Plusquellic, D. F.; Pratt, D. W. *J. Chem. Phys.* **1991**, 94, 7721.

16. Herschbach, D. R. *J. Chem. Phys*. **1959**, 31, 91.

17. Watson, J. K. G. in *Vibrational Spectra and Structure*; edited by Durig, J. R., Vol. 6, Ed.; Elsevier: Amsterdam, **1977**, pp 1.

18. Cvitas, T.; Hollas, J. M.; Kirby, G. H. *Mol. Phys*. **1970**, 19, 305.

19. Eisenhardt, C. G.; Pietraperzia, G.; Becucci, M. *Phys. Chem. Chem. Phys.* **2001**, 3, 1407.

20. Gordy, W.; Cook, R. L. *Microwave Molecular Spectra*; John Wiley & Sons: New York, **1984**, pp 570.

21. That the barriers to internal rotation might be different in different electronic states was first proposed by Hehre, W. J.; Pople, J. A.; Devaquet, A. J. P. *J. Am. Chem. Soc*. **1976**, 98, 664. See also Ref. 22.

22. For a complete summary of methyl group barrier heights in aromatic molecules, see Zhao, Z. -Q.; Parmenter, C. S.; Moss, D. B.; Bradley, A. J.; Knight, A. E. W.; Owens, K. G. *J. Chem. Phys.* **1992**, 96, 6362, and references therein.

23. It has been described in reference 15b that the A/E intensity ratio varies from 1.0 to 3.0 when the phase factor changes from 0° to 60°, for $V_3$ values of the order of 100 $cm^{-1}$.

# 6.0 ON THE ROLE OF METHYL TORSIONAL MODES IN THE INTERSYSTEM CROSSING DYNAMICS OF ISOLATED MOLECULES

This work has been accepted in *J. Phys. Chem. A* (2007).

## 6.1 ABSTRACT

Rotationally resolved fluorescence excitation spectra of the $0_0^0$ bands of the $S_1 \leftarrow S_0$ electronic transitions of 2- and 5-methylpyrimidine (2MP and 5MP, respectively) have been observed and assigned. Both spectra were found to contain two sets of rotational lines, one associated with the $\sigma = 0$ torsional level and the other associated with the $\sigma = \pm 1$ torsional level of the attached methyl group. Analyses of their structure using the appropriate torsion-rotation Hamiltonian yields the methyl group torsional barriers of $V_6'' = 1.56$ and $V_6' = 8.28$ cm$^{-1}$ in 2MP, and $V_6'' = 4.11$ and $V_6' = 58.88$ cm$^{-1}$ in 5MP. Many of the lines in both spectra are fragmented by couplings with lower lying triplet states. Analyses of some of these perturbations yields approximate values of the intersystem crossing matrix elements, from which it is concluded that the $\sigma = \pm 1$ torsional levels of the $S_1$ state are significantly more strongly coupled to the $T_1$ state than the $\sigma = 0$ torsional levels.

## 6.2 INTRODUCTION

Reported here are studies at high resolution of the $S_1 \leftarrow S_0$ fluorescence excitation spectra of 2-methylpyrimidine (2MP) and 5-methylpyrimidine (5MP) as isolated species in the collision-free environment of a molecular beam. Pyrimidine itself lies close to the small molecule limit in the language of radiationless transitions. It exhibits a zero-pressure fluorescence quantum yield of ~0.3 and a fluorescence decay that exhibits quantum beats, owing to spin-orbit coupling with a lower triplet state.[1] Hence, we reasoned that attachment of a single methyl group to pyrimidine might influence this process, by providing a low frequency torsional

coordinate along which state densities and/or coupling matrix elements might be enhanced. If this proves to be true, then 2MP and 5MP might be transformed into intermediate-case molecules with a significantly lower quantum yields and biexponential decay behaviors, and exhibit "intrinsically unassignable" high resolution spectra.

A radiationless transition is a change in the electronic state of a molecule that occurs without the absorption or emission of radiation. In bound states, there are two processes of this type, internal conversion (IC) and intersystem crossing (ISC). There has been a tremendous amount of research directed towards the study of these phenomena in the past fifty years. [Early work in the field has been reviewed by Kommandeur, *et al*.][2] Radiationless transitions in a polyatomic molecule occur *via* the transfer of energy from one multidimensional potential energy surface to another, and therefore are related to all types of chemical transformations. Intramolecular vibrational relaxation (IVR) is a related process that occurs on a single surface, which results in an apparent energy flow from one mode into another.[3]

IVR, IC and ISC are usually described by two sets of zero order levels, a bright state |s> that carries the oscillator strength and a bath of nearly isoenergetic dark states {|k>} to which the bright state is coupled, see Figure 6.1. The decay behavior of the prepared state depends upon the energy level density $\rho_k$, the decay widths $\gamma_k$, and the |s> - {|k>} couplings $\upsilon_{sk}$. The important parameters characterizing the different molecular limits are $x_k = \rho_k \gamma_k$ and $\upsilon_{sk}^2 \rho_k^2$. If $x_k << 1$, the average level spacing $\varepsilon_k$ is large compared to the radiative decay width $\gamma_k$. If there are no (or only a few) couplings between the two manifolds, then the initial state decays exponentially (sometimes showing quantum beats) with a rate that is equal (or slightly less than) the radiative rate and the emission quantum yield is high. This is the small molecule limit ($\upsilon_{sk}^2 \rho_k^2 << 1$). If $x_k >> 1$, the average level spacing is small; if further, $\left(\upsilon_{sk}^2 / \varepsilon_k\right) >> \gamma_s$, then there are a large number

of couplings between the two manifolds, and the oscillator strength is spread out over a large number of levels. If only a fraction of these are contained within the excitation bandwidth, then the initial state decays exponentially with a rate that is faster than the radiative rate and the emission quantum yield is low. This is the large molecule or statistical limit.

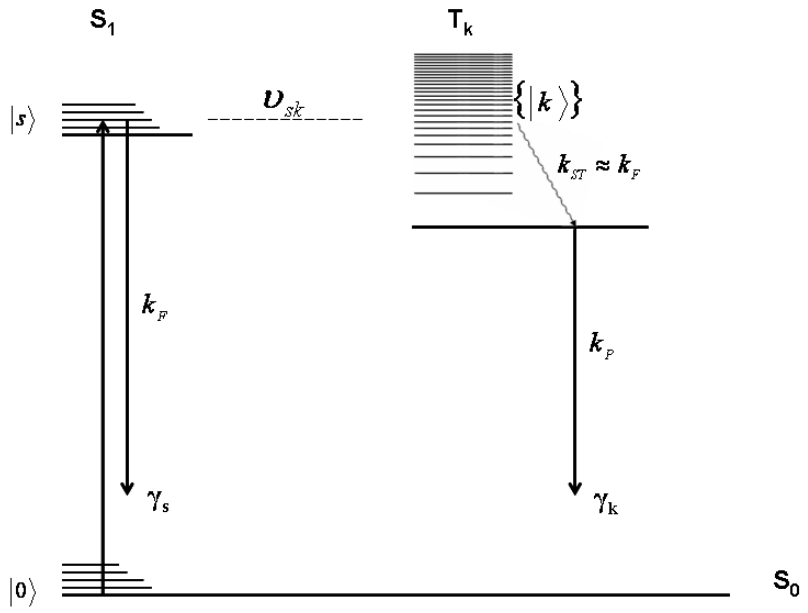


**Figure 6.1. Radiationless transitions in a large molecule. |s> denotes the bright state that is optically prepared by excitation of the ground state |0>, and coupled *via* matrix elements $v_{sk}$ to a dense manifold of nearly isoenergetic dark states {|k>}. In ISC, $S_1$ and $T_k$ are zero-order singlet and triplet states, respectively.**

As is often the case in science, valuable insight into the nature of dynamical processes is gained by studies of molecules that lie between the two limits, in the so-called "intermediate case". In such cases, radiationless transitions occur but are "reversible", and the decays are frequently non-exponential. A beautiful illustration of these effects can be found in the early work of Tramer and co-workers on pyrazine[4] and McDonald and co-workers on biacetyl.[5] G. ter Horst, *et al*.[6] and Y. Matsumoto, *et al*.[7] showed that the decay behavior of pyrazine is strongly dependent on the rotational state and the presence of magnetic fields. But probably the most dramatic demonstration of the existence of radiationless processes was provided by the direct

detection of the fragmentation of a single zero-order bright state into two or more molecular eigenstates using high resolution laser techniques; in benzene by Riedle, *et al*.,[8] in pyrimidine by Konings, *et al*.,[9] and in pyrazine by van der Meer, *et al*.[10] The analogous observation of IVR-induced fragmentation of C–H stretching modes in several small organic molecules was observed by Perry and co-workers,[11] McIlroy and Nesbitt[12] and Lehmann, Scoles and co-workers[13-14] at about the same time.

The increased level of detail provided by frequency-domain methods gives a more complete picture of energy redistribution processes. Much has been learned from studies of such spectra, including the measurements of relaxation rates and whether or not the process can be "manipulated" by excitation of certain modes, and not others. Scoles and his group have made notable contributions in this area, demonstrating in particular a "chromophore dependence of IVR" in several systems. Moore and co-workers[15] have reported similar studies of promoting modes in the photodissociation of $D_2CO$ and related small molecules. But analogous studies of promoting modes in the corresponding electronic processes of IC and ISC are lacking in larger molecules. This is the purpose of the work described here.

## 6.3 EXPERIMENTAL

2MP (>99% pure) was obtained from Koei Chemical Co. and 5MP (99% pure) was purchased from Sigma. Both chemicals were used without further purification. Dry argon and helium were used in all experiments as inert carrier gases.

In the vibrationally resolved experiments, samples were seeded into 40 psi of helium gas and expanded into a vacuum chamber ($10^{-5}$ torr) through a 1 mm diameter orifice pulsed valve

(General Valve Series 9) operating at 10 Hz. Two centimeters downstream of the valve, the free jet was excited with the second harmonic of a Quanta Ray $Nd^{3+}$:YAG (Model DCR-1A) pumped dye laser (Model PDL-1). The dye (DCM) laser output was frequency doubled with an external potassium dihydrogen phosphate (KDP) crystal providing a spectral resolution of ~0.6 $cm^{-1}$ in the ultraviolet (UV). From the point of intersection between the jet and the laser beam, the molecules were excited and the fluorescence was collected with a photomultiplier tube (PMT). Finally, the collected data were processed by a boxcar integrator (Stanford Research Systems) and recorded with Quick Data Acquisition software (Version 1.0.5).

Rotationally resolved electronic experiments were performed using a molecular beam laser spectrometer, described in detail elsewhere.[16] Briefly, the molecular beam was formed by expansion of the vaporized sample (either 2MP or 5MP) seeded in argon carrier gas (-17 psi) through a heated (~ 330 K) 200 $\mu$m quartz nozzle into a differentially pumped vacuum system. The expansion was skimmed 2 cm downstream with a 1 mm diameter skimmer and crossed 13 cm further downstream by a continuous wave (CW) $Ar^+$ pumped ring dye laser. The CW laser was operated with DCM dye and intracavity frequency doubled in a $LiIO_3$ crystal, yielding ~300 $\mu$W of UV radiation with a spectral resolution of about 1 MHz.

The fluorescence excitation spectrum was detected using spatially selective optics by a PMT and photon counting system. The PMT signal together with the iodine absorption spectrum and the relative frequency markers were simultaneously collected and processed by the JBA95 data acquisition system.[16] Absolute frequency calibration of the spectra was performed by comparison with the $I_2$ absorption spectrum. The relative frequency markers were obtained from a stabilized etalon with a free spectral range of 299.7520 ± 0.0005 MHz.

## 6.4 RESULTS

Figure 6.2 shows the vibrationally resolved fluorescence excitation spectra of 2MP and 5MP in the gas phase. Like Zwier and co-workers,[17,18] we observe strong $0_0^0$ transitions and no torsional bands near the electronic origins of both molecules. The origin ($0_0^0$) band in 2MP is at 30459.1 $cm^{-1}$ (~328.3 nm), red shifted from that of pyrimidine[7] by 614 $cm^{-1}$; whereas the $0_0^0$ band in 5MP is at 30799.9 $cm^{-1}$ (~324.7 nm), only 273 $cm^{-1}$ red shifted from the origin band of pyrimidine.

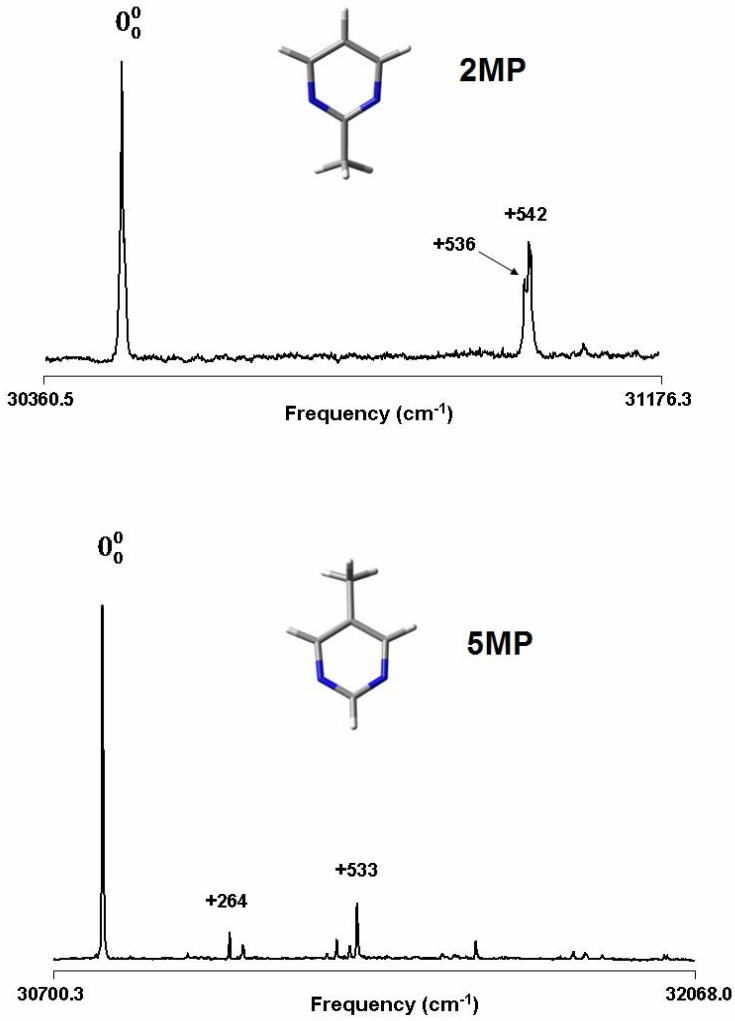


**Figure 6.2. Vibrationally resolved fluorescence excitation spectra of 2MP and 5MP in the gas phase.**

The absence of Franck-Condon progressions along the low frequency methyl torsional coordinate indicates that the preferred methyl group orientation is the same in both electronic states. The vibronic bands observed at about 535 $cm^{-1}$ mainly correspond to the $6a_0^1$ mode combined with torsional levels to give rise to the splitting observed in the 2MP spectrum.[18]

We have performed extensive studies of these spectra at high resolution, to examine the dynamic properties of their electronically excited states. Figure 6.3 shows the rotationally resolved $S_1 \leftarrow S_0$ fluorescence excitation spectrum of the origin band of 2MP in the gas phase. The entire spectrum contains about 3000 rovibronic lines and spans approximately 4.5 $cm^{-1}$ at a rotational temperature of about 5 K. Under the expansion conditions used in our experiments, only the lowest torsional levels ($\sigma = 0, \pm 1$) of 2MP are populated. Therefore, the transitions observed in the spectrum of Figure 6.3 are composed of two sub-bands, one associated with the $\sigma = 0$ (the *A* sub-band) and another with the $\sigma = \pm 1$ torsional levels (the *E* sub-band). The *A*

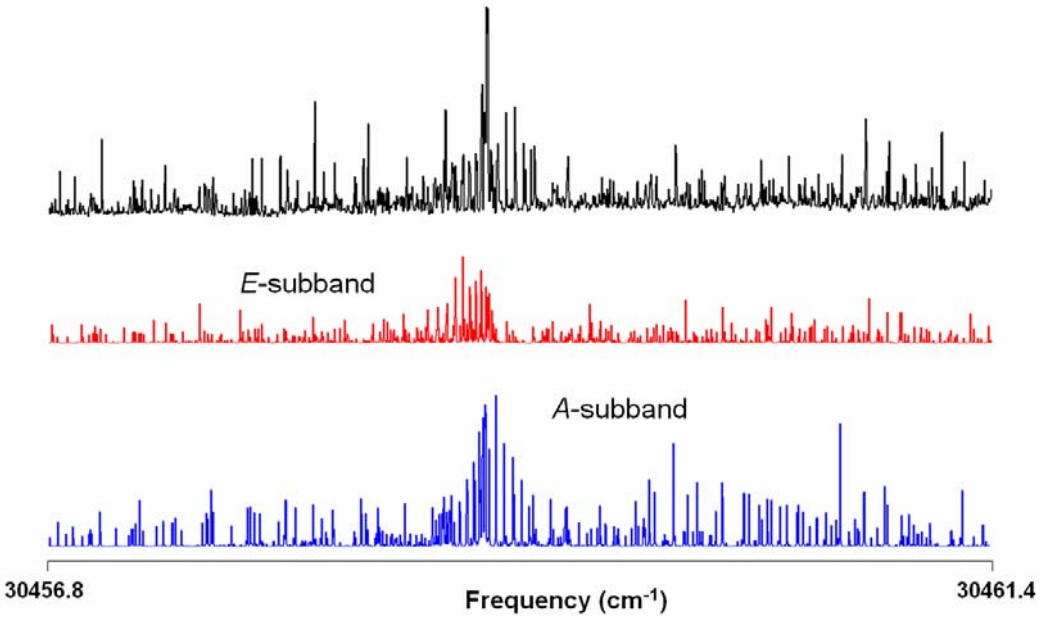


**Figure 6.3. Rotationally resolved fluorescence excitation spectrum of 2MP in the gas phase. Two simulated spectra (*A* and *E* sub-bands), due to the methyl group internal rotation, are required to fit the experimental trace. The splitting of the two sub-bands is about 157 MHz.**

sub-band was identified and assigned first and fit using rigid asymmetric rotor Hamiltonians for both electronic states. The fitting procedure was carried using the program *lbrot*,[19] which utilizes low barrier Hamiltonians and the graphic interface of JB95 fitting program.[20] The spectrum was found to be a pure *c*-type spectrum; the electronic transition moment vector is perpendicular to the plane of the aromatic ring. The final fit for the *A* sub-band utilized 129 rovibronic transitions and resulted in a standard deviation of 8.7 MHz; however, by performing a combination differences fitting procedure the standard deviation of the fit was reduced to 4.3 MHz.

The *E* sub-band contains rovibronic transitions whose degeneracies are lifted by the torsion-rotation interaction. Therefore, it was fit using the low barrier torsion-rotation Hamiltonian for a $G_{12}$ molecule,[21-23]

$$\hat{H} = \hat{H}_T + \hat{H}_R + \hat{H}_{TR} \quad \textbf{(6.1)}$$

with

$$\hat{H}_T = Fp^2 + \tfrac{1}{2} V_6(1-\cos 6\alpha), \quad \textbf{(6.2)}$$

$$\hat{H}_R = AP_z^2 + BP_x^2 + CP_y^2 + FP^2, \quad \textbf{(6.3)}$$

and

$$\hat{H}_{TR} = -2FPp. \quad \textbf{(6.4)}$$

Here, the torsional ($\hat{H}_T$) and the rotational ($\hat{H}_R$) Hamiltonians are treated separately, with the use of an extra term ($\hat{H}_{TR}$) that couples them. $A = \hbar^2/2I_z$, *etc*. are the rigid rotor rotational constants, $P = \sum_g \lambda_g \left( I_\alpha / I_g \right) P_g$ is the total angular momentum of the methyl rotor, and $\lambda_g \ (g = x, y, z)$ are the direction cosines of the symmetry axis of the methyl rotor with respect to the principal axes of inertia. $\alpha$ is the internal-rotation coordinate, $p$ is the torsional angular momentum, $F$ is the methyl group rotational constant, and $V_6$ is the six-fold potential barrier height hindering the torsional motion.[24] The reported microwave values for the $S_0$ rotational

constants and the corresponding barrier heights were taken as initial estimates for the fit of the experimental trace.[25] The final fit utilized 84 lines and resulted in a standard deviation of 15.5 MHz. The *E* sub-band was found to be red shifted from the *A* sub-band by ~157 MHz. A portion of the *Q* branch of this spectrum is shown in Figure 6.4, where the need for the two independent simulated spectra is clearly evident. Individual lines exhibit Voigt profiles, with 18 MHz Gaussian and 40 MHz Lorentzian contributions. The inertial parameters obtained from the fits are summarized in Table 6.1.

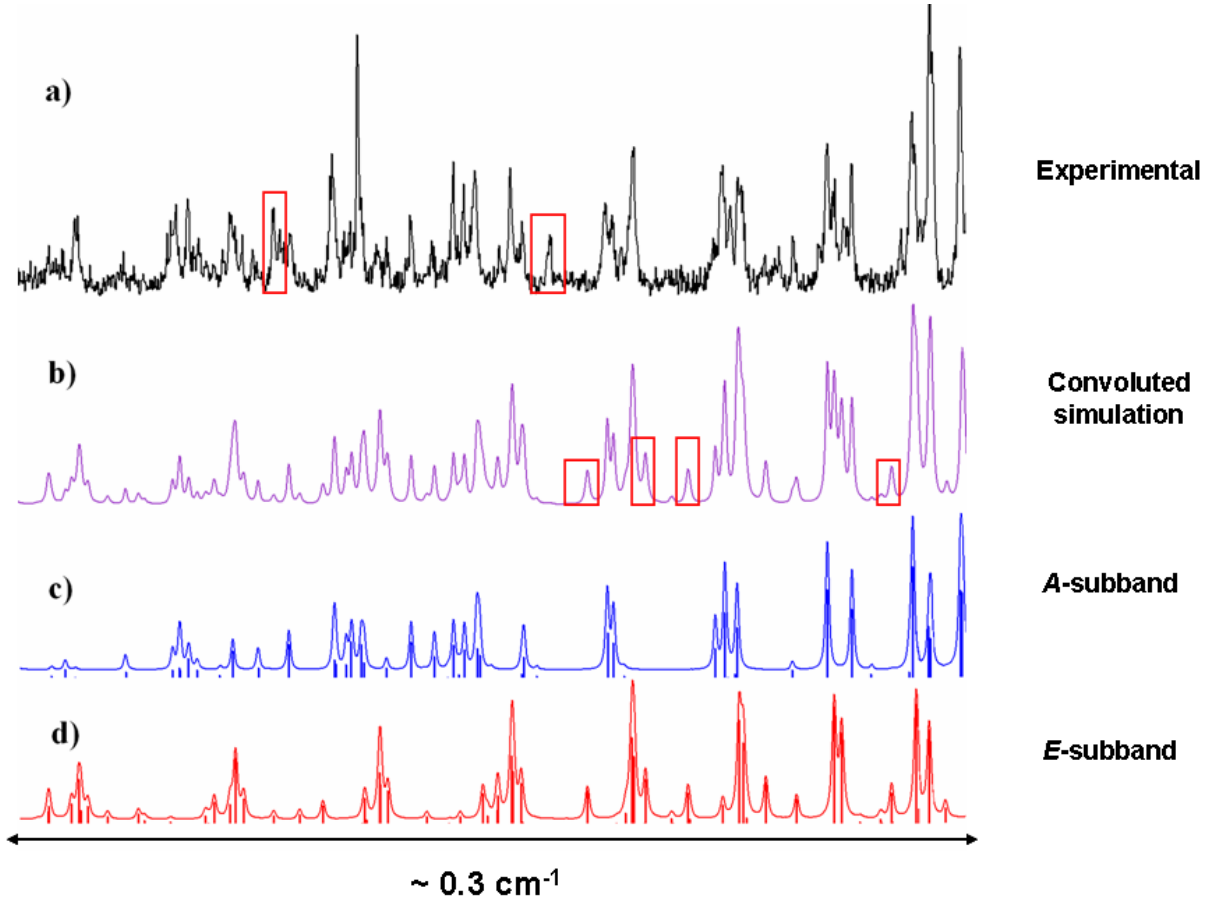


**Figure 6.4. A portion of the *Q* branch in the origin band of the $S_1 \leftarrow S_0$ electronic spectrum of 2MP illustrating the quality of the fit. The experimental spectrum is shown in a), the corresponding simulated spectrum is shown in b), and the contributions of the two sub-bands are shown separately in c) and d). Boxes denote either "extra" transitions in a) or "missing" transitions in b).**

**Table 6.1. Inertial parameters derived from fits of the high resolution spectra of the *A* and *E* sub-torsional bands of 2-methylpyrimidine.**

| Parameter[a] | *E* sub-band | *A* sub-band | Microwave[b] |
|---|---|---|---|
| **$S_0$** | | | |
| ***A″* (MHz)** | 6106.4 (1) | 6095.6 (1) | 6096.9 (1) |
| ***B″* (MHz)** | 2770.3 (1) | 2751.6 (1) | 2751.7 (<1) |
| ***C″* (MHz)** | 1867.7 (1) | 1895.5 (1) | 1895.6 (<1) |
| **$\Delta I''$ (amu Å$^2$)** | 5.40 (5) | 0.04 (5) | 0.06 |
| **$S_1$** | | | |
| ***A′* (MHz)** | 6397.8 (1) | 6373.4 (1) | |
| ***B′* (MHz)** | 2600.1 (1) | 2590.2 (2) | |
| ***C′* (MHz)** | 1823.7 (1) | 1842.0 (1) | |
| **$\Delta I'$ (amu Å$^2$)** | 3.76 (5) | -1.04 (5) | |
| **Band origin (cm$^{-1}$)** | 30459.06 | 30459.07 | |
| **OMC (MHz)** | 15.57 | 4.35 | |
| **Temp (K)** | 4.5 | 4.5 | |

[a] Numbers in parentheses are the standard deviations of the last significant figure.
[b] Values taken from Reference 25.

Also apparent in Figure 6.4 are significant differences between the experimental spectrum and the calculated one, highlighted by boxes. These differences include "missing" transitions that appear in the simulated spectrum b), and "extra" transitions that appear in the experimental spectrum a). These observations are a direct consequence of spin-orbit coupling to a lower triplet state.

Figure 6.5 shows the rotationally resolved fluorescence excitation spectrum of the $0_0^0$ band of 5MP in the gas phase. The spectrum spans about 4 cm$^{-1}$ and contains more than 2000 rovibronic lines. Upon a similar analysis, two sub-torsional bands were also found in the spectrum of 5MP; the *A* sub-band was fit using rigid rotor Hamiltonians in both electronic states, whereas the *E* sub-band required the first-order torsion-rotation coupling terms described above. For this molecule, the *E* sub-band was observed to be red shifted but by a larger magnitude (~7800 MHz) than in 2MP, which signals a larger difference in the methyl torsional barriers

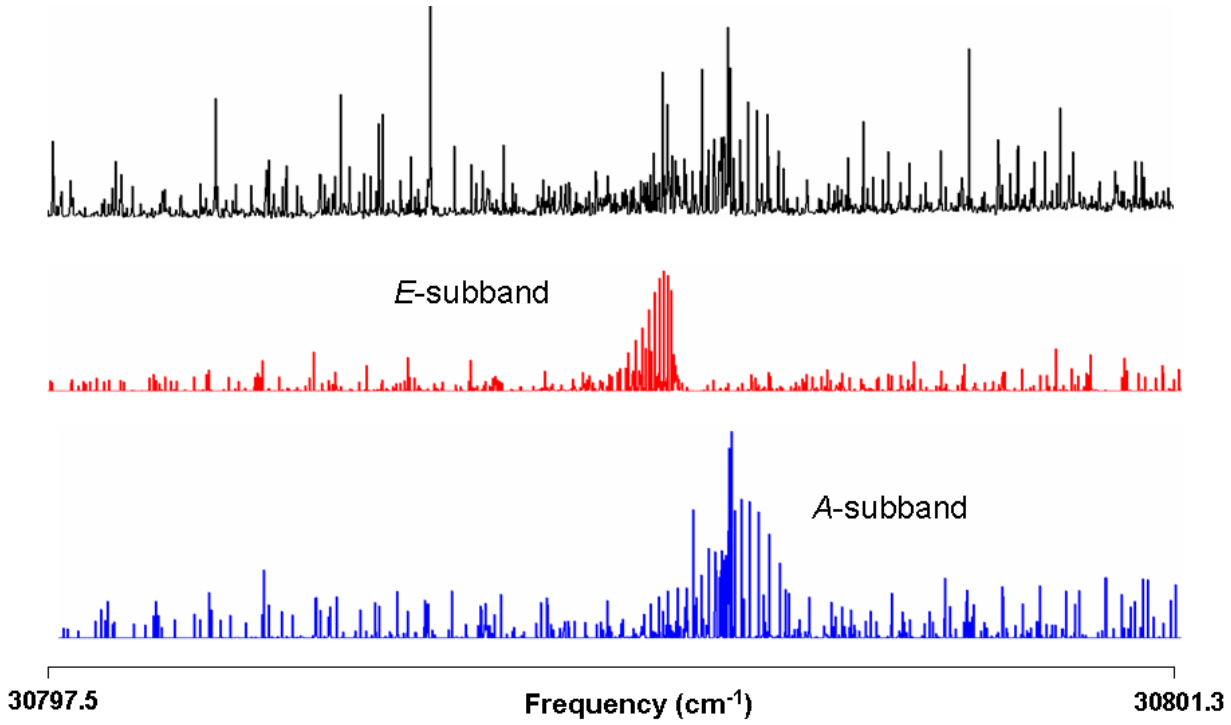


**Figure 6.5. Rotationally resolved fluorescence excitation spectrum of 5MP in the gas phase. Two simulated spectra (*A* and *E* sub-bands), due to the methyl internal rotation, are required to fit the experimental trace. The splitting of the two sub-bands is about 7,800 MHz.**

upon electronic excitation. This confirms the earlier results of Bandy, *et al.*[17] and Bitto and Gfeller.[26] Both sub-torsional bands in 5MP exhibit pure *c*-type rovibronic transitions. The final fit for the *A* sub-band utilized 116 transitions and yielded a standard deviation of 7.49 MHz, which was improved to 4.22 MHz after a combination difference analysis. On the other hand, the *E* sub-band utilized 80 transitions and resulted in a standard deviation of 9.86 MHz. Figure 6.6 shows a portion of the experimental spectrum in section where the two spectra overlap, including the two simulated *A* and *E* sub-bands. Note that this spectrum also exhibits several singlet-triplet perturbations. The inertial parameters obtained from the fits of the spectra of 5MP are reported in Table 6.2.

Finally, we have been able to obtain both vibrationally and rotationally resolved electronic spectra of 4-methylpyrimidine (4MP), which are not reported here. The acquisition

and analysis of this spectrum is in process of being improved, since the fluorescence quantum yield in 4MP seems to be extremely small.

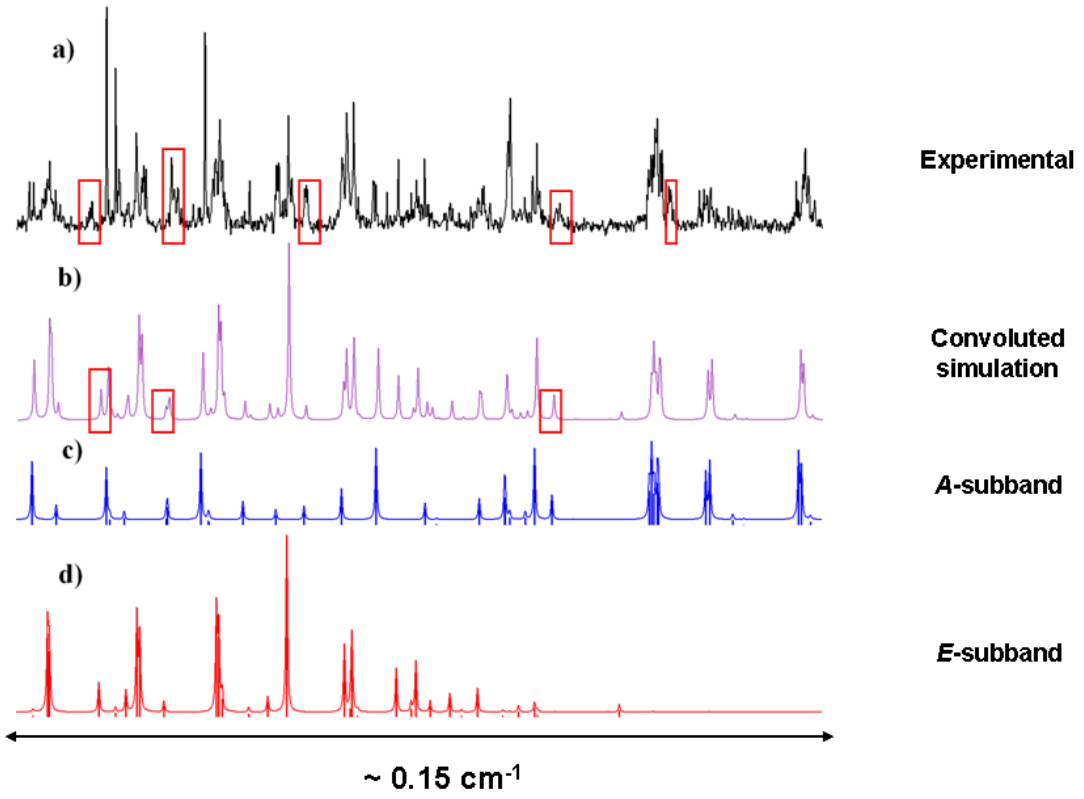


**Figure 6.6. A portion of the *Q* branch in the origin band of the $S_1 \leftarrow S_0$ electronic spectrum of 5MP illustrating the quality of the fit. The experimental spectrum is shown in a), the corresponding simulated spectrum is shown in b), and the contributions of the two sub-bands are shown separately in c) and d). Boxes denote either "extra" transitions in a) or "missing" transitions in b).**

## 6.5 DISCUSSION

### 6.5.1 Molecular structures upon excitation

Table 6.1 and 6.2 list the measured rotational constants of 2MP and 5 MP in their ground and electronically excited states. The ground state values are in excellent agreement with the earlier

microwave ones.[25,27] But the excited state values are quite different, owing to light-induced changes in the molecular geometries of the two species. 2MP has $\Delta A$ (= $A'$ – $A''$), $\Delta B$, and $\Delta C$ values of 277.8, -161.4, and -53.5 MHz, whereas 5MP has $\Delta A$, $\Delta B$, and $\Delta C$ values of 256.9, -103.4, and -27.4 MHz, respectively. (Both sets of values are from the *A* sub-band fits; the *E* sub-band values are slightly different owing to the second-order torsion-rotation contributions). The results for both molecules evidence significant contractions along directions perpendicular to *a*, and expansions along directions perpendicular to *b* and *c* when the photon is absorbed.

MP2 (second order Moller-Plesset) and CIS (configuration interaction-singles) *ab initio* calculations[28] were performed to determine the preferred orientation of the attached methyl group with respect to the plane of the ring in both electronic states. These calculations predict that the staggered orientation of the methyl (*i.e.*, one of the C–H bonds is perpendicular to the plane of the ring) is preferred in both states, by a few wavenumbers of energy. A similar result has been obtained for toluene.[29]

**Table 6.2. Inertial parameters derived from fits of the high resolution spectra of the *A* and *E* sub-torsional bands of 5-methylpyrimidine.**

| Parameter[a] | *E* sub-band | *A* sub-band | Microwave[b] |
|---|---|---|---|
| **$S_0$** | | | |
| ***A″* (MHz)** | 6100.6 (1) | 6108.3 (1) | 6108.4 (1) |
| ***B″* (MHz)** | 2640.5 (1) | 2642.4 (1) | 2642.2 (<1) |
| ***C″* (MHz)** | 1847.6 (1) | 1844.5 (1) | 1844.2 (<1) |
| **$\Delta I''$ (amu Å$^2$)** | -0.69 (5) | 0.00 (5) | 0.03 |
| **$S_1$** | | | |
| ***A′* (MHz)** | 6357.8 (1) | 6365.2 (1) | |
| ***B′* (MHz)** | 2537.2 (1) | 2538.9 (1) | |
| ***C′* (MHz)** | 1818.9 (1) | 1817.1 (1) | |
| **$\Delta I'$ (amu Å$^2$)** | -0.83 (5) | -0.32 (5) | |
| **Band origin (cm$^{-1}$)** | 30799.63 | 30799.89 | |
| **OMC (MHz)** | 9.86 | 4.22 | |
| **Temp (K)** | 5.0 | 5.0 | |

[a] Numbers in parentheses are the standard deviations of the last significant figure.
[b] Values taken from Reference 27.

Experimentally, the $S_1 \leftarrow S_0$ transition dipole moment vectors in both 2MP and 5MP were found to be oriented perpendicular to the plane of the aromatic ring (*i.e.*, only pure *c*-type rovibronic transitions were observed). Figure 6.7 illustrates the results obtained from the CIS calculations. In agreement with our observations, the pictures of the MOs for both molecules signal an evident transition from an *n*-orbital (no node in the plane of the ring and highly localized in the nitrogen atoms) to a $\pi^*$ orbital (benzene-like LUMO).

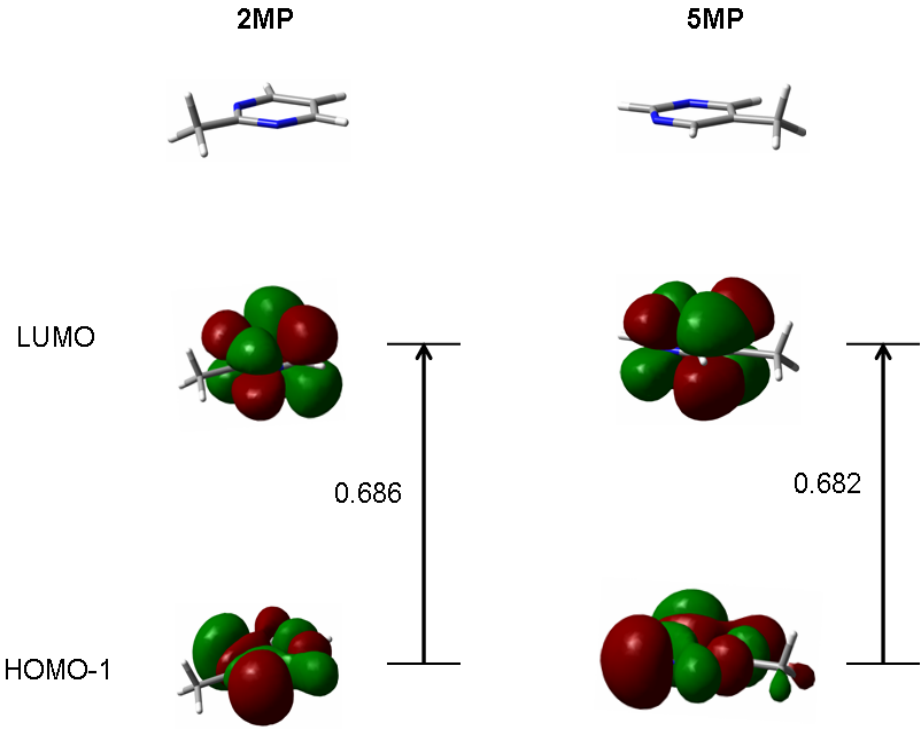


**Figure 6.7. CIS/6-31G(d,p) frontier molecular orbitals with their corresponding transition probabilities in 2MP and 5MP.**

Transfer of charge from the nitrogen lone pair(s) to the $\pi^*$ orbital of the ring produces significant structural changes in the isolated molecules. For example, the calculations suggest that the $N_1$–$C_2$ and $C_2$–$N_3$ bonds shorten by ~0.04 Å (from 1.34 to 1.30 Å); the $N_1$–$C_2$–$N_3$ angle decreases by ~11º (from 126º to 115º) in both molecules; and the $N_1$–$C_6$ and $N_3$–$C_4$ bond lengths increase by ~0.02 Å. [Interestingly, in the methyl eclipsed configurations (geometry-

optimization calculations performed by maintaining the methyl group torsional coordinate frozen), there is a remarkable difference in bond lengths of the $N_1$–$C_2$ and $C_2$–$N_3$ bonds in 2MP and $C_5$–$C_6$ and $C_4$–$C_5$ bonds in 5MP. Note that the only difference among these bonds is the relative orientation of the methyl group in the structures. Specifically, the $C_5$–$C_6$ bond is ~0.03 Å shorter than the $C_4$–$C_5$ bond in 5MP.] These structural changes are very different from those in the typical excitation of a $\pi\pi^*$ state in an aromatic molecule.[30]

### 6.5.2 Methyl group torsional barriers

The torsional barriers hindering the rotation of the methyl group about either the $C_2$–$C_{Methyl}$ bond in 2MP or the $C_5$–$C_{Methyl}$ bond in 5MP were determined from the relative spacing in frequency of the *A* and *E* sub-torsional bands in the high resolution spectra. The ground state torsional barriers, $V_6''$ = 1.56 for 2MP and $V_6''$ = 4.11 $cm^{-1}$ for 5MP, were taken from more accurate microwave results.[25,27] Then, the excited state torsional barriers, $V_6'$ = 8.28 for 2MP and $V_6'$ = 58.88 $cm^{-1}$ for 5MP were determined from the *A*-*E* splittings. The excited state barrier in 5MP is significantly larger than that in 2MP. Plots of the one-dimensional torsional energy surfaces along the torsional coordinate for 2MP and 5MP in both electronic states are shown in Figure 6.8. Note, that the lower the torsional barrier heights, the closer the experimental inertial defects to zero (*cf*. Tables 6.1 and 6.2). A similar trend was observed in 2- and 3-methylanisole.[31]

We believe that the observed methyl torsional barrier heights have their origin in $\pi$-bond order differences of two neighboring ring covalent bonds in the eclipsed configuration of these molecules. To further investigate this phenomenon, the $\pi$-covalent bond orders have been computed for both molecules in both staggered and eclipsed configurations in both electronic states.[32] When the methyl group is staggered in 2MP, the $\pi$-bond orders of the $N_1$–$C_2$ and $C_2$–$N_3$

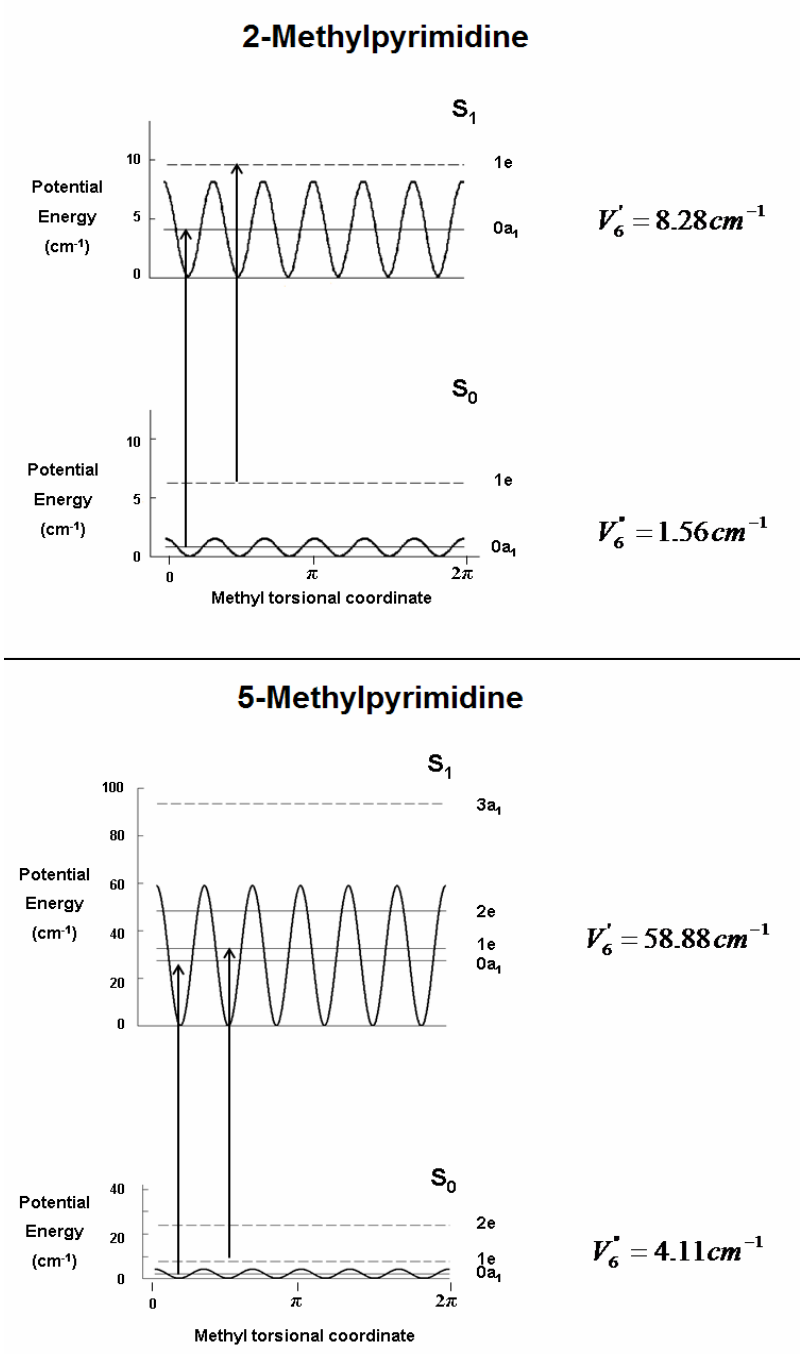


**Figure 6.8. Torsional energy surfaces of 2MP and 5MP in both electronic states.**

bonds are identical; $\rho_{12} = \rho_{23} = 0.458$ in $S_0$ and $\rho_{12} = \rho_{23} = 0.313$ in $S_1$. However, when the methyl group is eclipsed the $N_1$–$C_2$ bond, the $N_1$–$C_2$ and $C_2$–$N_3$ covalent bond orders are no longer the same; $\rho_{12} = 0.510$ and $\rho_{23} = 0.409$ in the $S_0$ state, and $\rho_{12} = 0.367$ and $\rho_{23} = 0.259$ in

the $S_1$ state. The difference in the two bond orders increases slightly from 0.101 in the $S_0$ state to 0.108 in the $S_1$ state, thereby explaining the small increase in $V_6$ in the electronically excited state. In contrast, the corresponding $C_4$–$C_5$ and $C_5$–$C_6$ covalent $\pi$-bond order differences in 5MP are 0.180 and 0.438 for the $S_0$ and $S_1$ states, respectively, thereby accounting for the much larger increase in $V_6$ when 5MP absorbs light.

### 6.5.3 Intersystem crossing dynamics

The intersystem crossing dynamics in 2MP and 5MP are revealed in Figures 6.4 and 6.6. There, it was shown that the experimental spectra exhibit "extra" lines that do not appear in the simulations, which otherwise accounts for most of the observed intensity. At the same time, the simulations contain "missing" lines that that do not appear in the experimental spectra. Both of these observations can be explained by interactions between the zero-order singlet state and an otherwise dark manifold of triplet states, the "talisman" of ISC. A similar effect has been observed in pyrimidine.[9]

Though qualitatively similar, the high resolution spectra of the two pyrimidine derivatives are quantitatively different from the spectra of the parent molecule. In pyrimidine itself, the number of extra lines is very small, typically 0-2 per zero-order state, and the fractional intensity that they exhibit is also very small, ~0-5%.[9] 2MP and 5MP exhibit, in contrast, many more extra lines with significantly higher intensity, betraying the existence of a larger number of perturbations between the zero-order states. The spectra of 2MP and 5MP are still quite far from the statistical limit, as individual transitions can still be resolved, identified, and approximately fit by an appropriate Hamiltonian. But since the spectra of 2MP and 5MP are significantly more perturbed than that of pyrimidine itself, we can safely conclude that methyl torsions enhance ISC

in the isolated molecule, and increase its rate. A similar finding has been made for the case of IVR by Parmenter and co-workers.[33] These authors argued that the increased IVR rate in molecules like *p*-fluorotoluene is primarily a reflection of a larger number of available states that can "couple through the exchange of energy between ring vibrations and internal rotation".[33]

Calculated densities of vibrational states in the nearby of the zero point vibrational level of the $S_1$ state (|s>), according to the Haarhoff formula,[34] are ~8.6, ~0.60, and ~66.88 levels/$cm^{-1}$ for pyrazine, pyrimidine, and 2MP respectively.

Unfortunately, groups of lines are so mixed and congested in the spectra of 2MP and 5MP that it is difficult to identify their $J\ K_a\ K_c$ parentage, and therefore to determine their zero-order character using the elegant Lawrance-Knight[35] deconvolution procedure. Application of this procedure to pyrimidine yielded zero-order energies spanning up to 1 GHz and spin-orbit couplings (SOC) matrix elements lying between 0 and 100 MHz.[9] However, it is still possible to extract some information about the analogous process in the methylpyrimidines from the existing data. Figure 6.9 shows a comparison of selected regions of the *A* and *E* sub-bands in 2MP; Figure 6.10 shows a similar comparison for 5MP. Contrasting the two *A* sub-bands, we see that the spectra exhibit many "extra" lines as well as "main" lines; the individual standard deviations range from 1-100 MHz, equivalent to a lifetime of the order of 1 ns or so. At most, then, individual SOC matrix elements in the methylpyrimidines do not seem to be much larger than these in pyrimidine itself. On the other hand, we see that the number of perturbations is much larger than in pyrimidine, and that this number increases still further in the two *E* sub-bands, leading to an apparent inhomogeneous broadening of individual "zero-order" lines in the spectrum and the formation of "clumps".[36] Clump widths approaching 100 MHz are observed, apparently deriving from a higher density of states, compared to the *A* sub-bands. Finally, we

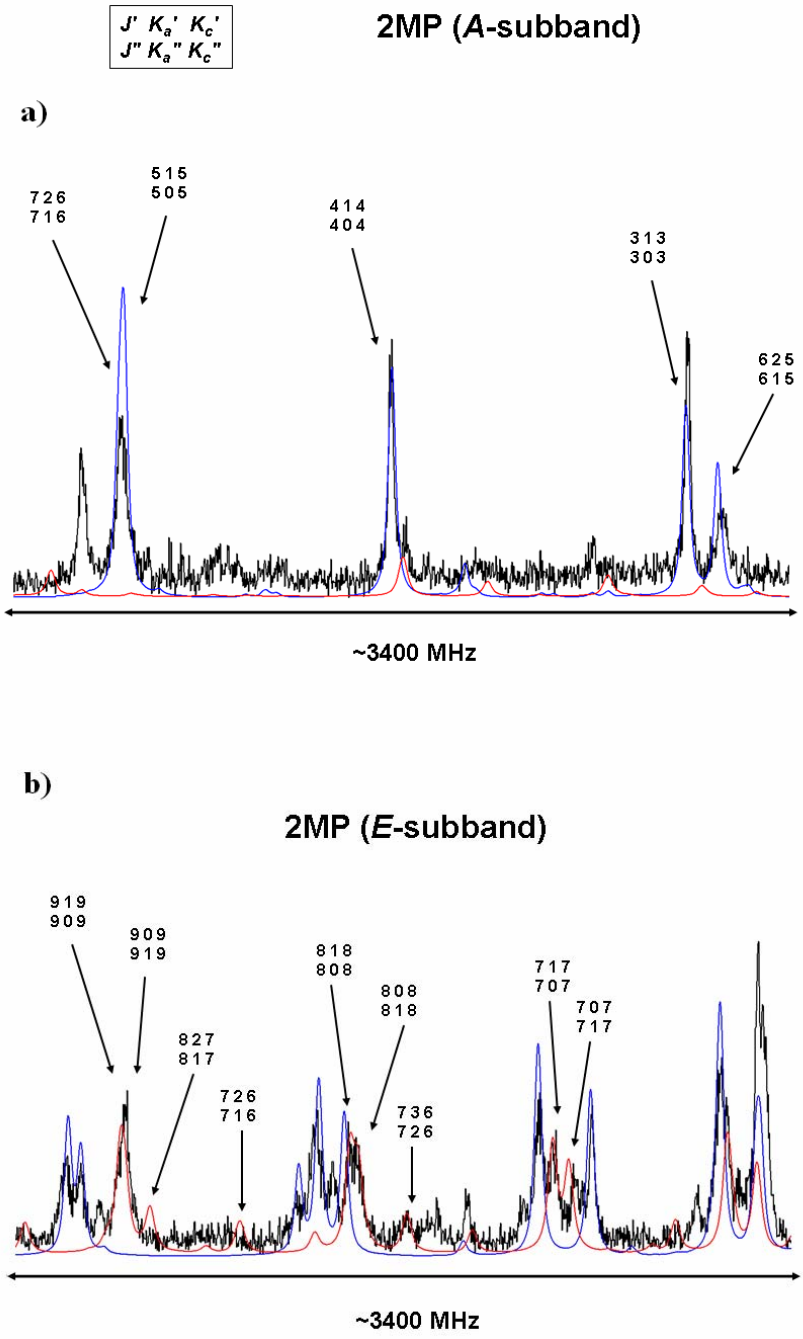


**Figure 6.9. Intersystem crossing in the high resolution electronic spectrum of 2-methylpyrimidine. The labeling of the transitions follows the quantum number pattern described in the box. a) The *A* sub-band exhibits some extra lines next to the simulated transitions. b) The *E* sub-band exhibits some frequency shifts and the degeneracy of the main transitions is broken.**

note that the number of perturbations is enhanced in 5MP, relative to 2MP, which may be a consequence of the significant difference in their torsional barriers in the $S_1$ state. A more

quantitative assessment of the factors responsible for these dynamics will require microwave-optical double resonance experiments to disentangle the spectra.

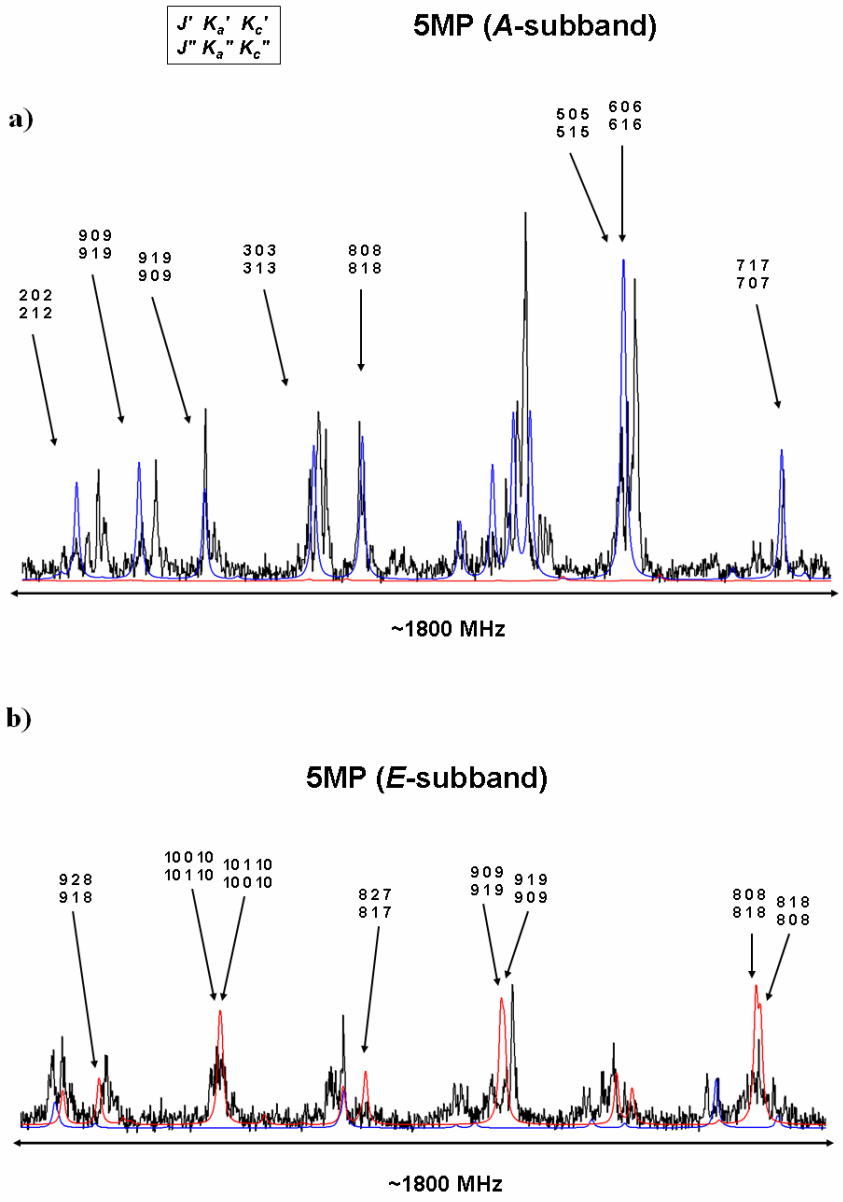


**Figure 6.10. Intersystem crossing in the high resolution electronic spectrum of 5-methylpyrimidine. The labeling of the transitions follows the quantum number pattern described in the box. a) The *A* sub-band exhibits extra lines around the simulated transitions forming localized "clumps". b) The *E* sub-band exhibits inhomogeneous broadening of peaks.**

## 6.6 SUMMARY

2MP and 5MP reveal intersystem crossing dynamics upon electronic excitation due to extra lines and line broadenings observed in their fully resolved $S_1 \leftarrow S_0$ fluorescence excitation spectra. Both spectra were found to be more congested than that of pyrimidine due to the low frequency motion of the attached methyl group. From the fits of the spectra, the $V_6$ methyl torsional barriers were determined for both molecules in their $S_0$ and $S_1$ electronic states. 5MP has a significantly larger barrier in its $S_1$ state than does 2MP, resulting in a higher density of coupled states and enhanced ISC in the isolated molecule.

## 6.7 ACKNOWLEDGMENTS

Giacinto Scoles has been a tremendous champion (and practitioner) of high resolution spectroscopy over the years, and we are grateful for his support. We also thank David R. Borst (INTEL) and David F. Plusquellic (NIST) for their helpful suggestions on the *lbrot* and JB95 fitting programs used for the data analysis, and the Koei Chemical Company for the kind donation of the 2-methylpyrimidine sample used in our experiments. This work has been supported by NSF (CHE-0615755).

## 6.8 REFERENCES

1. K. K. Innes, I. G. Ross, and W. R. Moomaw, *J. Mol. Spectrosc.* **132**, 492 (1988).

2. J. Kommandeur, W. A. Majewski, W. L. Meerts, and D. W. Pratt, *Annu. Rev. Phys. Chem.* **38**, 433 (1987), and references therein.

3. D. J. Nesbitt and R. W. Field, *J. Phys. Chem*. **100**, 12735 (1996).

4. F. Lahmani, A. Tramer, and C. Tric, *J. Chem. Phys.* **60**, 4431 (1974).

5. J. Chaiken, T. Benson, M. Gurnick, and J. D. McDonald, *Chem. Phys. Lett.* **61**, 195 (1979).

6. G. ter Horst, D. W. Pratt, and J. Kommandeur, *J. Chem. Phys.* **74**, 3616 (1981).

7. Y. Matsumoto, L. H. Spangler, and D. W. Pratt, *Laser Chem.* **2**, 91 (1983).

8. E. Riedle, H. J. Neusser, and E. W. Schlag, *J. Phys. Chem.* **86**, 4847 (1982).

9. J. A. Konings, W. A. Majewski, Y. Matsumoto, D. W. Pratt, and W. L. Meerts, *J. Chem. Phys.* **89**, 1813 (1988).

10. B. J. van der Meer, H. Th. Jonkman, J. Kommandeur, W. L. Meerts, and W. A. Majewski, *Chem. Phys. Lett.*, **92**, 565 (1982).

11. A. M. de Souza, D. Kaur, and D. S. Perry, *J. Chem. Phys*. 88, , 4569 (1988).

12. A. McIlroy and D. J. Nesbitt, *J. Chem. Phys*. **91**, 104 (1989).

13. A. McIlroy, D. J. Nesbitt, E. R. Th. Kerstel, B. H. Pate, K. K. Lehmann, and G. Scoles, *J. Chem. Phys*. **60**, 2596 (1994).

14. K. K. Lehmann, G. Scoles, and B. H. Pate, *Annu. Rev. Phys. Chem*. **45**, 241 (1994).

15. W. H. Green, Jr., C. B. Moore, and W. F. Polik, *Annu. Rev. Phys. Chem*. **43**, 591 (1992).

16. W. A. Majewski, J. F. Pfanstiel, D. F. Plusquellic, and D. W. Pratt, in *Laser Techniques in Chemistry*. T. R. Rizzo and A. B. Myers, Eds.; J. Wiley & Sons: New York, 1995, p 101.

17. R. E. Bandy, J. Nash, and T. S. Zwier, *J. Chem. Phys*. **95**, 2317 (1991).

18. R. E. Bandy, A. W. Garrett, H. D. Lee, and T. S. Zwier, *J. Chem. Phys*. **96**, 1667 (1992).

19. D. R. Borst, PhD thesis. University of Pittsburgh, 2001.

20. D. F. Plusquellic, *Jb95 spectral fitting program*; NIST: Gaithersburg, MD. http://physics.nist.gov/jb95.

21. L. H. Spangler and D. W. Pratt, in *Jet Spectroscopy and Molecular Dynamics*; J. M. Hollas and D. Phillips, Eds.; Chapman & Hall: London, 1995; p 366-398.

22. W. Gordy and R. L. Cook, *Microwave Molecular Spectra*; John Wiley & Sons: New York, 1984; p 607-617.

23. P. R. Bunker and P. Jensen, *Molecular Symmetry and Spectroscopy*; 2nd Edition, NRC Research Press: Ottawa, 1998; p 511.

24. In an earlier report [X. –Q. Tan and D. W. Pratt, *J. Chem. Phys*. **100**, 7061 (1994)], it has been shown that some molecules like the methylpyrimidines, exhibit a precessional motion of the symmetry axis of the top with respect the $C_2$ symmetry axis of the frame, originating a precessing angle $\theta$. We neglect this effect here.

25. W. Caminati, G. Cazzoli, and D. Troiano, *Chem. Phys. Lett*. **43**, 65 (1976).

26. H. Bitto and S. Gfeller, *Chem. Phys. Lett*. **265**, 600 (1997).

27. W. Caminati, G. Cazzoli, and A. M. Mirri, *Chem. Phys. Lett*. **31**, 104 (1975).

28. M. J. Frisch, *et al*., *Gaussian 03*, revision B.05; Gaussian, Inc.: Pittsburgh, PA, 2003.

29. D. R. Borst and D. W. Pratt, *J. Chem. Phys*. **113**, 3658 (2000).

30. See, for example, W. E. Sinclair and D. W. Pratt, *J. Chem. Phys*. **105**, 7942 (1996) for the contrasting case of aniline.

31. L. Alvarez-Valtierra, J. T. Yi, and D. W. Pratt, *J. Phys. Chem.* **110B**, 19914 (2006).

32. For details of the *Atoms in Molecules* calculations, see, for example a) J. Cioslowski, P. Piskorz, and P. Rez, *J. Chem. Phys*. **106**, 3607 (1997); b) J. Cioslowski and B. B. Stefanov, *J. Chem. Phys*. **105**, 8741 (1996).

33. D. B. Moss and C. S. Parmenter, *J. Chem. Phys*. **98**, 6897 (1993) and references therein.

34. P. C. Haarhoff, *Mol. Phys*. **7**, 101 (1964).

35. W. D. Lawrance and E. W. Knight, *J. Phys. Chem*. **89**, 917 (1985).

36. This term has extensively used for clusters of lines in spectral chaos and dynamics. See for example, R. L. Sundberg, E. Abramson, J. L. Kinsey, and R. W. Field, *J. Chem. Phys*. **83**, 466 (1985).

# 7.0 LIFETIME BROADENING IN THE ROTATIONALLY RESOLVED ELECTRONIC SPECTRA OF DIBENZOTHIOPHENE, 2,5-DIPHENYLFURAN AND 2,5-DIPHENYL-1,3,4-OXADIAZOLE IN THE GAS PHASE. INTERSYSTEM CROSSING DYNAMICS IN THE STATISTICAL LIMIT

## 7.1 ABSTRACT

The fluorescence lifetime of the zero-point vibrational level transition of dibenzothiophene (DBT) has been determined by analysis of its rotationally resolved $S_1 \leftarrow S_0$ fluorescence excitation spectrum to be $\tau_s$ = 1.0 ns. This lifetime of the $S_1$ state of DBT is contrasted with those observed for its chromophore analogs; fluorene (FLU), carbazole (CAR), and dibenzofuran (DBF), which are substantially longer. The electronic origin bands in the series CAR, FLU, DBF, and DBT exhibit a monotonic increase in Lorentzian broadening in their Voigt lineshape profiles. Two other heterocyclic molecules manifest similar photophysical properties; 2,5-diphenylfuran and 2,5-diphenyl-1,3,4-oxadiazole. Lorentzian lineshape broadenings of ~76 MHz were observed in the high resolution spectra of their origin bands. Possible reasons for the short fluorescence lifetimes observed in these heterocycles are further discussed.

## 7.2 INTRODUCTION

A radiationless transition is a change in the electronic state of a molecule that occurs without the absorption or emission of radiation. Radiationless transitions are transfers of energy from one part of a multidimensional potential energy surface to another, and therefore are related to all types of chemical transformations. The various types of nonradiative transitions in excited molecules, such as intramolecular vibrational relaxation (IVR), internal conversion (IC), and intersystem crossing (ISC), are usually described by two sets of zero-order levels, a bright state |s> that carries the oscillator strength and a bath of nearly isoenergetic dark states {|k>} to which the bright state is coupled, see Figure 6.1. The decay behavior of the prepared state depends upon

the energy level density $\rho_k$, the decay widths $\gamma_k$, and the |s> - {|k>} couplings $\upsilon_{sk}$. Using the classification scheme first proposed by Robinson[1] for the different types of decay behavior of chemical systems, we focus here on the large molecule (statistical) limit; *i.e.*, $x_k = \rho_k \gamma_k >> 1$. In this limit, the average level spacing $\varepsilon_k$ is small, there are a large number of couplings between the two manifolds, and the oscillator strength is spread out over a large number of levels. If only a fraction of these are contained within the excitation bandwidth, then the initial state decays exponentially with a rate that is faster than the radiative rate and the emission quantum yield is low.

Some heterocyclic aromatic molecules are known to exhibit fascinating photophysical properties in terms of ISC dynamics, in the large molecule limit, upon electronic excitation with monochromatic light.[2] Dibenzothiophene (DBT) is an excellent example of these heterocycles. Pioneering spectroscopic studies of DBT were performed by analyzing its electronic absorption spectrum in crystal lattices.[3-5] The orientations of the electronic transition moment vectors were determined for different electronic states.[4,5] Additionally, the transition energies, band polarizations, and dipole strengths of DBT, carbazole (CAR) and dibenzofuran (DBF) were measured in the condensed phase by UV linear and magnetic circular dichroism.[6,7] Important findings in terms of the effects of heavy atoms, planarity and rigidity of heterocyclic molecules on their photophysical properties and ISC rates have recently been reported.[8-10] Zander and Kirsch[8] have found that the fluorescence quantum yield decreases by a factor of 16 upon substitution of the oxygen atom in DBF by sulfur. Nijegorodov and co-workers[10] have shown that the change in fluorescence quantum yield in the series FLU-CAR-DBF-DBT can be entirely attributed to the internal heavy atom effect in the condensed phase experiments. This observation suggests a considerable increase in ISC rate constant $k_{ST}$, due to increases in magnitude of the

spin-orbit coupling operator in the molecular Hamiltonian and in the degree of conjugation of the heteroatom's electron lone pairs with the $\pi$-electron cloud. Thus, replacement of carbon atoms by either oxygen or sulfur always red-shifts the fluorescence excitation frequency, lowers the fluorescence quantum yield, and increases $k_{ST}$ in electronic excitation.[11]

Interestingly, some nitrogen- and oxygen-containing heterocycles also manifest different fluorescence and phosphorescence properties.[11,12] Hetereocycles such as 2,5-diphenylfuran (DPF) and 2,5-diphenyl-1,3,4-oxadiazole (DPO) are known to exhibit ($S_1$-$T_1$) spin-orbit coupling, facilitating the ISC efficiency.[13-15] What is not known is how these molecules behave as isolated species in the gas phase.

In this work, we report the rotationally resolved $S_1 \leftarrow S_0$ fluorescence excitation spectra of DBT, DPF and DPO in the collision-free environment of a molecular beam. These molecules lie in the statistical limit of ISC and therefore exhibit anomalous Lorentzian (lifetime) broadening in their rotational transitions, from which their fluorescence lifetimes can be determined. This makes possible an examination of the trends in ISC dynamics exhibited by the entire family of molecules.

## 7.3 EXPERIMENTAL

DBT, DPF, and DPO (>98% pure) were purchased from Aldrich and used without further purification. Either dry helium or argon was used as an inert carrier gas for our experiments.

In the vibrationally resolved experiments, samples were seeded into 55 psi of helium gas (for DBT) and 20 psi of argon gas (for DPF and DPO) and expanded into a vacuum chamber ($10^{-5}$ torr) through a 1 mm diameter orifice pulsed valve (General Valve Series 9) operating at 10

Hz. Two centimeters downstream of the valve, the free jet was excited with the second harmonic of a Quanta Ray $Nd^{3+}$:YAG (Model DCR-1A) pumped dye laser (Model PDL-1). The dye laser output (DCM for DBT and DPF, and Kiton Red 620 for DPO) was frequency doubled with an external KDP crystal providing a spectral resolution of ~0.6 $cm^{-1}$ in the UV. The molecules were excited at the point of intersection between the jet and the laser beam and the resulting fluorescence was collected with a photomultiplier tube (PMT). Finally, the collected data were processed by a boxcar integrator (Stanford Research Systems) and recorded with Quick Data Acquisition software (Version 1.0.5).

Rotationally resolved electronic experiments were performed using a molecular beam laser spectrometer, described in detail elsewhere.[16] Briefly, the molecular beam was formed by expansion of vaporized samples seeded either in helium (-5 psi) or argon (-16 psi) through a heated (~395 K) 200 $\mu$m quartz nozzle into a differentially pumped vacuum system. The expansion was skimmed 2 cm downstream with a 1 mm diameter skimmer and crossed 13 cm further downstream by a continuous wave (CW) $Ar^+$ pumped ring dye laser. The CW laser was operated with either DCM or Rhodamine 6G dye and intracavity frequency doubled in either a 630 nm $LiIO_3$ or a 600 nm $\beta$-barium borate (BBO) crystal, yielding ~250 $\mu$W of UV radiation with a resolution of ~1 MHz. The fluorescence excitation spectra were detected, using spatially selective optics, by a PMT and a photon counting system. The PMT signal together with the iodine absorption spectrum and the relative frequency markers were simultaneously collected and processed by the JBA95 data acquisition system.[16] Absolute frequency calibration of the spectra was performed by comparison with the $I_2$ absorption spectrum. The relative frequency markers were obtained from a stabilized etalon with a free spectral range of 299.7520 ± 0.0005 MHz.

## 7.4 RESULTS

Figure 7.1 shows the vibrationally resolved (low resolution) fluorescence excitation spectra of FLU, CAR, DBF, and DBT in a supersonic jet. Similar scans of some of these spectra have been previously reported elsewhere.[17-19] However, the jet-cooled low resolution LIF spectrum of DBT is presented here for the first time. Two relatively intense vibronic bands (marked in Figure 7.1d) appear in the spectrum of DBT at 202 and 482 $cm^{-1}$ above the origin band. These vibronic bands in DBT lie at frequencies similar to those previously observed in FLU, CAR, and DBF; some of these exhibit different band polarizations due to a Herzberg-Teller coupling mechanism involving the $S_2$ state.[20]

Figure 7.2 shows the rotationally resolved $S_1 \leftarrow S_0$ fluorescence excitation spectrum of the $0_0^0$ band of DBT, located at 31187.3 $cm^{-1}$ (about 2588 $cm^{-1}$ red-shifted from that of FLU[20]). It spans approximately 2.5 $cm^{-1}$ and exhibits an overall broad bandwidth and pure *b*-type character. To fit this spectrum, we first generated ~9000 rovibronic transitions based on *ab initio* estimates[21] of the $S_0$ rotational constants and rigid rotor Hamiltonians for both electronic states, using *b*-type selection rules. Then, we made quantum number assignments of single transitions in the simulated spectrum to corresponding transitions in the experimental spectrum, using the Windows-based program JB95.[22] Finally, we used a least squares fitting procedure to optimize the rotational constants, based on a comparison of observed and calculated line positions. The final fit utilized 176 rovibronic transitions and resulted in a standard deviation (OMC) of 3.5 MHz. The quality of this fit is shown in the bottom panel of Figure 7.2. Individual lines in the fit exhibit Voigt profiles, with a Gaussian linewidth of 18 MHz and a Lorentzian linewidth of 167 MHz. The rotational temperature of the fit is 9 K.

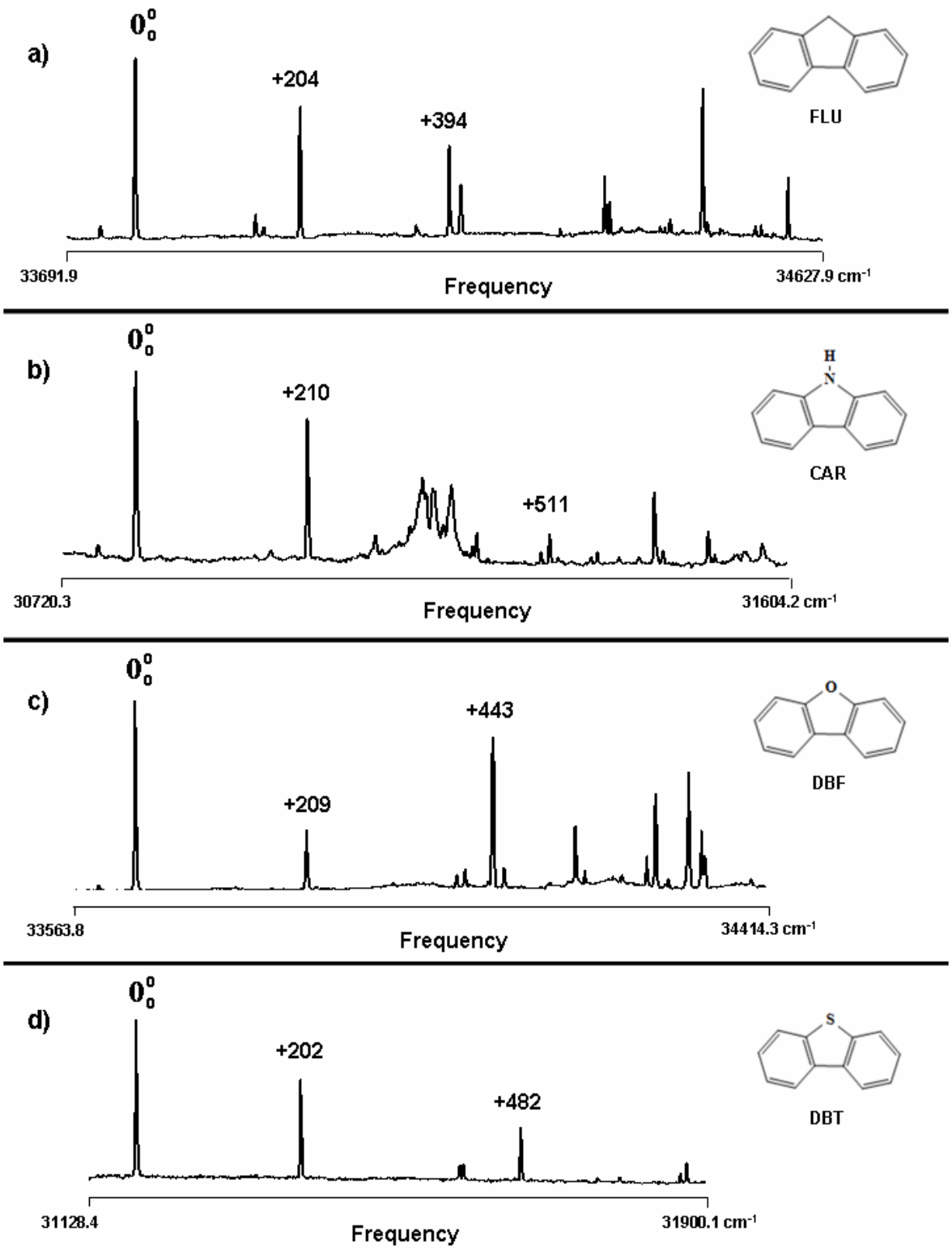


**Figure 7.1. Vibrationally resolved fluorescence excitation spectra of fluorene, carbazole, dibenzofuran, and dibenzothiophene in the gas phase.**

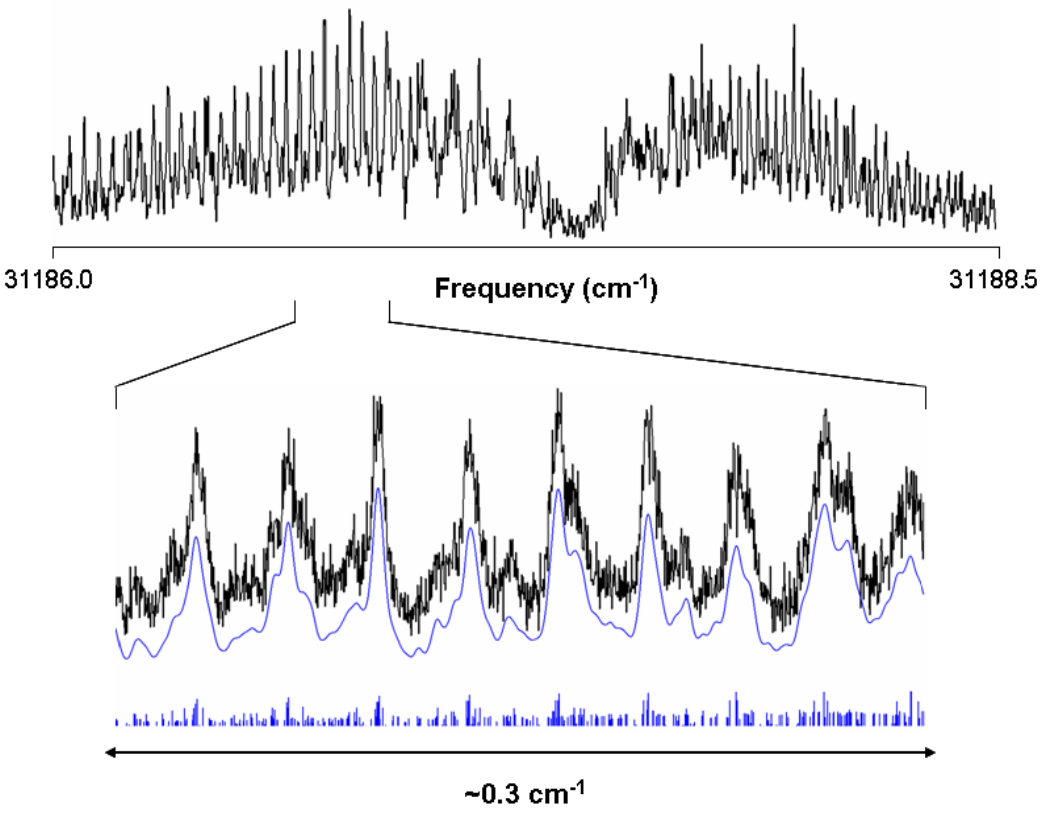


**Figure 7.2. Rotationally resolved fluorescence excitation spectrum of the $0_0^0$ band of DBT in the gas phase; the origin frequency is at 31187.3 cm$^{-1}$. Portions of the experimental trace and its corresponding simulated spectrum, with and without a lineshape function, are also shown in the bottom panel.**

Similarly, the DBT+202 vibronic transition also has been recorded and fully analyzed. The rotationally resolved electronic spectrum of this band spans approximately 2.5 cm$^{-1}$ and exhibits pure *b*-type rovibronic transitions. The Voigt profile used for the fit required 18 MHz Gaussian and 196 MHz Lorentzian contributions. The rotational temperature of the fit is 10 K. The inertial parameters of these two bands are reported in Table 7.1.

Figure 7.3 shows the corresponding low resolution LIF spectra of DPF and DPO in the gas phase. The features observed in both spectra agree with the ones previously reported by Topp and co-workers.[23] The $0_0^0$ band of DPF is red-shifted by ~18087 and ~3031 cm$^{-1}$ with respect to the $\pi\pi^*$ origin bands of furan[24] and DBF,[20] respectively. The two most intense vibronic

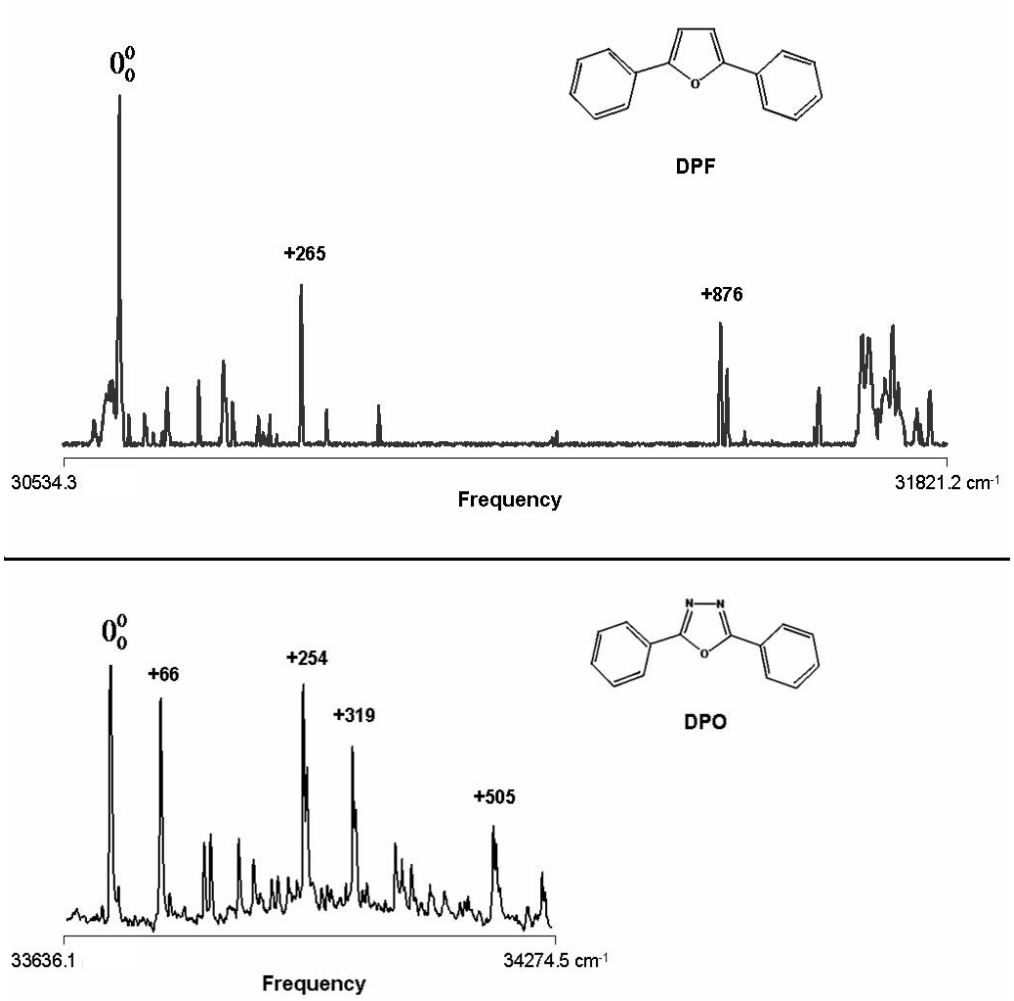


**Figure 7.3. Vibrationally resolved fluorescence excitation spectra of 2,5-diphenylfuran and 2,5-diphenyl-1,3,4-oxadiazole in the gas phase.**

transitions have been found at 265 and 876 $cm^{-1}$ away from the origin band. The $0_0^0$ band of DPO, however, is ~3000 $cm^{-1}$ blue-shifted from that of DPF and exhibits more vibronic activity in the region near the origin, such as the +66 and +254 $cm^{-1}$ bands.

Figure 7.4 shows the rotationally resolved $S_1 \leftarrow S_0$ fluorescence excitation spectrum of the $0_0^0$ band of DPF at 30613.3 $cm^{-1}$. It spans approximately 1.2 $cm^{-1}$ and exhibits pure *a*-type character, revealing that the $S_1 \leftarrow S_0$ transition moment vector is oriented parallel to the *a*-inertial axis. A procedure similar to that used for DBT was used to fit this band. The final fit,

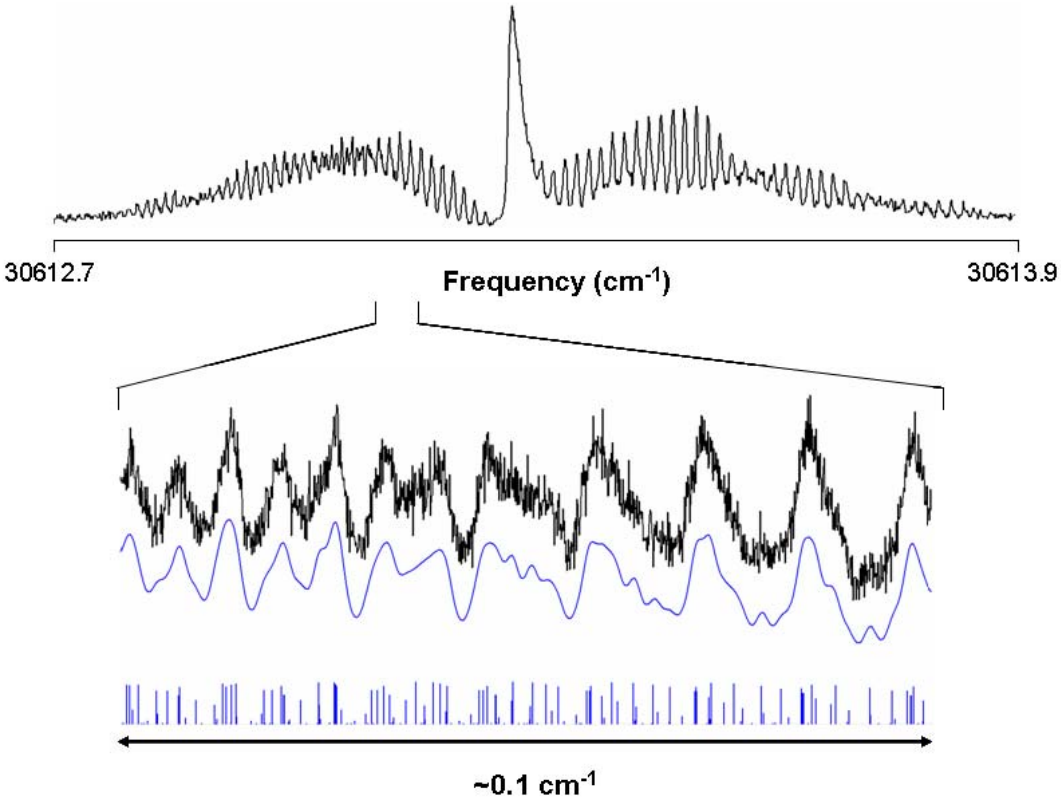


**Figure 7.4. Rotationally resolved fluorescence excitation spectrum of the $0_0^0$ band of 2,5-diphenylfuran in the gas phase; the origin frequency is at 30613.3 cm$^{-1}$. Portions of the experimental trace and its corresponding simulated spectrum, with and without a lineshape function, are also shown in the bottom panel.**

using rigid rotor Hamiltonians, utilized ~150 assigned transitions and resulted in a standard deviation of 2.98 MHz. The rotational temperature of the fit is 4 K. The Voigt lineshape profile required 18 MHz Gaussian and 75 MHz Lorentzian contributions. The quality of the fit is shown at the bottom of Figure 7.4, where a fully resolved portion of the experimental *P* branch is shown along with its simulated spectrum.

Finally, Figure 7.5 shows the rotationally resolved $S_1 \leftarrow S_0$ fluorescence excitation spectrum of the $0_0^0$ band of DPO in the gas phase. It spans approximately 1.3 cm$^{-1}$ and also exhibits pure *a*-type character. To fit this spectrum, rigid rotor Hamiltonians were used for both electronic states. Approximately 130 simulated rovibronic transitions were assigned to the

experimental spectrum, resulting in a standard deviation of 2.40 MHz. The rotational temperature of the fit is 5 K. The Voigt profile used 18 MHz Gaussian and 77 MHz Lorentzian contributions. The inertial parameters of the fits of these two bands are also reported in Table 7.1.

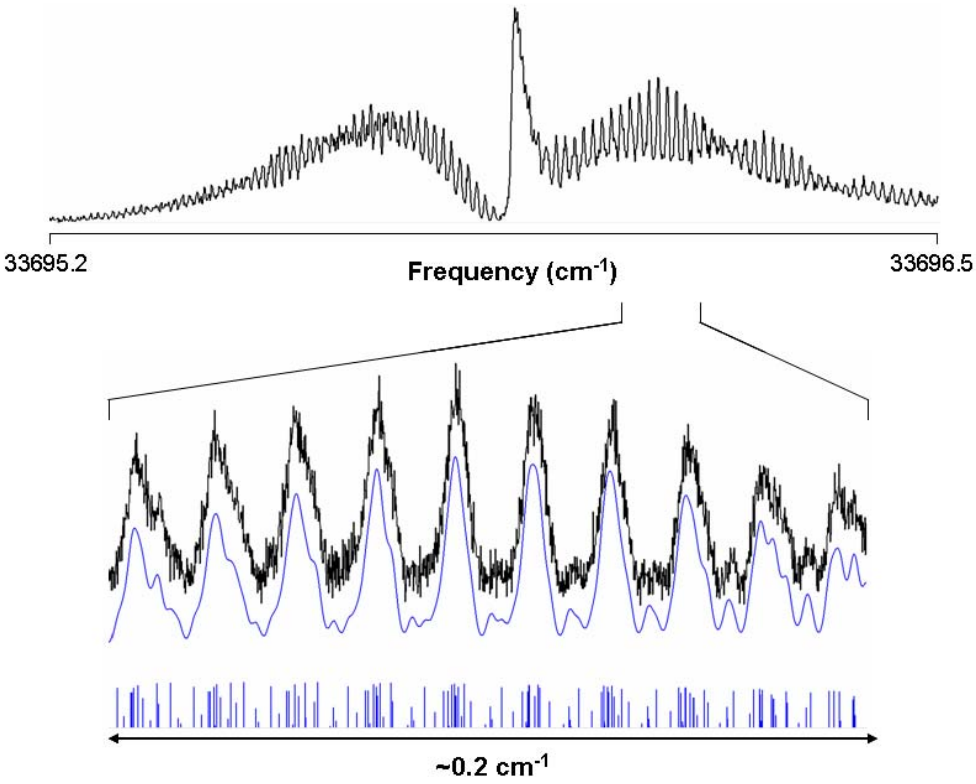


**Figure 7.5. Rotationally resolved fluorescence excitation spectrum of the $0_0^0$ band of 2,5-diphenyl-1,3,4-oxadiazole in the gas phase; the origin frequency is at 33695.9 cm$^{-1}$. Portions of the experimental trace and its corresponding simulated spectrum, with and without a lineshape function, are also shown in the bottom panel.**

## 7.5 DISCUSSION

The rotationally resolved $S_1 \leftarrow S_0$ fluorescence excitation spectra of fluorene (FLU), carbazole (CAR), and dibenzofuran (DBF) in the gas phase have been recently analyzed.[20] This analysis shows that some of the higher lying vibronic bands exhibit anomalous polarizations, suggesting a

**Table 7.1. Inertial parameters of the origin bands of DBT, DPF, and DPO in their ground and excited electronic states.**

| Parameter[a] | DBT[b] | DBT +202 | DPF[c] | DPO[d] |
|---|---|---|---|---|
| **$S_0$** | | | | |
| ***A″* (MHz)** | 1606.9 (1) | 1606.0 (1) | 1449.7 (1) | 1619.7 (1) |
| ***B″* (MHz)** | 578.7 (1) | 578.9 (1) | 217.8 (1) | 212.9 (1) |
| ***C″* (MHz)** | 425.7 (1) | 425.8 (1) | 189.2 (1) | 187.9 (1) |
| **$\Delta I''$ (amu Å$^2$)** | -0.74 (5) | -0.75 (5) | 1.86 (5) | 3.35 (5) |
| **$S_1$** | | | | |
| ***A′* (MHz)** | 1628.1 (1) | 1629.7 (1) | 1456.5 (1) | 1629.9 (1) |
| ***B′* (MHz)** | 569.7 (1) | 570.0 (1) | 218.8 (1) | 213.5 (1) |
| ***C′* (MHz)** | 422.3 (1) | 422.3 (1) | 190.0 (1) | 188.5 (1) |
| **$\Delta I'$ (amu Å$^2$)** | -0.73 (5) | 0.00 (5) | 3.22 (5) | 4.10 (5) |
| **Band origin (cm$^{-1}$)** | 31187.3 | 31389.3 | 30613.3 | 33695.9 |
| **OMC (MHz)** | 3.51 | 4.04 | 2.98 | 2.40 |
| **Band type** | *b* | *b* | *a* | *a* |

[a] The standard deviations in the last significant figure are shown in parentheses.
[b] MP2/6-31G** rotational constants: $A''$ = 1597.4 MHz, $B''$ = 579.0 MHz, $C''$ = 425.0 MHz.
[c] MP2/6-31G** rotational constants: $A''$ = 1420.5 MHz, $B''$ = 218.4 MHz, $C''$ = 189.3 MHz.
[d] MP2/6-31G** rotational constants: $A''$ = 1610.1 MHz, $B''$ = 212.7 MHz, $C''$ = 187.9 MHz.

Herzberg-Teller coupling of the $S_1$ state with a nearby $S_2$ state. Here, we analyze the lifetime (Lorentzian) broadening of single rovibronic transitions of DBT, and contrast its behavior with that of its analogs (FLU, CAR, and DBF) in greater detail.

From the fit of the spectrum in Figure 7.2, we find that DBT exhibits a *b*-axis polarized $S_1 \leftarrow S_0$ electronic transition, in agreement with previous results in crystal lattices.[4,5] The $S_1$ state of the isolated DBT is therefore an $L_a$ state in the Platt perimeter model (see Figure 7.6a).[25] This means that its photochemical behavior will be similar to that of CAR and DBF (which also have lowest $^1L_a$ states), but very different from that of FLU (which has a lowest $^1L_b$ state).[20]

The calculated ground state rotational constants (MP2/6-31G**) of DBT are in excellent agreement with the experimental ones (*cf.* Table 7.1). In most aromatic molecules, excited state $A'$, $B'$, and $C'$ values are less in magnitude than their ground state counterparts, owing to the small ring expansions that are typical of the $\pi\pi^*$ states. However, in DBT, $\Delta A$ ($A'$ - $A''$) is

positive (21.2 MHz), whereas Δ*B* and Δ*C* are slightly negative (-9.0 and -3.4 MHz, respectively). Similar effects were observed in CAR and DBF.[20] All three molecules appear to contract in directions perpendicular to *a* when the photon is absorbed. In contrast Δ*A* in fluorene is large and negative, suggesting an expansion in directions perpendicular to *a*. There also is more delocalization of the lone pair electrons in CAR and DBT, compared to DBF and FLU, since their origin bands are red shifted by relatively large amounts.

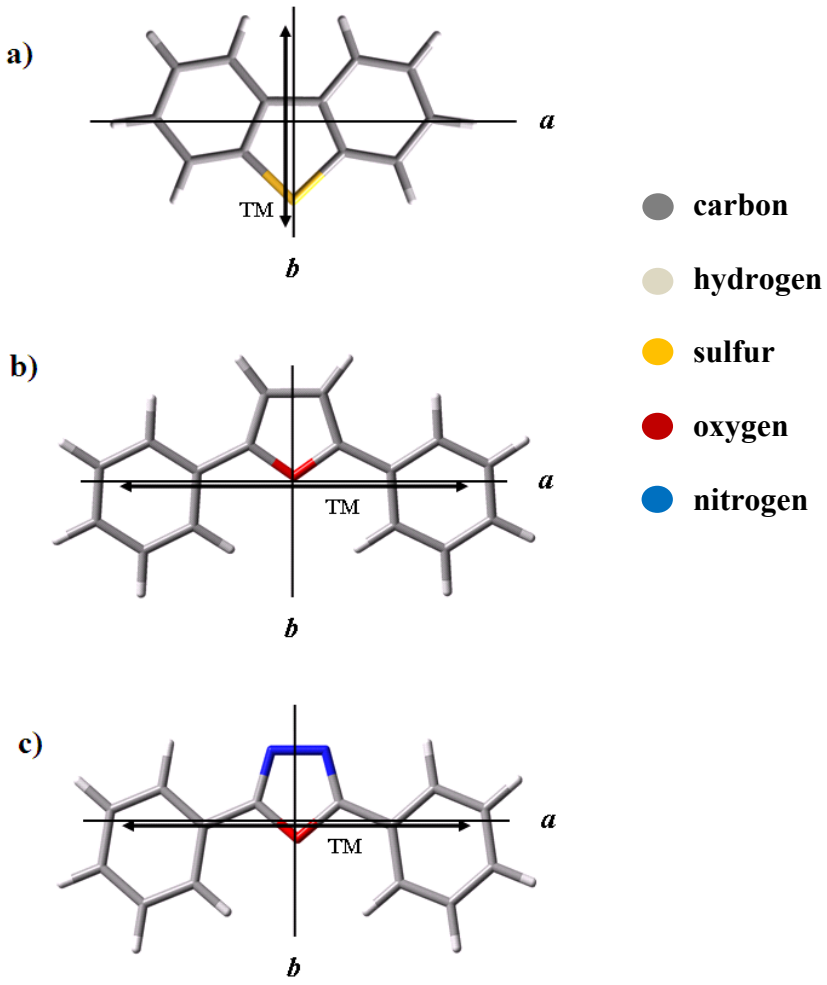


**Figure 7.6. $S_1 \leftarrow S_0$ electronic transition moment orientations in a) dibenzothiophene, b) 2,5-diphenylfuran, and c) 2,5-diphenyl-1,3,4-oxadiazole.**

DBT is essentially planar in both electronic states. It has inertial defect values ($\Delta I = I_c - I_a - I_b$) of -0.74 amu Å$^2$ in its $S_0$ state and -0.73 amu Å$^2$ in its $S_1$ electronic state, values that are consistent with a planar molecule ($\Delta I \approx 0$). These inertial defects do not seem to change substantially when the molecule absorbs light.

The analysis of the most intense vibronic band of DBT (202 cm$^{-1}$ away from its origin band) shows that the active mode is the totally symmetric in-plane ring bending mode, in analogy to what was observed for the CAR+210, and DBF+209 bands.[20] This assignment is in agreement with the parallel band polarization observed in the high resolution spectrum with respect to its $0_0^0$ band. Furthermore, the inertial defect values for this vibronic band follow the trend observed for the corresponding bands of CAR and DBF in both electronic states. The $\Delta I'$ value decreases in magnitude from -0.73 to 0.00 amu Å$^2$, whereas the $\Delta I''$ value does not change (-0.74 amu Å$^2$) when going from the $0_0^0$ to the +202 band in DBT (*cf.* Table 7.1). These observations are in excellent agreement with the theoretical results of Lee.[26]

A remarkable observation from the fits of the high resolution electronic spectra of DBT is the requirement of a significant Lorentzian contribution to the Voigt lineshape profiles, in contrast with those used in the fits of the corresponding spectra of FLU, CAR, and DBF. The vibronic bands DBT+202 and CAR+210 are compared in Figure 7.7. In DBT+202 a Lorentzian (natural) broadening of 195 MHz is required to properly fit the experimental trace, whereas in CAR+210, the Lorentzian contribution to the Voigt profile is only 18 MHz. The Gaussian contribution in both spectra is 18 MHz. Apparently, the presence of a heavy atom in the molecular structure contributes to the enhancement of the ISC dynamics by increasing the spin-orbit coupling terms ($\upsilon_{sk}$) in the Hamiltonian and increasing the density of dark states {|k>} available in the vicinity of the prepared singlet state |s>.

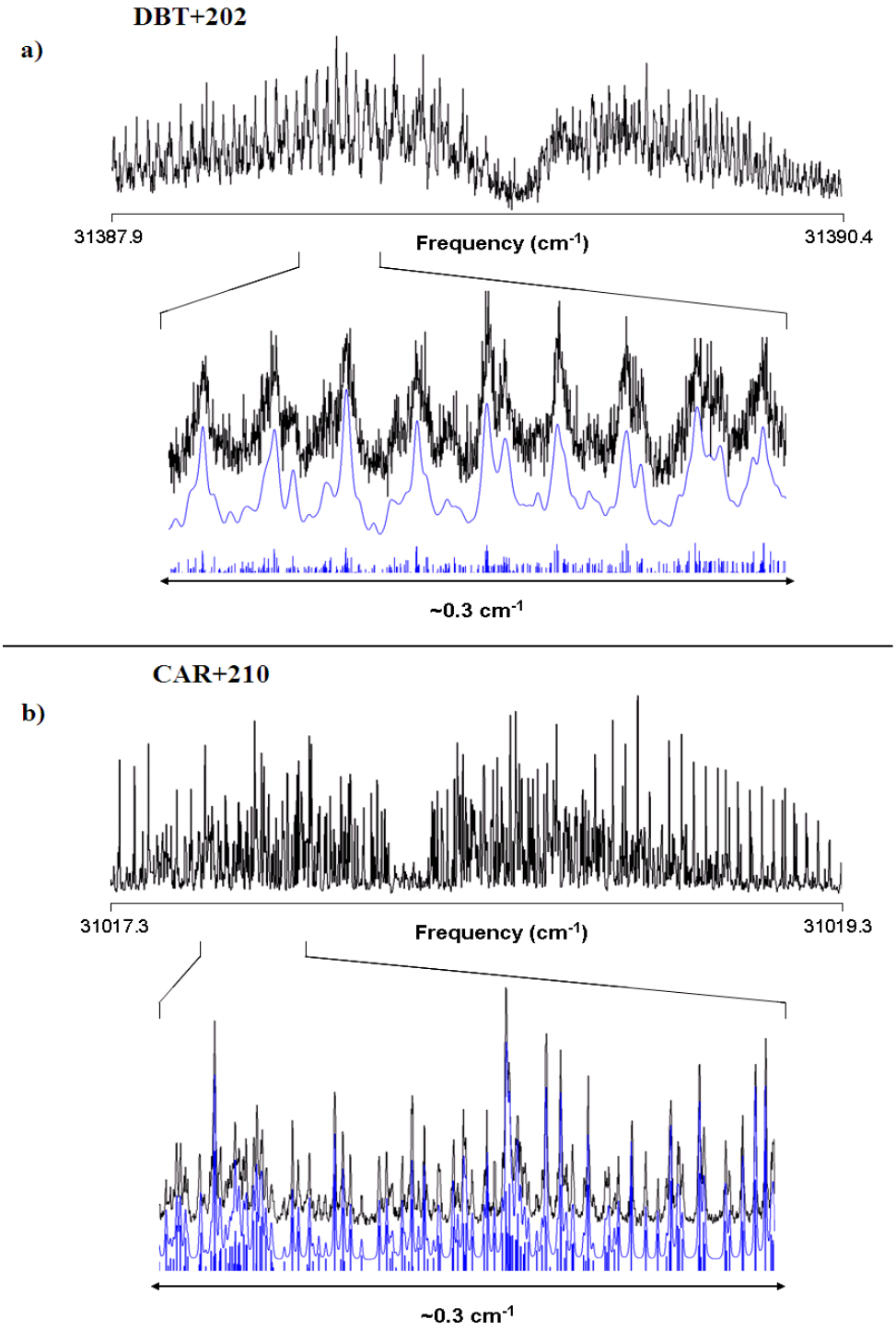


**Figure 7.7. a) Heavy atom effect in a vibronic band of dibenzothiophene (DBT+202) in the gas phase. A Lorentzian broadening of 195 MHz has been applied in the simulated trace. b) The analogous transition of carbazole (CAR+210) is shown for comparison. The Lorentzian broadening of the fit is 18 MHz. The Gaussian (Doppler) broadening is 18 MHz in both spectra.**

In order to further investigate the ISC dynamics in this family of molecules (FLU-CAR-DBF-DBT), the fluorescence decay widths $\gamma_s$ (in MHz) have been summarized in Table 7.2 for each transition in every molecule analyzed. Then, the corresponding fluorescence lifetimes $\tau_s$ (in ns) are computed using the relationship between $\gamma_s$ and $\tau_s$, given by

$$\gamma_s = \frac{1}{2\pi\tau_s}. \qquad \textbf{(7.1)}$$

Interestingly, the longest $\tau_s$ value is observed in the $0_0^0$ band of carbazole, 14.5 ns. We also observe that the vibrational motion decreases the lifetime in the $S_1$ state of the molecules, presumably by IVR. At some extent, it is promoted by means of internal conversion along different low frequency relaxation vibrational coordinates; even though the vibronic bands show significant oscillator strengths. However, the most remarkable finding is the decrease of the fluorescence lifetime of DBT by a factor of ~10 with respect to what is observed in FLU. This

**Table 7.2. Experimental fluorescence lifetime broadenings and $S_1$ lifetimes of some vibrational bands of FLU, CAR, DBF and DBT from fits of their high resolution spectra in the gas phase.[a,b]**

| Band | Fluorescence lifetime broadening $\gamma_s$ (MHz) | Lifetime in the $S_1$ state, $\tau_s$ (ns) |
|---|---|---|
| **FLU** | 15 (1) | 10.6 (7) |
| **FLU+204** | 24 (1) | 6.6 (4) |
| **FLU+394** | 30 (1) | 5.3 (2) |
| **CAR** | 11 (1) | 14.5 (8) |
| **CAR+210** | 18 (1) | 8.8 (6) |
| **CAR+511** | 23 (1) | 6.9 (4) |
| **DBF** | 21 (1) | 7.6 (4) |
| **DBF+209** | 31 (2) | 5.1 (2) |
| **DBF+443** | 27 (1) | 5.9 (3) |
| **DBT** | 167 (6) | 1.0 (<1) |
| **DBT+202** | 195 (6) | 0.8 (<1) |

[a] See Reference 20 for spectral details on the corresponding transitions of FLU, CAR, and DBF.
[b] The standard deviations in the last significant figure are shown in parentheses.

last observation is in good agreement with previous studies about the photophysical properties of several heterocycles in the condensed phase.[8,10]

As previously suggested by McClure,[27] the electronic Hamiltonian describing aromatic polyatomic molecules might require the incorporation of an extra term, namely a "spin-orbit interaction operator". As a consequence of these π-electronic spin-orbit interactions, perturbations which one ordinarily neglects are now relatively important causes of singlet-triplet mixing, and may well be responsible for the intercombination transitions that are actually observed.

From the earlier reports of McClure[27] and Gastilovich *et al*.[28], spin-orbit coupling (SOC) terms for the atoms C, N, O, and S have been obtained and analyzed in contrast with the fluorescence lifetime ($\tau_s$) obtained in this work for FLU, CAR, DBF, and DBT. As observed in Figure 7.8, apparently $\tau_s \propto \sqrt{\text{SOC}}$ in the series analyzed. CAR, however, does not fit in the same trend (it has been actually excluded); the anomalous behavior in CAR might be due to a reduced unpaired electron spin density on nitrogen in its $T_1$ state, since its lifetime is much longer than expected.

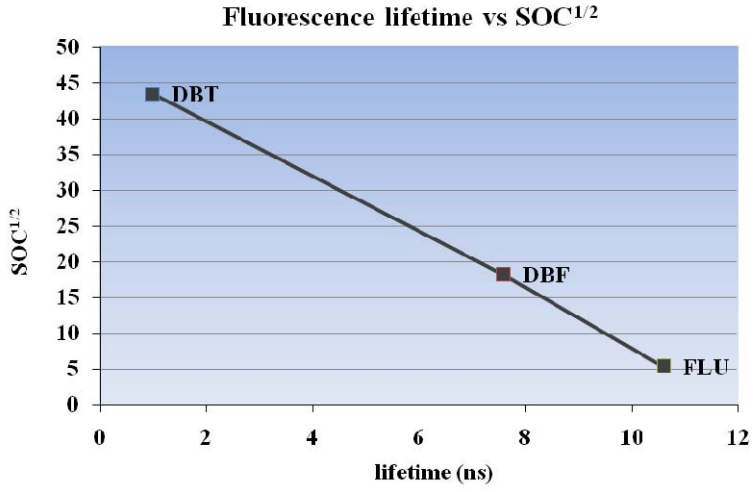


**Figure 7.8 Plot of the fluorescence lifetimes vs. the spin-orbit coupling terms of fluorene, dibenzofuran, and dibenzothiophene.**

The low resolution spectra of DPF and DPO exhibit several vibrational features in the low frequency range (*cf*. Figure 7.3). Topp and co-workers[23] have assigned the vibrational band at ~66 $cm^{-1}$ to an overtone (2 × 33 $cm^{-1}$) of the torsional motion of the phenyl groups with respect to the central ring. The band at ~260 $cm^{-1}$ has been assigned to a fundamental in-plane inter-annular bending motion in both molecules, whereas the group of lines at ~876 $cm^{-1}$ in DPF are strongly coupled, exhibit Franck-Condon progressions, and are assigned as an in-plane vibrational mode acting in the furan ring. We focus our study on the zero point vibrational level (ZPL) transition of each molecule here.

From the fits of the rotationally resolved spectra in Figures 7.4 and 7.5, we find that both molecules have long-axis polarized $S_1 \leftarrow S_0$ electronic transition moment vectors (*cf*. Figures 7.6b and 7.6c). The $S_1$ states of DPF and DPO are both $L_b$ states. This result indicates that the presence of the phenyl groups in the 2- and 5- positions of the central ring modify the electronic distribution of the frontier molecular orbitals; hence, the $S_1$ states are different from that exhibited by DBF ($^1L_a$ state).

In these two molecules, the calculated $S_0$ rotational constants are again in good agreement with the experimental values (see Table 7.1). Surprisingly, in these "more flexible" molecules, the changes in rotational constants upon excitation are all positive; $\Delta A$ = 6.8, $\Delta B$ = 1.0, and $\Delta C$ = 0.8 MHz in DPF and $\Delta A$ = 10.2, $\Delta B$ = 0.6, and $\Delta C$ = 0.6 MHz in DPO. Apparently, upon excitation the molecules contract in directions perpendicular to the *a*-axes of the molecules. Both molecules are essentially planar in both $S_0$ and $S_1$ states. DPF has an inertial defect value of 1.86 amu $Å^2$ in its $S_0$ state, a value that is consistent with a planar molecule having some in-plane degrees of freedom. However, by absorption of light this value increases in magnitude to 3.22 amu $Å^2$, which highlights the floppiness of the molecule along certain in-plane torsional

coordinates. DPO exhibits similar behavior in terms of inertial defect values, but these are somewhat larger in magnitude ($\Delta I''$ = 3.35 amu Å$^2$ and $\Delta I'$ = 4.10 amu Å$^2$). Electronically excited state calculations predict small changes within the central five-membered ring, due to the presence of the two nitrogen atoms in the structure.

At first glance, the appearances of the two rotationally resolved electronic spectra of DPF and DPO shown in Figures 7.4 and 7.5 are strange, even though the rotational temperature is fairly low (4 K) and the single rotational transition Doppler broadening is just 18 MHz. Therefore, the natural lineshape broadening exhibited in both spectra is a direct consequence of the enhanced ISC dynamics by the presence of the heteroatoms in the central five-membered ring. As it has been previously studied by Obukhov,[11,14] there are many variations in fluorescence properties due to the intramolecular interaction of nitrogen, oxygen, or sulfur atoms in 2-, 3-, 4- or 5- non-concatenated chains of either five- or six-member ring heterocycles. In the condensed phase (ethanol) experiments the excited state lifetimes for DPF and DPF are reported to be ~0.4 ns.[14] The estimated excited state lifetimes from our experiments in the gas phase are computed using Equation (7.1); the values are ~2.1 (1) ns for both molecules.

Presumably, in DPF and DPO there is a high density of vibrational states due to the low-frequency torsional motion of the phenyl groups with respect to the central ring. In a separate publication, we have studied the effect of the low-frequency methyl group torsional levels on the ISC dynamics of molecules containing a chromophore falling in the "intermediate" molecule limit; 2-methylpyrimidine and 5-methylpyrimidine.[29] In that work, we clearly observed the appearance of extra lines in the rotationally resolved electronic spectra, and a considerable increase of rovibronic transitions in contrast with what had been previously observed in pyrimidine itself.[30] Due to the fact that furan and oxadiazole heterocycles fall in the statistical

molecule limit, we believe that their corresponding phenyl derivatives, DPF and DPO respectively, do not exhibit well defined spectral signatures in the high resolution spectra analyzed here.

It would be interesting to complement the present study with the analysis of some of the representative vibronic bands of these two molecules, and some other non-concatenated polycycles with no heteroatoms present, such as *p*-terphenyl. This molecule is expected to exhibit ISC dynamics due to the presence of a nearby triplet state ($T_\beta$).[31]

## 7.6 SUMMARY

Rotationally resolved $S_1 \leftarrow S_0$ fluorescence excitation spectra of the $0_0^0$ bands of DBT, DPF, and DPO have been recorded in the collision-free environment of a molecular beam. Detailed analyses of these spectra make evident the existence of an ISC mechanism in the large molecule (statistical) limit upon excitation by UV light. DBT constitutes a special case in the family of FLU-CAR-DBF-DBT; since it exhibits a heavy atom effect by a considerable (factor of ~10) reduction of its excited state lifetime (~1 ns), with respect to the value exhibited by FLU (~10 ns). DPF and DPO also exhibit short excited state lifetimes (~2 ns), presumably due to the high density of dark state energy levels in the vicinity of the prepared state.

## 7.7 ACKNOWLEDGMENTS

L. Alvarez thanks Dr. M. Villanueva (U. Gto., Mexico) for his kind collaboration in some of the theoretical calculations described here. This work has been supported by NSF (CHE-0615755) to whom we are grateful.

## 7.8 REFERENCES

1. G. W. Robinson, *J. Chem. Phys.*, **47**, 1967 (1967).

2. P. W. Atkins, *Physical Chemistry*, 6th edition, W. H. Freeman and Co.: New York, 1998, pp 503-6.

3. A. Bree and R. Zwarich, *Spectrochim. Acta* **27A**, 599 (1971).

4. A. Bree and R. Zwarich, *Spectrochim. Acta* **27A**, 621 (1971).

5. E. Castellucci, P. Foggi, and P. R. Salvi, *Chem. Phys.* **63**, 437 (1981).

6. H. Yamaguchi and M. Higashi, *Spectrochim. Acta* **43A**, 1431 (1987).

7. J. Spanget-Larsen and E. W. Thulstrup, *J. Mol. Struct.* **661-662**, 603 (2003).

8. M. Zander and G. *Z.* Kirsch, *Naturforsch*. **44A**, 205 (1989).

9. X. Wang, J. Tian, W. G. Kofron, and E. C. Lim, *J. Phys. Chem.* **103A**, 1560 (1999).

10. N. Nijegorodov, P. V. C. Luhanga, J. S. Nkoma, and D. P. Winkoun, *Spectrochim. Acta* **64A**, 1 (2006) and references therein.

11. A. E. Obukhov, *Laser Physics* **13**, 847 (2003).

12. M. Kamiya, *Bulletin of the Chemical Society of Japan* **43**, 3344 (1970).

13. G. A. Abakumov, S. A. Drobakha, A. V. Klimanov, A. V. Ostrovskii, B. I. Polyakov, and A. P. Simonov, *Kvantovaya Elektron* **13**, 2364 (1986).

14. A. E. Obukhov, *Laser Physics* **9**, 699 (1999).

15. S. Luňák Jr., M. Nepraš, R. Hrdina, A. Kurfürst, and J. Kuthan, *Chem. Phys.* **170**, 77 (1993).

16. W. A. Majewski, J. F. Pfanstiel, D. F. Plusquellic, and D. W. Pratt, *Laser Techniques in Chemistry*. T. R. Rizzo and A. B. Myers, Eds. J. Wiley & Sons: New York, 1995, pp 101.

17. S. Leutwyler, U. Even, and J. Jortner, *Chem. Phys. Lett.* **86**, 439 (1982).

18. A. R. Auty, A. C. Jones, and D. Phillips, *J. Chem. Soc., Faraday Trans. 2* **82**, 1219 (1986).

19. T. Chakraborty and E. C. Lim, *Chem. Phys. Lett.* **207**, 99 (1993).

20. J. T. Yi, L. Alvarez-Valtierra, and D. W. Pratt, *J. Chem. Phys.* **124**, 244302 (2006).

21. M. J. Frisch, *et al*. *Gaussian 03*, Revision C.02; Gaussian, Inc.: Wallingford, CT, 2004.

22. D. F. Plusquellic, *JB95* Spectral fitting program, NIST, Gaithersburg, MD. http://physics.nist.gov/jb95.

23. E. A. Mangle, P. R. Salvi, R. J. Babbit, A. L. Motyka, and M. R. Topp, *Chem. Phys. Lett.* **133**, 214 (1987).

24. J. L. Roebber, D. P. Gerrity, R. Hemley, and V. Vaida, *Chem. Phys. Lett.* **75**, 104 (1980).

25. J. R. Platt, *J. Chem. Phys.* **19**, 101 (1951).

26. S. Y. Lee, *J. Phys. Chem.* **105A**, 8093 (2001).

27. D. S. McClure, *J. Chem. Phys.* **20**, 682 (1952).

28. E. A. Gastilovich, S. A. Serov, V. G. Klimenko, N. V. Korol'kova, and R. N. Nurmukhametov, *Mol. Spectrosc.* **99**, 897 (2005).

29. L. Alvarez-Valtierra, X. –Q. Tan, and D. W. Pratt, *J. Phys. Chem. A* (in press).

30. J. A. Konings, W. A. Majewski, Y. Matsumoto, D. W. Pratt, and W. L. Meerts, *J. Chem. Phys.* **89**, 1813 (1988).

31. N. Nijegorodov, D. P. Winkoun, and J. S. Nkoma, *Spectrochim. Acta*, **60A**, 2035 (2004).

## APPENDIX A

## MATHCAD CODE FOR TUNNELING SPLITING IN DHPH

In what follows, a program written in MATHCAD to solve the inversion motion tunneling problem of 9,10-dihydrophenanthrene is described.

| | |
|---|---|
| Conversion factors | $cf1 := 29979.2458\ MHz/cm^{-1}$<br>$cf2 := 1.9864.10^{-23}\ J/cm^{-1}$ |
| Molecular weight | $M := 180.1\ g/mol$ |
| From *ab initio* calculation | $red\_mass := 2.4507$ |
| Reduced mass of the molecule in Kg | $\mu := red\_mass \cdot 1.66054 \cdot 10^{-27}$<br>$\mu = 4.0695 \times 10^{-27}\ Kg$ |

$\upsilon\_cm := 254.7\ cm^{-1}$

Vibrational frequency of the model involved

$\upsilon := \upsilon\_cm \cdot cf1 \cdot 10^{6}$

$\upsilon = 7.6357 \times 10^{12}\ Hz$

hbar constant definition

$hbar := 1.05457 \cdot 10^{-34}\ J \cdot s$

Vibrational quantum number

$\nu := 1$

$\Delta E\_MHz := 26.69\ MHz$

Spectrocopic splitting of the sub-bands from the high resolution spectra

$\Delta E := \Delta E\_MHz \cdot cf2 / cf1$

$\Delta E = 1.7685 \times 10^{-26}\ J$

$\upsilon_0 := 385.25\ cm^{-1}$

Exponential frequency of the transition. “false origin”

$E_0 := \upsilon_0 \cdot cf2$

$E_0 = 7.6526 \times 10^{-21}\ J$

$CH_2$ distance away from plane (geometry optimized calculation)

$min := 4.149 \cdot 10^{-11}\ m$

Definition of the tunneling coordinate

$x := 3.5 \cdot 10^{-11}, 3.50001 \cdot 10^{-11} .. 4.8 \cdot 10^{11}$

Force constant

$k := 16.89\ N/m$

Single – well
Potential Energy Function $V(x) := 2\pi^2 \cdot \upsilon^2 \cdot \mu \cdot (x - \min)^2$

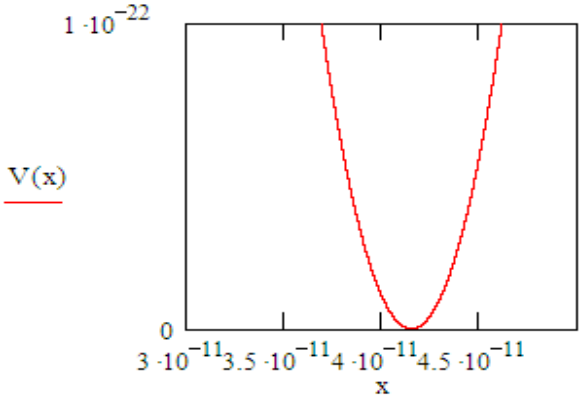


Turning point from
inertial defect plots $x1 := 3.207 \cdot 10^{-11}\ m$

$c := \upsilon^2 \cdot \mu \cdot (-2 \cdot \pi^2)$

Variable definitions to solve
the tunneling equation $y := -hbar \cdot \dfrac{\ln\left(\dfrac{\Delta E}{2 \cdot hbar \cdot \upsilon}\right)}{\sqrt{2\mu}}$

Energy variable $a := 1 \cdot 10^{-20}, 1.0001 \cdot 10^{-20} .. 1.5 \cdot 10^{-19}$

Tunneling equation to solve $z(a) := x1 \cdot \sqrt{a + c \cdot x1^2} + \dfrac{a}{\sqrt{-c}} \cdot a\sin\left(x1 \cdot \sqrt{\dfrac{-c}{a}}\right) - y$

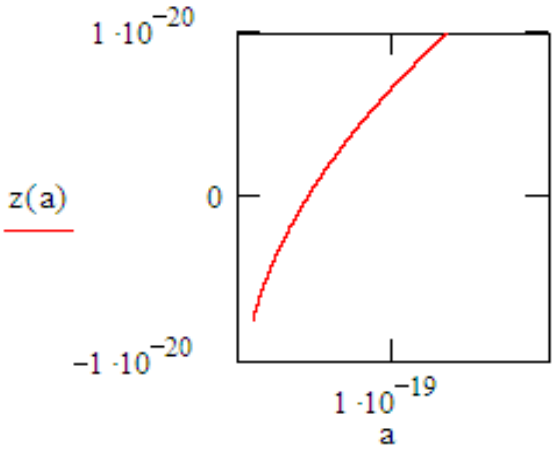


Potential barrier from interpolation

$V_0 := 4.4929 \cdot 10^{-20} + E_0$

$V_0 = 5.2582 \times 10^{-20}$ J

Potential barrier

$V_0\_wn := V_0/cf2$

$V_0\_wn = 2.6471 \times 10^{3}$ cm$^{-1}$

# APPENDIX B

## MATHCAD CODE FOR COMPUTING THE FIRST-ORDER PERTURBATION COEFFICIENTS FROM ESTIMATED TORSIONAL BARRIER HEIGHTS

The MATHCAD program to calculate 1st and 2nd order perturbation coefficients to be incorporated in the rigid rotor Hamiltonian to properly fit the methyl torsional transitions of the 2-methylanisole (2e) spectrum is described in the following code.

### B.1 GENERAL DEFINITION OF PARAMETERS

**2-Me-anisole (v = 1)**

Ground state rotational constants of the methyl rotor (in MHz):

Am_MHz := 273815.3

Bm_MHz := 273815.3

Cm_MHz := 164246.4

Ground state rotational constants of 2MA (in MHz):

AA_MHz := 2490.01

BA_MHz := 1558.96

CA_MHz := 970.71

conv_factor := 505379.007 amu $Å^2$ MHz

conv_factor2 := 29979.2458 $MHz/cm^{-1}$

Moments of inertia of Methyl group (in amu $Å^2$):

Iam := conv_factor/Am_MHz

Iam = 1.846

Ibm := conv_factor/Bm_MHz

Ibm = 1.846

Icm := conv_factor/Cm_MHz

Icm = 3.077

Moments of inertia of 2MA (in amu $Å^2$):

IaA := conv_factor/AA_MHz

IaA = 202.963

IbA := conv_factor/BA_MHz

IbA = 324.177

IcA := conv_factor/CA_MHz

IcA = 520.628

The relative motion is with respect to the ***c*** axis of the methyl group, so the value of **Icm** is the one used for the internal rotation.

For the anisole, it is necessary to calculate the internal-axes system and determine the relative position of the methyl rotor to them.

Angle of the internal rotor to the ***a*** axis of anisole (for 2MA):

$$\alpha := 67.21$$

Direction Cosines

$$\lambda a := \cos(\alpha \cdot deg)$$

$$\lambda b := \cos(90 \cdot deg - \alpha \cdot deg)$$

$$\lambda c := \cos(90 \cdot deg)$$

***Iα*** is the moment of inertia of the internal rotor, this value must be equal to **Icm**, but in this case, the value used is the one reported in Owen N. L., *Studies of internal rotation by microwave spectroscopy* in *Internal rotation in molecules*, Orville and Thomas, Eds. John Wiley and Sons. New York (1974) p. 189.

$$I\alpha := 3.15 \text{ amu } Å^2$$

$$\rho_a := (\lambda a \cdot I\alpha)/IaA$$

$$\rho_a = 6.012 \times 10^{-3}$$

$$\rho_b := (\lambda b \cdot I\alpha)/IbA$$

$$\rho_b = 8.958 \times 10^{-3}$$

$$\rho_c := (\lambda c \cdot I\alpha)/IcA$$

$$\rho_c = 0$$

Reducing factor:

$$r := 1- [(\lambda a^2 \cdot I\alpha)/IaA] - [(\lambda b^2 \cdot I\alpha)/IbA] – [(\lambda c^2 \cdot I\alpha)/IcA]$$

$$r = 0.98941$$

Reduced moment of inertia for internal rotation:

$$reduced\_moment := r \cdot I\alpha$$

$$reduced\_moment = 3.117$$

Internal rotational constant in wavenumbers:

$$F := conv\_factor/reduced\_moment$$

$$F = 162154.615 \text{ MHz}$$

$$FC := F/conv\_factor2$$

$$FC = 5.409 \text{ cm}^{-1}$$

Experimental barrier height from Ichimura and Suzuki (Reference 7 in chapter 5):

$$V3\_S1 := 48.0 \text{ cm}^{-1}$$

Mathieu parameter:

$$s1 := 4 \cdot V3\_S1/(9 \cdot FC)$$

$$s1 = 3.944$$

Barrier in ground state taken from reference 7 in chapter 5:

$$V3\_S0 := 418.0 \text{ cm}^{-1}$$

Mathieu parameter:

$$sg := 4 \cdot V3\_S0/(9 \cdot FC)$$

$$sg = 34.347$$

## B.2 EXCITED STATE

### B.2.1 Second order perturbation coefficients

From Herschbach (Reference 16 in chapter 5):

$$se := \begin{pmatrix} 16 \\ 20 \\ 28 \\ 36 \end{pmatrix} \qquad W2\_1A := \begin{pmatrix} -1.27334 \\ -0.654112 \\ -0.200728 \\ -0.069411 \end{pmatrix} \qquad W2\_1E := \begin{pmatrix} 0.590647 \\ 0.319985 \\ 0.100170 \\ 0.034699 \end{pmatrix}$$

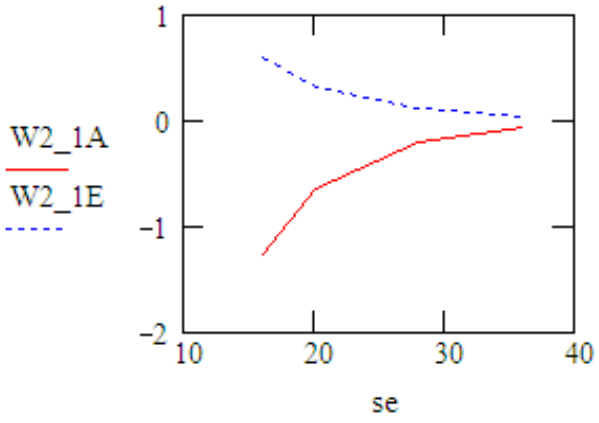

A level parameter:

interp(cspline(se, W2_1A), se, W2_1A, s1) = -6.041

W2_1A_intp := interp(cspline(se, W2_1A), se, W2_1A, s1)

W2_1A_intp = -6.041

E level parameter:

interp(cspline(se, W2_1E), se, W2_1E, s1) = 2.554

W2_1E_intp := interp(cspline(se, W2_1E), se, W2_1E, s1)

W2_1E_intp = 2.554

Second order perturbation coefficients:

$D2AA\_es\_MHz := F \cdot \rho_a^2 \cdot W2\_1A\_intp$

D2AA_es_MHz = -35.402

$D2BA\_es\_MHz := F \cdot \rho_b^2 \cdot W2\_1A\_intp$

D2BA_es_MHz = -78.610

$D2AE\_es\_MHz := F \cdot \rho_a^2 \cdot W2\_1E\_intp$

D2AE_es_MHz = 14.966

$D2BE\_es\_MHz := F \cdot \rho_b^2 \cdot W2\_1E\_intp$

D2BE_es_MHz = 33.231

### B.2.2 First order perturbation coefficients

From reference 16 in chapter 5:

$$se := \begin{pmatrix} 16 \\ 20 \\ 28 \\ 36 \end{pmatrix} \qquad W1\_1E := \begin{pmatrix} 0.7977206 \\ 0.4695574 \\ 0.1594403 \\ 0.0566696 \end{pmatrix}$$

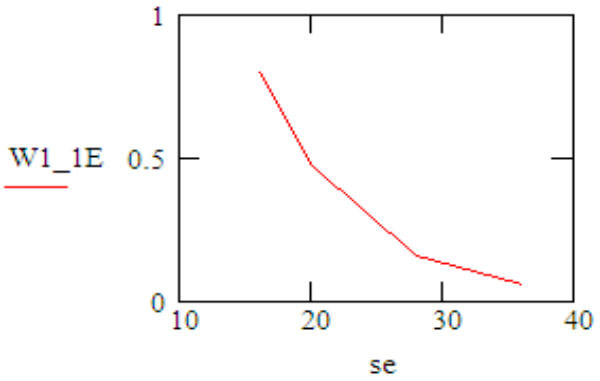


E level parameter:

interp(cspline(se, W1_1E), se, W1_1E, s1) = 2.947

W1_1E_intp := interp(cspline(se, W1_1E), se, W1_1E, s1)

W1_1E_intp = 2.947

First order perturbation coefficient:

$D1A\_es\_MHz := F \cdot \rho_a \cdot W1\_1E\_intp$

$D1A\_es\_MHz = 2.873 \times 10^3$

$D1B\_es\_MHz := F \cdot \rho_b \cdot W1\_1E\_intp$

$D1B\_es\_MHz = 4.281 \times 10^3$

## B.3 GROUND STATE

### B.3.1 Second order perturbation coefficient

From reference 16 in chapter 5:

$$s0:=\begin{pmatrix}16\\20\\28\\36\\40\\48\\56\\60\end{pmatrix} \quad W2\_0A:=\begin{pmatrix}0.052068\\0.024473\\0.006261\\0.001856\\0.001055\\0.0003643\\0.0001354\\0.0000845\end{pmatrix} \quad W2\_0E:=\begin{pmatrix}-0.026025\\-0.012236\\-0.003130\\-0.000928\\-0.0005272\\-0.0001819\\-0.00006769\\-0.00004227\end{pmatrix}$$

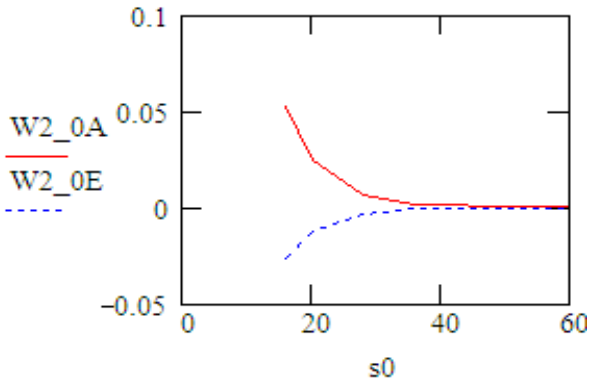


A level parameter:

interp(cspline(s0, W2_0A), s0, W2_0A, sg) = 2.413 x $10^{-3}$

W2_0A_intp := interp(cspline(s0, W2_0A), s0, W2_0A, sg)

W2_0A_intp = 2.413 x $10^{-3}$

E level parameter:

$$\text{interp}(\text{cspline}(s0, W2\_0E), s0, W2\_0E, sg) = -1.206 \times 10^{-3}$$

$$W2\_0E\_intp := \text{interp}(\text{cspline}(s0, W2\_0E), s0, W2\_0E, sg)$$

$$W2\_0E\_intp = -1.206 \times 10^{-3}$$

Second order perturbation coefficients:

$$D2AA\_gs\_MHz := F \cdot \rho_a^2 \cdot W2\_0A\_intp$$

$$D2AA\_gs\_MHz = 0.014$$

$$D2BA\_gs\_MHz := F \cdot \rho_b^2 \cdot W2\_0A\_intp$$

$$D2BA\_gs\_MHz = 0.031$$

$$D2AE\_gs\_MHz := F \cdot \rho_a^2 \cdot W2\_0E\_intp$$

$$D2AE\_gs\_MHz = -0.007$$

$$D2BE\_gs\_MHz := F \cdot \rho_b^2 \cdot W2\_0E\_intp$$

$$D2BE\_gs\_MHz = -0.016$$

### B.3.2 First order perturbation coefficients

From reference 16 in chapter 5:

$$s0 := \begin{pmatrix} 16 \\ 20 \\ 28 \\ 36 \\ 40 \\ 48 \\ 56 \\ 60 \end{pmatrix} \qquad W1\_0E := \begin{pmatrix} -0.0437764 \\ -0.0203828 \\ -0.0051860 \\ -0.0015359 \\ -0.0008723 \\ -0.0003012 \\ -0.0001120 \\ -0.00006992 \end{pmatrix}$$

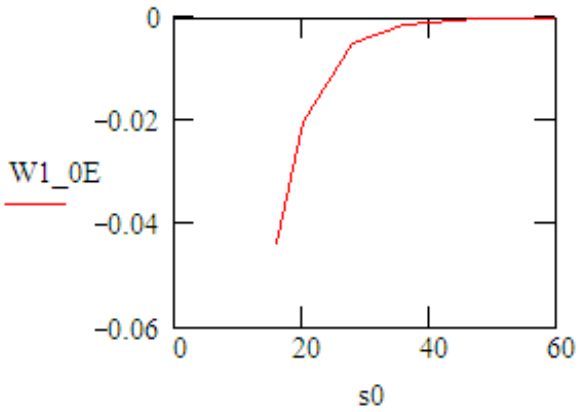


E level parameter:

interp(cspline(s0, W1_0E), s0, W1_0E, sg) = -2.001 x $10^{-3}$

W1_gs_intp := interp(cspline(s0, W1_0E), s0, W1_0E, sg)

W1_gs_intp = -2.001 x $10^{-3}$

First order perturbation coefficient:

D1A_gs_MHz := $F \cdot \rho_a \cdot W1\_gs\_intp$

D1A_gs_MHz = -1.951

D1B_gs_MHz := $F \cdot \rho_b \cdot W1\_gs\_intp$

D1B_gs_MHz = -2.907

# APPENDIX C

# WORK IN PROGRESS AND COLLABORATIONS

## C.1 THE TORSIONAL MOTION OF METHYL GROUPS IN SOME OTHER RELEVANT AROMATIC MOLECULES

Molecules studied are 2-toluidine, 3-toluidine, and 2-tolunitrile. This project is in collaboration with Dr. John Yi, Phil Morgan, and Justin Young. Phil and Justin are eventually planning to get better spectra of the 3-toluidine than the ones shown below. 3-tolunitrile is a molecule in the queue to be recorded and analyzed.

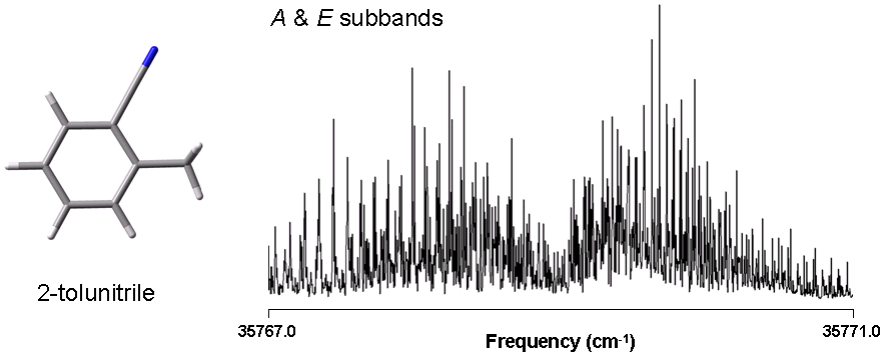

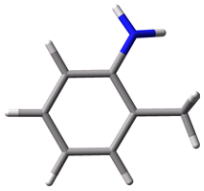

2-toluidine

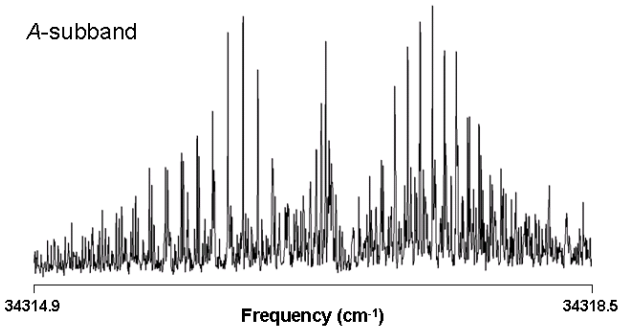


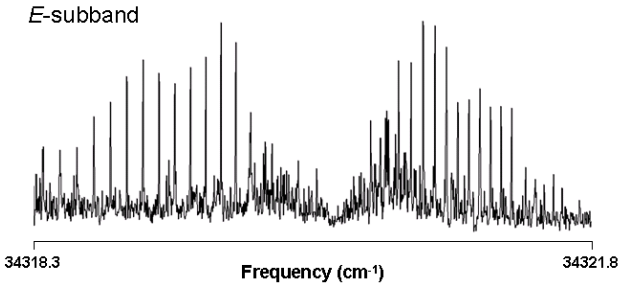


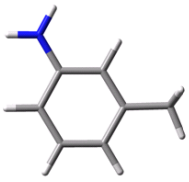

3-toluidine

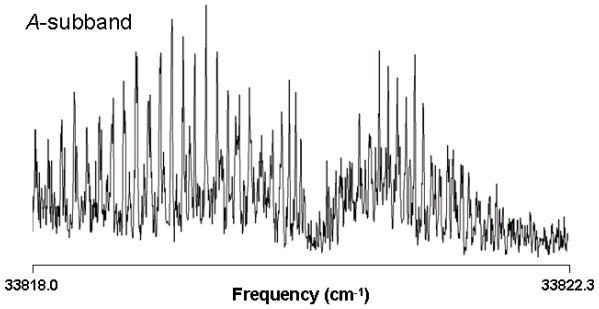


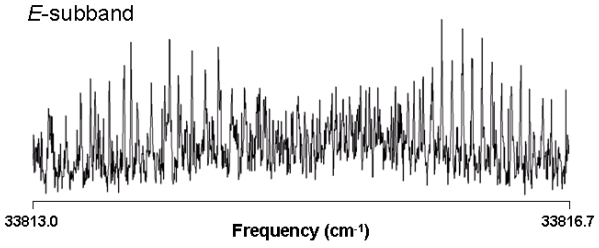

## C.2 THE AR VDW COMPLEXES OF FLUORENE, CARBAZOLE, AND DIBENZOFURAN

We were able to record spectra of the complexes corresponding to the ZPL and some vibronic transitions of these molecules. I am in the process of improving some of the fits. This project is in collaboration with Dr. John Yi. The spectra of the Ar complex of each molecule in their ZPL transitions are shown below.

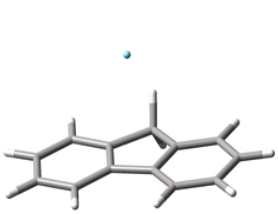

Fluorene-Ar

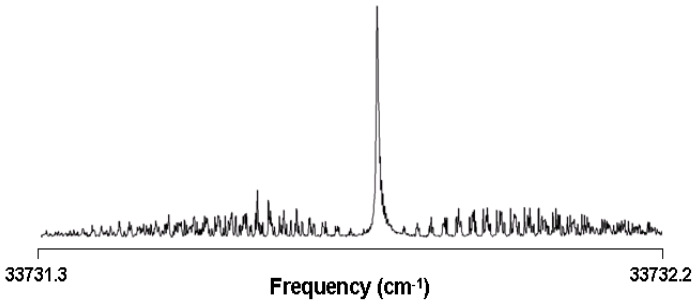


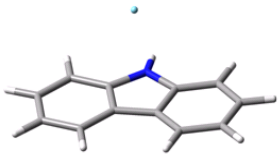

Carbazole-Ar

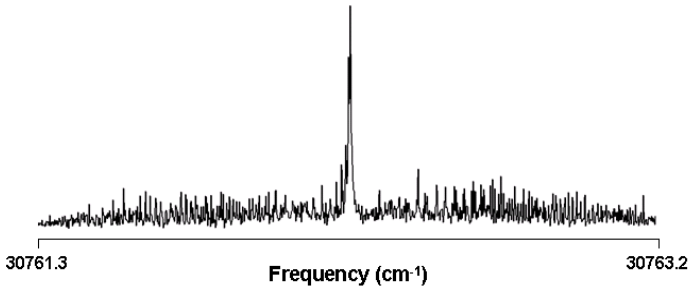


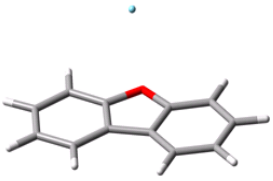

Dibenzofuran-Ar

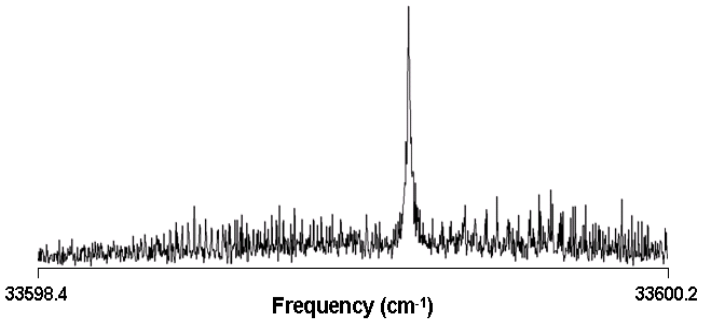

## C.3 HIGH RESOLUTION SPECTRUM OF 4-METHYLPYRIMIDINE

The 4-methylpyrimidine high resolution spectrum has been recorded, but its fit has been extremely difficult to accomplish due to the low-quantum yield of this molecule. It might be worth to give a second trial in our high resolution machine using the new Wavetrain to enhance the UV power. The spectrum obtained using intracavity frequency doubling is shown below.

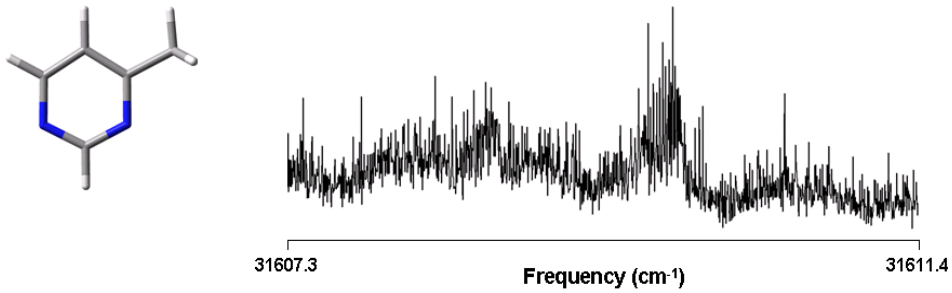


## C.4 ANOMERIC EFFECT STUDY IN AROMATIC MOLECULES

1,3-benzodioxole and coumaran are two molecules that exhibit anomeric effect. These projects are in collaboration with Jessica Thomas. 1,3-benzodioxole has been previously published by Castelluci and co-workers [*Chem. Phys. Lett*. **385**, 304 (2004)], but Jessica is in process of refining the inertial parameters of the different vibronic bands studied. Coumaran is a similar molecule that has not been studied in high resolution spectroscopy yet. The origin bands of these two molecules are shown below.

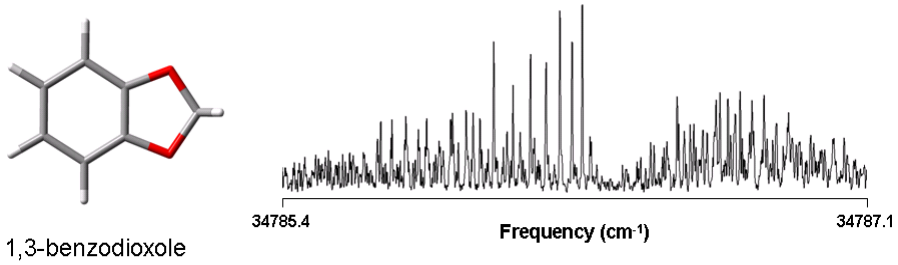


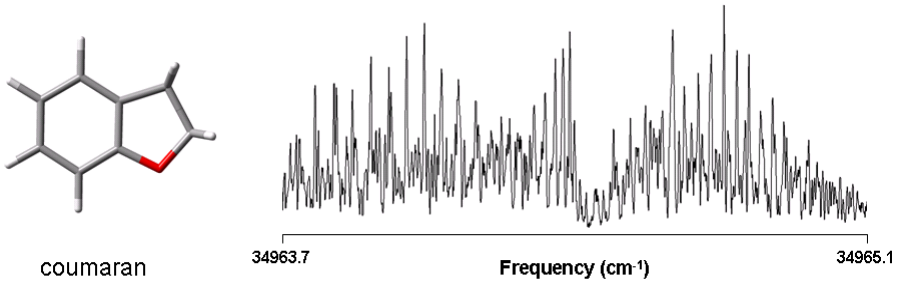


## C.5 STARK EFFECT IN 3-AMINOBENZONITRILE

3-aminobenzonitrile is an interesting molecule whose electronic spectrum is currently under investigation by applying external electric field (Stark effect). This project is in collaboration with Diane Mitchell. The spectrum of the origin band in this molecule is shown below.

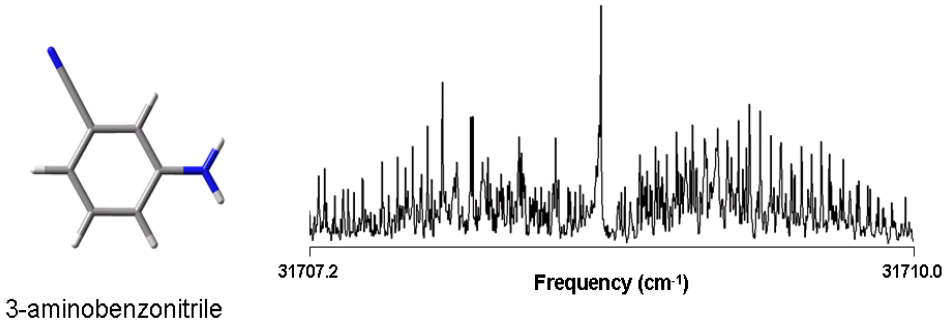

## C.6 HIGH RESOLUTION SPECTRA OF *S*-(+)- AND *R*-(-)-NAPROXEN

Naproxen is a project that is still in process of being further analyzed; Justin Young is planning on getting high resolution spectra with better signal/noise ratio than the ones shown in Chapter 2, so he may disentangle the apparent spectral differences exhibited by the two enantiomers on this molecule.